Marino Filipe Alves dos Santos

Mestre em Biotecnologia

Structural and Functional studies on the Reactivity of CORMs with plasma proteins

Dissertação para obtenção do Grau de Doutor em Bioquímica,
Especialidade Bioquímica Estrutural

Orientador: Doutora Teresa Sacadura Santos-Silva,
Investigadora Auxiliar, FCT/UNL
Co-orientador: Doutora Maria João Lobo de Reis Madeira
Crispim Romão, Professora Catedrática, FCT/UNL

Júri

Presidente: Prof. Doutora Maria Paula Pires dos Santos Diogo
Arguentes: Doutor João Domingos Galamba Correia
Doutora Isabel Maria Travassos de Almeida de Jesus Bento

Vogais: Prof. Doutor Carlos José Rodrigues Crispim Romão
Prof. Doutor João Emídio da Silva da Costa Pessoa
Prof. Doutor Eurico José da Silva Cabrita
Doutor Tiago Miguel Guerra Miranda Bandeiras
Doutora Teresa Sacadura Santos Silva

FACULDADE DE CIÊNCIAS E TECNOLOGIA
UNIVERSIDADE NOVA DE LISBOA

Julho de 2016

Marino Filipe Alves dos Santos

Mestre em Biotecnologia

Structural and Functional studies on the Reactivity of CORMs with plasma proteins

Dissertação para obtenção do Grau de Doutor em Bioquímica,
Especialidade Bioquímica Estrutural

Orientador: Doutora Teresa Sacadura Santos-Silva,
Investigadora Auxiliar, FCT/UNL
Co-orientador: Doutora Maria João Lobo de Reis Madeira
Crispim Romão, Professora Catedrática, FCT/UNL

Júri

Presidente: Prof. Doutora Maria Paula Pires dos Santos Diogo
Arguentes: Doutor João Domingos Galamba Correia
Doutora Isabel Maria Travassos de Almeida de Jesus Bento

Vogais: Prof. Doutor Carlos José Rodrigues Crispim Romão
Prof. Doutor João Emídio da Silva da Costa Pessoa
Prof. Doutor Eurico José da Silva Cabrita
Doutor Tiago Miguel Guerra Miranda Bandeiras
Doutora Teresa Sacadura Santos Silva

FACULDADE DE CIÊNCIAS E TECNOLOGIA
UNIVERSIDADE NOVA DE LISBOA

Julho de 2016

"Structural and Functional studies on the Reactivity of CORMs with plasma proteins"

O trabalho apresentado nesta Dissertação foi realizado com o apoio financeiro da Fundação para a Ciência e Tecnologia (FCT–MEC), através da atribuição da Bolsa de Doutoramento individual SFRH/BD/77894/2011 e do projecto PTDC/QUI-BIQ/117799/2010.

O trabalho desenvolvido ao longo da presente Dissertação resultou na publicação dos seguintes artigos em revistas internacionais:

1) – **Marino F. A. Santos**, João D. Seixas, Abhik Mukhopadhyay, Patrícia M. Reis, Maria J. Romão, Carlos C. Romão, Teresa Santos-Silva, New insights into the chemistry of fac-$[Ru(CO)_3]^{2+}$ fragments in biologically relevant conditions: The CO releasing activity of $[Ru(CO)_3Cl_2$(1,3-thiazole)], and the X-ray crystal structure of its adduct with lysozyme, *Journal of Inorganic Biochemistry* **2012**, *117*, 285-291.

2) – Sameena Mehtab, Gisela Gonçalves, Somnath Roy, Ana Isabel Tomaz, Teresa Santos-Silva, **Marino F.A. Santos**, Maria J. Romão, Tamás Jakusch, Tamás Kiss, João Costa Pessoa, Interaction of vanadium (IV) with human serum apo-transferrin, *Journal of Inorganic Biochemistry* **2013**, *121*, 187-195.

3) – João Costa Pessoa, Gisela Gonçalves, Somnath Roy, Isabel Correia, Sameena Mehtab, **Marino F.A. Santos**, Teresa Santos-Silva, New insights on vanadium binding to human serum transferrin, *Inorganica Chimica Acta* **2014**, *420*, 60-68.

4) – **Marino F. A. Santos**, Isabel Correia, Ana R. Oliveira, Eugenio Garribba, João Costa Pessoa, Teresa Santos-Silva, Vanadium Complexes as Prospective Therapeutics: Structural Characterization of a V^{IV} Lysozyme Adduct, *European Journal of Inorganic Chemistry* **2014**, *2014(21)*, 3293-3297.

5) – João D. Seixas, **Marino F. A. Santos**, Abhik Mukhopadhyay, Ana C. Coelho, Patrícia M. Reis, Luís F. Veiros, Ana R. Marques, Nuno Penacho, Ana M. L. Gonçalves, Maria J. Romão, Gonçalo J. L. Bernardes, Teresa Santos-Silva, Carlos C. Romão, A contribution to the rational design of $Ru(CO)_3Cl_2L$ complexes for in vivo delivery of CO, *Dalton Transactions* **2015**, *44*, 5058-5075.

6) – João Costa Pessoa, Eugenio Garribba, **Marino F.A. Santos**, Teresa Santos-Silva, Vanadium and proteins: uptake, transport, structure, activity and function, *Coordination Chemistry Reviews* **2015**, *301-302*, 49-86.

Agradecimentos

Acknowledgements

"O passado é a chave do futuro." Foi assim que comecei os Agradecimentos da minha Tese de Mestrado. Quatro anos volvidos, e porque há tradições que se devem manter e preservar, assim começo os Agradecimentos da minha Tese de Doutoramento.

Obrigado a todos. E, usando esta tão simples e sucinta expressão, podia ficar por aqui. Todavia, parece-me que se gerou uma infundada expectativa sobre esta secção pelos mais variados quadrantes da sociedade civil que, pese embora o seu manifesto exagero, me faz sentir na obrigação de não a defraudar por simples desistência. Em alternativa, será defraudada lenta e gradualmente à medida que a leitura da secção avance. Quer isto dizer que se não pretendem ficar desiludidos com o conteúdo destas parcas linhas, aconselho vivamente que parem a leitura por aqui embora, claro, sejam livres para continuar por vossa conta e risco.

Se, após todo este palavreado, ainda estão a ler, merecem os meus parabéns pela persistência e o meu reparo pela teimosia. Perguntei-me várias vezes qual seria a melhor maneira de começar esta narrativa. Como não a encontrei, opto por uma saída diplomática sublinhando o meu apreço pelo Benfica e por História. O que tem isso a ver com os Agradecimentos? Pouco, mas não se devem perder oportunidades de mostrar o quanto "me envaidece" a fé inabalável no clube que "nunca encontrou rival neste nosso Portugal". Já a História, tem que aparecer em qualquer apontamento biográfico da minha parte até porque, qual gloriosa epopeia camoniana, esta secção não pretende mais do que registar para a posterioridade todos aqueles que contribuíram de forma decisiva, quiçá, estrutural – um excelente jogo de palavras – para o desenrolar deste trabalho. Posto isto, comecemos (finalmente) os Agradecimentos devidos.

À Teresa, como não podia deixar de ser, ficam as primeiras palavras pela entusiástica e abrangente orientação ao longo destes seis anos. Enquanto seu primeiro aluno de Mestrado e de Doutoramento, disse-lhe, algures no espaço e no tempo, algo como que eu seria "o seu primeiro ciclo de refinamento" enquanto orientadora. Muitos alunos depois, acho que tal previsão se confirmou. Espero que, para primeiro refinamento, tenha obtido uns valores de R e R_{free} aceitáveis.

À professora Maria João Romão, por ter possibilitado a realização desta Tese no grupo de Cristalografia de Proteínas assim como pela sua co-orientação. No meio de tantos assuntos burocráticos, conseguiu nunca deixar o laboratório e respectiva investigação para trás.

Ao professor Carlos Romão, agradeço não apenas a sua acção vital no desenvolvimento do projecto dos CORMs, mas também a sua boa disposição e optimismo. À Catarina por todo o (muito) auxílio durante a minha breve estadia no mundo da síntese organometálica.

Ao professor João da Costa Pessoa, pela oportunidade de ter contactado com o vasto "mundo do vanádio" e pela prontidão com que sempre respondeu às nossas (muitas) dúvidas. À Isabel, pela medição dos espectros de EPR e disponibilidade para as minhas dúvidas.

Tempo agora para recordar que, nos idos tempos de 2011, agradeci a um espaço físico (a sala de BCM) o que, porventura, terá ajudado na popularidade da obra. Poderia agradecer agora à FCT como um todo (o que não seria mentira alguma), mas vou arriscar e eleger dois espaços em específico: os laboratórios 605 e 607 (com uma menção honrosa para o 621). Tal como disse em 2011, é bem possível que a importância dos espaços se deva aos seus ocupantes pelo que agradeço a todos os membros e "amigos" do XTAL pela ajuda ao longo desta Tese. Desde a Ana Luísa, a Angelina e a Isabel, todos deixaram a sua marca como se pretende transmitir de seguida.

Às "minhas" alunas de Projecto – Joana, Rita e Marta – pela valiosa oportunidade de exploração desumana que me proporcionaram (deve ler-se "pela sua contribuição para os resultados").

To Abhik for his availability to help me, first in the lab and then directly from the PDBe headquarters. To Shabir for the tips and patience in my first trips to the Synchrotron and for the dinners in one of the fanciest French restaurants: Pizza Hut at Lyon Airport.

Ao Jorge, pelos seus mordazes e pertinentes comentários da vida em geral bem como por todo o "apoio moral" que nunca me negou nos (raros a tender para raríssimos) resultados menos conseguidos do Benfica. Que a Estrutura esteja contigo!

À Cecília, por todas as encomendas, orçamentos, cristais congelados, soluções, dicas de cristalização, manutenção e operação do robot, envios de *dewars* e organização logístico-moral de tantos e tantos eventos. Tomara o *Quartzy* conseguir tal eficiência.

A um excelente Trio d'Ataque pós-doutoral sempre com "a genica que as engrandece": à Benedita, à Catarina e à Márcia. À Benedita, pelas eloquentes conversas de fim de tarde e salutares tentativas (vãs é certo) de me instruir em diferentes variantes sócio-artístico-culturais. À Catarina, pela organização de vários pequenos/grandes aspectos do dia-a-dia do laboratório e pelo passeio ao SLS. À Márcia, pelas peripécias no Diamond (já incluindo o Miguel), pelas (muitas) dicas de SAXS e pela já longínqua paciência enquanto "orientadora" aquando da minha chegada ao laboratório.

À Diana Vieira, pela ajuda de longa data que se prolongou pelo doutoramento – em Portugal (desde as aulas até ao passeio a Coimbra) ou em Inglaterra (com o jantar de boas-vindas). Note-se a total ausência de recursos de *stand-up* sublinhando, tristemente, a minha total inaptidão para tal arte.

Aos meus dois prezados "companheiros de armas" que durante algum tempo completaram com a minha pessoa um outro Trio d'Ataque: o dos alunos de Doutoramento. À Rita, pelo baptismo (de fogo) nas idas ao Sincrotrão e por tentar melhorar o desolador desterro que é a Margem Sul com a sua presença – cá estarei quando chegar a tua vez. Ao Hugo, pela épica viagem à BM30, pelas muitas boleias e por todas as dicas cristalográficas e afins – deixaste uma importante marca neste caminho e lamento que não assistas à sua conclusão; sem grandes palavras, deixo apenas um obrigado por tudo.

Às duas futuras *experts* em açúcares e afins, Diana e Viviana, seja pela aula de microarrays ou pelo passeio a Grenoble (que, com mais ou menos sono, foi, obviamente, *magnifique!*).

Ao Francisco que, chegando a meio desta Tese, rapidamente fez parecer que já estava no grupo desde há largos anos. Uma aquisição de enorme potencial, tendo sempre na "alma a chama imensa" e um excelente formando (e formador) que adoptou os valores da FCT e da Margem Sul com distinção e classe. Um orgulho!

Ao Filipe, por todos e mais alguns motivos que, se fossem exaustivamente mencionados, iriam ocupar tanto ou mais espaço que a restante Tese. Desde finais de 2008, nunca nenhuma dúvida, observação, reparo ou nota de âmbito académico, profissional, lúdico ou de avaliação de situações e comportamentos (estes então…) deixou de ser analisada e respondida. Sem a eloquência do ROC, resta-me tentar demonstrar o meu profundo reconhecimento invocando um simples lema que, ainda assim, poderá ser tão grande como os maiores da Europa: "Esforço, Dedicação, Devoção e Glória"!

Há muitas outras pessoas que, ao longo de mais de 20 anos, deixaram também a sua marca em diferentes etapas lectivas do Secundário à faculdade. Sendo virtualmente impossível referi-los a todos, não se deve deixar de fazer esta menção colectiva destacando, ainda assim, os heróicos aventureiros de BCM – Ana Filipa, Filipa, Nadine, Rui, Tânia Leandro, Tânia Perestrelo, Vasco Gordicho e Viviana entre muitos outros – que, de acordo com as minhas palavras de 2011, formaram uma "equipa sempre munida com um belo baralho de cartas e pronta a ajudar o próximo" e que, hoje, espalham a marca, orgulho e prestígio do curso e da própria FCT um pouco por todo o lado neste nosso mundo.

À Filipa, seja em Portugal, em Espanha, na Holanda, em Inglaterra ou na Suíça, pelas várias visitas à casa-mãe e pelo frequente despoletar dos e-*mails* comuns dos supracitados heróis de BCM. Estou certo que as noções laboratoriais adquiridas no XTAL te ajudam a brilhar por esta Europa fora.

À Tânia Perestrelo, já que nunca é demais lembrar, pela sua providencial escolha da BII (com mais ou com menos juízo) além dos muitos trabalhos (e outras tantas "sessões de estudo") na licenciatura, pelas visitas à casa-mãe e pela constante "presença não-presencial" com as modernas modernices comunicacionais dos nossos dias. Seja "no" Machico (ou outras zonas de Marrocos como o aeroporto Ronaldo), em Lisboa, em Coimbra ou no outro lado do Atlântico – seja com caneta, lápis ou porta-minas – mais um exemplo da formação XTAL a singrar pelo mundo.

À Tânia Leandro, pela sua intervenção decisiva na conversão de almas menos crentes para a causa de História da Ciência, pelas (muito) frequentes visitas à casa-mãe e, sobretudo, pelas várias sessões terapêuticas nas já referidas modernices comunicacionais sobre muitos e variados aspectos da vida seja a recordar o passado, comentar o presente ou projectar o futuro. Mantendo a convicção que, mais tarde ou mais cedo, a tão ansiada colaboração se vai concretizar, resta-me terminar (já que "aprecias" de sobremaneira o idioma) com um singelo (mas sentido) *gracias!*

Ao Rui, pelo facto de, resumidamente, me ter feito uma licenciatura, um mestrado e ainda ter tempo para me apresentar ao mundo da investigação. E assim se resumem os últimos dez anos. Todavia, muito mais há a dizer. O profissionalismo irrepreensível na elaboração de numerosos resumos, apresentações, discussões, relatórios, portfólios e outros trabalhos afins em 30 disciplinas partilhadas entre dois ciclos de estudos. A mítica frase "amanhã às 8h" e respectivas sessões de estudo intensivas na sala de BCM. O esmiuçamento de tantos programas e/ou segmentos cómicos e a criação dos nossos próprios, vamos lá, peculiares *sketches*. As profícuas visitas ao 3º e/ou ao 6º piso para a actualização detalhada dos pormenores e curiosidades da vida. E tantos outros episódios de relevo. Temos, em breve, de avançar com um livro de memórias, mas, para já, fica um simples "*Danke schön* e que continuemos a *'legislelar bué'* por mais umas boas (e longas) décadas".

Não podia terminar tão nobre secção sem uma referência à minha família que, indubitavelmente, possibilitou a realização desta Tese. Em especial aos meus pais (José e Ilda) e aos meus avós (Daniel e Céu) pelos 28 anos de trabalho constante (seja à semana, Sábados, Domingos ou feriados) para eu poder andar a brincar por estes lados. Uma igualmente importante palavra para a minha avó Álida e para a Maria sempre presentes nas visitas à terrinha nas *mui* nobres e académicas proximidades de Coimbra. Por último, fica uma simbólica palavra de saudade para o meu avô Eduardo que, não tendo a oportunidade de ver o culminar deste longo trajecto, foi estando presente em grande parte do mesmo.

E, muitos caracteres depois, parece-me que estou a chegar ao fim dos Agradecimentos. Para alguma dúvida ou esclarecimento adicionais, façam o obséquio de entrar em contacto com a minha pessoa. Contudo, não posso terminar sem uma breve, mas sentida, palavra para um grupo de bons rapazes que resolveram subir ao lugar mais alto do futebol europeu de selecções na véspera da minha defesa – o que um golo (até do Éder) pode fazer pela confiança e alegria de um país.

E, se comecei esta secção com a auto-citação inicial de 2011, parece-me apropriado finalizá-la com a auto-citação terminal da mesma publicação: "muito obrigado a todos os que ajudaram neste caminho".

E pluribus unum

"Não somos 11, Somos 11 milhões"

Omnis Civitas Contra Se Divisa Non Stabit

Abstract

Drug design is a multidisciplinary field involving several methodologies namely X-ray crystallography. This Thesis reports the results obtained in two drug design projects related to the interactions of putative metal-based drugs (Carbon Monoxide Releasing Molecules, CORMs, and vanadium complexes) with different proteins.

Carbon monoxide, beyond its toxic potential, is a signaling molecule with biological and potential therapeutic roles. CORMs are able to transport CO in the blood stream delivering it at the damaged tissues and their pharmacokinetics strongly depends on the interactions with blood proteins (hemoglobin, albumin and transferrin).

Soaking and co-crystallization trials have been tried and crystal structures were obtained, namely two 1.9 Å resolution hemoglobin structures and a 2.7 Å resolution transferrin structure soaked with ruthenium- and iridium-based CORMs. Several $[Ru(CO)_3Cl_2L]$ CORMs have been soaked with lysozyme (HEWL) to understand their mechanism of action. The 1.5 Å resolution HEWL•ALF850 structure shows the adduct $[His15•Ru(CO)(H_2O)_4]^{2+}$ revealing the importance of the stepwise decay of $[Ru(CO)_3]^{2+}$ for the delivery of CO *in vivo*. The subsequent 1.7 Å resolution structures corroborate such proposal: an adduct $[His15•Ru^{II}(COOH)(CO)(H_2O)_3]$, found in the HEWL•ALF486 structure, corresponds to a metallacarboxylate intermediate of the decarbonylation pathway. This suggests that the aqueous chemistry of these complexes is governed by the water-gas shift reaction initiated with the nucleophilic attack of HO^- on coordinated CO.

Vanadium is an element with biological and therapeutic roles namely as insulin-enhancer agent and transferrin has been proposed as a natural carrier. The conformation adopted by transferrin upon vanadium binding was addressed by X-ray crystallography, urea gel electrophoresis and SAXS but no definitive answers were obtained.

HEWL was also used in different soaking experiments and a 1.3 Å resolution structure with picolinate was solved showing that $V^{IV}O(pic)_2$ covalently binds to the COO^- group of the side chain of Asp52 in the active site. The long $V^{IV}=O$ bond is explained by the reduction of V^{IV} to V^{III} during exposure to the X-ray beam as further confirmed by EPR and DFT. Picolinate was used with trypsin and similar results have been obtained: the 1.1 Å resolution structure exhibits a $V^{IV}O(pic)_2$ adduct bound to Ser195 in the active site. The ability of picolinate complex to bind to the active center of proteins – glycoside hydrolases and serine proteases – has been demonstrated suggesting that similar vanadium compounds can act as protein inhibitors, accounting for eventual side effects derived from the use of these metal complexes as therapeutic agents.

Keywords: Carbon monoxide and Carbon Monoxide Releasing Molecules (CORMs) • Vanadium and vanadium complexes • Drug design • X-ray crystallography • Blood proteins • Lysozyme • Trypsin

Resumo

O processo de *drug design* é uma área interdisciplinar envolvendo várias técnicas nomeadamente a cristalografia de raios-X. A presente Tese aborda dois projectos de *drug design* relacionados com as interacções de potenciais fármacos – Moléculas Libertadoras de Monóxido de Carbono (CORMs) e complexos de vanádio – com diferentes proteínas.

O monóxido de carbono, além do seu potencial tóxico, é uma molécula sinalizadora com efeitos biológicos e terapêuticos. Os CORMs transportam o CO na corrente sanguínea libertando-o nos tecidos afectados e a sua farmacocinética depende das interacções estabelecidas com proteínas sanguíneas (hemoglobina, albumina e transferrina).

Realizaram-se ensaios de *soaking* e de co-cristalização com estas proteínas obtendo-se estruturas de hemoglobina (resolução de 1.9 Å) e transferrina (resolução de 2.7 Å) com diferentes CORMs de ruténio e de irídio. Usaram-se diferentes compostos $[Ru(CO)_3Cl_2L]$ em ensaios de *soaking* com lisozima (HEWL) para compreender o seu mecanismo de acção. A estrutura de HEWL•ALF850 (resolução de 1.5 Å), mostra o aducto $[His15•Ru(CO)(H_2O)_4]^{2+}$ sugerindo que a descarbonilação progressiva de $[Ru(CO)_3]^{2+}$ é fundamental para a libertação do CO *in vivo*. Outras três estruturas (resolução de 1.7 Å) reforçam tal ideia: o aducto $[His15•Ru^{II}(COOH)(CO)(H_2O)_3]$, identificado na estrutura HEWL•ALF486, corresponde a uma espécie intermediária da descarbonilação indicando que tal processo é iniciado pelo ataque nucleofílico do grupo HO^- ao grupo CO.

O vanádio possui diversas acções biológicas e terapêuticas nomeadamente como mimetizador da insulina sendo que a transferrina foi proposta como o transportador natural. A sua conformação após a ligação ao vanádio foi investigada por diferentes metodologias – cristalografia de raios-X, electroforese em gel de ureia e SAXS – mas sem resultados conclusivos.

Realizaram-se diversos ensaios de *soaking* com a lisozima obtendo-se uma estrutura com picolinato (resolução de 1.3 Å) mostrando o aducto $V^{IV}O(pic)_2$ covalentemente ligado ao grupo COO^- da cadeia lateral do Asp52 no centro activo. A longa ligação $V^{IV}=O$ deve-se à redução do V^{IV} a V^{III} durante a exposição ao intenso feixe de raios-X como posteriormente mostrado por EPR e DFT. O mesmo composto foi também usado com a tripsina obtendo-se resultados semelhantes com o aducto $V^{IV}O(pic)_2$ ligado à Ser195 no centro activo (resolução de 1.1 Å). A capacidade de ligação do complexo de picolinato ao centro activo de proteínas – glicosil hidrolases e proteases de serina – foi demonstrada sugerindo que compostos de vanádio semelhantes possam actuar como inibidores de proteínas o que, por sua vez, pode interferir no seu uso como agentes terapêuticos.

Termos chave: Monóxido de carbono e Moléculas Libertadoras de Monóxido de Carbono (CORMs) • Vanádio e complexos de vanádio • Desenvolvimento de fármacos • Cristalografia de raios-X • Proteínas sanguíneas • Lisozima • Tripsina

Table of Contents

Figures Index

Table Index

Abbreviations and symbols

$\|F_{hkl}\|$	Amplitude
1,10-phen	Phenanthroline
ADME	Absorption, Distribution, Metabolism and Excretion
ADMET	Absorption, Distribution, Metabolism, Excretion and Toxicity
AOX	Aldehyde oxidase
Bipy	2,2'-bipyridine
BK	Large-conductance Ca^{2+}-and voltage-gated K^+ channels
BPG	2,3-biphosphoglycerate
BSA	Bovine Serum Albumin
Ca_V	Voltage-gated Calcium Channels
cGMP	Cyclic Guanosine Monophosphate
CO	Carbon monoxide
COHb	Carboxyhemoglobin
CORM	Carbon Monoxide Releasing Molecule
CORM-1	Dimanganese decacarbonyl, $[Mn_2(CO)_{10}]$
CORM-2	Tricarbonyldichloro ruthenium (II) dimer, $[Ru(CO)_3Cl_2]_2$
CORM-3	Tricarbonyldichloro(glycinato)ruthenium (II), $[Ru(CO)_3Cl(glicinate)]$
CORM-A1	Sodium boranocarbonate, $[Na_2H_3BCO_2]$
Cryo-EM	Cryo Electron Microscopy
CSD	Cambridge Structural Database
Da	Dalton
DCM	Dichloromethane/Methylene chloride
DFT	Density Functional Theory
d_{hkl}	Distance between the planes in the crystal lattice
DLS	Diamond Light Source
EMA	European Medicines Agency
ERK	Extracellular signal Regulated Kinases
ESRF	European Synchrotron Radiation Facility
ET-CORM	Enzyme-triggered CORM
FBDD	Fragment-based Drug Discovery
F_{calc}	Calculated Structure Factor
FDA	Food and Drug Administration
FDT	Free Drug Theory
F_{hkl}	Structure Factor

F_{obs}	Observed Structure Factor
FTIR	Fourier Transform Infrared Spectroscopy
GI tract	Gastrointestinal tract
GPCRs	G-protein-coupled receptors
GTP	Guanosine Triphosphate
H_2dipic	Dipicolinic acid
H_2S	Hydrogen Sulfide
Hdhp	1,2-dimethyl-3-hydroxy-4-pyridinone
HEPES	4-(2-hydroxyethyl)-1-piperazineethanesulfonic acid
HEWL	Hen White Egg Lysozyme
HO	Heme oxygenase
HO-1	Heme oxygenase-1
HO-2	Heme oxygenase-2
Hpic	Picolinic acid
HSA	Human Serum Albumin
Hs-apoTF	Human Serum Transferrin
HSF1	Heat Shock Factor 1
HSP70	Heat Shock Protein 70
HTS	High Throughput Screening
I/R	Ischemia/Reperfusion
IL-10	Interleukin-10
IL-1β	Interleukin-1β
IRS	Insulin Receptor Substrate
ITC	Isothermal Titration Calorimetry
JNK	c-Jun NH2-terminal kinases
K_{Ca}	Calcium-activated Potassium Channels
logP	Logarithm of the octanol-water partition coefficient
MAD	Multiple-wavelength Anomalous Dispersion
Maltol	3-Hydroxy-2-methyl-4H-pyran-4-one
MAPK	Mitogen-activated protein kinase pathway
MCC	Metal Carbonyl Complex
MIP-1α	Macrophage Inflammatory Protein-1α
MIR	Multiple Isomorphous Replacement
MR	Molecular Replacement
$NaVO_3$	Sodium metavanadate
NMR	Nuclear Magnetic Resonance

NO	Nitric Oxide
p38	p38 MAPK
PD	Pharmacodynamics
PDB	Protein Data Bank
PEG	Polyethylene glycol
PK	Pharmacokinetic
PKG	cGMP-dependent Protein Kinase or Protein Kinase G
PTPase	Phosphatases with affinity to tyrosine-phosphate proteins
RO5	Rule-of-five or Lipinski's rule
ROS	Reactive Oxygen Species
SAD	Single-wavelength Anomalous Dispersion
SAR	Structure-Activity Relationship
SAXS	Small Angle X-ray Scattering
sGC	Soluble Guanylyl Cyclase
SLS	Swiss Light Source
SPR	Surface Plasmon Resonance
TNFα	Tumor Necrosis Factor
Tris	Tris-(hydroxymethyl)-aminomethane
TS	Fluorescence-based Thermal Shift
V	Vanadium
VBPO	Bromoperoxidases
VCPO	Chloroperoxidases
VHPO	Vanadium-containing Haloperoxidases
$VO(acac)_2$	Vanadyl acetylacetonate
$VOSO_4$	Vanadyl sulfate tetrahydrate
θ	Angle between the incident wave and the crystal plane
λ	Wavelength
Φ_{hkl}	Phase

CHAPTER 1

INTRODUCTION

1.1 – Drug Design and Development

1.1.1 – General concepts and historical perspective

The 20th century, as well as the earlier years of the 21st century, led to deep and significant geographic, political, economic, technologic and social changes in the world. Greatly connected with such modifications, it is commonly recognized that the current life conditions are much better than those 100 years ago, particularly in the developed countries in Europe and North America.

The improvement of the health conditions was an essential step for such progress as proven by the raising of the life expectancy. This improvement is partially explained by a better nutrition and basic hygiene procedures but the development of new, better and safer drugs was absolutely vital for such achievement. Remarkably, former deathly diseases as smallpox, poliomyelitis and diphtheria were largely eradicated, a large range of antibiotics were made available and many other chronic or minor conditions – as simple as a cold or a headache – could be effectively treated or, at least, controlled (Figure 1.1).[1,2]

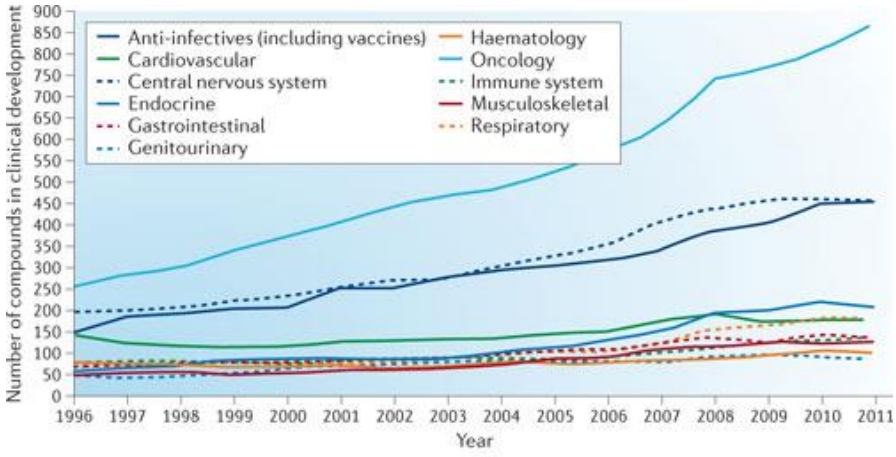

Figure 1.1 – Compounds in clinical development by therapeutic area between 1996 and 2011.[2] Oncology is the more representative area with 26% of the total of the products in development in 2011.

At this point, one very important question emerges: what is a drug? In general, a drug can be defined as "an agent that has a desired biological effect on the human body or some other living system" or, even in a more broad definition, agents that "interact with a biological system and produce a biological response".[3] These definitions can be ambiguous covering many compounds. Can penicillin and ecstasy belong to the same group? And some other compounds like caffeine, nicotine and alcohol? In order to try to clarify these situations, drugs were described as: "good drugs" and "bad drugs". The "good drugs", also called pharmaceutical drugs or medicaments, are used to prevent or treat diseases (like penicillin and other antibiotics). On the opposite side, "bad drugs", normally

associated to addiction and habituation, do not have medicinal goals (heroin and cocaine can be cited as belonging to this group).

However, such classification is not entirely satisfactory. The line between both sides is very flexible meaning that the same compound could be classified as a "good drug" or as a "bad drug" depending on the situation. A classic example is morphine: known as a potent analgesic, but also addictive and responsible for respiratory problems.[3] Other illustrative example is heroin: one of the most well-known "bad drugs", heroin is a very effective painkiller used in terminal cancer cases as diamorphine.[3,4]

These two straightforward examples illustrate that, by one hand, is very hard, or virtually impossible, to distinguish between "good drugs" and "bad drugs" and, by the other hand, that no drug is entirely safe. Helping to explain these facts, it should be taken into account the famous citation of Paracelsus – the "father" of Toxicology – in the 16th century: "All things are poison and nothing is without poison; only the dose makes a thing not a poison" or, more simpler, "The dose makes the poison" (*Sola dosis facit venenum* in Latin).[5]

Apart from all the possible discussions related with this nomenclature, the terms drug development and drug design are usually associated to the research conducted by large pharmaceutical companies with very significant financial costs (around US $800 million according some studies).[1,6]

Nevertheless, long before the foundation of these companies, scientists were already involved in this subject. The following paragraphs aim to give a brief historical perspective on the evolution of drug discovery.

The search for medicinal substances is nearly as old as man himself and there are evidences of the use of drugs in the Neolithic period.[7] Natural products were the source of the drugs used – particularly herbs and other vegetal products, but also arising from animal and mineral origin – and nowadays continue to be important in the drug discovery processes.[5,8]

Moving to some ancient civilizations (Mesopotamia, Egypt, India and China, among others), it is possible to asseverate the use of drugs thanks to the available documents and artifacts that survive until modern ages.[5,7] That's the case of several pieces of clay from Mesopotamia, dated around 1700 B.C., found about one century ago and interpreted by R. Campbell Thompson.[7] Also importantly, an Egyptian document was also found in 1872; written in c. 1550 B.C., the so-called Ebers Papyrus (named in honor to George Ebers who found it) contains information on prescriptions, drugs and medicinal plants (Figure 1.2). Regarding the Oriental cultures, some compositions should be also mentioned: the Indian *Ayurveda* ("Science and Knowledge of Life") and the Chinese *Shen Nong Ben Cao Jing* ("Shen Nong's Canon on Materia Medica").[5,7]

As expected, the classic civilizations – Greece and Rome – made significant contributions to the development of this subject. Numerous medical schools appeared, many of them working in temples dedicated to Asklepios, the god of medicine, and, interestingly, the term *pharmakon* is used to describe a drug in the epic poem Odyssey, written by Homer. Some personalities are inevitably

mentioned as Hippocrates (the "Father of Medicine" and leader of the Cos school, he is associated to the *Hippocratic Oath* and the *Hippocratic Corpus* where medical and ethical questions are considered), Aristotle and Teophrastus (the authors of *Historia Plantarum* and *De Causis Plantarum*, respectively, which present a classification for over 500 plants and describes the vegetal physiology).[5,7]

In Rome, in the first and second centuries after Christ, Pedanius Dioscorides and Claudius Galen or Ganelus should be also highlighted. Dioscorides was the author of *De Materia Medica* (Figure 1.3) which presents a detailed study not only on over 900 drugs (from animal, vegetal and mineral sources) but also on some elementary chemical techniques (as distillation). Galenus was the author of *Opera Omnia* which describes several drugs and respective applications; he also developed the use of the so-called "galenicals" – complexes resulting from the junction of several ingredients.[5,7]

Figure 1.2 – Piece of the Ebers Papyrus.[5]
Found in Thebes by the German George Ebers, the document was deciphered by B. Ebbell in 1937 allowing the identification of more than 700 drugs and recipes used in Ancient Egypt. Currently, it is held at the University of Leipzig (Germany).

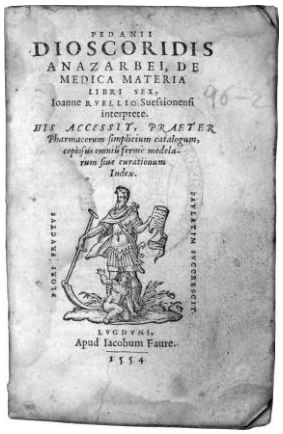

Figure 1.3 – Cover of *De Materia Medica* (edition dated from 1554, in Latin).[5]
The original edition was written in Greek and, due to the details presented on several drugs and some of the side effects, it was one of the main pharmacology books until the 18th and 19th centuries.

After the end of the West Roman Empire (5th century) and the beginning of the Medieval period, the focus on science was moved to the Arab world, merging the occidental and the oriental knowledge in different areas. It should be emphasized that Iberian Peninsula was particularly influenced by the Arabian culture due to several centuries of occupation (from 711 to 1492) as proven, for instance, by the vocabulary, architecture and technology adopted by the Portuguese and Spanish people. Concerning pharmacology, the Arabian thinking is similar to the Greek one; Rhazes (Abu Bakr al-Razi), Avicenna (Abu Ali al-Hussain ibn Abdallah ibn Sina) and Abulcasis (Abu al-Qasim al-Zahrawi) are some of the greatest names in the 10th and 11th centuries. For instance, in first years of the 11th century, Avicenna published the book *al-Qanun fi at-tibb – Canon Medicinae* – containing, among other details, the description of the uses and efficacy of 760 drugs alphabetically ordered.[5,7]

During the Middle Ages, Europe is not recognized as a fruitful and fertile land for the development of the scientific questions with exceptions of some medicinal works namely the book

published in the last half of the 13th century *Thesaurus Pauperum* attributed to the Portuguese Pope John XXI (born Pedro Julião and also known as Pedro Hispano Portucalense).[9,10]

The Renaissance was the stage for a noteworthy change in this paradigm and science, among architecture, painting and sculpture, gained new life. The already referred Paracelsus (born Philippus Teophastrus Bombastus von Hohenheim) was one of the exponents of this period; in addition to the introduction of the concept of dose, Paracelsus used metal salts for the treatment of some disorders in what can be considered as an ancestor of medicinal chemistry.[5]

One of the facts closely related to such development was the Portuguese Discoveries (the famous *Descobrimentos* brilliantly described in the equally famous Portuguese epic poem *Os Lusíadas* by Luís Vaz de Camões). Following the example of Portugal, some other European countries also started its discoveries namely Spain (the *Treaty of Tordesillas* – by which the two Iberian countries divided the world between them, shortly after the discovery of America – became well-known). Starting in 1415 and prosecuting into the 15th and 16th centuries, the Portuguese people were able to reach very widespread regions such as Africa, Orient (India, China and Japan) and Brazil. As result, in addition to the expansion of the Portuguese Empire, it was possible to contact with other civilizations as well as to study new herbs and other pharmacological agents introducing them in Europe. New compendia were written as "The Colloquies on the Simples and Drugs of India" (*Coloquios dos simples, e drogas he cousas mediçinais da India*) published in 1563 by Garcia de Orta.[11]

The progressive advances in biology and chemistry that occurred in the following centuries paved the way into the modern drug discovery processes from the 19th century until nowadays (Figure 1.4).[5,12,13] In fact, by the 19th century, more than the simple use of herbs or other agents with medicinal properties, the goal was to identify, isolate and characterize the respective active substances. This approach was determinant for the development of the pharmacology as an experimental and systematic scientific field thanks to the work conducted by some European scientists as François Magendie, Claude Bernard, Rudolph Buchheim and Oswald Schmiedeberg. The foundation of specialized journals has also contributed for the mentioned development; as example, Schmiedeberg and Bernhard Naunyn founded, in 1873, the journal *Archiv für experimentelle Pathologie und Pharmakologie* which is still active nowadays under the name "Naunyn-Schmiedeberg's Archives of Pharmacology".[5]

The first example of this new methodology took place in the first years of the 19th century when Friedrich Sertürner was able to isolate morphine from opium testing it in dogs. From this point, several other alkaloids were identified and isolated like emetine (by Pierre Pelletier), quinine and caffeine (both by Pierre Pelletier and Joseph Caventou), atropine (by Philipp Geiger), papaverine (by Georg Merck) and cocaine (by Albert Niemann).[5,7] As important as these findings, was the raising of the first pharmaceutical manufactures. In 1826, six years after its isolation, quinine was massively produced by Pelletier and Caventou, in what is considered the basis of the pharmaceutical industry.

Shortly after, some other factories were created or reconverted for such purpose as Merck – still a world giant of the pharmaceutical industry nowadays.[5]

Figure 1.4 – Summary of some important findings on drug discovery over the last 200 years. Adapted from [12] Starting with the isolation of the active principles from plants, the significant advances in Chemistry, Molecular Biology, Genetics, Bio-informatics and Biochemistry were essential for the development of new drugs.

In the subsequent years, different approaches led to the emergence of new drugs as represented in Figure 1.5. During the 19th century, the introduction of different vaccines, as anthrax, rabies and cholera by Louis Pasteur, was crucial avoiding thousands of deaths by year. In the first years of the 20th century, new concepts were introduced, as the term chemoreceptor by Paul Ehrlich, which is on the basis of the modern studies of ligand-receptor interactions.[5,12]

Moving to the second period (from the middle of 1930s to nowadays), the discovery of antibiotics – penicillin was the first to be identified by Alexander Fleming – was also a remarkable progress in the evolution of drug discovery. Penicillin played an important role during the Second

World War and, from then to now, several other natural and semisynthetic antibiotics were produced helping to reduce the number of deaths caused by bacterial infections, around the world. A large range of new drugs has been developed in the last 40 years covering an increasing number of conditions. The expansion of the drug discovery process is closely related to the improvement of the available methodologies and tools: molecular biology, computational chemistry, genetic engineering and structural biology (namely X-ray crystallography) are some examples of the techniques that contributed to the boost of this already well established field.[5,12]

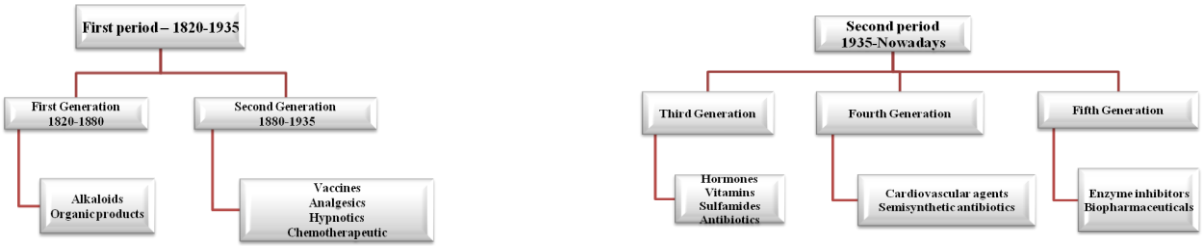

Figure 1.5 – Schematic representation of the major periods of drug development. Adapted from [5] The modern drug discovery process is divided into two periods which are subdivided in different generations of drugs spanning from the beginning of the 19th century until the 21st century. Vaccines and antibiotics are some of the most representative compounds in the drug development area.

Nevertheless, this amazing journey is not finished or not even close to its end. Research is conducted daily in order to try to improve our knowledge on different diseases – cancer is, perhaps, the most paradigmatic case – leading to the identification of new potential usable drugs.

1.1.2 – Principles of Drug Design

As previously mentioned, the development of new drugs is a very expensive and time-consuming process.[6] In fact, from the thousands potential compounds studied, only a minor percentage will reach the market after approval by some legal institutions as the US Food and Drug Administration (FDA) or the European Medicines Agency (EMA): from 1950 to 2008, only 1222 new drugs were approved by the FDA (Figure 1.6).[14,15]

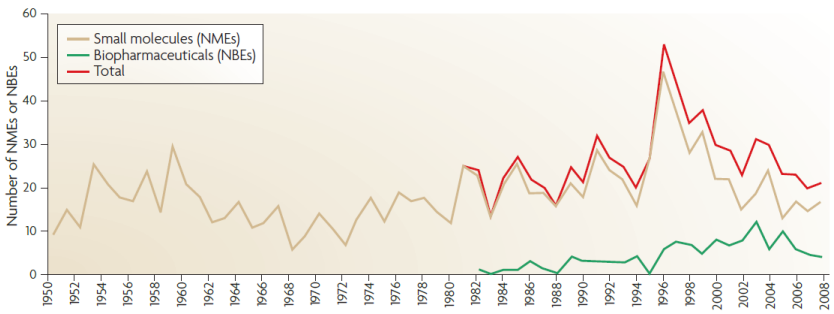

Figure 1.6 – Graphical representation of the approval of new drugs by the FDA between 1950 and 2008.[14] Out of a total of 1222 approved drugs, 1103 correspond to small molecules and 119 are biological molecules. Reflecting the high costs of the process, only 261 companies have released at least one new drug to the market since 1950.

The low number of successfully approved drugs is a clear indicator of the complexity of the process. Several steps are required in order to obtain a suitable therapeutic agent (Figure 1.7) and all of them must be entirely satisfactory. That means that, for instance, a drug candidate could be very effective against a given disorder but is useless if it is also toxic or not bioavailable. In fact, bioavailability and toxicity are the common factors for rejecting the use of different molecules as drugs, covering 39% and 21% of the causes of the unsuccessful cases, respectively.[4,16,17]

The creation of a new drug could be divided into two different stages: discovery and development. The first stage leads to the identification of a drug candidate (after identifying the target and optimizing the lead) while the second stage encompasses the preclinical, clinical (phases I, II and III) and post-clinical trials in animals and humans

Only after all these steps, which usually take 10-15 years to be completed, a molecule can be considered as a safe drug and reach the market. Regardless of the importance of the clinical trials, they will be not addressed herein. Instead, a brief outline on the discovery process of a new drug candidate will be covered.

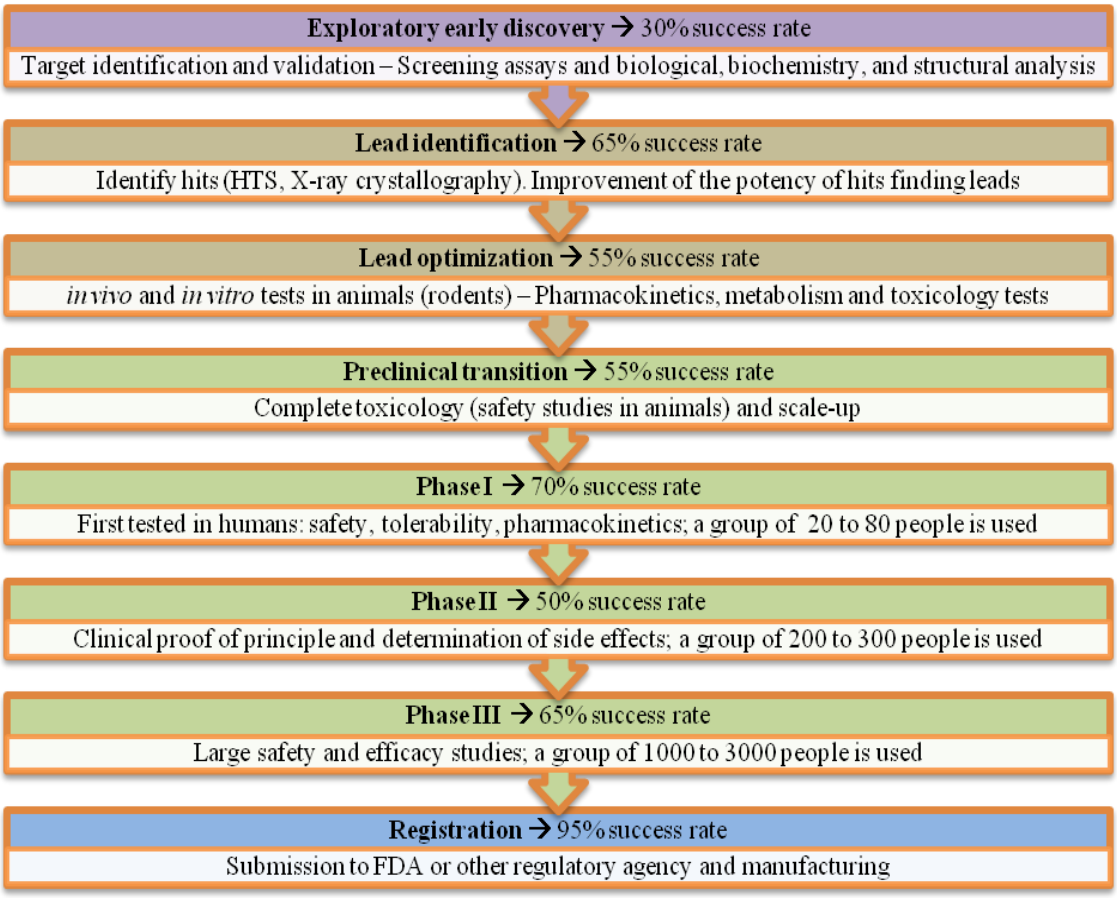

Figure 1.7 – Schematic representation of the different stages involved in the drug design process from the target identification until the market release. Adapted from [17] Following the identification of a biological target, several steps are conducted in order to find appropriate molecules. Only a reduced number of drug candidates will enter into the clinical tests phases and, from those, usually just one will be commercial available for the general public.

1.1.2.1 – Drug Discovery steps

As previously referred, before starting the clinical trials phases, it is necessary to determine suitable drug candidates. Figure 1.8 summarizes the principal steps involved in the discovery of drug candidates: target identification and validation, hit identification, hit-to-lead and lead optimization.[18]

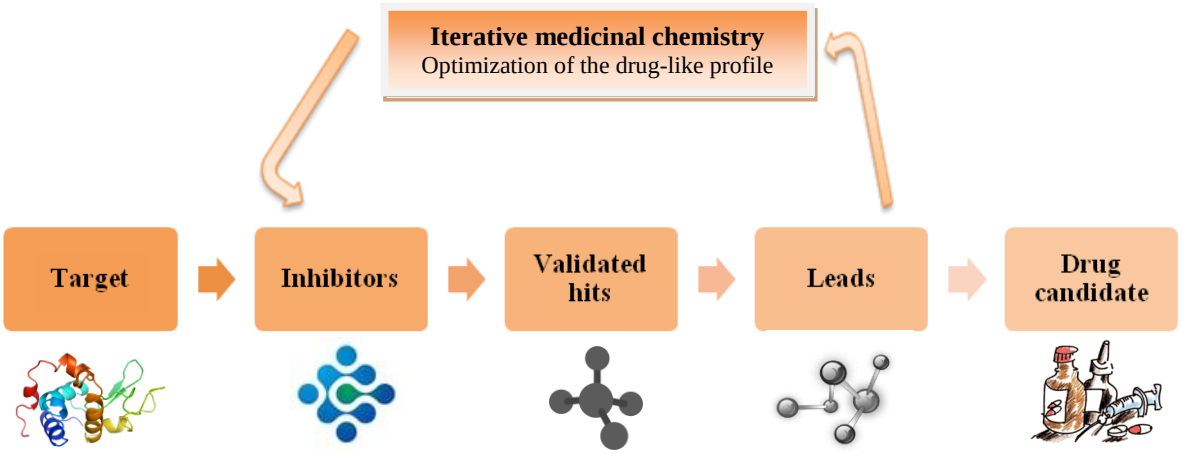

Figure 1.8 – Workflow of the stages involved in the discovery of putative drug candidates. Adapted from [17] For each stage, different methodologies are required in order to achieve the desired goal: obtaining a new and safe drug. The great number of required steps and respective associated techniques explains partially why drug design is an expensive and time-consuming process.

- **Target identification and validation**

Keeping in mind the current paradigm, a given disease should be characterized as accurately and detailed as possible. Therefore, it makes sense thinking in the target identification as the first stage of the drug design process.

A target could be defined as a biological molecule – usually proteins, DNA or RNA – able to interact with a potential drug (small molecules or other biomolecules like antibodies) producing a beneficial effect. An important consequence from this definition is the existence of a binding site – a particular region of the target capable of accommodating the drug through covalent interactions or, more commonly, intermolecular interactions (for example, ionic bonds, hydrogen bonds, van der Waals interactions and hydrophobic interactions). A "druggable" target must follow some specific characteristics namely to be directly involved in a given disorder, to be locally expressed in some tissues or organs and to be functionally and structurally characterized.[3,18,19,20,21]

Currently, proteins are the most well studied targets being grouped into different classes such as enzymes, receptors, ion channels and transport proteins. Particular attention has been given to proteases and kinases and also to G-protein-coupled receptors (GPCRs).[22] The progressive studies on the area allow to identify an increasing number of targets.[19,20,21]

Different approaches could be applied in order to identify new targets.[23] In addition to a careful examination on the available literature of a desired molecular mechanism, it is normal to analyze the gene expression profile, comparing the expression levels of RNA and proteins observed in the normal and in the affected tissue. Other techniques are related to proteomics (example of the determination of the enzymatic activity in the affected tissues) or to phenotype analysis approaches.[20,21] It is still possible to use the so-called data mining approach – a bioinformatic method that combines biological, computational and statistical knowledge to discover, select and prioritize potential targets.[24]

After its identification, a target must be experimentally validated in order to confirm the proposed mechanism of action. For that, different animal models are used and several approaches can be adopted including the gene knockout and the gene knockdown/silencing, through RNA interference or antisense methods.[20,21]

- **Hit identification**

Following the target identification and validation, the drug design process enters into a new stage of screening tests in order to identify, from the thousands compounds available, hits and the respective leads.[18]

At this point, it is convenient to define the terms hit and lead. A hit can be defined as a primary compound that shows some activity to a given target in a screening assay. A lead, deriving from the hit, is a chemical structure with activity and selectivity to a target, proved by specific pharmacological or biochemical screens. Upon optimization, a lead eventually originates a clinical candidate.[18,25]

In order to obtain a considerable number of hits and leads for a given target, there are several possible assays that could be grouped into two big categories: biochemical assays, also named "isolated target", where the target protein is overexpressed and purified allowing the quantification of the ligand affinity to the target; and cell-based assays, where the activity of the ligand is directly inferred by the behavior of the cells. Different factors should be taken into account to decide the best assay for a given biological problem. These assays could be used in different screening approaches including the High Throughput Screening (HTS) and the Fragment-based Drug Discovery (FBDD).[18,26]

The HTS is a method based in the screening of large chemical compound libraries, with a variable number of molecules (up to millions), for activity against the previously identified targets, usually relying on different fluorescence and absorbance techniques. This method was introduced in 1990s and since then significant advances were observed, not only by its progressive automation and miniaturization (Figure 1.9), but also by the optimization of important parameters such as time, cost

and quality of the process (reproducibility and robustness are important characteristics to evaluate the quality of the HTS method).[27,28,29]

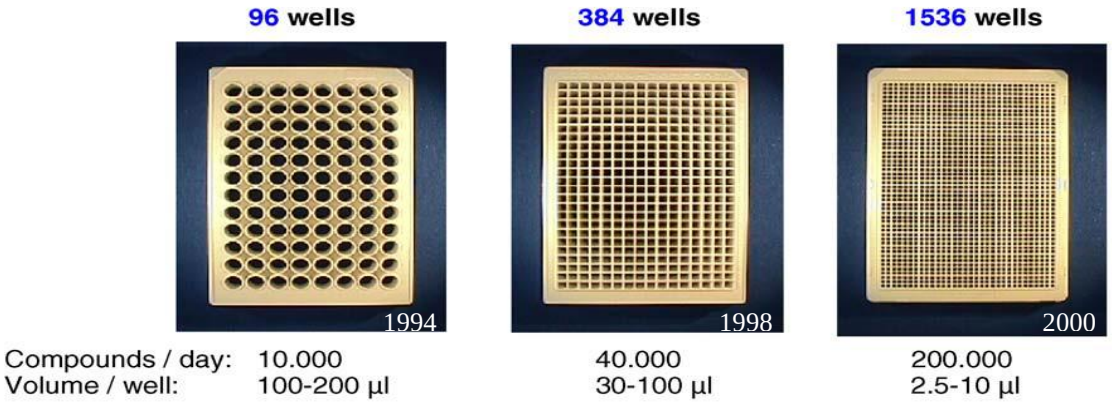

Figure 1.9 – Evolution of the type of microtiter plates used in HTS assays through the years. Adapted from [27] In the beginning, 96-well plates were used but they were progressively replaced by 384-well and 1536-well plates. Such miniaturization was crucial to increase the efficacy of the HTS methods which allowed screening of many more compounds with a smaller volume per well, as indicated for each plate.

Despite their utility, HTS methods present some disadvantages such as the maintenance of the libraries and the existence of some compounds that, by their physic-chemical properties, are not suitable to be used as drugs. In order to overcome these limitations, FBDD methodologies have emerged. In the FBDD method, libraries of fragments (small molecules with no more than 300 Da) are designed rather than using the entire molecules allowing to recognize the determinants of the binding to the desired target. Once an interaction is detected, the initial fragment is progressively improved in order to optimize the binding or some other desired characteristics (Figure 1.10).[30,31]

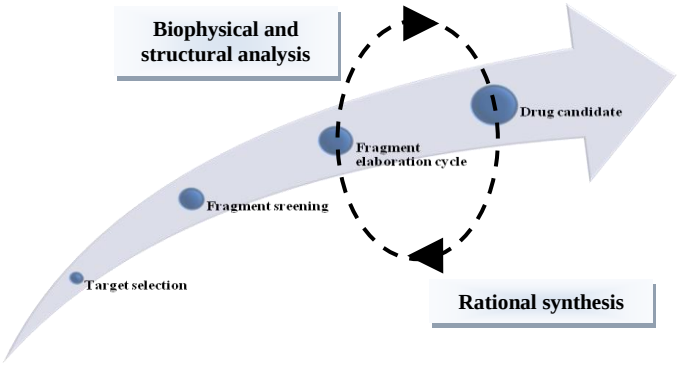

Figure 1.10 – Scheme of the steps of FBDD methodology. Adapted from [30] A combined and interdisciplinary approach allows the design of more potent drug candidates. In addition to X-ray crystallography and several biophysical techniques, *in silico* methods are also precious tools, often saving time and financial resources.

FBDD methods require a strong interdisciplinary approach, intertwining structural biology and synthetic chemistry. In fact, the structural characterization of the biological target is essential in the iterative re-synthesis of the fragment and X-ray crystallography plays a crucial role in this process as "potentially the most powerful primary screening technique" in the words of Abell and coworkers.[30]

Some other complementary biophysical techniques such as Fluorescence-based Thermal Shift (TS), Surface Plasmon Resonance (SPR), Isothermal Titration Calorimetry (ITC) and Nuclear Magnetic Resonance (NMR) are usually performed prior to X-ray analysis to confirm the fragment-target interaction.[30]

After the screening methods reveal different hits, they are grouped into the so-called hit series according to the results of a Structure-Activity Relationship (SAR) analysis (identification of a given chemical group or structural aspect responsible for the activity of the hit) and also to their physicochemical properties.[18,25]

- **Hit-to-lead phase**

Following the determination of the hit series, the hit-to-lead or lead generation phase relies on the manipulation of the compounds in order to increase its potency and selectivity but also to maintain or gain favorable pharmacokinetic (PK) and pharmacodynamic (PD) properties. In order to achieve such objective, after the design of new leads, different assays are conducted including *in vivo* (using animal models) and *in vitro* to study the toxicity, solubility, permeability, microsomal stability and inhibition of cytochrome P450 among other characteristics.[18] Broadly speaking, the hit-to-lead phase could be performed by three approaches – hit evolution, (bio)isosteric replacement and hit fragmentation – and a combination of them (Figure 1.11).

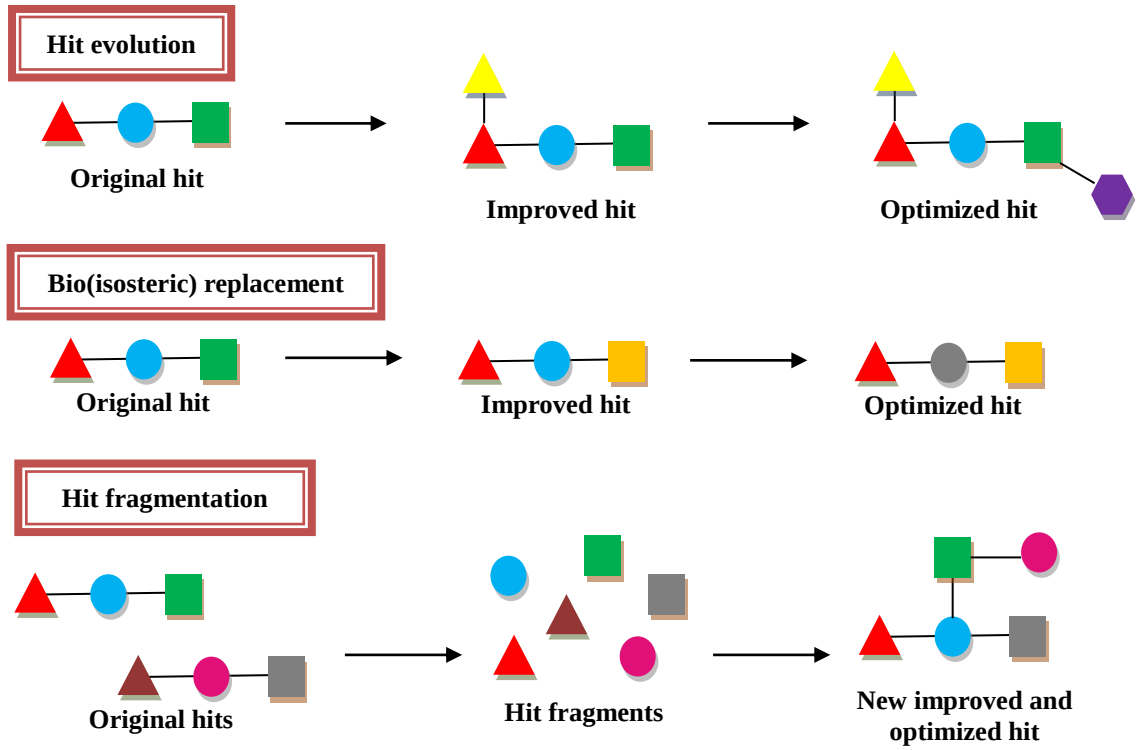

Figure 1.11 – Schematic representation of the three methods used in the hit-to-lead phase. Adapted from [32] In addition to the details mentioned, the fragment-based techniques include the fragment self-assembly in which the formation of the new lead is favored by the biological target itself.

In the first method, new chemical groups are added or removed from the hit, to maximize a given desired property and SAR analysis is an important tool in this process. The (bio)isosteric replacements can be considered as a particular situation of the hit evolution in which a given group is substituted by its bioisostere, a related group with similar biological effects. Finally, the hit fragmentation method is used when large hits are not suitable for further optimization operations and the generated fragments are analyzed for identification of new potential leads, for example, by joining fragments from two individual hits.[18,32]

- **Lead optimization**

Before entering the pre-clinical trials, the drug candidate is subjected to the lead optimization stage, in which the lead structure is ultimately refined to exhibit the desired properties, as efficiently as possible. For that, different assays – namely *in vivo* trials – are performed to confirm the genotoxicity and the PK/PD behavior of the putative drug candidates.[18]

Following all these steps, from the thousands or even millions compounds initially tested, only one or two are suitable to be classified as a drug candidate. Such low success rate could be explained by various causes including not finding an appropriate hit or lead, high *in vitro* or *in vivo* toxicity, an inappropriate PK/PD profile and the detection of putative adverse side effects. In addition to all those mentioned potential difficulties, more challenges emerge after the entrance into the clinical trials phase. Therefore, the pharmaceutical companies are trying to reduce the so-called rate of attrition in drug development in order to partially overcome the high financial costs involved in these projects being able to manufacture a growing number of new and safe drugs, accessible to the world population.[33,34]

1.1.2.2 – Drug-like molecules properties

Although the main objective of this section is not a complete description of all the properties that a compound should have, a briefly overview of such subject is useful to partially understand the difficulties associated to obtaining a suitable drug candidate and simultaneously the vital importance of the drug-like properties on the drug design process.[35]

As implicitly described over the text, the source of the compound is the first step to be decided and, unlike to what can be thought, natural products obtained from microorganisms, plants and animals are still important and an invaluable source of potential new molecules in the drug development process.[8,36,37]

One of the major properties that a drug-like molecule should have is to be bioavailable. Bioavailability could be defined as the fraction of the dose of a given molecule in the systemic

circulation reaching the desired target. Traditionally, such property is predicted by the four Lipinski's rules or "rule-of-five" (RO5) originally suggested in 1997 by Christopher A. Lipinski and co-wokers and republished in 2001.[38,39,40] According to this set of rules, a compound is more probable to have a satisfactory absorption and permeability if it has a molecular weight no greater than 500Da, a logP (logarithm of the octanol-water partition coefficient, which is a measure of lipophilicity) minor than 5, less than 5 hydrogen-bond donor groups and less than 10 hydrogen-bond acceptor groups.[4,38,39,40]

Using this practical approach, the design of no useful compounds could be significantly reduced. However, it should be highlighted that, despite the indications provided by Lipinski's rules, it is possible to have bioavailable compounds which do not follow all the criteria, explaining the continuing design of new and innovative drugs against different diseases.[41,42,43]

One of the Lipinski's rules – logP less than 5 – is related to the solubility of the compound. The partition coefficient is calculated as the ratio of un-ionized drug distributed between the immiscible phases at equilibrium and a high logP value corresponds to a high lipophilicity. Even though the Lipinski's rule points towards a low lipophilicity, an excessive hydrophilicity should be also avoided. A suitable drug candidate should be carefully designed with an appropriate number of non-polar and polar groups in order to have an acceptable solubility in both aqueous and hydrophobic media. A moderate lipophilicity is necessary to allow the transport of the drug through biological membranes while hydrophilicity is required to the transport of the drug to the respective target.[4]

Other important characteristic of a potential drug is its stability and different tests are carried out to confirm it. A drug should be stable enough to preserve its activity prior to be taken, due to microbiologic or chemical degradation (the so-called shelf-life stability). Moreover, a drug should also be stable after administration, in order to effectively get to the action site in adequate concentrations to produce its effects. However, once again, a fine equilibrium needs to be found regarding stability and reactivity: if a drug is too stable, it will not produce any effect raising, in addition, problems concerning its posterior metabolism and excretion.[4,44] On the other hand, if it is too reactive, the chances of reach the respective target are also significantly lower.

In order to improve stability some approaches are used including the use of prodrugs. These are inactive compounds related to the original molecule that are converted, *in vivo,* into the active drug by some triggering mechanism, namely an, enzymatic reactions. The use of prodrugs allows not only to improve stability but also other desired properties as low aqueous solubility or inappropriate PK/PD profile, as well as targeting.[4,45,46,47,48]

In addition to the addressed questions, several other properties should be taken into account during the development of a new drug. Stereochemistry is one of these properties: there is vital to design the enantiomer that possesses the desired pharmacological effect and not the one with no effect or with some other biological activities.[4,49,50]

1.1.2.3 – Pharmacokinetics and pharmacodynamics

To finalize the chapter dedicated to the drug design principles, some basic notions of pharmacokinetics and pharmacodynamics will be given.

An accurate characterization of both parameters is required to classify a given compound as a putative drug, being related to the interaction of the compound with the respective target. Hence, pharmacokinetics can be defined as the mechanisms occurring from drug administration until it reaches the respective target, while pharmacodynamics is the effect of the drug in the target and, consequently, in the organism (Figure 1.12).[4,51,52,53,54]

Due to the main goals of this thesis, a bigger focus will be given to pharmacokinetics. Nevertheless, it should be referred that pharmacodynamics play also an essential role in the process, allowing, for instance, to determine the potency of a given drug by understanding the mode of binding to the target.[4]

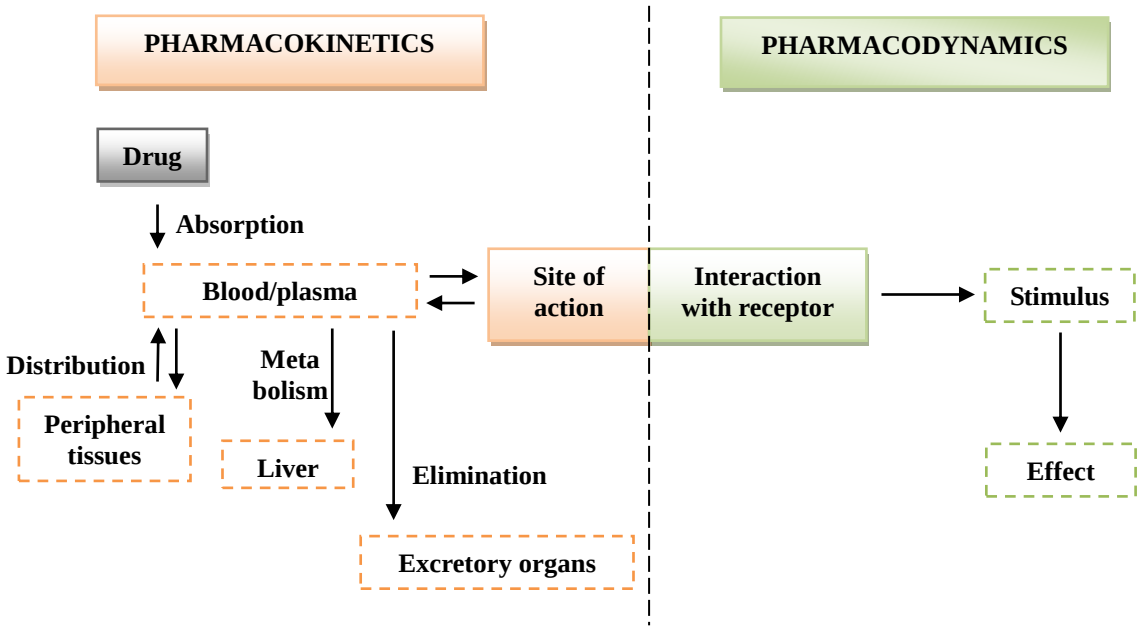

Figure 1.12 – Schematic representation of the concepts related to pharmacokinetics and pharmacodynamics. Adapted from [51] Quoting Benedetti and co-workers, pharmacokinetics answers to "what the body does to the drug" and pharmacodynamics answers to "what the drug does to the body system".

Pharmacokinetics is usually divided into four main steps: Absorption, Distribution, Metabolism and Excretion (ADME) as illustrated in Figure 1.13. Often, Toxicity is also included in these steps (ADMET) and *in silico* studies are a precious tool in this research area.[55,56] A brief description of each ADME step will be given in the next paragraphs.

The first phenomenon to take place is absorption, consisting on the passage of the drug, from the site of administration to the circulatory system and being related to the bioavailability term previously referred. Such definition implies that the concept of absorption is only used with

extravascular administered drugs (most commonly by oral administration), since the intravascular drugs are administered directly into blood.[4,51]

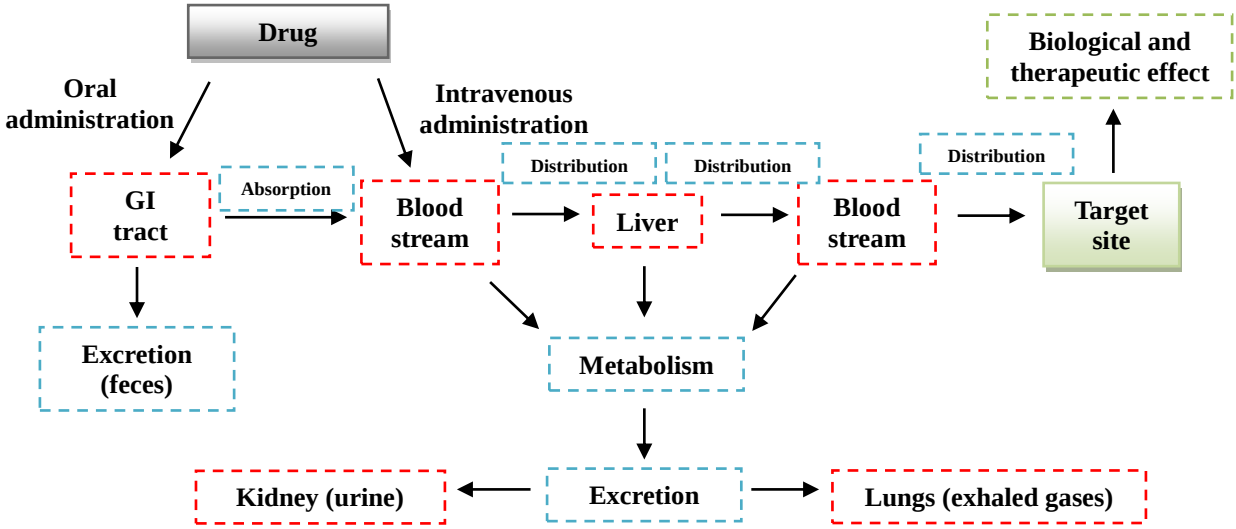

Figure 1.13 – Schematic representation of the steps of pharmacokinetics. Adapted from [4] After the drug oral administration, its absorption into the blood stream is required from the GI tract (namely stomach and intestines). Once the drug reaches the blood (or if it is administered directly into the circulatory system), it is distributed to the desired biological target. However, part of the drug is metabolized, mainly in the liver, for excretion, not reaching the target.

Several parameters influence the absorption of a drug, as the pH – usually, neutral compounds are easily absorbed through membranes, although one should take into account that the gastrointestinal (GI) tract has different values of pH, acid in stomach and basic in intestines. Other important parameter is to know how fast a given drug will be dissolved, which is related to the dosage form – solid, liquid, emulsion – and the respective optimization (for instance, a certain drug can be more effective as tablets than as ointment or *vice-versa*).[4,51]

The absorption of a drug is followed by its distribution, which is the transport of the drug from the administration site to the final site of action – its target – essentially by the blood. The different characteristics of the drug influence its distribution, such as lipophilicity (a very lipophilic compound could be trapped in the body fat which will lead to an unsuccessful action) and stability (a high level of decomposition implies a higher dosage, although it is often a good strategy when prodrugs are used).[4,51]

A very important point related to the distribution step is the binding of the drugs to plasma proteins. In fact, most of the drugs are able to bind to serum proteins such as albumin, transferrin, α-1 acid glycoprotein, lipoproteins and α-,β- and γ-globulin, depending on the characteristics of the drugs themselves (for example, usually acidic drugs have a greater affinity for albumin while basic drugs have a greater affinity for α-1 acid glycoprotein). Particular attention has been given to albumin as the most abundant protein in plasma, at approximately 600μM. However, the concentration of other serum proteins can increase in cases of disease, namely α-1 acid glycoprotein which is at 12-31 μM in normal conditions but can reach 60 μM in response to inflammation.[4,54,57,58]

The drug binding to plasma proteins has multiple consequences namely the fact that a bound drug has no pharmacological effect. Normally, this binding is reversible and an equilibrium between the protein-bound and the free form of the drug is established in plasma. This is important because the percentage of bound and unbound drug determines the concentration of the drug effectively available to interact with its target and produce the desired pharmacological effect. According to the Free Drug Theory (FDT), after reaching the steady state equilibrium, the free drug concentration should be the same in extracellular and intracellular spaces (plasma and tissues, respectively) and only the unbound drug in plasma should be taken into account in this calculation. This means that if a drug is highly bound to plasma proteins, the administered dose of the drug should be adjusted since the concentration of the free form might not be enough to elicit the desired effect and, at the same time, the drug cannot be easily metabolized and excreted. The binding constants of target-ligand complexes is an important parameter to take into account and different techniques as equilibrium dialysis, ultrafiltration and ultracentrifugation are commonly used.[4,57,58,59,60]

Nevertheless, binding to plasma proteins has some advantages, often explored by medicinal chemists. Plasma proteins are able to significantly extend the action of the respective bound drug by releasing it progressively over time and by minimizing its excretion as it would be the case for the free form. Finally, more hydrophobic molecules can be transported to the biological targets thanks to the binding to plasma proteins.[4,57,58,59]

There are other causes that influence the availability of a drug to, effectively, reach the target. Metabolism is one of such causes, being defined as the mechanisms responsible for the chemical conversion of a drug into other compounds (metabolites), normally more hydrophilic and, consequently, more likely to be excreted through urine or bile. A suitable drug must be designed in order to be metabolized properly: not too fast, to be in circulation in order to elicit a given action, but also not too slow to avoid accumulation and potential toxicity or other side effects.[4,51] Metabolism is a very variable process depending on age, gender, genetic variations, species and, even, environmental factors. Therefore, it is difficult to be properly characterized during the drug design process. On the other hand, it is also important to determine the nature of the formed metabolites that can be either inactive, with a similar function compared to the original drug, with a different function compared to the original drug or toxic. The role of metabolism is vital when prodrugs are used, since this process is responsible for producing the desired pharmacology active metabolite.[4,51]

The liver is the major site of metabolism although it may happen in other tissues as the brain, GI tract, lungs and kidneys. Usually, metabolism is divided into Phase I and Phase II. In Phase I, functional groups become exposed or are introduced, commonly through oxidation, reduction or hydrolysis, leading to a more water soluble metabolite. Phase II is characterized as a conjugation step in which a functional group or molecule is added to the previous metabolite (or alternatively to the original drug) – by, for example, sulfation, N-acetylation, glucuronidation and glutathione conjugation – increasing the hydrophilicity as well as the molecular weight and the negative charge of the

metabolite.[4,51,60,61] Several enzymes perform the two phases. Particular attention has been given to the cytochrome P450 family whose members are able to oxidize a significant percentage of drugs.[62,63] However, other enzymes are also involved in the process, namely aldehyde oxidase (AOX), which is a molybdenum containing protein responsible for the oxidation of several drugs and xenobiotics, many of those not metabolized by cytochrome P450.[64,65] This enzyme has been recognized by the pharma industry as an important player in drug design and the respective human tridimensional structure was recently solved by X-ray crystallography by our group.[66]

Finally, the last step of ADME is the excretion by which the unnecessary drug or its related metabolites are removed from the organism. There are different excretion mechanisms – as exhalation, saliva, tears, sweat, breast milk and bile – but all of them represent a minor source when compared to the kidneys glomerular filtration and active tubular secretion. Although the excretion mechanisms are no further analyzed herein, it should be highlighted that part of the excreted substances can be recovered by tubular reabsorption. As previously emphasized, drugs bound to plasma proteins are not eliminated by glomerular filtration increasing their life time in blood.[4,51,60]

Altogether, the steps of ADME must be rigorously characterized in order to achieve a suitable drug candidate. If any of these requirements is not fulfilled, it is likely to find future complications with the compound, namely at the level of drug-drug interactions.[67]

1.1.3 – Metal-based pharmacological compounds

The previous subchapters are mainly focused on different aspects that are taken into account by the industry, in order to produce an adequate drug for a given disease. However, the first research steps in this process are often executed by a great number of scientists working in several academic institutes. In fact, fundamental research provides valuable information to the pharmaceutical industry, in the drug design process. One example is metal-based drugs, designed by medicinal/biological inorganic chemistry.

As described previously, metals and related metal-complexes – for example, arsenic, gold and iron – have been used since ancient civilizations through empiric approaches regarding dose, toxicity or side effects. Over the time, the study of these compounds became more systematic and medicinal inorganic chemistry establishes itself as a scientific discipline in the 1970s and 1980s, although earlier reports proposing some metal complexes as drugs can be found (as example, in the beginning of the 20th century, Paul Ehrlich investigated an arsenical compound – commercially known as salvarsan – to treat syphilis).[68,69,70,71]

Hydrogen, oxygen, carbon and nitrogen represent 99% of the human body (62.8%, 25.4%, 9.4% and 1.4%, respectively). However, many other elements are required in order to keep the homeostasis – approximately 25 elements in total (Figure 1.14). Therefore, it is not a surprise to find

several metals playing an essential role in different biological processes. The role of iron in oxygen transport and calcium in cellular signaling are a few examples.

Nowadays, different metals are routinely used for different medical purposes namely as therapeutic or diagnostic agents (Figure 1.14 and Table 1.1).[72] Although a detailed characterization of each metal and respective therapeutic action is not the purpose of this section, some examples will be given in the next paragraphs.

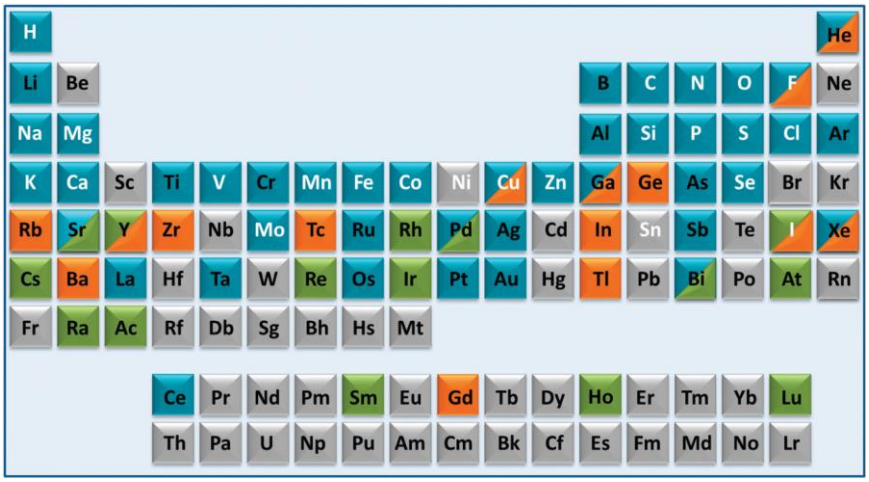

Figure 1.14 – Schematic representation of the "Medical Periodic Table".[70] The essential elements for humans are indicated in white letters and metals are significantly represented. In addition, some others elements are medically used, indicated with the following color code: green – elements used as medical radioisotopes; blue – elements used in therapy; orange – elements used in diagnosis

Particular attention has been given to the use of transition metals in this field. Nevertheless, elements as gallium and tin have been, also, implicated as putative anticancer and antimicrobial agents. Other related metals are currently in the market as arsenic, antimony and bismuth, used to treat cancer, leishmaniasis and stomach ulcers, respectively.[73]

Considering transition metals, there are several studies showing their relevance in different pathologies namely cancer. Platinum, palladium, ruthenium and gold are good examples of metals used for such purpose.[74,75,76,77]

Platinum is a landmark in medicinal inorganic chemistry being the first metal to be associated with anticancer activity in 1969 by Barnet Rosenberg and collaborators. Ten years later, cisplatin – cis-diamminodichloridoplatinum(II) – has been approved for the treatment of different cancers namely ovarian, testicular, lung and bladder; based on cisplatin, other related platinum(II) compounds were developed as carboplatin and oxaliplatin. The anticancer activity of cisplatin is based on its binding to the DNA preventing the DNA replication and the consequent multiplication of cancer cells (Figure 1.15). However, cisplatin presents some disadvantages regarding toxicity (only a minor percentage of the drug reaches the DNA and the free drug can interact with different proteins and inactivate metabolic processes) and resistance (DNA repair mechanisms can still be activated, counteracting the effect of the drug). This has lead to the development of, not only, new platinum compounds, but also to the design of complexes with other metals.[69,75,78]

Table 1.1 – List of some metals and the respective medical applications.Adapted from [69] The metals are ordered according to their position in the Periodic Table. MRI – Magnetic Resonance Imaging; PET – Positron Emission Tomography; SPECT – Single Photon Emission Computed Tomography

Metal name	Metal symbol	Medical application
Lithium	Li	Treatment of bipolar disorders
Magnesium	Mg	Laxative; Antacid; Dietary supplement
Aluminum	Al	Adjuvant; Antacid; Treatment of hyperphosphatemia; Peptic ulcer disease
Calcium	Ca	Antacid
Chromium	Cr	Dietary (trace mineral) supplement
Manganese	Mn	MRI contrast agent
Iron	Fe	MRI contrast agent; Dietary supplement
Cobalt	Co	Treatment and diagnosis of pernicious anemia; Dietary supplement
Nickel	Ni	Dietary (trace mineral) supplement
Copper	Cu	Treatment for Menke's disease; ^{64}Cu-PET radio-imaging
Zinc	Zn	Treatment of eczema; Dietary supplement
Gallium	Ga	^{67}Ga-SPECT radio-imaging; $^{66/68}$Ga-PET radio-imaging
Arsenic	As	Treatment of leukemia
Rubidium	Rb	^{82}Rb-PET radio-imaging
Strontium	Sr	Osteoporosis
Yttrium	Y	^{90}Y-therapeutic radionuclide; ^{86}Y-PET radio-imaging
Zirconium	Zr	^{89}Zr-PET radio-imaging
Molybdenum	Mo	Treatment for Wilson's disease (copper chelator); Dietary (trace mineral) supplement
Technetium	Tc	^{99m}Tc-SPECT radio-imaging
Silver	Ag	Antimicrobial
Indium	In	^{111}In-SPECT radio-imaging
Antimony	Sb	Anti-leishmanial
Barium	Ba	Radiographic contrast medium
Lanthanum	La	Treatment of hyperphosphatemia
Cerium	Ce	Treatment of burns
Samarium	Sm	^{153}Sm-therapeutic radionuclide
Gadolinium	Gd	MRI contrast agent
Rhenium	Re	^{188}Re-therapeutic radionuclide
Gold	Au	Antiarthritic
Bismuth	Bi	Antibacterial; Treatment of gastrointestinal and skin disorders

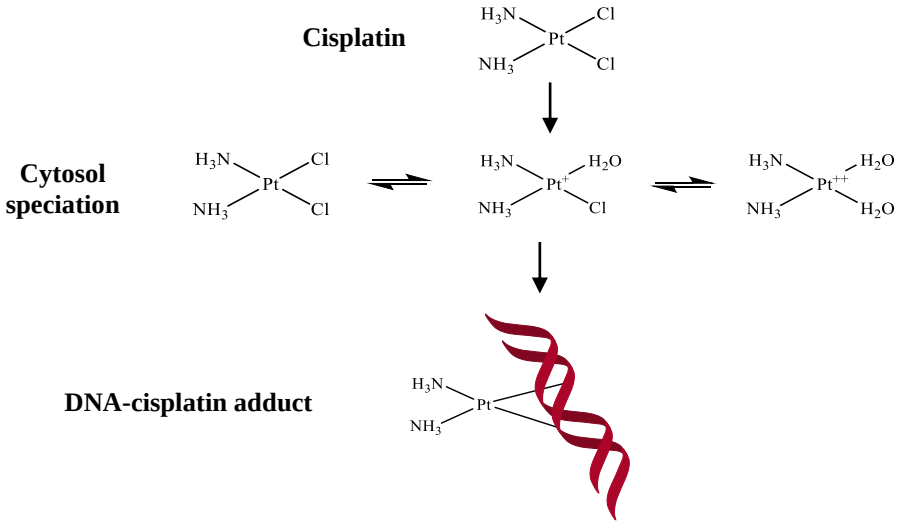

Figure 1.15 – Schematic representation of the mode of action of cisplatin. Adapted from [78] Cisplatin remains intact in plasma but, due to the low chloride concentration in the cells, the chloride ligands are replaced by water molecules. The formed species, positively charged, can then interact with DNA in the nucleus. The scheme was prepared in ChemDraw.

Independently of the used metal, adequate ADME parameters should be followed. Again, the binding to proteins is very important for the distribution of the metal-based drug. In particular, transferrins are able to transport several metals in addition to iron, their natural metal ligand, acting as possible carriers of this type of drugs.[78]

In the next two sections, a detailed characterization of different families of metal-based complexes, used in this Thesis, will be presented.

1.2 – Carbon monoxide – Biological and therapeutic applications

1.2.1 – General concepts and toxicity

Carbon monoxide (CO) is mainly recognized as a colorless, odorless, tasteless and highly toxic gas. CO was firstly produced in 1776 by Joseph de Lassone (after heating a mixture of zinc oxide and coal) but its chemical composition was determined only in 1801 by F. Clement and J. B. Desormes. Currently, CO is industrially used in hydrogen production and as a reducing agent for the production of metals among other applications.[79,80]

Table 1.2 summarizes some of the physical properties of CO. Chemically, CO is an unsaturated molecule with a triple bond between carbon and oxygen (bond length of 112.82 pm) and a bond dissociation energy of 1070 kJ/mol contributing for its stability in the normal temperature and pressure conditions.[79,80]

Carbon monoxide is formed by the incomplete combustion of organic molecules rich in carbon, being possible to identify two major sources: natural (degradation of organic matter, volcanic activity, forest fires) or anthropogenic (mainly by the consumption of fossil fuels). Therefore, human activities which are used since Industrial Revolution have an impact in the atmospheric CO levels and high concentrations can be found next to the most industrialized and urban zones.[79,81,82,83]

Table 1.2 – Physical properties of carbon monoxide. Adapted from [79,80]

Molecular mass	28.01 g mol^{-1}
Density **(at 273.15K and 101.3 kPa)**	1.25 kg m^{-3}
Molar heat capacity **(at 273.15K and 101.3 kPa)**	C_p=29.05 J mol^{-1} K^{-1} C_v=20.68 J mol^{-1} K^{-1}
Thermal conductivity **(at 273.15K and 101.3 kPa)**	0.02324 W m^{-1} K^{-1}
Boiling point (at 101.3 kPa)	81.65 K
Melting point (at 101.3 kPa)	74.15 K
Critical temperature	132.29 K
Critical pressure	3496 kg m^{-3}
Autoignition temperature	ca. 880 K
Solubility in water (at 273 K)	35.37 ml L^{-1}
Solubility in water (at 293 K)	23.19 ml L^{-1}
Solubility in water (at 323 K)	16.15 ml L^{-1}
Solubility in methanol (at 293 K)	18.30 ml L^{-1}
Solubility in ethanol (at 293 K)	19.01 ml L^{-1}
Solubility in acetone (at 293 K)	25.38 ml L^{-1}

Interestingly, CO is also found in comets and asteroids, which were an important source of the gas in early Earth's atmosphere. This highly reducing atmosphere has been implicated in the early origin of life, contributing to the formation of important biological molecules such as amino acids and nitrogen bases.[84,85,86]

Nevertheless, as referred in the beginning of this chapter, CO is largely known by its toxicity. In fact, "silent killer" is a common nickname attributed to CO, highlighting its non-irritating properties and, along history, several accidental or suicidal deaths were caused by the inhalation of such gas. Periodically, news about CO poisoning appear in different media – newspapers, radio, television and online sources – which are usually associated with places with poor ventilation or with the use of heating systems. Different studies point to this reality with more than 15000 cases related to CO poisoning observed between 2001 and 2003, only in the United States of America.[85,87,88,89]

The described toxicity is due to the CO ability to reversibly bind to hemoglobin with the concomitant formation of carboxyhemoglobin (COHb), reducing the efficacy of the oxygen transport. Historically, this ability was firstly suggested by Claude Bernard in 1857 and it arises from the much higher affinity of CO (about 230 times higher) for the heme ferrous iron atom than oxygen. Therefore, the generated hypoxia is the cause of the symptoms associated to CO, varying from a simple headache

to death: Figure 1.16 shows the correlation between the levels of CO and COHb and the respective effects in the human health. CO is also able to inhibit some other enzymes (example of cytochrome-c oxidase) but the effects are not so significant when compared to those resulting from its binding to hemoglobin.[81,83,86,90,91]

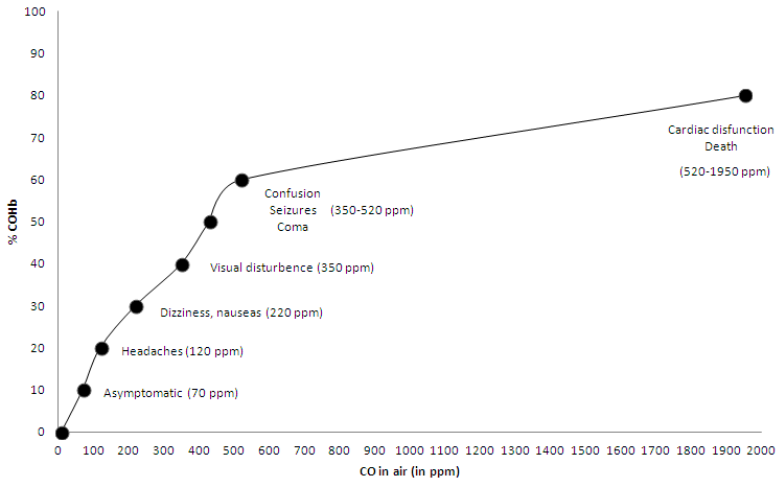

Figure 1.16 – Graphical correlation of the harmful effects of CO with its concentration and percentage of COHb in human health.[91] Values up to 10-20% COHb are tolerated and no toxic symptoms are observed. The progressive increase of such percentage leads to more serious consequences and levels of 50-60% COHb are already very dangerous. Levels above 80% COHb are normally fatal.

1.2.2 – Endogenous production of carbon monoxide

Although the potential toxicity presented by CO described in the previous section, important advances led to a progressive change on how this molecule is seen by the scientific community namely its production by a wide range of organisms from bacteria to eukaryotes, including the humans.

The discovery of the endogenous production of CO took place at less than 70 years ago. In the early 1950s, Torgny Sjöstrand – a Swedish physician – was involved in some experiments proving, not only the endogenous presence of CO in humans, but also that it derives from heme degradation. The continuous research in this area allowed the identification of the enzyme responsible for heme catabolism – named heme oxygenase (HO) – by R. Tenhunen and co-workers in 1968. In fact, heme oxygenase is responsible for about 86% of the CO endogenously generated (the remaining production results from other reactions such as lipids peroxidation and the photo-oxidation of organic compounds).[83,85,91,92]

The heme degradation by heme oxygenase results in three distinct products: CO, ferrous iron (Fe^{2+}) and biliverdin-IX, which is converted into bilirubin-IX by the enzyme biliverdin reductase (Figure 1.17). All of the mentioned products have biological actions as described in the next sections.[83,85,93,94,95]

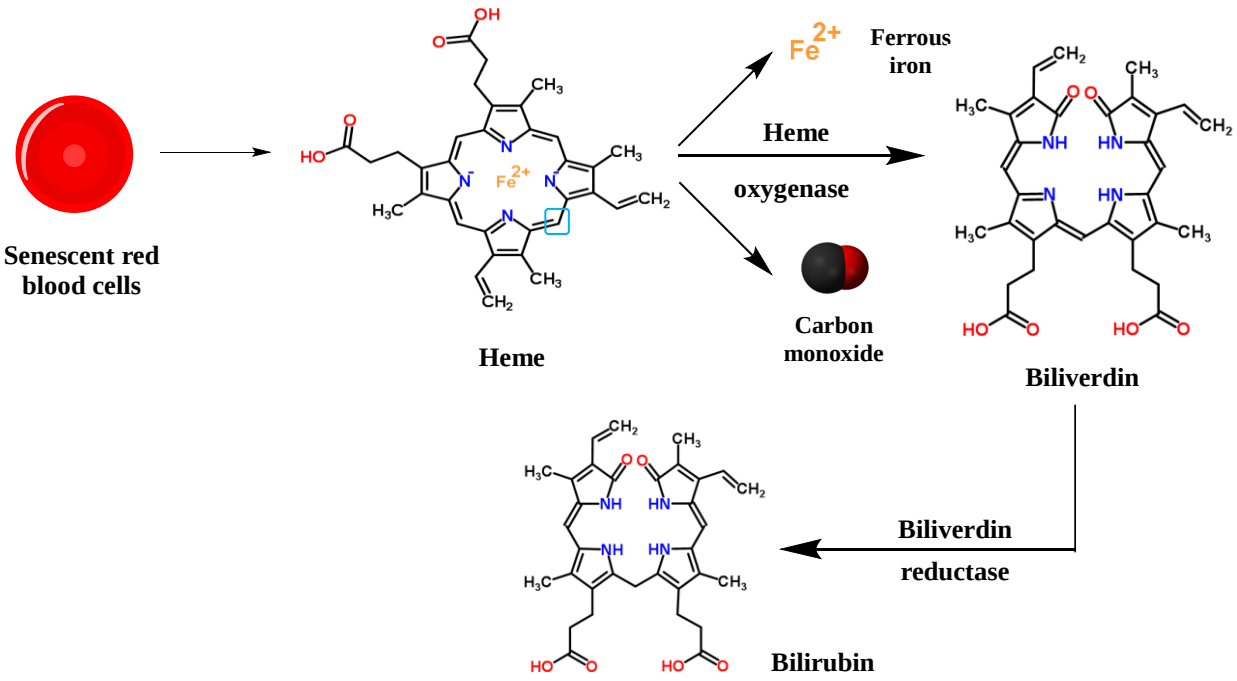

Figure 1.17 – Schematic representation of the products generated from the heme degradation by heme oxygenase.Adapted from [93] The degradation of heme requires the presence of NADPH and oxygen. In addition, this is a regiospecific reaction and only the α-CH (blue circled in the figure) of the heme is oxidized, forming the intermediate α-mesohydroxyheme (not shown in the figure) which is then be converted to biliverdin through the release of a CO molecule and the iron Fe^{2+}. The structures shown were obtained in the free chemical structure database *ChemSpider*.

Heme oxygenase has two isoforms in humans: heme oxygenase-1 (HO-1) and heme oxygenase-2 (HO-2). A third isoform was also identified in rats (in brain, liver and kidneys) in the later 1990s but its function is not yet clear. HO-1 and HO-2 share an elevated residue sequence homology (43%) and the principal difference is that HO-1 is inducible while HO-2 is constitutive.[83,85,94,96]

HO-1, also designed by HSP32, was the first isoform to be identified and it has a molecular mass of 32 kDa. Mainly located at the endoplasmic reticulum, it is an inducible enzyme, meaning that its expression largely increases in response to a great range of chemical and physical stresses, including ultraviolet radiation, hydrogen peroxide and sodium arsenite (Table 1.3). Therefore, it has been postulated that HO-1 is involved in cellular defense mechanisms contributing for the cell homeostasis. The described activation occurs in the majority of the tissues while the basal expression of HO-1 is mainly restricted to spleen and other tissues responsible for the degradation of senescent red blood cells.[81,83,85,96,97]

HO-2, lately found in 1980s, is a constitutive protein meaning that its expression does not depend on the existence of stimuli. It is also mainly located at endoplasmic reticulum in organs like brain, liver and kidneys. The protein has a molecular weight of 36 kDa exhibiting two functional domains (heme regulatory domains) in addition to the catalytic domain also found in HO-1 suggesting its participation in other heme-related processes involved in cellular protection.[81,83,85,96,97]

Table 1.3 – List of some agents responsible for the activation of HO-1.Adapted from [81,97]
IL – Interleukin; TNF – Tumor Necrosis Factor; TGF – Transforming Growth Factor; PDGF – Platelet-derived Growth Factor; VEGF – Vascular Endothelial Growth Factor.

Type of inducer	Examples
Oxidants	Hydrogen peroxide
Tiol-reactive substances	Sodium arsenite, Iodoacetamide, Cadmium chloride
Heavy metals	Tin, Lead
Nitric oxide and derivatives	Nitric oxide, Angeli's salt (α-oxyhyponitrite)
Cytokines	IL-1 α/β, IL-6, IL-10, IL-11, TNF-α
Growth factors	TGF-α, TGF-β, PDGF, VEGF
Others	Endotoxins, Ultraviolet radiation

Both HO-1 and HO-2 were structurally characterized by X-ray crystallography and several structures are available in the Protein Data Bank (PDB) from different organisms (mainly *Homo sapiens* and *Rattus norvegicus*), with different ligands and with different mutations. Historically, the first human HO-1 structures were released approximately 15 years ago at 2.1Å resolution (apo-form) and 2.6Å resolution (heme-bound) while the first human HO-2 structures were released in 2007 at 2.4Å resolution (apo-form) and 2.6Å resolution (heme-bound).[98,99,100]

As expected, the two isoforms have an identical overall tridimensional structure, mainly constituted by α-helices, which is maintain in the apo-forms. The structures also provide valuable information allowing, among other features, the characterization of the heme binding pocket and the rearrangements of some residues to accommodate the heme moiety (Figure 1.18).[98,99,100]

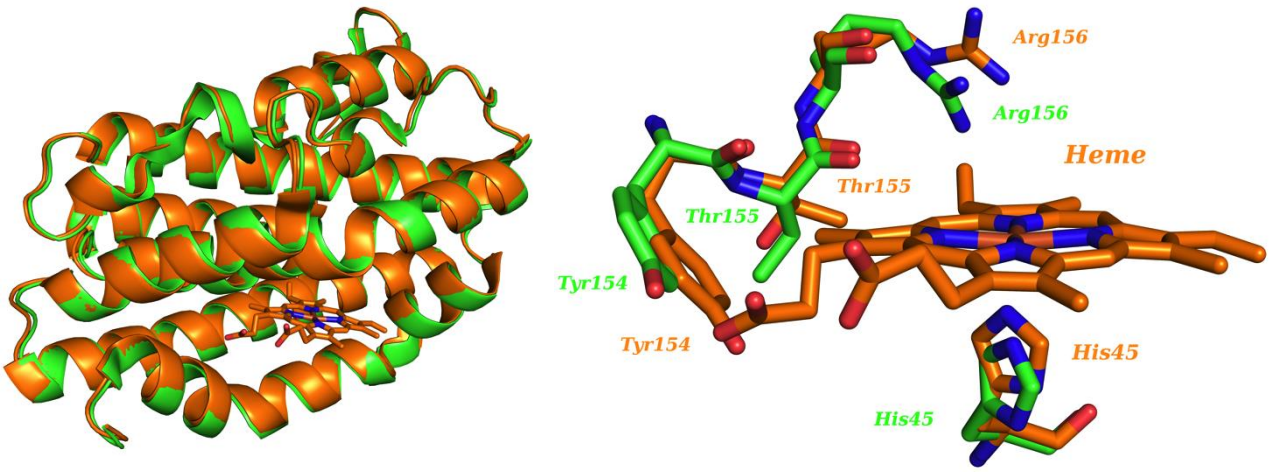

Figure 1.18 – Structural representation of the human HO-2 in the apo-form (PDB: 2Q32, green) and heme-bound form (PDB: 2QPP, orange). In the left, the overall structure of the protein is shown, confirming an identical organization in the presence and in the absence of the heme. In the right, a detailed view of the heme binding pocket; some rearrangements of residues are visible in order to accommodate the heme, particularly histidine 45 which is positioned to coordinate the heme iron atom and tyrosine 154 is forming an hydrogen bond (not shown) with the heme propionate group. The figure was prepared in Pymol.

1.2.3 – Biological effects of carbon monoxide

With an increasing knowledge of HO activity and reaction mechanism, the enzyme has been proposed to be involved in different pathologies and diseases. Therefore, not surprisingly, HO has gained a pharmacological interest namely due to its ability to efficiently control the heme and iron intracellular concentrations. Such concentrations, conversely, are important to control different cellular mechanisms. However, closely related to the potential benefits of heme oxygenase, its respective products – CO, iron and biliverdin/bilirubin – have been also investigated from a new perspective.[96,101]

In fact, the three products were usually seen merely as harmful molecules but, beyond its toxicity, beneficial effects are now also recognized. The CO effects will be more deeply addressed but some brief words about the other products will be given here.

Biliverdin is rapidly converted into bilirubin, which, in high concentrations, is responsible for jaundice, and neurotoxicity in babies. Nevertheless, bilirubin is also able to act as an antioxidant due to its ability to scavenge reactive oxygen species (ROS) helping to control the cellular oxidative stress.[92,96,101]

On the other hand, in spite of its essential role in life, free iron is also known to form reactive oxygen species which largely interfere with the cell survival. However, the release of iron by HO is accompanied by an increasing expression of ferritin, a protein responsible for the maintenance of the correct levels of intracellular iron, contributing for the cell protection.[92,96,101]

Concerning CO, in adequate concentrations, it is recognized as a molecule with anti-inflammatory, anti-apoptotic and anti-proliferative properties being an excellent example of the Paracelsus' maxim previously mentioned: "The dose makes the poison" (Table 1.4).[101,102,103]

Table 1.4 – Correlation between the CO concentration and the respective effect. Adapted from [103]

CO concentration	Effect
10000 ppm (1%)	Fatal in minutes
10-500 ppm (0.001 a 0.05%)	Preclinical efficacy
10 ppm (0.001%)	No effect (atmospheric air)

In fact, CO is nowadays recognized as a member of an important family of gasotransmitters, together with nitric oxide (NO) and hydrogen sulfide (H_2S). These three gases have some physical similarities in addition to the fact that all of them were initially identified as pollutant gases and later on identified as endogenously produced by several organisms and associated with some different cell processes. As illustrated in Figure 1.19, these three signaling molecules, although produced by different enzymes, participate in identical processes, being progressively studied as putative therapeutic agents.[104,105,106,107]

Very briefly, all of them have been implicated as vasodilators in addition to their cytoprotective and anti-inflammatory effect. As example, NO has been proposed to be used in the treatment of pulmonary conditions in children and adults and the enzyme responsible for its synthesis – nitric oxide synthase – has been indicated as an intervenient in some cellular processes. H_2S is involved in several processes in different systems including the cardiovascular and nervous systems.[108,109,110]

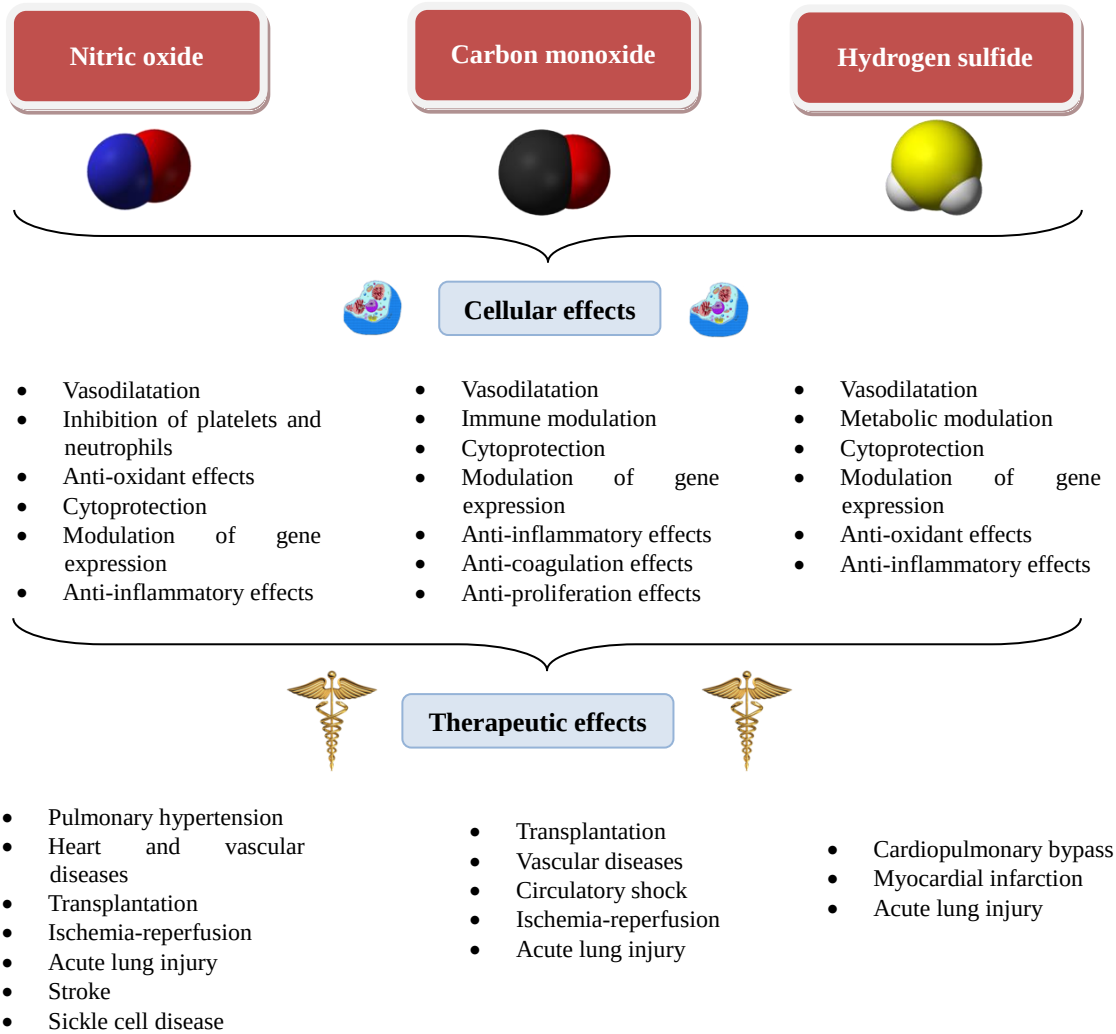

Figure 1.19 – Representation of the mechanisms in which the gasotransmitters are involved: nitric oxide (left), carbon monoxide (middle) and hydrogen sulfide (right). Adapted from [104] Modulating different processes implicated in different pathologic conditions, these three molecules are now considered agents with pharmacological interest. Importantly, the mode of administration needs to be properly defined in order to avoid their potential toxicity as hereafter discussed for CO.

1.2.3.1 – Carbon monoxide as a signaling molecule

Multiple investigations were conducted intending to better characterize the cellular mechanisms in which CO is involved, producing the observed beneficial effects. As depicted in Figure

1.20, CO has been proposed to modulate different mechanisms. It should be noted that, in addition to those pathways, heme-containing proteins are also targets for CO, as previously discussed. Cytochromes are included in this group and, in fact, low CO concentrations are able to positively modulate mitochondrial cytochrome-c oxidase and the generation of ROS, which, act as signaling agents, protect against cell damages. Similarly, nitric oxide synthase (NOS) is also a putative target for CO.[85,104,111]

Three pathways in which CO is involved are relatively well characterized and were selected for a more deep description: soluble guanylyl cyclase, ion channels and MAPK pathway.

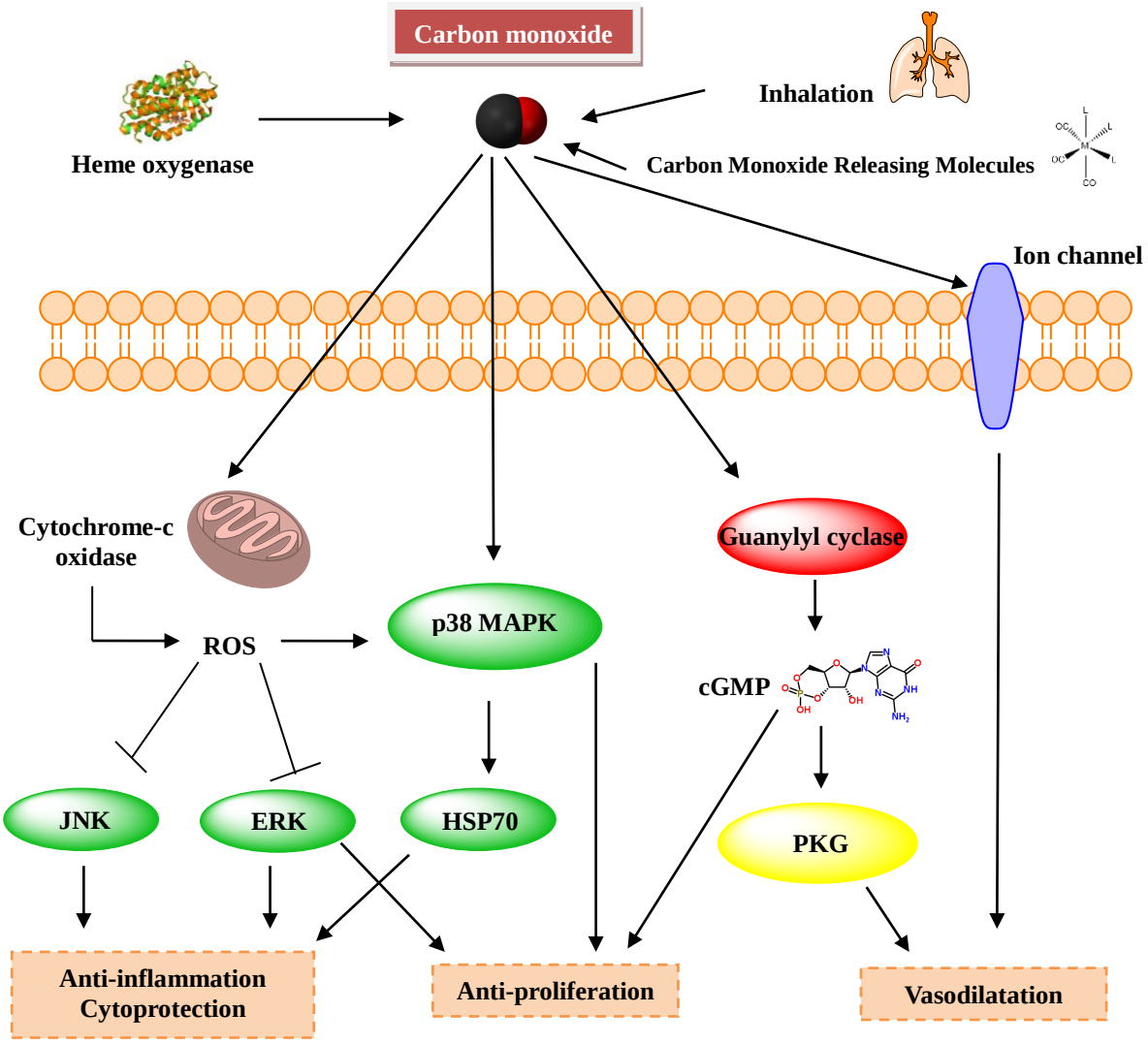

Figure 1.20 – Schematic representation of the cellular mechanisms in which CO is involved. Adapted from [104] Depending on the type of cells and environmental conditions, different pathways are activated. As observed, different pathways contribute for the same final protective action. Abbreviations are indicated in the text.

- **Soluble guanylyl cyclase**

Soluble guanylyl cyclase (sGC) is an enzyme responsible for the conversion of guanosine triphosphate (GTP) into cyclic guanosine monophosphate (cGMP) as shown in Figure 1.21. cGMP, known as a second messenger, is involved in different mechanisms including the regulation of protein kinases, ion channels and phosphodiesterases.[85,94,104]

sGC was firstly identified as a NO sensor and, in fact, the presence of NO increases the enzyme activity more than 100-fold explaining the effects of vasodilatation observed due to this mediator. The enzyme has two subunits (α1 and β1) with different domains including a heme-containing domain, responsible for NO binding (named H-NOX) and spectroscopic and structural studies revealed some insights on this binding.[85,94,112,113]

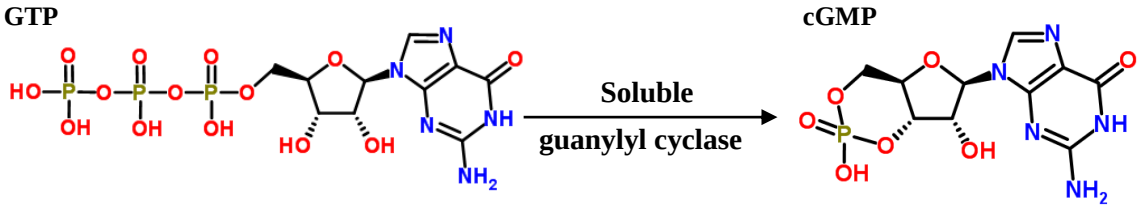

Figure 1.21 – Schematic representation of the reaction catalyzed by soluble guanylyl cyclase. The structural representations of GTP and cGMP were obtained in the free chemical structure database *ChemSpider*.

However, it was found that CO is able to enhance also the production of cGMP by sGC although with a reduced effectiveness (2- to 10-fold increase) when compared to the NO action and spectroscopic and structural studies are also available.[85,94,112,114]

Interestingly, some molecules were identified as activators of the effects of NO and CO on sGC, namely, 3-(5'-hydroxymethyl-3'-furyl)-1-benzylindazole and 5-cyclopropyl-2-[1-(2-fluorobenzyl)-1H-pyrazolo[3,4-b]pyridin-3-yl]pyrimidin-4-ylamine (YC-1 and BAY41-2272, respectively).

The high levels of cGMP – produced in response to the action of CO (or NO) – stimulate the production of cGMP-dependent protein kinase or protein kinase G (PKG) capable of decreasing the intracellular calcium levels by interacting with different ion channels as explained in the next section (Figure 1.22). Ultimately, the variation of the Ca^{2+} concentration is responsible for the vasodilatation of vascular smooth muscle cells properties, attributed to CO.[81,94,115,116]

- **Ion channels**

As mentioned, CO is able to promote vasodilatation due to the action of PKG on some ion channels. PKG directly inhibits voltage-gated calcium channels (Ca_V) preventing the influx of Ca^{2+} (Figure 1.22).[116]

In addition, PKG can also activate some potassium channels namely calcium-activated potassium channels (K_{Ca}). Large-conductance Ca^{2+}-and voltage-gated K^+ channels – usually referred to

as BK ("big potassium"), maxi K or Slo1 – activation implies a membrane hyperpolarization, which also inhibits the calcium channels. PKG phosphorylates some serine residues of BK channels leading to its activation; as example, Ser855, Ser869 and Ser1072 have been implied in this mechanism.[85,94,117,118]

On the other hand, carbon monoxide was also identified as capable of directly activate potassium channels but the mechanisms by which the activation is achieved are not fully explained.[94]

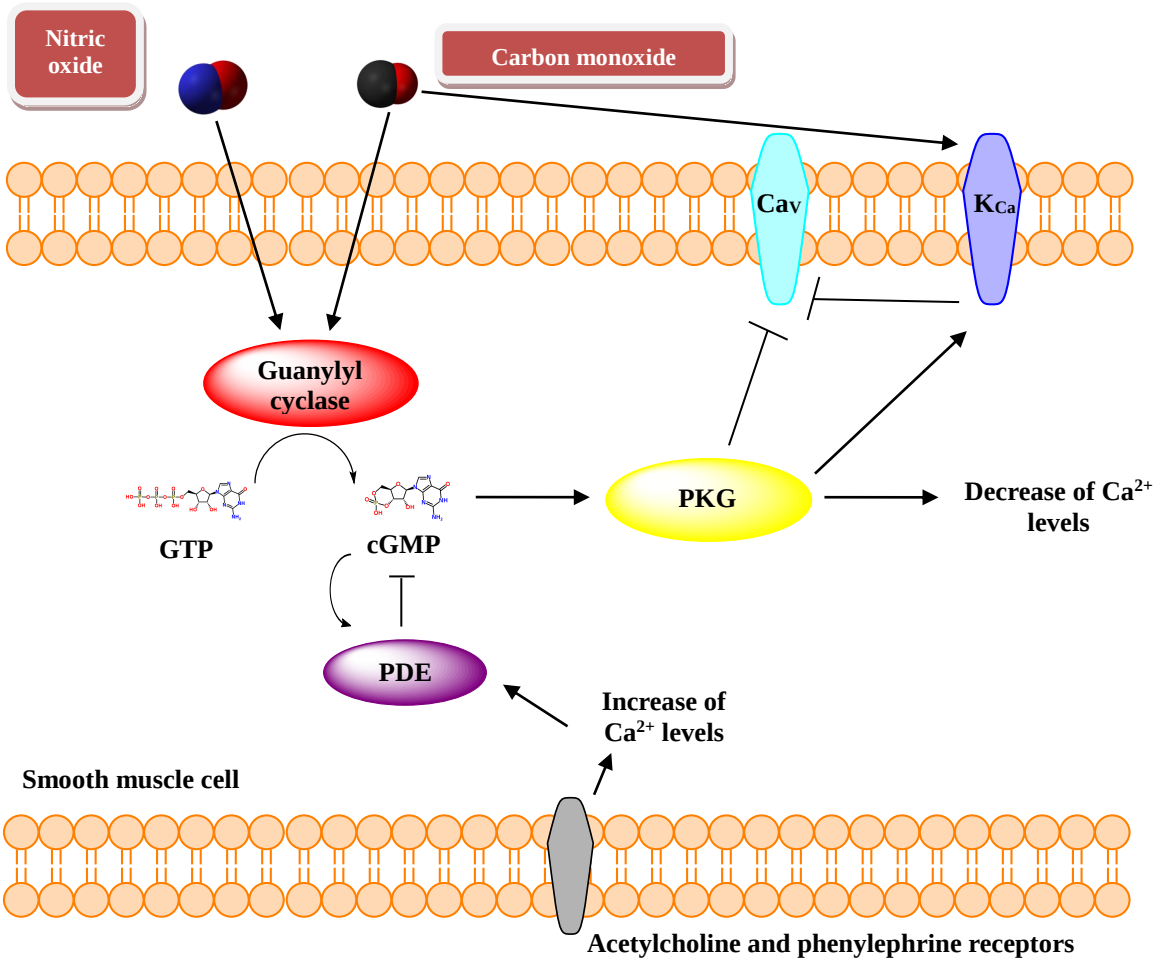

Figure 1.22 – Schematic representation of the effects of CO and NO on soluble guanylyl cyclase, ion channels and associated pathways.Adapted from [116] In addition to the described mechanisms leading to the decrease of calcium levels, cells are also prepared to increase these levels if necessary due to the action of agents such as acetylcholine and phenylephrine. The increase of calcium leads to cGMP degradation by phosphodiesterases (PDE).

- **MAPK pathway**

Mitogen-activated protein kinase pathway (MAPK) is an eukaryotic evolutionarily conserved pathway involved in several signal transduction processes participating in important cellular events such as cell proliferation, cell differentiation and apoptosis.[81,119,120,121,122]

This pathway is characterized by the presence of three kinases that sequentially phosphorylate and activate the respective downstream target kinase: MAPK proteins are phosphorylate by MAPK

kinases (MKK) which are phosphorylate by MKK kinases (MAPPKKK). The initial phosphorylation occurs in response to different chemical and physical agents including cytokines, growth factors and neurotransmitters. This is a highly regulated pathway and it is largely studied in some pathological situations such as cancer.[81,122,123,124]

In mammals, three MAPK pathways are particularly important: the extracellular signal regulated kinases (ERK), the c-Jun NH2-terminal kinases (JNK) and the p38 MAPK (p38). Although not fully elucidated, it is known that CO is able to modulate different MAPK pathways (namely p38) being responsible for some of the verified beneficial effects; anti-inflammatory, anti-apoptotic and anti-proliferative effects are particularly remarkable as next described.[81,83]

Firstly, inflammation is a defense process developed by the cells in response to several damaging agents belonging to the innate immune system.[125,126] Nevertheless, a chronic inflammation is also associated to some diseases such as atherosclerosis and cancer explaining the need of finding effective therapeutic agents to control it.[127,128]

CO participates in inflammatory processes by either inhibit the expression of pro-inflammatory cytokines or by enhance the production of anti-inflammatory cytokines (namely interleukin-10, IL-10). Thus, CO is able to modulate the p38 pathway increasing the production of the transcription factor Heat Shock Factor 1 (HSF1) which, consequently, activates the expression of Heat Shock Protein 70 (HSP70). The high levels of these proteins decrease the production of several pro-inflammatory cytokines such as Tumor Necrosis Factor (TNFα), interleukin-1β (IL-1β) and Macrophage Inflammatory Protein-1α (MIP-1α). All together, the described signaling mechanisms help to effectively control the pathologies originated by inflammatory processes.[81,83,129,130]

Secondly, apoptosis or programmed cell death is also a natural phenomenon being an alternative to necrosis. Apoptosis is involved in several crucial biological processes such as cell turnover and embryonic development acting also as a protective mechanism against damaged cells resulting, for example, from DNA replication errors. Nonetheless, a decontrolled apoptosis is prejudicial being involved in different pathologies such as autoimmune diseases and cancer.[131]

Considering the mentioned roles, it can be easily concluded that elucidation of the mechanisms involved in apoptosis and respective modulation are essential to fight such diseases. In addition, apoptosis could be also one of the causes responsible for organ transplantation failures; generally transplantation causes ischemia/reperfusion (I/R) injuries capable of triggering apoptosis (namely from the endothelial cells of the blood vessels).[81,83,131]

CO is also capable of modulating the apoptosis mechanisms contributing for organ transplantation success. In fact, different experiments were conducted showing the feasibility of this approach namely in procedures involving the transplantation of organs such as heart, lung, liver, intestine and kidney in rats or mice (Table 1.5). CO was also used in xenotransplantation with positive results.[132,133,134,135,136,137,138]

Table 1.5 – List of organ successfully transplanted organs (in rats) and the respective CO concentration used in the procedure (in parenthesis, the administration method is indicated). Adapted from [132]

Transplanted organ	CO concentration
Heart	20-400 ppm (Gas administration)
Lung	250-500 ppm (Gas administration)
Liver	100-300 ppm (Gas administration)
Intestine	250 ppm (Gas administration)
Kidney	20-250 ppm (Gas administration)

Studies point to the activation of p38 MAPK by CO in vascular endothelial cells decreasing the expression of different apoptotic agents such as TNFα, Fas and caspase 3.[132,139,140] In parallel, apoptosis of vascular smooth muscle cells is also reduced by the action of sGC activated by CO due to the inhibition of other apoptotic agent (protein p53) proving that these mechanisms are tightly regulated by different pathways.[141]

Finally, decontrolled cell proliferation is associated to some diseases from vascular stenosis to, in more severe cases, different types of cancer. Different experiments were conducted showing that excessive proliferation is reduced by CO application as shown in a case of neointimal proliferation associated with inflammatory lesions *in vivo* (Figure 1.23).[142] CO decreases the proliferation of different cells such as vascular smooth muscle cells and T cells modulating different cell cycle-related factors.[81,83,143,144,145]

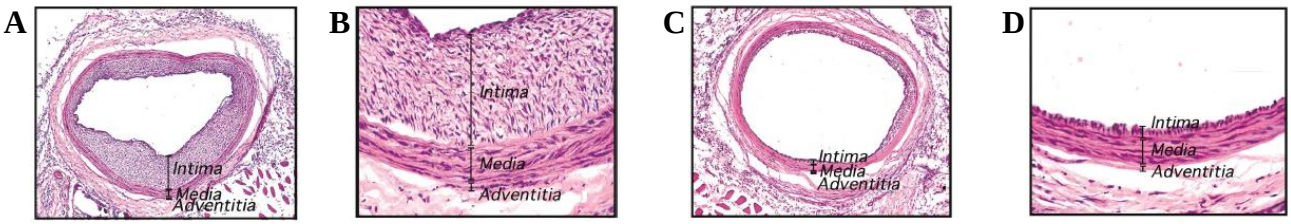

Figure 1.23 – Carbon monoxide effects on cell proliferation verified after a vascular balloon angioplasty.[142] On the left – A (10-times magnification) and B (50-times magnification) – rat carotid arteries (14 days post-balloon angioplasty) without any CO treatment (air exposed) are shown being possible to observe a massive cell proliferation next to the tunica intima. On the right – C (10-times magnification) and D (50-times magnification) – similar samples are presented but the rats were exposed to CO (250 ppm, 1 hour) before the balloon angioplasty; a clear reduction of the excessive cell proliferation is visible confirming the anti-proliferative properties of carbon monoxide.

1.2.4 – Therapeutic application of carbon monoxide

Keeping in mind the previously described mechanisms in which CO acts as a modulator, different studies were published focusing on beneficial effects of CO in different organs and model diseases.[81,146]

Therefore, not surprisingly, the use of CO as a putative therapeutic agent has been suggested, leading to a simultaneously simple and complex question: how to deliver CO in an effective and safe way?

A first possibility is to stimulate the activity of heme-oxygenase-1 to increase the levels of CO both by genetic or non-genetic methodologies. In the first approach, HO gene transfer is performed choosing an appropriate vector such as adenovirus. In the second approach, different agents (e.g hemin) are used to induce the production of HO-1. Both methods should carefully follow safety criteria: vectors should not be pathogenic and the selected inducers should be properly characterized in order to show their lack of toxicity.[83,147,148]

A second possibility consists in the application of exogenous CO. Following this approach, it is necessary to define the method by which carbon monoxide is delivered. CO inhalation is an almost intuitive method for such purpose keeping in mind the gaseous state of the molecule. In fact, tests with cells and model animals were performed allowing adjustments on the exposure time and concentration and producing therapeutically relevant results. However, several questions arise from such approach. The principal one is related to the general toxicity of CO, which could be responsible for severe consequences meaning that the inhalation could be impracticable if high concentrations of CO are required. In addition, studies point that a considerable amount of CO remains bound to hemoglobin forcing the application of higher concentrations for a given biological effect. Another major shortcoming of CO inhalation is related to its lack of tissue specificity meaning that both damaged and healthy tissues would be saturated with CO.[83,85,86,91,93,111,149]

In order to overcome the presented CO inhalation weaknesses, other methodologies have been developed namely the use of prodrugs, which are widely used in several drug design processes as described in the previous chapter. As example, dichloromethane/methylene chloride (DCM, formula CH_2Cl_2) is oxidized by P450 cytochrome generating carbon monoxide among other products. This methodology was successfully applied in cases of liver injure and transplantation but it raises some doubts due to the toxicity of DCM.[83,85,150,151]

In this context, an intense research has been dedicated to some other prodrugs and Carbon Monoxide Releasing Molecules (CORMs) emerged as promising therapeutic agents in this field.

1.2.4.1 – Carbon Monoxide Releasing Molecules – CORMs

The initial development of CORMs as biological and therapeutic agents was attributed to Roberto Motterlini in the first years of 21st century.[85] A collaborative work with Brian Mann (responsible for the synthesis of the compounds) led to a patent submission in 2002 almost immediately followed by a new one from Werner Haas, Carlos Romão and collaborators.[152,153] The first scientific paper described the use of CORMs was also published in 2002.[154]

The main idea associated to CORMs is easily understandable: CORMs are CO containing molecules capable of transport CO in the blood, delivering it at the damaged tissues, in controlled amounts. This approach avoids, the existence of free CO in the blood stream preventing the formation of high levels of COHb and other CO-associated toxic effects. On the other hand, the lack of specificity exhibited by inhalation is also, in theory, overcome allowing the application of smaller quantities of CO for producing a similar effect.[83,85,86,91,94,111,149,155,156,157]

A great number of pertinent questions are associated with the use of CORMs as putative therapeutic agents. The type of compound to use for such purpose is perhaps one of the most obvious. Moreover, it is important to have compounds stable enough to transport CO in the blood but also reactive enough to deliver it efficiently. In the next sections, some important aspects on the design of such complexes will be given as well as some examples of CORMs.

1.2.4.1.1 – CORMs and transition metals

As described previously, one of the first – if not the first – decisive steps in the formulation of a CORM is the type of compound to be used. A common feature to all of the suitable candidates is the ability of release CO under biological conditions and five different classes of compounds obeying this rule were recognized: organometallic complexes, aldehydes, oxalates, boroncarboxylates and silacarboxylates.[91]

Notwithstanding, most of the representatives of the last four groups fail in some parameters essential for their use as CORMs namely a low CO release rate or a toxic behavior. Some exceptions should be mentioned such as CORM-A1 (an early CORM that will be covered in the next sections being an example of a boroncarboxylate complex) and two recent organic photo-CORMs.[91,143,158,159]

Therefore, the use of organometallic complexes involving transition metals remains the best studied class of compounds for CO delivery.[160,161] In fact, as indicated by Carlos Romão and collaborators, this approach mimics the natural carrier of CO: the heme group of hemoglobin.[91]

On the other hand, metals are suitable candidates to form complexes with CO due to the chemistry associated to the process. CO has ten valence electrons (four from carbon and six from oxygen) with a lone pair on carbon and other lone pair on oxygen, which is responsible for a small dipole moment (negative charge on carbon and positive charge on oxygen). Under appropriate conditions, CO is then able to interact with several transition metals in low oxidation states, forming complexes named metal carbonyl complexes (MCCs) with M–CO bonds. The electron lone pair on carbon is donated to an empty metal orbital forming a σ bond. The stability of M–CO bond is significantly increased by a back-donation mechanism by which metal electrons (from filled d orbitals) are donated to empty antibonding orbitals on CO forming π bonds (CO is considered a π acceptor). Both processes are represented in Figure 1.24. This is an example of synergistic binding

(stronger σ bonds lead to stronger π bonds) and it also explains the affinity to low oxidation state metals that possess high-energy d electrons.[79,86,91]

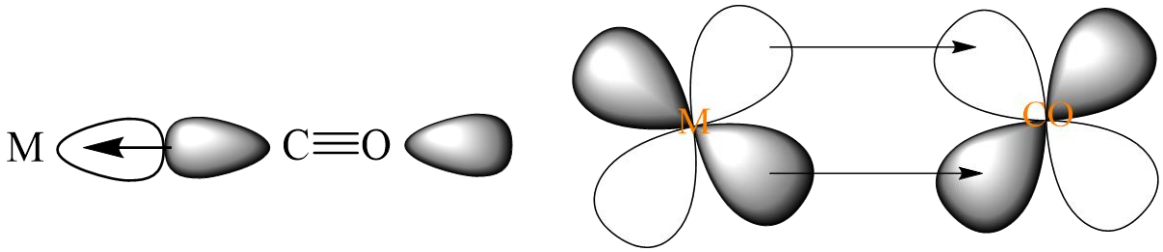

Figure 1.24 – Schematic representation of a M–CO bond.Adapted from [86] On the left, a σ overlap is represented resulting from the donation of the electron lone pair on carbon to an empty metal orbital as indicated by the arrow. On the right, π overlaps are represented resulting from the back-donation of electrons from filled d orbitals of the metal to empty antibonding orbitals on CO as indicated by the arrows. The scheme was prepared in ChemDraw.

MCCs are represented by the general formula $M(CO)_xL_y$ where M is the metal and L the different ancillary ligands that can be used to stabilize the complex (the role of the ligands will be addressed lately). Logically, the presence of, at least, one CO moiety is required.[91]

This field was intensely explored in order to evaluate the use of MCCs as viable *in vivo* CO carriers capable of being used as safety drugs. Nevertheless, that is not an easy task due to the great number of parameters that should be taken into account. Briefly, a good candidate should: a) be soluble in water, b) have a controlled CO release in order to not excessively raise the COHb levels and c) not be toxic (the CORM itself but also the products resulting from the CO release). This means that a great range of compounds synthesized and characterized iin the literature as capable of releasing CO are not appropriate drugs because they do not obey to one or multiple ADME rules. Over the years, a growing attention has been given to this factor explaining the differences between the early and the newest CORMs as pointed lately in the text.

A common and important question to all this type of compounds is related to the mechanisms by which the CO is released. This question is explored in the next section.

1.2.4.1.2 – Mechanisms of CO release from CORMs

As mentioned, the use of CORMs rather than CO inhalation has the capacity of confining the CO release to the damaged tissues and, by that, minimizing the risks of high levels of COHb. Following such idea, a very immediate and pertinent question emerges: how it is possible to control the CO release in order to occur in specific tissues?

The answer to that question is given by the design of the compound itself. The metal, the number of CO groups and the type and number of ligands must be carefully analyzed from a chemical point of view allowing one or multiple mechanisms capable of liberating the carbon monoxide in response to a given stimulus. Often, these stimuli are characteristic of the target tissue, namely the

presence of enzymes or specific pH values. Alternatively, the CORM could be administered and then locally activated for instance by irradiation. Figure 1.25 summarizes some of the mechanisms responsible for CO release.[85,86,91,156]

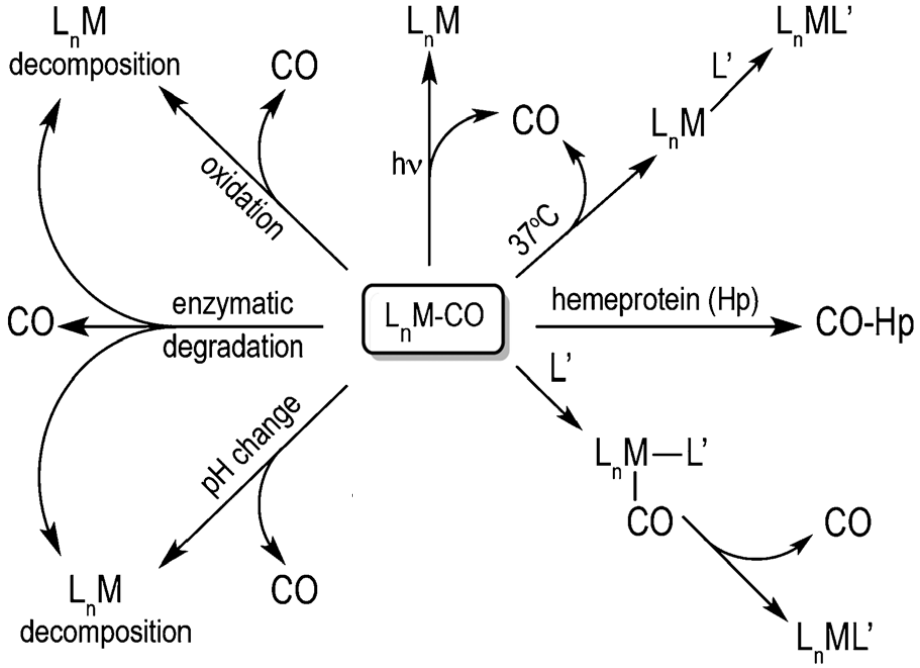

Figure 1.25 – Schematic representation of possible trigger mechanisms responsible for CO release from a general MCC represented by L_nM-CO. Adapted from [91] The release of CO can be achieved by physical, chemical or biological methods.

A first mechanism leading to CO release is the thermal dissociation by which the M-CO bond is broken. In this case, a temperature increase facilitated CO release which is followed by the binding of a different ligand to the metal. Such method is though limited to the corporal temperature which is, usually, lower than the temperature necessary for dissociation; this limitation could be partially overcome by the presence of certain ligands in the CORM that induce CO dissociation such as primary amines.[85,91,111] Moreover, as mentioned, CO is a π acceptor so, if the adjacent ligands of the CORM act as π donors, the CO moiety can be labilized and released. The adjacent ligands can be further deprotonated forming π donor molecules (for example, hydroxide groups can evolve to oxide groups upon deprotonation and π binding) according to the pH. This approach is useful to design tissue specific compounds that preferably release CO in a given range of more acidic or basic pH values.[85,91] The dissociation mechanism is verified in different complexes including the iron carbonyl complexes $[(SBPy_3)Fe(CO)]^{2+}$ and $[(Tpmen)Fe(CO)]^{2+}$ ($SBPy_3$ and Tpmen are pentadentate polypyridine ligands).[162]

Oppositely, association is also a viable mechanism by which a new ligand binds to the metal promoting the M-CO bond breaking.[85,91] Some rhenium-based CORMs of general formula $[Re^{II}(CO)_2Br_2L_2]$ (where L_2 is a N ligand) follow this mechanism.[163]

A third valid option to release CO is the oxidation of the metal present in MCCs by biological oxidizing molecules such as O_2 or ROS. Such oxidation is responsible for making the M-CO bond weaker (the π back-donation is affected) and, consequently, CO is released. Tissue specificity is also possible by the presence of ancillary ligands that are preferably removed by chemical species existing exclusively in those tissues.[85,91,111]

A different possibility is to use the so-called bioactivated or enzyme-triggered CORMs (ET-CORMs) that are biologically activated to release CO by the action of a given enzyme. If the enzyme is intimacy related to a pathological condition, being produced uniquely (or at least largely) in the damaged areas, effective tissue specific complexes could be designed.[85,91,111] Some iron tricarbonyl compounds have been described as ET-CORMs activated by esterases and phosphatases.[164,165]

Finally, light activated CORMs or photoCORMs were the first to be used in the earlier CORMs development. As suggested by their nomenclature, photoCORMs are able to release CO when activated by light at different wavelengths (according to the M-CO bond characteristics) and they are particularly used in photodynamic therapy.[166] Often the application of photoCORMs requires surgery to reach the target (some given tissues or tumors) but their use is also possible in skin disorders.[85,91,111] Several photoCORMs were characterized and some literature on this subject is available.[167,168]

Independently of the used trigger mechanism, it is necessary to have methods to detect the released CO. Infrared spectroscopy and gas chromatography are well-known techniques for such purpose. The so-called myoglobin assay was also widely used (CO interacts with reduced deoxy-myoglobin forming CO-myoglobin in a reaction monitored by UV-visible spectroscopy).[94,149] However, this test presents some drawbacks namely the effect of sodium dithionite that interfere with the CO release.[169] New methods have been suggested including the use of a palladium complex (CO Probe 1, COP-1) as a reaction-based fluorescent CO probe capable of triggering a fluorogenic carbonylation reaction. Therefore, this reaction is able to show efficiently the CO release not only in aqueous buffered solutions but also in living cells.[170]

1.2.4.1.3 – Early CORMs

As mentioned before, the field corresponding to the development of putative *in vivo* CO carriers has begun to be explored at approximately 15 years ago and different complexes with distinct characteristics were synthesized and used in several experiments. However, at this stage, the design of the complexes was mainly focused merely in the ability to release CO neglecting some other important features namely those related to ADME properties. Nevertheless, these early CORMs were extremely useful to prove that the concept of CO releasing was possible. Moreover, such CORMs were also associated to several pathologies allowing further investigations. Four early complexes were particularly analyzed being possible to catalog them into two distinct groups: lipid soluble and water soluble CORMs (Figure 1.26). Dimanganese decacarbonyl (CORM-1, $[Mn_2(CO)_{10}]$) and

tricarbonyldichloro ruthenium (II) dimer (CORM-2, $[Ru(CO)_3Cl_2]_2$) belong to the first group while tricarbonyldichloro(glycinato)ruthenium (II) (CORM-3, $[Ru(CO)_3Cl(glycinate)]$) and sodium boranocarbonate (CORM-A1, $[Na_2H_3BCO_2]$) belong to the second group.[85,171]

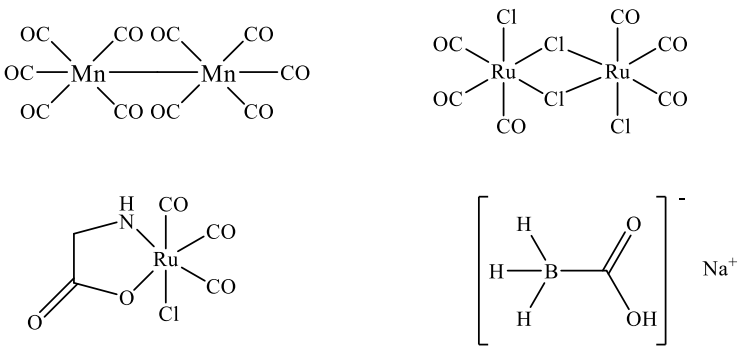

Figure 1.26 – Structural representation of the paradigmatic early CORMs. Adapted from [85] Top: CORM-1 (left) and CORM-2 (right); bottom: CORM-3 (left) and CORM-A1 (right). The structures were prepared in ChemDraw.

Lipid soluble CORMs were the first ones to be developed, being soluble only in organic solvents such as ethanol or dimethyl sulfoxide (DMSO). In addition to potential biocompatibility issues, CORM-1 needs also photolysis activation to trigger CO release, which is not attractive for its development as a therapeutic agent. Nonetheless, CORM-1 was related to vasodilatation properties from the first biological testes.[85,154,156]

CORM-2, also a water insoluble ruthenium-based complex, presents the advantage of not being activated by light and it is still today used as a CORM model. Besides vasodilatation, CORM-2 was recognized as anti-inflammatory and protection against I/R injuries agent.[85,154,156,172,173]

The development of water soluble complexes was a major breakthrough in the study of the biological actions of CORMs. CORM-3 was the first example of this class of compounds being presented in 2003.[174] Closely related to the structure of CORM-2, the addition of a glycine ligand allows a significant increase of its water solubility explaining why CORM-3 is, perhaps, the most "famous" CORM and the more widely used as a model compound. In spite of its instability in water leading to the formation of different intermediate species, the beneficial effects of CORM-3 were associated to a multiple number of conditions including vasodilatation, inflammation and transplantation.[172,174,175]

The last early CORM herein mentioned is CORM-A1 identified not longer than 11 years ago. Contrarily to the other three mentioned complexes, this compound is a nonmetal-based CORM and its CO release is pH and temperature dependent. Despite its reducing character, CORM-A1 was shown to be particularly useful in cases of vasodilatation.[111,176]

1.2.4.1.4 – Drug-like CORMs

In addition to the four CORMs described in the previous section, many other complexes were designed and investigated over the years using a great range of metals such as chromium, molybdenum, tungsten, manganese, rhenium, iron, ruthenium and cobalt.[85]

However, a significant percentage of the developed compounds will, most likely, not be suitable for *in vivo* application as CO carriers due to their lack of drug-like properties. Keeping this in mind, Carlos Romão and collaborators proposed a rational method to produce drug-like MCCs in which three aspects should be carefully taken into account: the metal, the inner/ligand coordination sphere and the outer/drug coordination sphere as illustrated in Figure 1.27.[91,111]

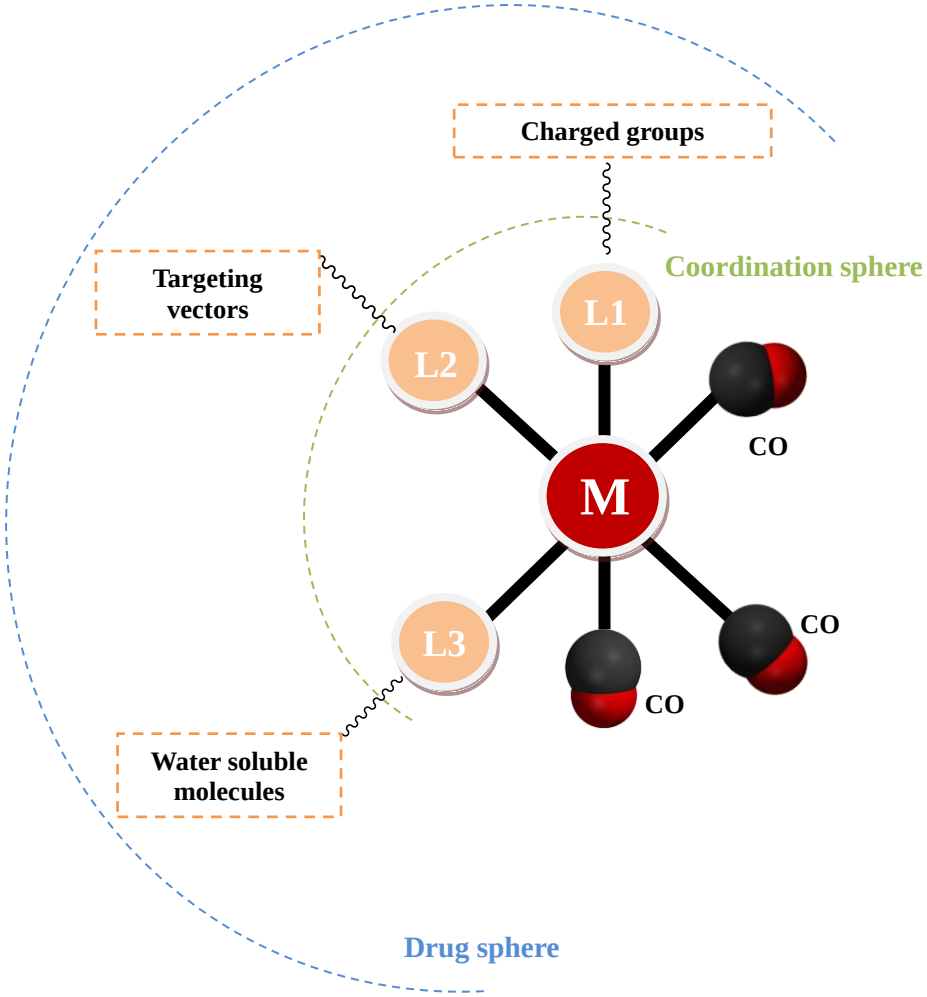

Figure 1.27 – Schematic representation of a drug-like CORM. Adapted from [91] The two spheres are depicted. The use of CORMs as viable drugs requires a particular attention to the drug sphere. The addition of some molecules to the ancillary ligands is often used to improve several pharmacological characteristics. As example, carbohydrates and peptides are used to increase water solubility; enzyme substrates are used to target a given tissue; amino and carboxylate groups are used to modulate the charge of the complex controlling different aspects such as solubility and membrane permeation.

Virtually, the almost totality of transition metals can be used to produce MCCs. However, the most stable elements – forming complexes with 18 valence electrons – are often preferred, namely

those from groups 6, 7 and 8 such as chromium, molybdenum, manganese, rhenium, iron and ruthenium. However, the toxicity issues are also important explaining why manganese complexes are not so explored. For that reason, labile complexes and those in which M-CO bond are formed under non-biologic conditions are usually discarded.[91,111]

The inner/ligand coordination sphere is mainly related to the number of CO moieties and the number and properties of the ancillary ligands. There is no consensus on the ideal number of CO groups but it is clear that ancillary ligands play an essential role for the design of viable CORMs. In fact, such ligands largely control the rate of CO release by modulating the electronic environment of the metal, making it more or less susceptible to different processes responsible for the CO loss, as previously explained. Moreover, a potential high toxicity of the metal could be attenuated by these ligands. There are multiple molecules able to be used as ancillary ligands and the choice of the appropriate ones depends not only on the used metal but also on the eventual required modifications to originate a drug-like molecule.[91,111,149]

Finally, the outer/drug coordination sphere is responsible, as suggested by the name, for the pharmacological characteristics that any viable drug should follow, including water solubility, appropriate ADME and pharmacokinetic profiles and the targeting to the affected tissues or organs. A slight modification of a given ancillary ligand – adding some substituents – could be enough to improve significantly the desired acceptable pharmacological parameters. In addition, drug sphere is useful to adequate a compound to a given mode of administration.[91,111,149]

These criteria were used to find viable drug-like CORMs and different complexes were designed by Alfama Inc to treat acute liver failure induced by acetaminophen (paracetamol) overdose. In fact, several compounds were tested and the best results were obtained with the compound $[Mo(CO)_3(CNCMe_2CO_2H)_3]$ designated by ALF794 (Figura 1.28). Compared with some other related-complexes, ALF794 exhibits considerable higher liver specificity being present in residual concentrations in other organs such as the heart, the lungs and the kidneys. Moreover, it was also found that liver microsomes accelerate the release of CO from the complex meaning that ALF794 can be bioactivated in the liver without the need of further mechanisms of release. All these properties make ALF794 a very suitable drug candidate to be used against acute liver failure.[111,177]

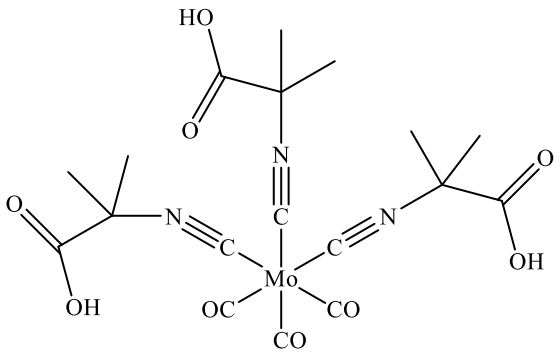

Figure 1.28 – Structural representation of ALF794. The structure was prepared in ChemDraw.

1.3 – Vanadium – Biological and therapeutic effects

1.3.1 – General concepts and historical perspective

Vanadium (V) is a bright silver-white and ductile transition metal (group 5, atomic number 23 and atomic mass 50.94). Widely distributed in nature (soil, crude oil, water and air), vanadium is a trace metal found in different organisms from different domains.[178,179,180]

Vanadium is an abundant element not only in Earth (0.013% w/w) but also in the space namely in meteorites and comets.[181] Different minerals have vanadium in their composition (Figure 1.29 and Table 1.6) and concentrations of 30-35nM ($Na^+H_2VO_4^-$) are found in sea waters meaning that vanadium is the second most common transition metal in sea waters immediately after molybdenum (100nM, MoO_4^{2-}).[179]

Figure 1.29 – Minerals containing vanadium: vanadinite (left), carnonite (center) and descloizite (right). Photos obtained from: http://www.galleries.com/

Table 1.6 – List of some of the most common minerals containing vanadium. Adapted from [179]

Mineral name	Formula	Type of compound
Vanadinite	$Pb_5[VO_4]_3Cl$	Orthovanadate
Patronite	VS_4 or $(VS_2)_2$	Disulfide
Roscoelite (vanadium mica)	$K(Al,V)_2(OH,F)_2[AlSi_3O_{10}]$	V^{3+} aluminosilicate
Carnotite	$K(UO_2)[VO_4]$	Orthovanadate
Descloizite	$Pb(Zn,Cu)OH[VO_4]$	Orthovanadate

From an historical point of the view, separated events contributed to the discovery of vanadium in what can be considered a "two-step process". In 1801, the Spanish mineralogist Andrés Manuel del Rio, then professor at the *Real Colegio de Minas* in Mexico City, firstly identified a new element as consequence of his work with a brown lead ore (today known as vanadinite). del Rio originally named it panchromium (meaning "all colours" in Greek) lately changed to erythronium (meaning "red" in Greek). Visiting del Rio, Alexander von Humboldt thought that such element was chromium and brought some samples to Europe. A sample was shortly after analyzed by the French

chemist Hippolyte Victor Collet-Descotils postulating the existence of chromium in the mineral. Later, in 1828, Humboldt gave other sample to the German chemist Friedrich Wöhler who concluded that the element had distinct properties from those observed in chromium.[179,182,183,184]

In parallel, in 1831, the Swedish chemist Nils Gabriel Sefström found a new element from an iron mineral further analyzed by Jöns Jacob Berzelius. Sefström designed such element as vanadium in honor to the beauty and fertility Nordic goddess Vanadis also known as Freya. Finally, Wöhler had the opportunity to compare this element with the one described by del Rio concluding, 30 years after its initial finding, that both samples are the same element: vanadium.[179,182,183,184]

These were the first steps into a long journey, which is still today very challenging. In fact, vanadium and vanadium oxides play several roles in very different fields, ranging from industry to medicine.[182,185] Briefly, industrial applications include the use of vanadium as component of different metal alloys, as catalyst in different processes (namely in the oxidation of sulfur dioxide to sulfur trioxide for sulfuric acid production) and production of batteries.[186,187,188,189]

Biological implications and medical applications of vanadium were pointed since the last quarter of the 19th century. As most remarkable examples, the presence of vanadium was indicated both in plants (sugar beets) and animals (ascidians, commonly known as sea squirts) by Edmund O. von Lippmann and Martin Henze, respectively, could be cited.[184] On the other hand, the hospital L'Hôtel-Dieu (Lyon) was the first stage for the therapeutic use of vanadium. A group of 44 people were treated with metavanadate and positive results were registered. Only more than 100 years later, already in the 21st century, successful clinical tests could be achieved with the use of a vanadium compound – VO(ethylmaltolate)$_2$, BEOV – in the treatment of type 2 diabetes. In the time elapsed between these two events, significant efforts were done to a better comprehension of the subject, particularly since the 1980s, by several groups worldwide spread.[184,185,190] A deeper analysis on the biological and medical roles of vanadium will be addressed in the next sections.

It should be mentioned that a lot of research is daily conducted by several teams on different aspects related to this element. In fact, the "vanadium community" is very active as proven by the multiple meetings and congresses organized over the years. In addition, the Vanadis Award was created in 2004 rewarding scientists with outstanding contributions for the field. So far, Vanadis Award has been attributed to Debbie C. Crans (USA, 2004), Dieter Rehder (Germany, 2006), Toshikazu Hirao (Japan, 2008), Vincent L. Pecoraro (USA, 2010), Israel E. Wachs (USA, 2012) and João Costa Pessoa (Portugal, 2014).

1.3.2 – Vanadium chemistry and vanadium complexes

The chemistry of vanadium is complex and an exhaustive overview of such topic is not the objective of the present section. Nevertheless, some concepts will be covered.

Vanadium, as a transition metal, has different oxidation states namely +II, +III, +IV and +V. According to the oxidation state, different colours are observed in aqueous solutions: violet, green, blue and yellow, respectively. From a biological point of view, V^{2+} is not so significant because it is not stable in water being quickly oxidized again to V^{III}. When in aqueous media, these oxidation states are susceptible to hydrolysis, originating different species as briefly explained next.[180,191,192]

V^{III} forms different non-oxo (O^{2-}) monomeric and oligomeric species depending on pH and vanadium concentration. As example, the deprotonation of the monomeric species is common and different aquanonoxovanadium(III) forms – $[V(H_20)_6]^{3+}$, $[V(OH)(H_20)_5]^{2+}$ and $[V(OH)_2(H_20)_4]^{+}$ – are known (Figure 1.30). This oxidation state is particularly important in ascidians and in Polychaeta fan worms, both organisms able to store V^{III}. Associated with such storage, sulfate is able to bind to V^{III} forming aqua-sulfato species as $[V(HSO_4)(H_20)_5]^{2+}$ and $[V(HSO_4)_2(H_20)_4]^{+}$.[180,191,192]

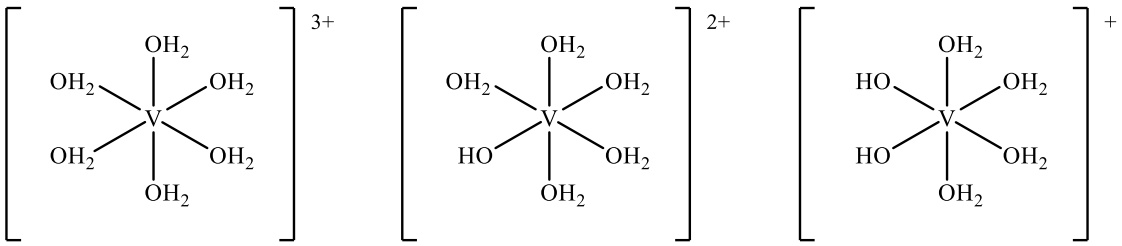

Figure 1.30 – Structural representation of some V^{III} aqueous monomeric species: $[V(H_20)_6]^{3+}$ (left), $[V(OH)(H_20)_5]^{2+}$ (center) and $[V(OH)_2(H_20)_4]^{+}$ (right). Adapted from [192] The structures were prepared in ChemDraw.

Despite the existence of some non-oxo vanadium(IV) complexes (namely amavadin, a vanadium-containing molecule existing in *Amanita muscaria* mushrooms), V^{IV} exists mainly as mono-oxo complexes containing a stable vanadyl ion – VO^{2+} (Figure 1.31). Stable at low pH, vanadyl ion tends to form precipitates – $VO(OH)_2$ – at higher pH values if not complexed with other ligands.[180,191,192]

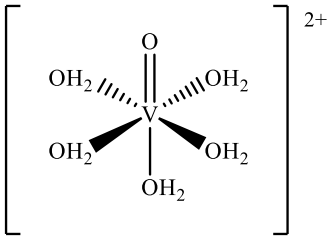

Figure 1.31 – Structural representation of a V^{IV} aqueous species: $[VO(H_20)_5]^{2+}$ Adapted from [180] The structure was prepared in ChemDraw.

Finally, V^{V} exists usually as oxo-vanadates. Vanadate(V) presents multiple oligomeric forms (V_1, V_2, V_4, V_5 and V_{10} for example) depending on pH, vanadium concentration and environment ionic conditions. As example, the simplest vanadate – $(VO_4)^{3-}$ – exists only in very basic pH conditions while decavanadate – $(V_{10}O_{28})^{6-}$ – is formed under conditions of moderate acidity (Figure 1.32).[180,191,192,193] Decavanadate is particularly studied from a biological point of view.[194,195]

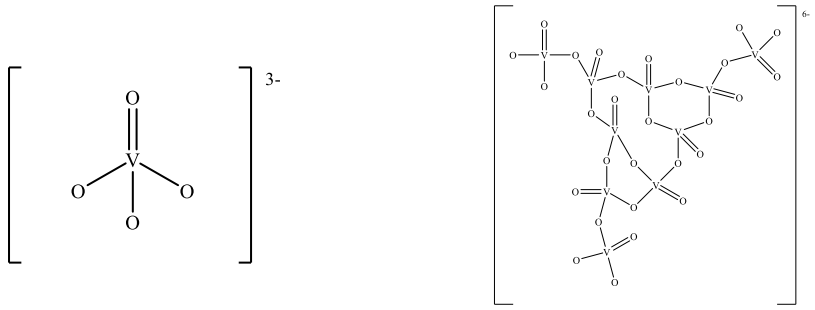

Figure 1.32 – Structural representation of two V^{V} vanadates: monovanadate [$(VO_4)^{3-}$] (left) and decavanadate [$(V_{10}O_{28})^{6-}$] (right). Adapted from [193] The structures were prepared in ChemDraw.

Both V^{IV} and V^{V} are able to form complexes with a great range of inorganic and organic ligands. Oxygen-, nitrogen- and sulfur-containing ligands are particularly important. The vanadium coordination complexes have different coordination numbers (4 to 8) and different coordination geometries namely square pyramidal and octahedral. The presence of the ligands increases the stability of vanadium – as example, oxidation of V^{IV} is not so likely to occur when the metal is forming a organometallic complexed. Moreover, such feature is also useful from a biological and therapeutic point of view allowing the interaction with several biogenic ligands or contributing for a more drug-like profile of the vanadium coordination complexes.[180,191,192,193]

1.3.3 – Vanadium in Biology and Medicine

As mentioned, vanadium is commonly found in Nature and, not surprisingly, it has been implied in different biological functions and, in parallel, as a putative therapeutic agent. As example, studies with animals suggested the role of vanadium on thyroid and carbohydrate metabolism.[196,197]

Concerning humans, vanadium is found at approximately 0.3μM. Major vanadium sources are diet (food and water) and inhalation. Studies point a daily ingestion of 10 to 30μg of vanadium; some aliments rich in vanadium include shellfish, mushrooms, parsley and black pepper while beverages like beer and wine have also a considerable amount of the element (drinkable water presents a medium concentration of 10 nM).[178,184,196,198] In addition to food and water, the vanadium oxides existing in the atmosphere – particularly in polluted environments – are also relevant. Proving, once again, that Paracelsus was correct about his famous sentence, a prolonged vanadium inhalation can originate toxic effects namely lung diseases and DNA damage.[184,198,199,200,201] On the other hand, vanadium can be stored in bones (vanadate replaces phosphate in apatite) leading to different osteogenic effects with potential therapeutic interest.[184,202]

A considerable amount of literature is available on the role of vanadium in biology and medicine.[180,184,195,196,198,203,204,205,206,207,208,209,210] Herein, a brief overview will be given divided into two major subjects: interaction of vanadium with proteins and therapeutic actions of vanadium.

1.3.3.1 – Vanadium and proteins

Very recently, a review covering different aspects – namely from a structural point of view – related with vanadium and proteins was published.[210] In fact, a considerable number of vanadium-related proteins are available in the PDB (Protein Data Base) most of which were solved by X-ray crystallography.[210,211]

Largely contributing for its biological relevance, the vanadate(V)-phosphate analogy should be mentioned (Figure 1.33). Due to their structural analogy, vanadate(V) can mimic phosphate in different processes leading, in most of the cases, to the inhibition of the enzymes by the formation of a stable transition state analogue.[198,203,210]

Vanadium is closely related to a great variety of proteins as summarized in Table 1.7. Next sections are dedicated to V uptake and transport, the role of V in the protein activity and function and, finally, to the V action as substrate analogue or inhibitor.

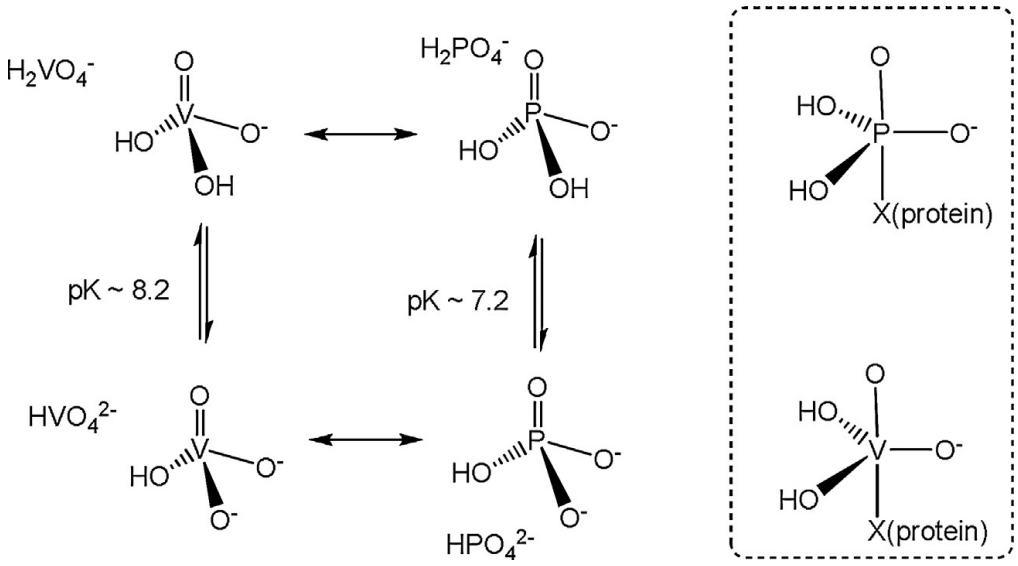

Figure 1.33 – Schematic representation of the analogy between phosphate and vanadate (V).[210] The structural analogy allows the formation of vanadate-protein adducts similar to those formed with phosphate as depicted in the dashed rectangle. However, there are also differences between the two anions. As example, vanadate(V) is able to form stable complexes with coordination numbers 5 and 6 while phosphate only form complexes with coordination number 5. The pKa values are also different being responsible for an unequal distribution of $H_2VO_4^-/HVO_4^{2-}$ and $H_2PO_4^-/HPO_4^{2-}$ at physiological conditions (vanadate exists mainly as $H_2VO_4^-$ while phosphate exists in the two forms).

Table 1.7 – Summary of function and/or reaction of proteins related to vanadium.[210]

Protein	Function/reaction	PDB code
Vanabins	Vanadium storage/carrier	1VFI
Nitrogenases	$16\ ATP + 8\ H^+ + 16\ H_2O + N_2 + 8\ e^- \rightarrow 2\ NH_3 + H_2 + 16\ ADP + 16\ Pi$	–
Haloperoxidases	$H_2O_2 + X^- + H^+ \rightarrow H_2O + HOX$ (X = Halogen)	1VNC, 1IDQ, 1IDU, 1VNI, 1VNH, 1VNG, 1VNF, 1VNE, 3W36, 1QI9, 4USZ, 4CIT
V-Nitrate reductases	$NO_3^- + NADH \rightarrow NO_2^- + NAD^+ + OH^-$	–
Phosphatases	$aa\text{-}OPO_3^{2-} + H_2O \rightarrow aa\text{-}OH + P_i$	4KKZ, 2D1G, 3F9B, 1B8J, 1H2F, 3ZWK, 4QIH, 4HGP, 4ERC, 3ZX5, 4KNW, 3QKQ, 3ZWU, 3QCC, 3QCD, 3S3F, 3OMX, 3I7Z, 3I80, 2I42, 2HY3, 2I4E, 1Z12, 1RPT, 1J9L
Kinases	$ATP + substrate\text{-}OH \rightarrow ADP + substrate\text{-}OPO_3^{2-}$	1M7G, 3GQI, 1DKT, 4DZ6, 3Q8Y
Other Transferases	Transfer of functional groups between different molecules	1UZI, 1RXS, 1C4G, 4HGO, 3E81, 2RAR, 2RBK, 2AZD, 1BO6
EctoNTPDases	$NTP \xrightarrow{H_2O} NDP + P_i \xrightarrow{H_2O} NMP + 2\ P_i$	4BRE, 4BRH, 4BRL, 3ZX2, 3QVF
Phosphodiesterases	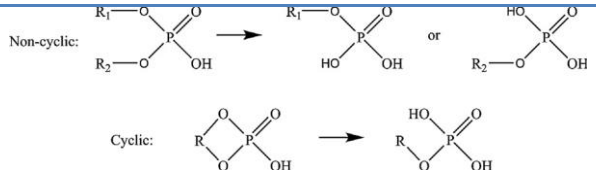	1JH7, 2GSO, 1RFF, 1RFI, 1RG1, 1RG2,1RGT, 1RGU, 1RH0, 1NOP, 1MU9
Phosphomutases	$HO\text{-}substrate\text{-}OPO_3^{2-} \rightarrow PO_4^{2-}\text{-}substrate$	1E59, 3GW8, 3GP5
ATPases	$ATP + H_2O \rightarrow ADP + P_i$	1L7V, 3PUV, 3B5Z, 2XEL, 2XO8, 2X9H, 3MJX, 3MNQ, 2JHR, 2JJ9, 4BYF, 4AE3, 2YCU, 4DBR, 4E7S, 4E7Z, 3MKD, 3MYH, 3BZ7, 3BZ8, 3BZ9, 2V26, 1YV3, 1VFZ, 1QVI, 1LKX, 1DFL, 1VOM
ATP synthases	$ADP + P_i \rightarrow ATP$	2F43, 3P20
DNA binding (Topoisomerases)	Regulation of the overwinding or underwinding of DNA	3IGC, 2B9S, 3MGV, 2XEL, 2XO8, 2X9H
DNA binding (Aprataxin)	Removal of AMP from DNA ends	4NDG
DNA binding (Protelomerases)	Generation of closed hairpin ends in linear DNA	4E0G, 2V6E
Ribonucleases	Degradation of RNA	1RUV, 6RSA, 2G8H, 3RNT
Ribozymes	Catalysis of biochemical reactions by RNA	1M5O, 2P7E

1.3.3.1.1 – Vanadium uptake and transport

There are three major examples of vanadium hyper-accumulator organisms: Polychaete worms, *Amanita muscaria* fungus (as amavadin as previously mentioned) and ascidians (also known as seasquirts or tunicates).[208,212,213,214]

From those, ascidians will be briefly addressed herein. About one century ago, Martin Henze was the first to point the high levels of vanadium in the blood cells of ascidians – the highest amount of V was found for *Ascidia gemmata* (350 mM).[210,214,215]

The specific blood cells involved in the vanadium accumulation are designed by vanadocytes, which contain vacuoles where vanadium is stored. Although vanadium uptake occurs as V^{V}, in the vanadocytes it is reduced to V^{IV}, using NADPH and/or glutathione from the pentose phosphate pathway, and in the vacuoles it is further reduced to V^{III}.[203,210, 214,215,216]

Vanabins are a family of proteins located in the vanadocytes' cytoplasm. Involved in the V^{IV} uptake, they act as a metallochaperones, responsible for the transport of the metal from the cytoplasm to the vacuoles. The characterization of these proteins shows that vanabin1 (12.5 kDa) and vanabin2 (15 kDa) are able to bind up to ten and twenty V^{IV} ions, respectively. There is a deposited vanabin2 structure from *Ascidia sydneiensissamea* (PDB: 1VFI) solved by NMR. The structure does not contain V^{IV} bound to the protein showing four α-helices in a bow-shaped conformation. Out of 91 residues, 18 are cysteines, which form nine disulfide bonds, involved in the stabilization of the structure and in the binding of V^{IV} ions (Figure 1.34). Moreover, NMR experiments allowed the identification of the residues involved in the binding of V^{IV}; the residues are placed on the same face of the molecule and V^{IV} ions are coordinated by amine-N donors from lysines, arginines and histidines.[210,216,217]

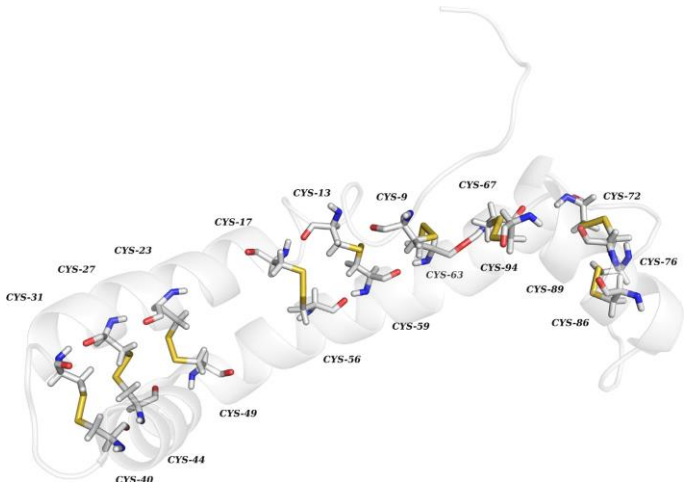

Figure 1.34 – Structural representation, in cartoon, of vanabin2 (PDB: 1VFI).[210] The nine disulfide bonds are also depicted (yellow, stick representation). It is visible the importance of the disulfide bonds on the correct protein folding.

On the other hand, different classes of proteins have been proposed to be involved in vanadium transport namely transferrins, albumin, immunoglobulins, hemoglobin and ferritin.[210]

However, this subject will be further addressed later in this introduction and also in the Chapter 3 related to the interactions of proteins with vanadium and vanadium compounds.

1.3.3.1.2 – Vanadium in protein activity and function

Vanadium was identified as an essential element for the activity of three different families of proteins: nitrogenases (enzymes capable of transforming molecular nitrogen into nitrogen compounds), nitrate reductases (enzymes that catalyze the reduction of nitrate to nitrite) and haloperoxidases. From those, uniquely haloperoxidases are structurally characterized and the discussion will be focused on them.[208,210]

Haloperoxidases are enzymes that catalyze the oxidation of halides, by hydrogen peroxide (as indicated in Table 1.7). There are three classes of haloperoxidases: co-factor free, heme-dependent and with vanadium as a relevant entity in the active site, the vanadium-containing haloperoxidases (VHPOs). The naming of the VHPOs is based on the most electronegative halide that the enzyme can oxidize: the chloroperoxidases (VCPOs) can catalyze the oxidation of Cl^-, Br^- and I^-, the bromoperoxidases (VBPOs) can catalyze the oxidation of Br^- and I^- and iodoperoxidases are specific for I^-.[203,207,210]

VBPO and VCPO were found in the middle of 1980s leading to an intense research from a chemical, biochemical and industrial point of view. The first structure of a VHPO was determined in 1996 by Messerschmidt and Wever at 2.1Å resolution by X-ray crystallography (PDB: 1VNC) corresponding to a chloroperoxidase from the fungus *Curvularia inaequalis* (CiVCPO) where V is bound to His496, three O-atoms and to an azide ligand from the crystallization conditions in a trigonal-bipyramidal geometry (Figure 1.35).[210,218]

Progressively, other structures of native and mutant CiVCPOs were solved allowing a better understanding of its mode of action. A good example of that are the structures in the apo form (PDB: 1IDQ) and in the presence of peroxide (PDB: 1IDU). During the catalytic reaction, V adopts a reasonably stable five-coordinated state upon binding of H_2O_2 which, in turn, is attacked by the halide. The hypohalide species formed is very susceptible to nucleophilic attack producing halogenated compounds and singlet oxygen.[210,219]

Bromo- and iodoperoxidases were also structurally characterized from algae (PDBs: 1QHB, 1UP8 and 1QI9) and bacterial sources (PDBs: 4USZ and 4CIT), respectively. As expected, similar structures to those described for VCPOs were obtained suggesting similar reaction mechanisms.[210]

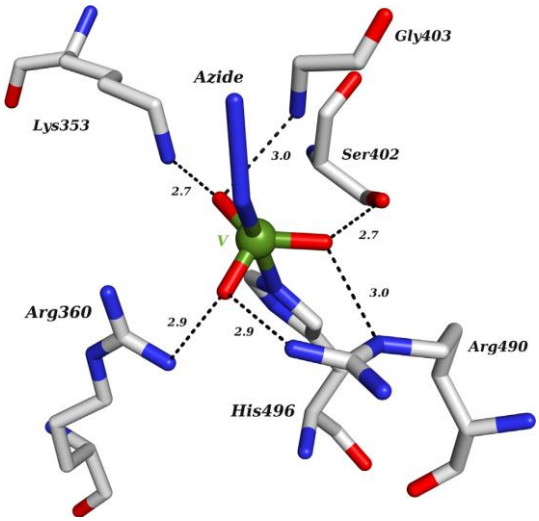

Figure 1.35 – Structural representation of the adduct formed between the CiVCPO and the vanadate(V) moiety (PDB: 1VNC).[210] In addition to the described in the text, the residues hydrogen bonded to the vanadate(V) moiety are also shown (bond lengths are indicated in Å). The vanadate(V) is deeply buried in the protein, accessible via a highly positively charged funnel-shaped channel.

1.3.3.1.3 – Vanadium as substrate analogue or inhibitor

There are many classes of proteins where vanadium, mainly as vanadate(V), acts as a substrate analogue or inhibitor contributing to the elucidation of the catalytic reaction mechanism. These enzymes can be grouped as those mainly involved in phosphate binding or release, proteins responsible for DNA binding and proteins responsible for RNA binding as indicated in Table 1.7. Some significant examples of each class will be selected to a further description.

Phosphorylation is one of the major signaling pathways controlling a cascade of different physiological effects and is commonly observed in all organisms. Kinases and phosphatases are the key enzymes in this reversible reaction being responsible for the addition or removal of a phosphate group, respectively. Protein phosphorylation mainly occurs in residues (serine, threonine and tyrosine) with hydroxyl-containing side chains; dephosphorylation is achieved by hydrolysis of the ester bond with the formation of a high-energy five coordinate phosphorous transition state. The $V^{IV}O^{2+}$ cation also inhibits different enzymes and in some cases with a greater potency than vanadate(V). Several structures of vanadium-bound phosphatases and kinases have been determined (Table 1.7).[210]

Vanadate(V) is not a specific inhibitor of all phosphatases, but can be a potent inhibitor of such activity. Vanadate(V) may mimic the 5-coordinate transition state of phosphate formed during the phosphatase catalytic cycle, by its ability to form a stable 5-coordinate complex at the active site of the enzyme. Among this vast family, phosphatases with affinity to tyrosine-phosphate proteins (PTPases) are particularly important being implicated in inflammation, atherosclerosis, diabetes and cancer. Vanadate(V) has been widely used as analogue for studying the reaction mechanism of this class of enzymes providing important information regarding transition state conformation and structural determinants for catalysis. As example, two relevant transition state analogues of PTP1B have been

obtained by crystallizing the enzyme with a short Tyr-containing peptide that was previously incubated with vanadate(V). In the first one, the vanadate(V)–tyrosyl peptide is bound to the active site (PDB: 3I7Z); the vanadium adopts a trigonal–bipyramidal geometry with the nucleophylic cysteine and the tyrosyl oxygen in apical positions. The second one corresponds to the Cys-bound vanadate(V) species (PDB: 3I80) similar to the phosphoenzyme prior to inorganic phosphate release. These models represent snapshots of the reaction mechanism of PTPases (Figure 1.36).[210,219]

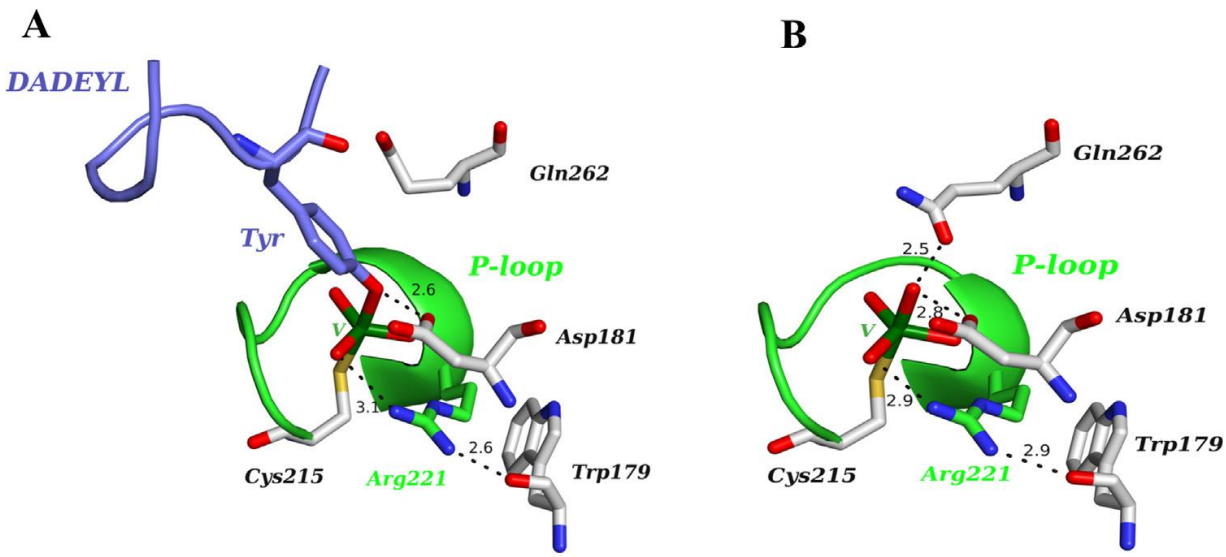

Figure 1.36 – Structural transition state analogues models of the reaction mechanism of PTP1B.[210] (A) In the first transition state analogue (PDB: 3I7Z), the vanadate(V) moiety adopts a trigonal–bipyramidal geometry with Cys215, the tyrosine of the peptide DADEYL (a fragment of the epidermal growth factor receptor) and three O-atoms. These atoms are hydrogen bonded (not shown) to the backbone N-atoms of the P-loop (residues 215–222) and to one N-atom of the side chain of Arg221. This residue is hydrogen bonded to the backbone carbonyl of Trp179 allowing Asp181 to be positioned next to the oxygen of the leaving group. Gln262 is not interacting with the vanadate(V) moiety. (B) In second transition state analogue (PDB: 3I80), the structure simulates the protein prior to the inorganic phosphate release; the vanadate(V) moiety remains in a trigonal-bipyramidal geometry. Gln262 is rotated being hydrogen bonded to one of the O-atoms of the vanadate(V). Some distances are indicated in Å.

Vanadium can interact with DNA binding proteins in a similar way to what has been described. As example, some structures of topoisomerases where vanadate(V) was used to obtain information regarding the transition state of the catalytic reaction have been determined. In 2006, a transition state structure of topoisomerase I from *Leishmania donovani* (PDB: 2B9S), a potential clinical target against leishmaniases, encompassing a nicked double-stranded DNA and vanadate(V) was solved at 2.3Å resolution. The vanadate(V) moiety presents a distorted trigonal–bipyramidal geometry with the 5-hydroxyl end of the DNA nick and the nucleophilic Tyr222 residue in the apical positions. His453, Lys314 and Lys352 residues are hydrogen bonded to the apical or equatorial ligands, contributing for the stabilization of the transition state analogue; furthermore, the Arg410 residue and a water molecule are next to the phenolic oxygen of Tyr222 being implicated in the

respective nucleophile activation process.[210,221] Some other structures of vanadium-related DNA binding proteins are also available in the PDB (Table 1.7).

Finally, ribonucleases, also known as RNases, catalyze the cleavage of RNA and vanadate(V), $V^{IV}O^{2+}$ and some of their complexes are strong inhibitors of the hydrolysis of the phosphodiester bond in RNA. As example, RNase A (bovine pancreatic ribonuclease A) is involved in two reactions: the cleavage of the 3'-5' phosphate bond and the hydrolysis of the produced 2'-3'-cyclic phosphate intermediate. Uridine vanadate(V) was used as a 2',3'-cyclic phosphate due to their structural similarities leading to a 1.3Å resolution structure (PDB: 1RUV). A 5-coordinate trigonal–bipyramidal geometry adduct was obtained in the active site of the protein; the reaction involves the formation of a cyclic ester with V coordinated across the 2' and 3' positions of ribose (Figure 1.37).[203,210,222] A brief mention should be done also concerning ribozymes; there are around 220 deposited structures of these RNA molecules capable of catalyzing some reactions including two vanadium-containing structures which mimic the transition state of these peculiar enzymes.[210]

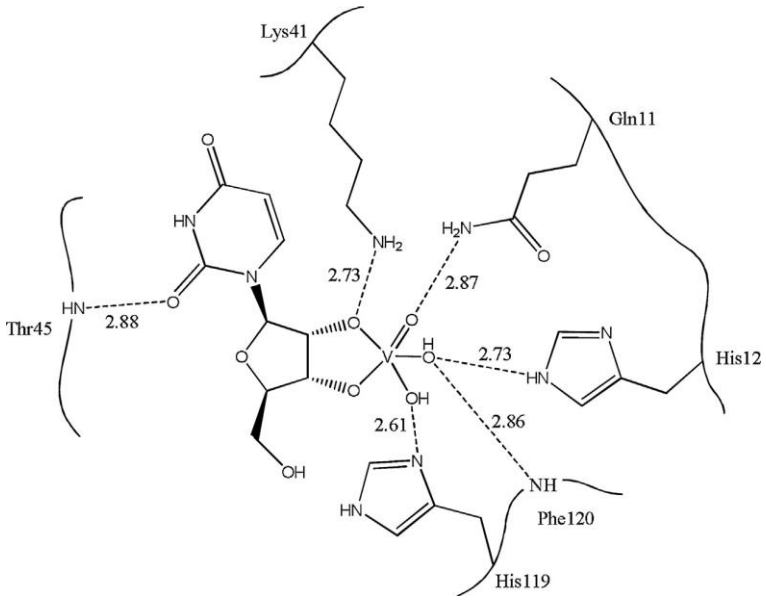

Figure 1.37 – Structural representation of the vanadate(V)-RNase A adduct (PDB: 1RUV).[210] The vanadate(V) moiety is also stabilized by a hydrogen bond network established between the O-atoms and different residues namely His12, His119, Lys41 and Gln11. Some distances are indicated in Å.

1.3.3.2 – Therapeutic applications of vanadium

Different medical and therapeutic applications involving vanadium have been proposed. Commonly to all putative drugs, a properly characterization of the uptake and the routes of distribution in the organism is required, as illustrated in Figure 1.38.

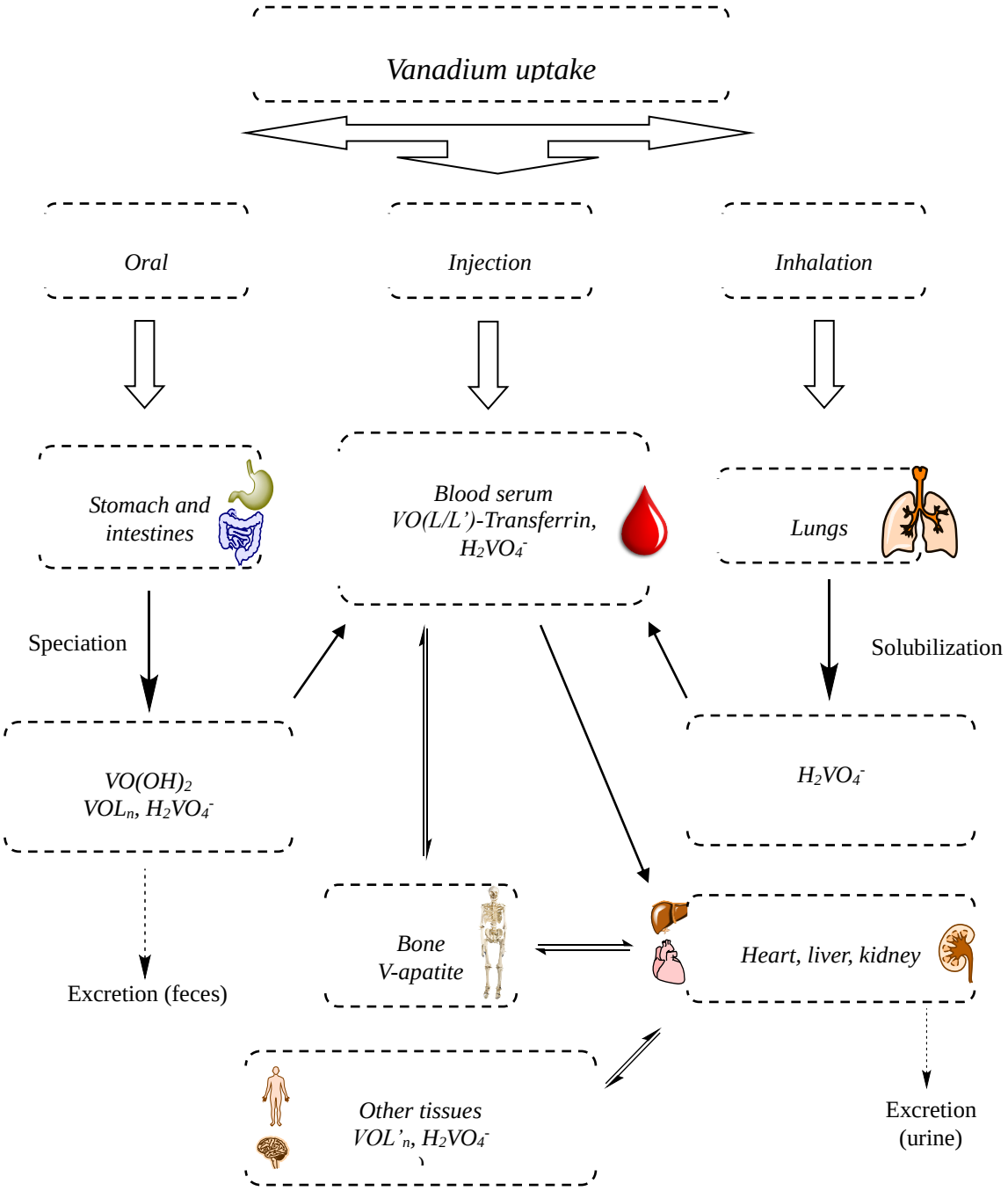

Figure 1.38 – Schematic representation of the uptake, distribution and excretion of vanadium and vanadium compounds in the organism. Adapted from [198] Organic and inorganic V^{IV} and V^{V} complexes are administered mainly orally or by injection. Inhalation is responsible for the uptake of vanadium oxides such as V_2O_5 as previously described. The absorbed vanadium reaches the blood stream and is subjected to different speciation processes by the interaction with different proteins namely serum transferrin. Finally, vanadium is distributed to the different organs or can be stored in the bones.

Once in the blood, V^{IV} and V^{V} are able to interconvert the respective oxidation state interacting with a great range of bio-ligands of low molecular mass, like citrate, lactate, phosphate, and bio-ligands of high molecular mass, such as serum transferrin, albumin and immunoglobulins, which provide a significant stability to the ion. In fact, it is known that free $V^{IV}O^{2+}$ is almost inexistent

because it precipitates as $V^{IV}O(OH)_2$ but $V^{IV}O$-compounds are quite stable; bio-ligands also allow the presence of $[V^{V}O]^{3+}$ and $[V^{V}O_2]^{+}$ compounds in addition to the existing $H_2VO_4^-$ species.[196,198,223]

Remarkably, vanadium can also be absorbed by red blood cells; V^{V} is then reduced to V^{IV} by glutathione binding to hemoglobin.[196,198,224] The uptake of vanadium by the cells is an essential step in this process and different possibilities for such uptake have been proposed including the use of phosphate channels and the use of the transferrin receptors.[196,198]

These aspects are important to be properly characterized in order to design useful drugs. Briefly, a general overview on the therapeutic action of vanadium in different areas will be given in the next sections.

1.3.3.2.1 – Anti-diabetic activity

Diabetes mellitus, usually referred as diabetes, is wide spread in the world affecting both developed and developing countries, with a total of 346 million patients but with a significant percentage of deaths occurring in the poorest regions.[225] Symptoms associated with diabetes have been described since ancient times but significant advances in the correct characterization of the disease just took place in the 19th and 20th centuries.[226]

Diabetes is a disorder associated with a deregulation of glucose and fatty acids metabolism, as consequence of an inexistent or deficient insulin production by the β-cells of the Langerhans' islets in the pancreas or an inappropriate response to this hormone. In normal conditions, insulin stimulates the glucose uptake by the cells (inhibiting simultaneously the degradation of glycogen in a process known as glycogenolysis) and inhibits an excessive lipolysis (formation of glycerol and free fatty acids, lately converted into ketoacids). Consequently, malfunctions of insulin will be responsible for hyperglycemia (high blood glucose levels depriving the normal use of glucose by the cells) raising also the occurrence of ketoacidosis responsible for blindness, vascular complications and limb amputation among other diseases.[198,204,205,209,227,228,229]

There are two main types of diabetes: Type 1 and Type 2. The first one is related to the non-production or basal production of insulin in the β-cells. The second one is doubtless the most common type (almost of 90% of the world registered cases) and it is characterized by the normal production of insulin but an inadequate response of the insulin receptors.[198,205,209,230,231]

From a molecular point of view, the transmembranar insulin receptor – existing in several types of cells such as muscle and fat cells – is a tetramer α2β2 acting as a tyrosine kinase (two extracellular subunits α and two intracellular subunits β). The binding of insulin to the subunits α is responsible for the autophosphorylation of tyrosine residues of subunits β. The described phosphorylation initiates a signaling cascade pathway culminating in the cellular absorption of glucose. The subunits β are able to phosphorylate some other proteins designated insulin receptor substrates (IRSs) such as phosphatidylinositol 3-kinase5 and protein kinase B that, ultimately, are

responsible for the activation of the intracellular glucose transporter (GLUT4). In both types of diabetes, the problems with insulin lead to the interruption of the described signaling cascade pathway; in fact, if insulin is not present, the phosphorylation of the subunits β of the insulin receptor is counteracted by a protein tyrosine phosphatase (PTP1B) which, preventing the phosphorylation of the IRSs, prevents also the normal activity of the GLUT4 transporter. A simplified representation of both mechanisms – normal and abnormal function of insulin – is depicted in Figure 1.39.[198,205,232]

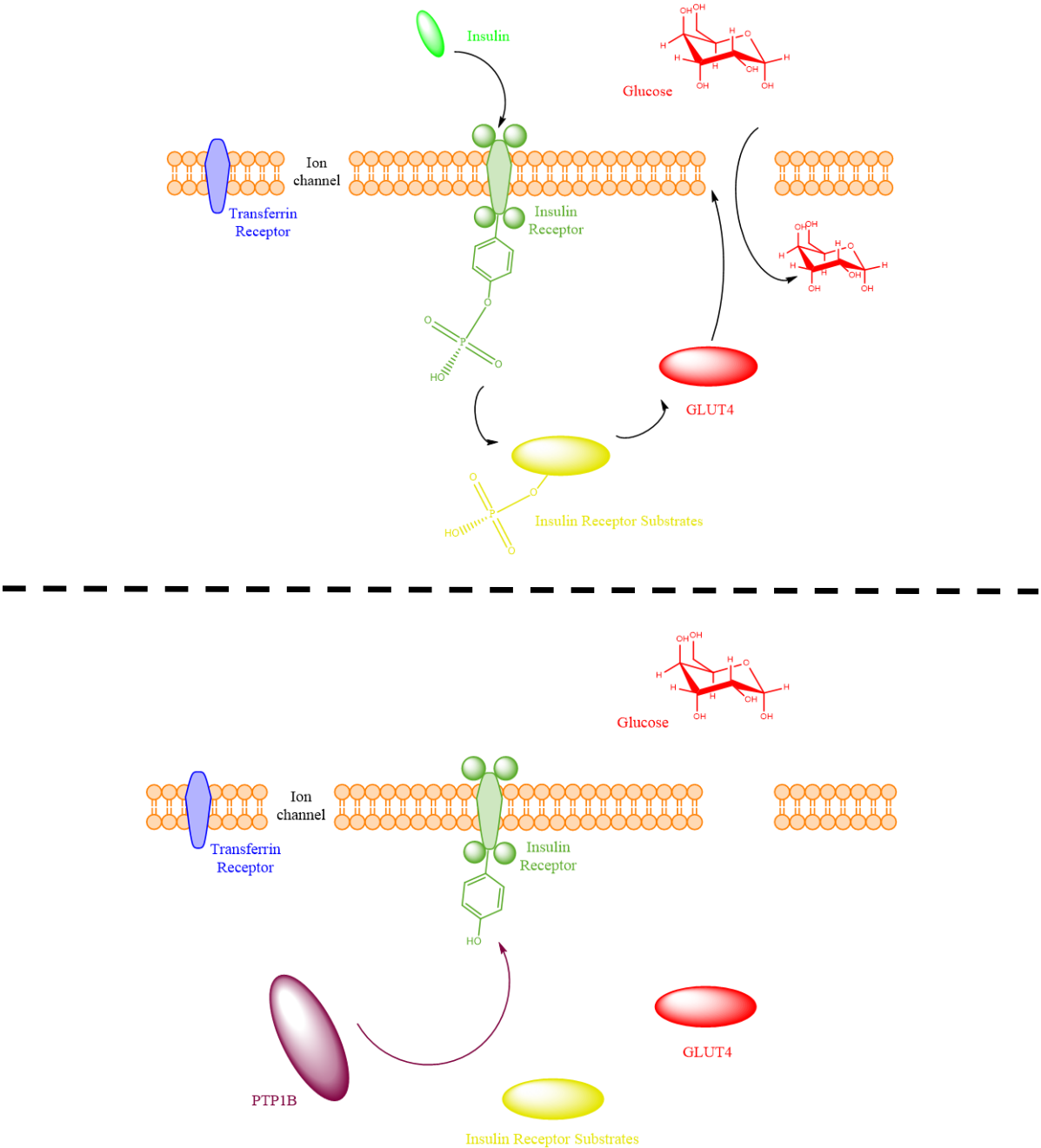

Figure 1.39 – Schematic representation of the molecular mechanisms responsible for the normal glucose uptake (top) or the absence of the glucose uptake (bottom). Adapted from [198,205] The presence of insulin or an adequate insulin response is vital for the correct cellular glucose uptake by controlling a complex signaling cascade pathway responsible for the activation of the glucose transporter.

Following the normal procedures in drug design processes, the knowledge of the molecular mechanisms involved in the glucose uptake and metabolism is an invaluable contribution for the development of useful drugs. As example, sitagliptin phosphate was developed as an oral and bioavailable drug for the treatment of diabetes type 2 by inhibiting dipeptidyl peptidase IV which, in turn, is responsible for the inactivation of incretin hormones.[233]

Adopting a similar thinking, vanadium has also been tested as a potential drug against diabetes. As mentioned in the first section of this chapter, the first experiments with vanadium go back to the last years of the 19th century. A more systematic approach was followed in 1970s and 1980s where it has been postulated the efficiency of inorganic vanadium (V^{IV} and V^{V}) compounds in different processes related to diabetes; studies with streptozotocin-induced diabetic rats were particularly important for such findings.[205,234,235]

That was the beginning of the study of vanadium as an insulin-mimetic agent or, more accurately defined, as an insulin-enhancing agent. Looking again to the molecular mechanism of glucose uptake, it is believed that vanadium is able to inhibit PTP1B due to the vanadate(V)-phosphate analogy as previously indicated. Such inhibition allows the successive phosphorylation steps responsible for the activation of GLUT4 even in the absence (or low response) of insulin (Figure 1.40).[198,205,207,209]

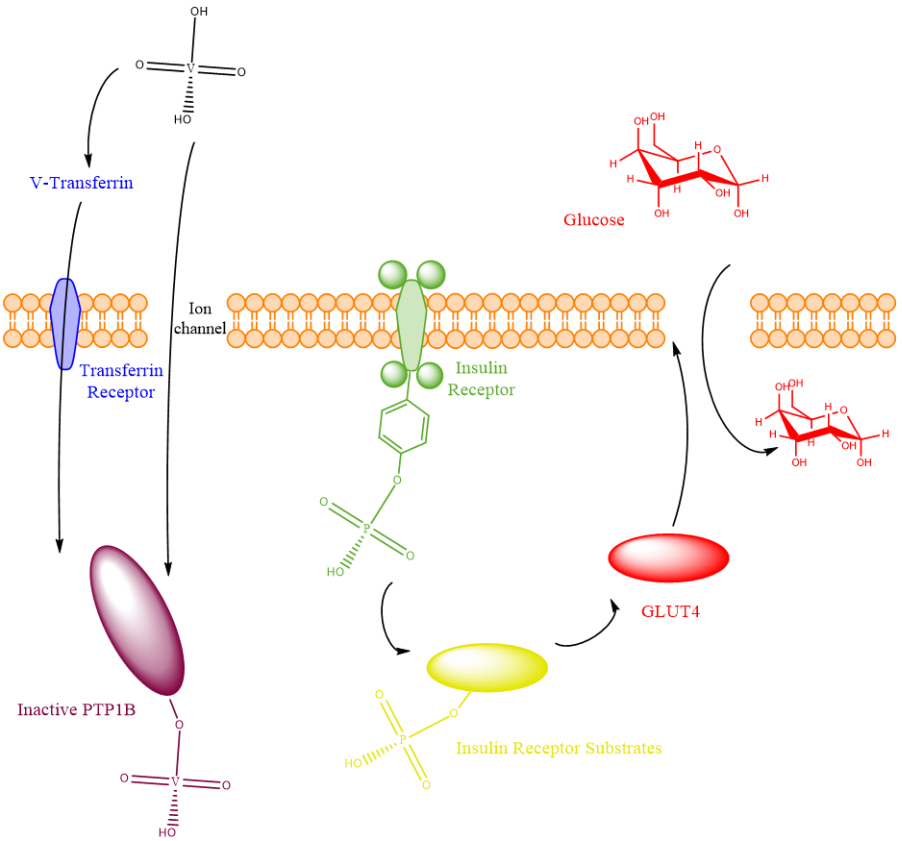

Figure 1.40 – Schematic representation of the action of vanadium as insulin-enhancing agent. Adapted from [198,205] The vanadate could enter in the cells using different strategies – namely using ion channels or the transferrin/transferrin receptor system if bound to that serum protein – being available to binding to the active site of PTP1B. Hence, even without insulin, the phosphatase is deactivated and the phosphorylation signaling cascade results in the activation of GLUT4.

Vanadium compounds with organic ligands have also been studied in order to overcome the low oral absorption rate of the inorganic salts, forming $V^{IV}O(carrier)_n$ complexes. The addition of such organic ligands – maltol and pyridine derivatives are notable examples – allows a better pharmacokinetic profile of the complex improving different characteristics including the stability (namely in different pH values), the recognition of the complex by the cells due to the presence of a specific ligand and the decrease of toxicity.[198,205,236,237] These complexes can also suffer different speciation processes in the blood originating different compounds or inorganic vanadium.[198]

Several tests were carried out with animals and humans using a great range of vanadium complexes and promising results were obtained namely with bis(maltolato)oxovanadium(IV) and bis(ethylmaltolato)oxidovanadium(IV) – BMOV and BEOV, respectively. BEOV has been inclusively used in clinical tests (phases I and II).[198,205,238 and references therein]

Despite the positive results obtained, possible side effects of vanadium-based drugs should be taken into account. Inhibition of different phosphatases and generation of ROS – with the concomitant deregulation of several cell functions – are important putative drawbacks in this process. Moreover, a properly characterization of all speciation processes that a vanadium-based drug can suffer is also required. Therefore, more research work should be conducted in order to design useful vanadium-related insulin-enhancing agents.[198]

1.3.3.2.2 – Other therapeutic actions

The use of vanadium and vanadium complexes has been proposed for the treatment of other pathologies than diabetes. Anti-cancer, anti-parasitic, anti-viral, anti-bacterial and anti-fungal are some of most relevant cases.[198,205,207]

Being one of the most studied diseases, it seems quite natural that some approaches using vanadium have been tried in different types of cancer.[239,240,241,242] The mechanisms by which vanadium acts are not clear but it is admitted that such compounds are able to prevent DNA replication inducing the apoptosis of the cancerous cells. This process mimics the action of cis-platin. Metvan, containing V^{IV} and 1,10-phenanthroline, is a notable example of a complex with anti-tumoral properties in a great range of cancers (breast, ovarian, prostate and testicular) without significant toxicity.[198,205,207,240]

Regarding anti-parasitic action of vanadium complexes, particular attention has been given to trypanosomiasis, leishmaniasis and amoebiasis causing by the protozoa *Trypanosoma cruzi*, *Leishmania* spp. and *Entamoeba histolytica*, respectively.[243]

1.4 – X-ray crystallography

1.4.1 – General concepts and historical perspective

A general overview of the previous chapters allows depicts the importance of proteins in different processes of drug design projects. However, the biological role of these molecules is beyond that. The transport of oxygen, the regulation of different signaling pathways and the activity of many enzymes are three illustrative examples of such importance.

Therefore, different fields have been developed in order to improve the proper characterization of such biomolecules particularly in the last two centuries. Biochemistry and molecular biology – with different techniques and procedures – are two notable examples of that. Not surprisingly, soon after the beginning of a deeper study of proteins, the scientific community felt the need to determine their three-dimensional structure to a better understanding of the respective function and, by that, of the biological processes in which they participate. This was the basis for the development of structural biology, which is used to characterize not only proteins but also DNA and RNA. Usually, the groups working in projects with a structural biology component argue that "structure is function" and this short sentence perfectly reflects reality.

Keeping the described scenario in mind, a relevant question arises: how to obtain the three-dimensional structure of proteins and other biomolecules? Three major techniques are available for such purpose: cryo Electron Microscopy (cryo-EM), Nuclear Magnetic Resonance (NMR) and X-ray crystallography. Although a growing number of structures have been determined by cryo-EM and NMR in the recent years, X-ray crystallography is still the main technique applied for the structure determination of macro-biomolecules. Similarly, the study of protein-ligand interactions is also widely addressed by X-ray crystallography being one of the most used techniques in drug design processes. The advances in molecular biology, the emergence of more potent synchrotrons, the development of more sophisticated software (data collection, structure resolution and structure refinement) and more powerful computational resources can be cited as factors contributing to the progress registered in X-ray crystallography.

The supremacy of X-ray crystallography over the two other techniques is clear when the number of PDB entries is analyzed. Currently (July 2016), 120879 structures are deposited in the PDB from which 108012 structures were determined by X-ray crystallography, corresponding to 89% of the total number of entries.[244] It is also interesting to observe that, in September 2011, only 75694 structures were deposited meaning that more than 40000 structures were made available during the time course of this Thesis and proving the dynamism of the structural biology field.

The year of 2014 was proclaimed as the International Year of Crystallography by UNESCO, celebrating the 100th anniversaries of the attribution of Nobel Prizes to Max von Laue (1914), William

H. Bragg and William L. Bragg (1915), the 50th anniversary of the Nobel Prize to Dorothy Hodgkin and the 400 years of Kepler's observation of symmetry in ice crystals. Multiple commemorative events were organized in several points of the globe and this is one more example of the referred dynamism of the community. Portugal was not an exception in this movement and the three major structural biology groups, held in Caparica, Oeiras and Porto were involved in different initiatives to promote the importance of the technique; as example, the FCT/UNL group organized a series of conferences to celebrate the International Year of Crystallography including the presence of three Nobel Prize winners: Robert Huber (Chemistry, 1988), Ada Yonath (Chemistry, 2009) and Brian Kobilka (Chemistry, 2012).

From a historical point of view, an outstanding moment took place in 1895 when the German scientist Wilhelm Conrad Röntgen discovered a new type of electromagnetic radiation. He named it "X-rays" due to its unknown characteristics and it is still today the more recognized nomenclature worldwide, although the term "Röntgen radiation" is also used. The first years of the 20th century were dedicated to the elucidation of the nature of X-rays; in 1912, Max von Laue, Walter Friedrich and Paul Knipping confirmed that X-rays are electromagnetic radiation, providing also the first demonstration of X-ray diffraction from a crystal lattice. Shortly after, the Braggs – father (William Henry) and son (William Lawrence) – were able to postulate the famous "Bragg's Law", in addition to the determination of the first structures of some salts such as sodium chloride. In the following decades, a growing number of inorganic, organic and mineral structures were solved; the work conducted by Dorothy Hodgkin is particularly relevant determining three-dimensional structures of different molecules such as vitamin B12 and penicillin.[245,246,247,248]

The first structures of biomolecules were proposed only in the 1950s. Particularly known, the famous "double helix" structure of DNA was presented in 1953 by James Watson and Francis Crick. Concerning proteins, in later 1950s/early 1960s, John Kendrew and Max Perutz were pioneers, presenting the structures of sperm whale myoglobin and horse hemoglobin, respectively. Soon after, other protein structures were released such as lysozyme and insulin, thanks to the work of David C. Phillips and Dorothy Hodgkin, respectively. Over the decades, several others structures were determined including some complex membrane proteins and assemblies such as the photosynthetic reaction centre and the ribosome.[245,246,247,248]

The importance of X-ray crystallography is clearly proved by the considerable number of Nobel Prizes attributed to findings related to the methodology including several prizes awarded to works related to structural biology (Table 1.8). Such importance is also understandable by the words of different remarkable crystallographers.[249]

Table 1.8 – List of Nobel Prizes winners associated with X-ray crystallography. The information presented was retired from the official website of the Nobel Prize (http://www.nobelprize.org/).

Year/Nobel Prize	Winner(s)	Scientific achievements
1901, Physics	W. C. Röntgen	Discovery of X-rays
1914, Physics	M. Von Laue	Diffraction of X-rays by crystals
1915, Physics	W. H. Bragg and W. L. Bragg	Use of X-rays to determine crystal structure
1917, Physics	C. G. Barkla	Discovery of the characteristic Röntgen radiation of the elements
1929, Physics	L.-V. de Broglie	The wave nature of the electron
1936, Chemistry	P. J. W. Debye	Knowledge of molecular structure through his investigations on dipole moments and on the diffraction of X-rays and electrons in gases
1937, Physics	C. J. Davisson and G. Thompson	Diffraction of electrons by crystals
1946, Chemistry	J. B. Sumner	Discovery that enzymes can be crystallized
1954, Chemistry	L. C. Pauling	Research into the nature of the chemical bond and its application to the elucidation of the structure of complex substances
1962, Chemistry	J. C. Kendrew and M. Perutz	Studies of the structures of globular proteins
1962, Physiology or Medicine	F. Crick, J. Watson and M. Wilkins	The helical structure of DNA
1964, Chemistry	D. Hodgkin	Structure of many biochemical substances including Vitamin B12
1972, Chemistry	C. B. Anfinsen	Folding of protein chains
1976, Chemistry	W. N. Lipscomb	Structure of boranes
1982, Chemistry	A. Klug	Development of crystallographic electron microscopy and discovery of the structure of biologically important nucleic acid-protein complexes
1985, Chemistry	H. Hauptman and J. Karle	Development of direct methods for the determination of crystal structures
1988, Chemistry	J. Deisenhofer, R. Huber and H. Michel	Determination of the three-dimensional structure of a photosynthetic reaction centre
1991, Physics	P.-G. de Gennes	Methods of discovering order in simple systems can be applied to polymers and liquid crystals
1992, Physics	G. Charpak	Discovery of the multi wire proportional chamber
1994, Physics	C. Shull and N. Brockhouse	Neutron diffraction
1996, Chemistry	R.Curl, H. Kroto and R. Smalley	Discovery of the fullerene form of carbon
1997, Chemistry	P. D. Boyer, J. E. Walker and J. C. Skou	Elucidation of the enzymatic mechanism underlying the synthesis of adenosine triphosphate (ATP) and discovery of an ion-transporting enzyme
2003, Chemistry	P. Agre and R. MacKinnon	Discoveries concerning channels in cell membranes
2006, Chemistry	R. D. Kornberg	Studies of the molecular basis of eukaryotic transcription
2009, Chemistry	V. Ramakrishnan, T. A. Steitz and A. E. Yonath	Studies of the structure and function of the ribosome
2010, Physics	A. Geim and K. Novoselov	Groundbreaking experiments regarding the two-dimensional material graphene
2011, Chemistry	D. Shechtman	Discovery of quasicrystals
2012, Chemistry	R. J. Lefkowitz and B. K. Kobilka	Studies of G-protein-coupled receptors
2013, Chemistry	M. Karplus, M. Levitt and A. Warshel	Development of multiscale models for complex chemical systems

Following the growing number of solved structures, it becomes necessary to create useful databases to organize such information. In 1971, Protein Data Bank (PDB) was created with 7 structures. Since 2003, three institutions are responsible for the maintenance of the world wide PDB: Research Collaboratory for Structural Bioinformatics (RCSB-PDB, San Diego, USA), European Bioinformatics Institute (PDBe, Hinxton, United Kingdom) and Institute for Protein Research (PDBj, Osaka, Japan). [250,251]

The use of X-rays in structural investigations is justified by their wavelength – 0.1 to 100Å (0.01 to 10 nm) – in the same range as interatomic bond distances (approximately 1Å). If properly organized into an ordered crystal, molecules are able to diffract the incident X-rays producing diffraction patterns. From the obtained diffraction patterns, using Fourier methods and solving the Phase Problem, it is possible to determine the electron density maps and the initial protein model. This model is progressively refined until a final model is obtained, which is validated prior to its deposition in the PDB.[251,252,253,254,255,256,257] Figure 1.41 summarizes the main steps involved in the determination of a protein structure by X-ray crystallography which will be covered in the next sections.

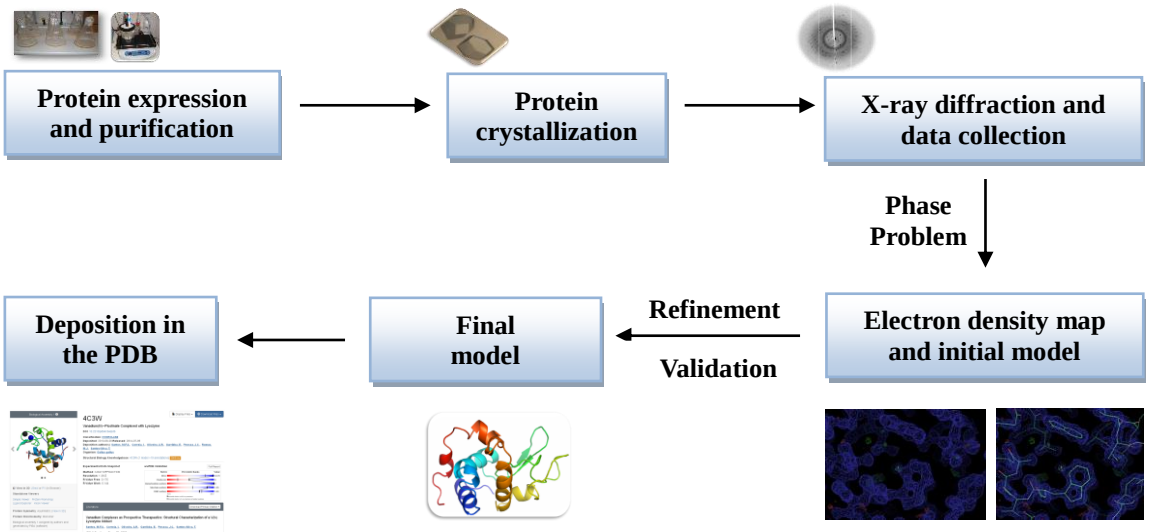

Figure 1.41 – Schematic overview of the major steps involved in the determination of a protein structure by X-ray crystallography. Adapted from [253] Very often, prior to start the crystallization trials, it is necessary to express and purify the protein of interest using different molecular biology and biochemistry procedures. After obtaining suitable crystals for the x-ray diffraction experiment – usually the limiting step in crystallography – electron density maps are obtained which are used to build the initial model. This preliminary model is then refined several times and validated leading to the final model which is ready to be deposited in the PDB.

1.4.2 – Crystals and protein crystallization

As previously mentioned, X-rays can be diffracted by protein molecules but the diffraction originated by a unique molecule is very weak. This limitation is overcome by the use of crystals, which allows to detect a measurable diffraction signal.

A crystal can be defined as an ordered solid entity, periodically repeated in the three dimensional space. Protein crystals can have different sizes (usually from 0.03 to 0.5 mm depending a lot on the protein) and shapes. Moreover, these crystals are fragile due to the high solvent content (30-70% of the total volume).[251,252,256]

Each crystal is constituted by the repetition of its simplest units called unit cells. In the words of Bernhard Rupp, the unit cell is defined as "the transitionally repeating building blocks of a crystal comprising a unit lattice filled with motifs according to the space group symmetry of the crystal" meaning that the unit cell originates the crystalline lattice (corresponding to the position of each molecule in the crystal) by translation operations. Associated with the unit cell concept, a second is defined: the asymmetric unit which is, again in the words of Bernhard Rupp, "the smallest part of a crystal structure from which upon application of space group symmetry operations the complete unit cell of the crystal is generated". Figure 1.42 illustrates the relation between asymmetric unit, unit cell and crystalline lattice. Importantly, such definition describes also the concept of space group: the set of symmetry operations by which the unit cell is generated from the asymmetric unit.[251,252]

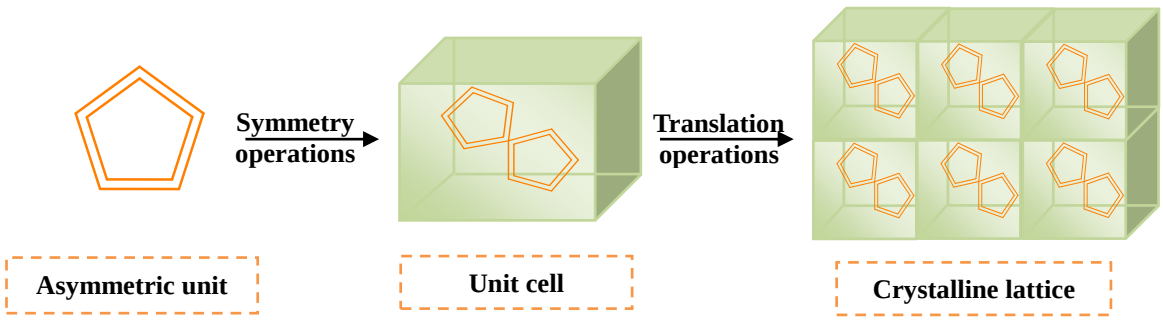

Figure 1.42 – Schematic representation of the concepts of asymmetric unit, unit cell and crystalline lattice. Adapted from [252] For details, see the text above.

The unit cell is characterized by six parameters designated as unit cell constants: the lengths of the three axes (a, b and c) and the angles formed between these same axes (α, β and γ) as schematized in Figure 1.43.[251,252]

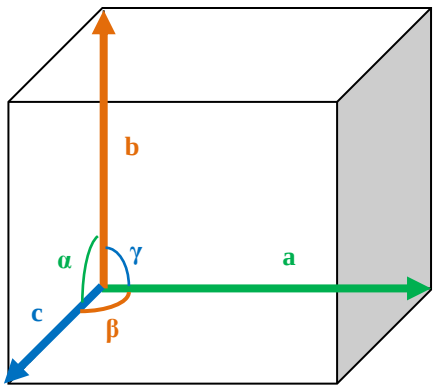

Figure 1.43 – Schematic representation of the unit cell constants. Adapted from [252] The unit cell is characterized by three vectors – a, b and c – and by three angles – α (between b and c), β (between a and c) and γ (between a and b).

According to the unit cell constants, seven different crystal systems can be defined. There are also four different types of unit cells (Figure 1.44) leading to the existence of the 14 so-called Bravais lattices. Such lattices are the basis of 230 different space groups but this number is reduced to 65 in proteins due to their chiral nature (mirror planes and inversion centers are not allowed).[251,252,256,258] Table 1.9 summarizes the existing crystal systems, Bravais lattices and space groups.

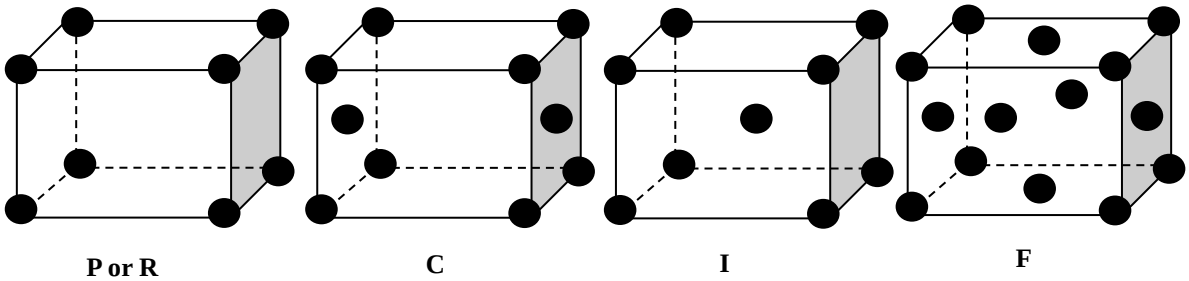

Figure 1.44 – Schematic representation of the unit cell types. The unit cells can be divided into four different types: primitive (P or R), face-centered on a single face (C), body-centered (I) and face-centered on the six faces (F).

Table 1.9 – List of crystal systems, Bravais lattices and space groups allowed for proteins. The variation of unit cells constants leads to different crystal systems which, combined with the four possible unit cell types, originate the 14 Bravais lattices.

Crystal system	Bravais lattice	Space group
Triclinic $a \neq b \neq c$ $\alpha \neq \beta \neq \gamma \neq 90^o$	P	P1
Monoclinic $a \neq b \neq c$ $\alpha = \gamma = 90^o$ $\beta \neq 90^o$	P and C	P2, $P2_1$, C2
Orthorhombic $a \neq b \neq c$ $\alpha = \beta = \gamma = 90^o$	P, C, F and I	P222, $P2_12_12_1$, $P2_12_12$, $P222_1$, C222, $C222_1$, F222 I222, $I2_12_12_1$
Tetragonal $a = b \neq c$ $\alpha = \beta = \gamma = 90^o$	P and I	P4, $P4_1$, $P4_2$, $P4_3$, P422, $P42_12$, $P4_122$, $P4_12_12$, $P4_222$, $P4_22_12$, $P4_32_12$, $P4_322$, I4, $I4_1$, $I4_122$, I422
Hexagonal $a = b \neq c$ $\alpha = \beta = 90^o$ $\gamma = 120^o$	P	P6, $P6_5$, $P6_1$, $P6_4$, $P6_3$,$P6_2$, P622, $P6_122$, $P6_222$, $P6_322$, $P6_422$, $P6_522$
Trigonal $a = b \neq c$; $\alpha = \beta = 90^o$;$\gamma = 120^o$ or **Rhombohedral** $a = b = c$; $\alpha = \beta = \gamma \neq 90^o$	P or R	P3, $P3_1$, $P3_2$, P312, P321, $P3_121$, $P3_112$, $P3_221$, $P3_212$ R3, R32
Cubic $a = b = c$ $\alpha = \beta = \gamma = 90^o$	P, I and F	P23, $P2_13$, P432, $P4_132$, $P4_232$, $P4_332$ I23, $I2_13$, I432, $I4_132$ F23, F432, $F4_132$,

The bottleneck of X-ray crystallography is, still today, obtaining suitable crystals for a diffraction experiment. In fact, crystallization is often the more time-consuming step in the pipeline illustrated in Figure 1.41 and without good diffracting crystals is very difficult – if not impossible – to solve the structure.

Different methodologies are used in protein crystallization but all of them require the achievement of a supersaturated state of the protein. In other words, some procedures must be applied in order to decrease the solubility of the protein usually by adding precipitant agents to the protein solution: ionic salts or organic polymers (polyethylene glycol molecules, PEGs, with different molecular sizes are often used). The analysis of the crystallization phase diagram is useful to better understand the crystallization process (Figure 1.45). Crystallization occurs in two distinct stages – nucleation and growth – which take place in two different supersaturated zones (labile and metastable zone, respectively).[251,252,259,260,261,262,263]

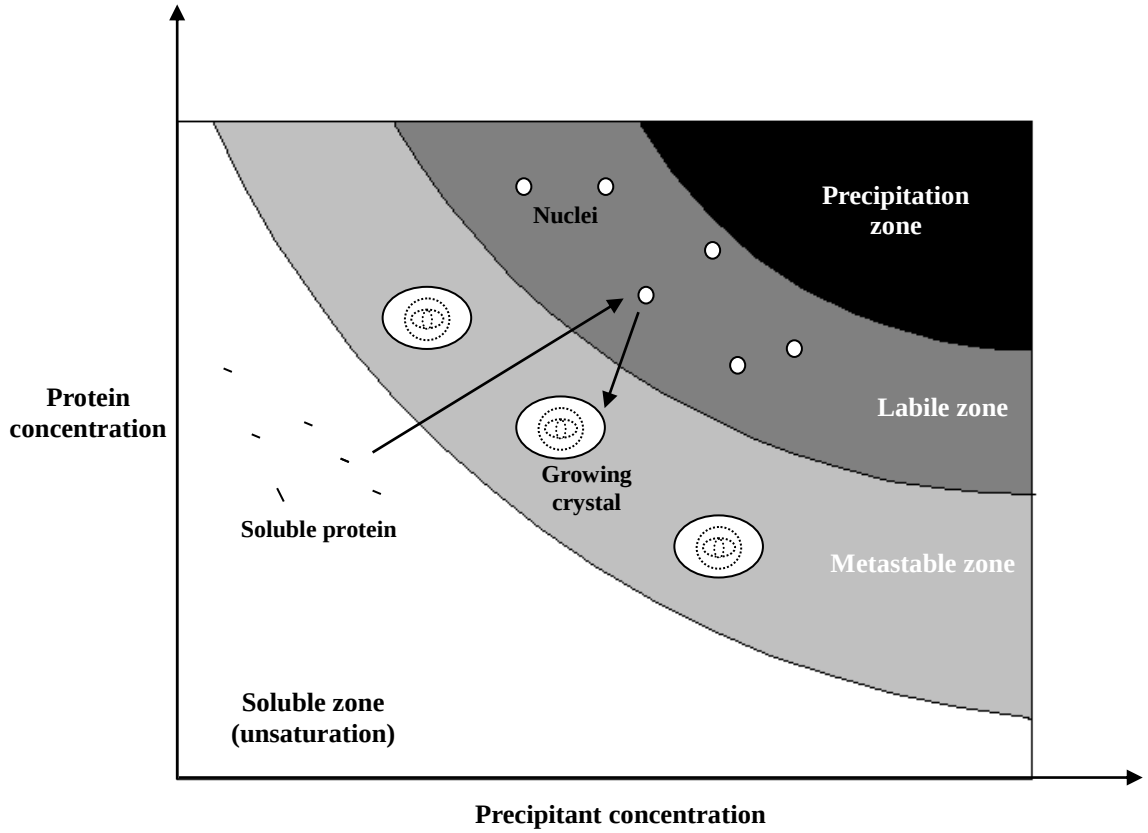

Figure 1.45 – Crystallization phase diagram. Adapted from [263] The diagram is divided into two major zones: soluble (white) and supersaturated (colored). The supersaturated zone is subdivided into three zones: metastable (light grey), labile (dark grey) and precipitation (black). If the ideal concentrations of protein and precipitant are found, crystallization can take place in a two-step process: nucleation and growth.
In the described situation, the soluble protein molecules (small lines) will move from the soluble zone into the labile zone where small clusters (small circles) are formed (nucleation). These nuclei will slowly and orderly growth to form the crystals (bigger dotted circles) essentially in the metastable zone. If the ideal conditions are not achieved, it is possible to enter into the precipitation zone where a non-diffracting amorphous aggregate is formed.

The most common crystallization procedure is the vapor diffusion method in which the slowly solvent evaporation is responsible for the supersaturated state. In a closed reservoir, a variable size drop (protein/precipitant) is equilibrated against a precipitant solution meaning that the precipitant is more concentrated in the reservoir than in the drop. An equilibrium is then established promoting the water evaporation from the drop, which increases the concentration of the precipitant to the same value as in the reservoir. Concomitantly, the concentration of protein in the drop is also increased, which might be enough to reach a supersaturated state where crystallization can occur. The vapor diffusion method can be performed in two distinct techniques (Figure 1.46): hanging-drop (the protein/precipitant drop is placed in a siliconized cover slip) and sitting drop (the drop is placed in a support/microbridge inside the reservoir).[251,252,255,259]

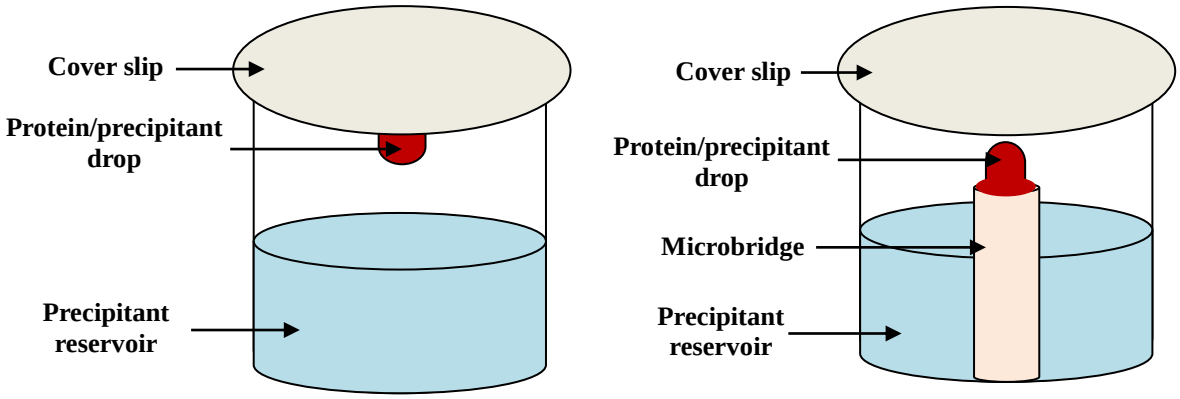

Figure 1.46 – Schematic representation of the vapor diffusion method: hanging-drop (left) and sitting-drop (right) techniques. According the method, the protein/precipitant drop is placed in the cover slip or in a microbridge (hanging and sitting-drop, respectively). This slight variation could be enough to obtain suitable crystals by varying the thermodynamic and kinetic parameters.

As largely referred, obtaining a good diffracting crystal is very often a time-consuming step due to the multiple parameters that influence such process. As example, the protein construct itself can influence the ability for a given protein to crystallize or not. Protein concentration, purity, freshness and conformation are other important parameters that should be taken into account. Other factors not directly related with the protein are also vital for the success of the experience: the type of precipitant and buffer used as well as the pH and temperature range tested are illustrative examples. Screening assays, compassing a considerable amount of different conditions, are often used in the first trials to determine the proper crystallization conditions.[251]

Different approaches have been followed in order to increase the success rate of protein crystallization.[264,265] The use of ionic liquids as additives is one of the possibilities.[266] The introduction of crystallization robots for automated crystallization was also an innovative step allowing to test a great variety of conditions with a small amount of protein.[251,264]

1.4.3 – X-ray diffraction and data collection

Once an ordered crystal is obtained, an X-ray diffraction experiment is performed. For that, the X-ray source must be selected. Home-sources, in which the X-rays are produced by shooting a metal (usually cupper or molybdenum) with an accelerated beam of electrons, have been developed over the years allowing a progressively more efficient data collection. However, the use of synchrotron radiation was one of the decisive steps to the *boom* verified in X-ray crystallography, producing a highly intense and bright X-ray beam (improving the data quality and decreasing the acquisition time) and also allowing to select the desired wavelength which is indispensable for solving some crystal structures, as further explained. Several synchrotron facilities are worldwide installed in Europe, North and South America, Asia and Oceania (Figure 1.47).[251,252,256,267]

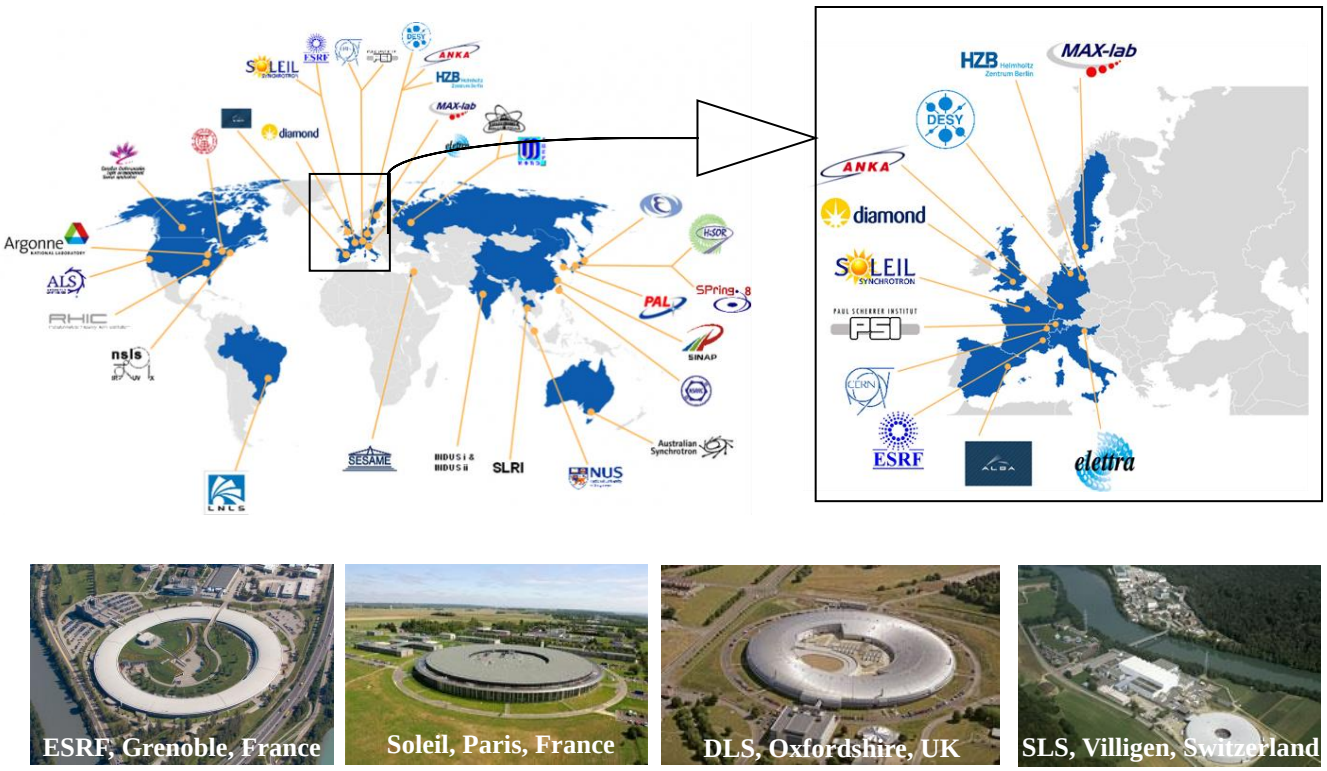

Figure 1.47 – Synchrotron facilities in the world. Adapted from http://www.veqter.co.uk/residual-stress-measurement/synchrotron-diffraction (top) and http://www.lightsources.org/ (bottom) In the top, the distribution of the synchrotrons facilities in the world is shown (in the insert, a more detailed vision of the Europe is presented). In the bottom, four representative European synchrotrons facilities are depicted: European Synchrotron Radiation Facility (ESRF), Soleil Synchrotron, Diamond Light Source (DLS) and Swiss Light Source (SLS). Different data collection experiments – covering the objectives of this Thesis – were performed in all these four facilities.

Keeping in mind the already mentioned fragile nature of protein crystals, some procedures are normally adopted prior the data collection. Usually, after growing, the crystals are transferred to a harvesting buffer (similar to the precipitation solution but with a higher precipitant concentration) in order to minimize/prevent their degradation. Also importantly, the crystals should be preserved in an adequate cryo-protector solution prior to data collection. Normally, the cryo-protector solution is

prepared by adding a given concentration of glycerol (20 to 30% in most of the cases) to the harvesting buffer but different PEGs and sugars can be also used. The use of a cryo-protector avoids the formation of ice in the solvent channels of the crystal during the data collection carried at cryogenic temperatures (around 100K). Cryo-crystallography techniques significantly have contributed for the development of the field by minimizing the radiation damages suffered by the crystals (particularly severe in very intense synchrotron beams) due to the formation of free radicals capable of disrupting the internal order of the crystal. This explains the reason why crystals are normally flash-cooled in liquid nitrogen slowing down the diffusion of such species.[251,252,256,268]

In a diffraction experiment, the X-ray beam reaches the crystal interacting with the protein electrons. The X-rays are then scattered by these electrons originating a diffraction pattern with different reflections (also designed by spots) recorded in an adequate detector. The data collection can be considered as the last experimental step in a crystallographic study, immediately followed by an intense computational work. Therefore, special attention should be given to it because a defective data collection will compromise the success of the protein structure determination; an appropriate strategy is vital and different parameters should be taken into account including some intrinsic features of the crystal (namely the space group) but also some technical decisions such as the distance between the crystal and the detector, the time of exposure and the oscillation angle.

As strongly indicated before, getting good crystals is the principal bottleneck of X-ray crystallography. But, what is a good crystal? Much more important than the morphological aspect, a good crystal is characterized by its diffracting ability. In fact, not all crystals are able to diffract the X-rays. About one century ago, William Henry Bragg and William Lawrence Bragg investigated such theme concluding that diffraction only occurs in specific conditions. Assuming the existence of imaginary planes (*hkl* planes) in the crystal lattice, their work is summarized in the so-called "Bragg's Law" (Equation 1.1):

$$n\lambda = 2d_{hkl}.\sin\theta \qquad \textbf{Equation 1.1}$$

In this equation, n is an integer, λ is the wavelength of the incident X-ray, d_{hkl} is the distance between the planes in the crystal lattice and θ is the angle between the incident wave and the crystal planes (Figure 1.48). In other words, diffraction occurs when the wavelength of the incident beam is proportional to the distance between planes in the crystal lattice: constructive interference. If the "Bragg's Law" is not obeyed, no diffraction is produced (destructive interference).[251,252] The difference between constructive and destructive interference is shown in Figure 1.49.

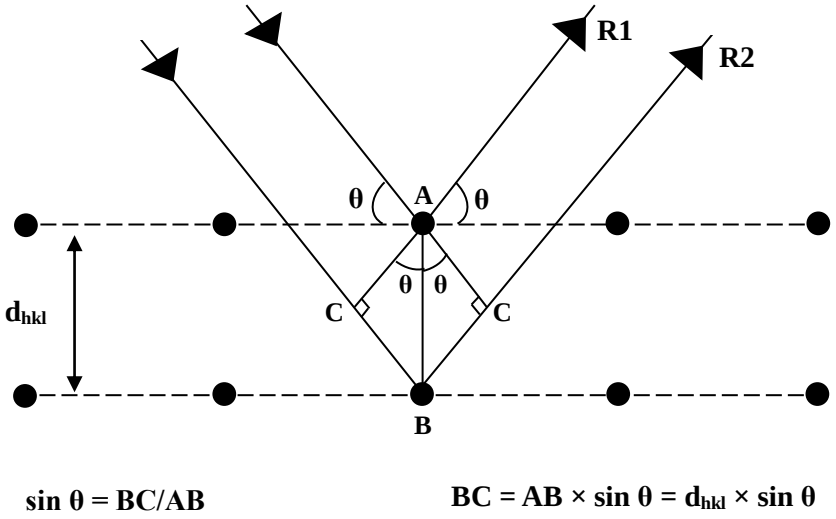

Figure 1.48 – Geometric representation of the "Bragg's Law". Adapted from [252] Using this geometric and trigonometric approach, it is possible to observe that the wave R2 has an identical distance to wave R1 plus the CB and BC (2BC) distance; the incidence angle θ in similar to the one (CAB) verified in the right triangle ABC as the distance d_{hkl} (AB) is perpendicular to the plane. Applying some trigonometric formulas, the sine of the angle θ is equal to BC/AB (opposite side/hypotenuse) meaning that $2BC = 2.d_{hkl}.\sin\theta$. If this value is proportional to the incident wavelength beam (nλ), the "Bragg's Law" is obeyed and a reflection (or spot) will be recorded.

The d_{hkl} distances are closely related to the resolution obtained in a diffraction experiment: a higher resolution is observed with small interplanar distances. Also importantly, the crystal is rotated during the diffraction experiment in order to test all possible sets of planes and assuring that all possible reflections are included in the resulting diffraction pattern. The recorded reflections are located in the so-called reciprocal space according the respective hkl indices (Miller indices). Conversely, the real space corresponds to the crystal itself and each atom is placed in the unit cell according x,y,z coordinates meaning that large unit cells will produce small reciprocal cells and vice-versa.[251,252]

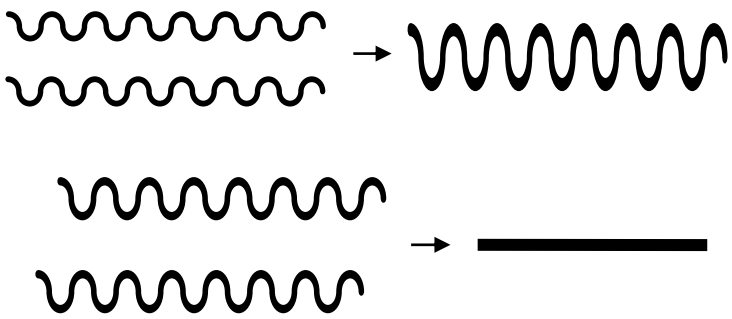

Figure 1.49 – Schematic representation of the constructive and destructive interference (top and bottom, respectively). A wave is characterized by its wavelength, amplitude and phase and two situations can occur. When the waves are in the same phase, a constructive interference is observed and a reflection will be produced. By the contrary, if the waves are out of phase, a destructive interference is originated and no diffraction will be produced.

1.4.4 – The "phase problem" and structure solution

After data collection, a major challenge is presented: how to transform the recorded reflections into a structural model of a protein or, alternatively, how to solve a protein structure? Nowadays, modern algorithms implemented in several crystallographic tools are able to solve a structure almost automatically in a user-friendly interface. However, a lot of mathematics is behind such programs as briefly discussed in the next paragraphs.

As electromagnetic radiation, X-rays can be described as a periodic function characterized by three parameters (wavelength, amplitude and phase) and any periodic function can be represented by a Fourier sum: the structure factor equation (Equation 1.2). The structure factor (F_{hkl}) is a function that describes the X-ray wave responsible for a given reflection in the diffraction pattern being the sum of the diffraction of all the electrons in the unit cell. In this equation, f_j represents the scattering factor of the atom j and x_j, y_j and z_j represent the position of the atom j in the unit cell.

$$F_{hkl} = \sum_{j=1}^{n} f_j e^{2\pi i(hx_j + ky_j + lz_j)} \qquad \textbf{Equation 1.2}$$

The previous equation can be rewritten considering the volume of the unit cell (Equation 1.3) introducing the electron density term –ρ(x,y,z).

$$F_{hkl} = \int_V \rho(x,y,z) e^{2\pi i(hx + ky + lz)} dV \qquad \textbf{Equation 1.3}$$

Applying an inverse Fourier transform to the Equation 1.3, the electron density can be defined according Equation 1.4. This operation allows commuting from the reciprocal space (structure factor) into the real space (electron density) as the Fourier transform describes the relation between an object and its inverse.

$$\rho(x,y,z) = \frac{1}{V} \sum_{hkl} |F_{hkl}| e^{i\varphi_{hkl}} e^{-2\pi i(hx+ky+lz)} \qquad \textbf{Equation 1.4}$$

Analyzing the Equation 1.4, it is possible to observe that electron density depends on amplitude ($|F_{hkl}|$) and phase (φ_{hkl}) of the diffracted wave. Experimentally, it is possible to correlate the intensities of the reflections and the respective structure factor amplitudes: $|F_{hkl}|$ is proportional to the square root of its intensity ($|F_{hkl}|=\sqrt{I}$). However, the phase information is lost during data collection: it is not possible to determine which is the phase angle when the wave reaches the detector. This leads to the so-called "phase problem" in crystallography. Therefore, different methodologies capable of solving the "phase problem" have been designed. Common to all of them, initial phases are estimated allowing a first electron density map.[251,252,269,270]

Nowadays, with the increasing number of structures available in the PDB, the most common method used to overcome the "phase problem" is Molecular Replacement (MR). MR is based in the existence of a related protein structure (usually with, at least, 25% sequence identity) to estimate the initial phases of the protein in study. This approach has two different steps: in the first one (rotation), the model protein is properly orientated into the unit cell of the protein of interest due to the superposition of the respective Patterson maps; in the second one (translation), the orientated model is correctly positioned in the unit cell by comparing the structure factors of both model and protein studied. A potential disadvantage of this method is the introduction of "model bias": the obtained electron density could contain some features related to the known model protein and not to the target protein. Nevertheless, MR is widely used in projects related to drug design.[251,252,255,256]

If the studied protein is completely new and no other related models are available, some other methodologies are used: isomorphous replacement and anomalous scattering are the most important being based on the determination of an atomic substructure. Among the first methods used in the early years of crystallography, Multiple Isomorphous Replacement (MIR) was the most common one. Here, heavy atoms (namely mercury and platinum) are incorporated into crystals and, comparing the difference in the intensities between the native crystal and the isomorphous derivative crystal, initial phases are found. The second methods include Single-wavelength Anomalous Dispersion (SAD) and Multiple-wavelength Anomalous Dispersion (MAD); both methods are based on the fact that elements diffract differently the X-rays at specific wavelengths allowing the determination of the position of such elements and consequently, the protein phases. As suggested by the name, SAD uses only one wavelength and MAD uses more than one wavelength implying that synchrotron radiation is required for a MAD experiment; it should be also emphasized that selenomethionines are often used in anomalous scattering experiments.[251,252,255,256]

1.4.5 – Refinement and structure validation

Once the "phase problem" is solved and the first electron density maps are obtained, it is possible to move to the next step: building, refinement and validation of the model. Nowadays, people from distinct scientific areas use the deposited protein models but often they are not aware that a model is merely an interpretation of the electron density by the crystallographer and it can contain errors – the electron density is effectively a reconstruction of the intensities experimentally obtained with the guessed phases. Thus, an accurate and truthful model is imperative.

At this stage, the model should be built in order to explain satisfactorily the electron density. In other words, during the refinement, the initial solution is characterized by the so-called observed structure factors (F_{obs}); however, the correct interpretation of the electron density (with the concomitant model building) leads to new and improved phases allowing to recalculate the structure

factors (calculated structure factores – F_{calc}).[252,254,255]

Therefore, the refinement could be considered an iterative process in which the differences between F_{obs} and F_{calc} should be progressively minimized. R-factor (or R-work) is a statistic parameter created to quantify the fit between the experimental data and the respective model (Equation 1.5).

$$Rfactor = \frac{\Sigma \left\| F_{obs} \right| - \left| F_{calc} \right\|}{\Sigma \left| F_{obs} \right|} \qquad \textbf{Equation 1.5}$$

High R-factor values (expressed in percentage or decimal fractions) indicate a significant difference between F_{obs} and F_{calc} and a real correct solution has not been achieved: values higher than 50% mean a complete arbitrary solution. With a proper model refinement, the R-factor progressively decreases and it is accepted that values below 20% point for a global satisfactory protein model. Usually, this parameter depends on the resolution of the structure and values of 10 to 15% are often obtained for proteins.[252,254,255]

Almost 25 years ago, in 1992, other parameter has been introduced by Axel Brunger: R_{free}. This is calculated similarly to R-factor but using a small random set of the experimental data (5-10% of the reflections) which is not used in the refinement steps. This parameter is considered a cross-validation tool reflecting an eventual over-interpretation of the electron density. R-factor and R_{free} should have a similar behavior meaning that a decrease of R-factor without the associated decrease of R_{free} indicates the introduction of errors into the model. In acceptable models, usually, R_{free} does not exceed R-factor by more than 5%.[252,254,255]

Other parameters are also taken into account namely the root-mean-square deviations (RMSD) of bond lengths and bond angles which measure the discrepancies between the model and the typical values of these stereochemical parameters.[254,255,271]

Both R-factor and R_{free} uniquely described the global errors found in the model. However, local errors are not detected by them and other parameter is used for such purpose: B factor (also named temperature factor or atomic displacement parameter or Debye-Waller factor). The B factor (expressed in $Å^2$) is related to the thermal vibration of an atom around its position increasing if the atom is not properly located into electron density. Moreover, this value also quantifies the relative mobility of the atoms in the crystal allowing to identify more mobile zones of the protein.[252,254,255]

Virtually, the refinement is an endless procedure. However, when the electron density is greatly explained by the model, this step is considered done. This means that the point at which the refinement is concluded greatly depends on the person who conducts it. The final step in a structure determination by X-ray crystallography, prior the deposition in the PDB, is the validation of the obtained model. Different programs can be used to guarantee that the model is reliable such as Procheck and Molprobity.[272,273] The analysis of the Ramachandran plot is a classical example of the analyses performed at this stage. The plot shows the values of the dihedral angles of the protein

backbone: phi (φ) and psi (ψ) – the angles formed by N, Cα and by Cα, C=O, respectively – which are responsible for the secondary structure of the protein.[254,255]

After the deposition of the final model of a protein in the PDB, the structure can be used not only by crystallographers but also by other scientists with various backgrounds including biochemists, geneticists and biologists. This is, indubitably, one of the reasons by which the validation step should be carefully respected. The final model of a protein can be used for different purposes including the analysis of the overall structure and, very often, the analysis of the active site or other ligand binding sites. As previously mentioned, this is particularly important in the drug design field allowing the identification of new molecules with potential biological or therapeutic applications.

Following the idea expressed in the last sentence, in this Thesis, X-ray crystallography was selected as the main technique to study the interactions established between two different classes of putative metal-based drugs and several proteins as further discussed in the next two chapters.

CHAPTER 2

INTERACTION OF PROTEINS WITH CARBON MONOXIDE RELEASING MOLECULES

2.1 – Introduction and objectives

As mentioned in the respective introductory chapter, the general perception of carbon monoxide has changed from a deadly substance to a molecule with biological and therapeutic effects. Consequently, it is necessary to develop viable and safe methodologies to use carbon monoxide as a drug. CORMs are one of the most promising approaches for such goal even if their pharmacological use depends on several factors.

In fact, it was also previously indicated that a set of characteristics should be followed in order to design a drug-like CORM namely by controlling the type of metal, the number of CO ligands and the nature of the ancillary ligands. Among these characteristics, an acceptable pharmacokinetic profile *in vivo* is required: if a given compound fails in the ADME parameters, it will be not possible to use it in further studies.

Remembering what it was written before, the binding of drugs to plasma proteins strongly modulates their pharmacokinetic profile as it controls their distribution in the organism. CORMs are not exception and the interactions established with plasma proteins are crucial for their *in vivo* behavior. In fact, the behavior of the CORM in the blood stream depends on the interactions with plasma cells and proteins namely serum albumin and serum transferrin. Among the referred cells, red blood cells are particularly relevant making probable the involvement of hemoglobin in these interactions.

On the other hand, X-ray crystallography is a powerful technique to study the mentioned interactions at an atomic level revealing the details behind such interactions. Therefore, not surprisingly, a structural approach to this theme has been proposed recently and some results have been published with CORM-3 and ALF186. In both works, hen egg white lysozyme (HEWL) was used as a robust crystallographic model allowing to observe the formation of adducts between the protein and the tested CORMs.[274,275]

Keeping in mind the previous lines, the principal aim of the experimental work described in this chapter was to characterize – structurally and functionally – the interactions established between several CORMs and the proteins above mentioned: HEWL (crystallographic model) and blood proteins (bovine hemoglobin, human serum albumin, bovine serum albumin and human serum apo-transferrin).

For such purpose, different types of CORMs – namely ruthenium-, iridium- and platinum-related CORMs – have been selected and the interactions established with the proteins were characterized mainly by X-ray crystallography. Following this systematic approach, relevant information is expected to be collected contributing for a future successful drug design strategy.

2.2 – Structural and functional studies with proteins

2.2.1 – Ruthenium-based CORMs

Ruthenium-based CORMs have been widely studied. Perhaps the most remarkable examples are found in the early stage of development of this type of compounds: CORM-2 and CORM-3. In fact, numerous results have been obtained with both compounds, which are still today often used as models.[85 and references therein]

In this section, different ruthenium-based CORMs have been used with the mentioned proteins mainly in different structural studies, using X-ray crystallography. Particularly relevant results were obtained with lysozyme and hemoglobin. Albumin (human and bovine) and transferrin were also used but no significant results have been obtained; therefore, the protein purification steps and crystallization optimization trials performed with these proteins will be addressed in the next chapter (iridium- and platinum-based CORMs). Moreover, the synthesis of one ruthenium-based CORM was also performed.

2.2.1.1 – Synthesis of $Cs_2[Ru(CO)_2Cl_4]$ complex (ALF_MS1)

The vast majority of the ruthenium-based compounds used in the structural studies with proteins were previously synthesized by the team of Alfama or by the group of Professor Carlos Romão at ITQB/UNL (*Instituto de Tecnologia Química e Bioquímica António Xavier*). Nevertheless, the ruthenium-based CORM cesium tetrachlorodicarbonylruthenate(II), $Cs_2[Ru(CO)_2Cl_4]$, named ALF_MS1, was synthesized during the time of this thesis.

2.2.1.1.1 – Materials and Methods

Ruthenium trichloride, hydrochloric acid and formic acid were purchased from Sigma-Aldrich. Cesium chloride was purchased from Alfa Aesar. Absolute ethanol was obtained from Carlo Erba Reagents.

The synthesis was carried out under a nitrogen atmosphere, using standard schlenk techniques, based in the procedure described by Cleare and Griffith.[276]

Ruthenium(III) trichloride (0.5 g) was refluxed with a mixture (1:1 v/v) of 37% of hydrochloric acid and 90% of formic acid (10 ml) at 105ºC (approximately 5 hours). Cesium chloride (0.725 g) was then added and a green supernatant was formed. Several washes with distilled water were performed and the resulting solution was evaporated using a rotary evaporator

(Büchi, Rotavapor R-114, Waterbath B-480) at 65ºC. Finally four ethanol extraction steps were performed (10ml of ethanol using a stirring water bath at 40ºC for 10 minutes) followed by a new cycle of evaporation using the rotary evaporator. A brownish powder was obtained. An infrared spectrum was traced in an IFS66/S FTIR spectrophotometer (Bruker) using KBr pellets (potassium bromide from Sigma-Aldrich).

2.2.1.1.2 – Results and Discussion

The synthesis of cesium tetrachlorodicarbonylruthenate(II), $Cs_2[Ru(CO)_2Cl_4]$ named ALF_MS1, was performed following the reaction scheme depicted in Figure 2.1.

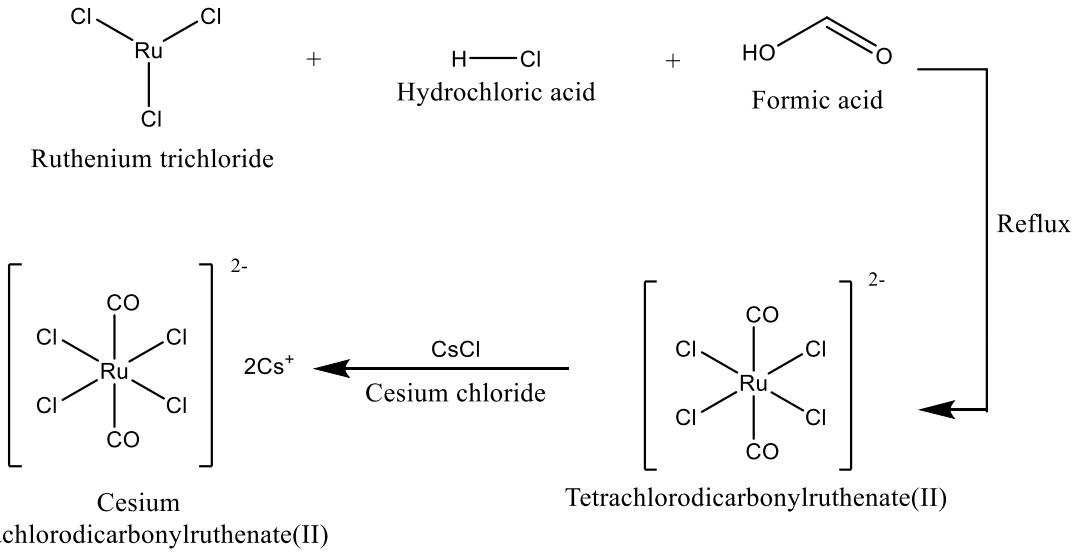

Figure 2.1 – Reaction scheme of the synthesis of the compound ALF_MS1 according the followed experimental procedure. The addition of cesium chloride allows the precipitation of the final salt.

Unexpectedly, the five hours reflux of ruthenium trichloride with the mixture of hydrochloric acid and formic acid did not produce a yellow solution; instead, a brownish/reddish solution was obtained.

Nevertheless, cesium chloride was added and a more yellowish solution was obtained. Then, 2 ml of distilled water was added to remove potential contaminants and the solution was filtered. An orange supernatant was obtained indicating the formation of a water-soluble ruthenium complex. Further washes using water (10 ml) were carried out in order to increase the complex recovery, following an ethanol extraction: a brownish powder (0.268 g) was obtained.

Probably these unexpected results are explained by the use of distilled water to dilute the formic acid (98%) instead of using an originally manufactured 90% formic acid as described in protocol.[276] Water could react with ruthenium trichloride producing a different intermediate than the expected tetrachlorodicarbonylruthenate(II).

In order to characterize the synthesized compound, FTIR (Fourier Transform Infrared) spectroscopy was used. A KBr pellet of ALF_MS1 was analyzed and the respective spectrum is shown in Figure 2.2. A distinct peak is located in the CO stretching region at 1942 cm^{-1} differently from the reported characteristic wavenumber for the $Cs_2[Ru(CO)_2Cl_4]$ complex (2036 cm^{-1}). The experimentally obtained wavenumber value is close to the one reported for other ruthenium-based chlorocarbonyl species: $Cs_2[Ru(CO)(H_2O)Cl_4]$ (1951 cm^{-1}).[276]

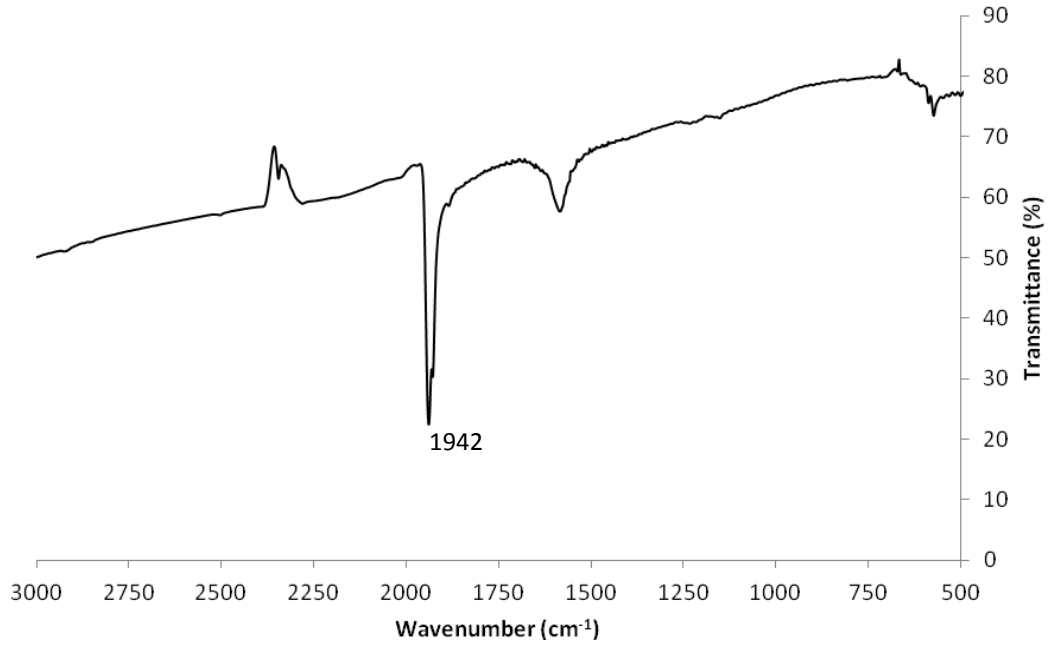

Figure 2.2 – FTIR spectrum of solid ALF_MS1 in KBr pellet. A sharp peak at 1942 cm^{-1} is clearly observable.

Consequently, the synthesized compound ALF_MS1 corresponds very likely to the mentioned monoaqua complex as result of the use of water during the experimental procedure. Elemental Analysis was performed to fully elucidate the nature of ALF_MS1 revealing the presence of hydrogen. This result is currently under analysis in order to be compared with the calculated percentage (0.36%).

Even though ALF_MS1 doesn't correspond to the originally intended complex, $Cs_2[Ru(CO)(H_2O)Cl_4]$ can still be used as a CORM, likely with different properties than the ones expected. Therefore, the ALF_MS1 was kept to be used in the proposed structural studies – particularly with albumin and transferrin – in order to understand its potential reactivity towards proteins.

2.2.1.2 – Interactions with Hen Egg White Lysozyme

HEWL is often used as a robust protein model in structural studies involving potential metal-based pharmacological compounds mainly due to the high resolutions obtained.[277,278,279,280] An

analogous approach has been followed in the beginning of the fruitful collaboration between Professor Carlos Romão and the X-ray crystallography Group at FCT/UNL.[274,275] Therefore, not surprisingly, a similar experimental methodology was adopted in the structural studies herein covered.

2.2.1.2.1 – Materials and Methods

The complexes ALF850, ALF475, ALF486 and ALF487 were synthesized by the team of Alfama. ALF_MS1 was synthesized as described in the chapter 2.2.1.1. HEWL, sodium acetate buffer and glycerol were purchased from Sigma-Aldrich. Sodium chloride was acquired from Scharlay.

- **Infrared Spectroscopy**

The interaction of ALF850 with HEWL was studied by incubating the complex with the protein for 1 hour. The protein was then separated from the soluble compounds by dialysis and the isolated fraction was lyophilized. A FTIR spectrum was traced in a Perkin Elmer Spectrum1000 spectrophotometer using KBr pellets.

- **X-ray crystallography – Crystallization, data collection, structure solution and structure refinement**

A solution of HEWL was prepared (50 mg/ml in 0.1 M acetate buffer pH 4.5) and crystallized using 6-8% (w/v) NaCl in 0.1 M acetate buffer pH 4.5. Hanging drops were prepared at 20°C using the vapor diffusion method (drops with 2 μl of protein and 2 μl of precipitant solution with 700 μl of the precipitant solution in the reservoir) in 24-well plates from Molecular Dimensions. Crystals of approximately 0.2×0.2×0.2 mm^3 appeared within 24 hours and were stabilized with a harvesting buffer containing 12% (w/v) NaCl. Crystals were observed either with a SZH10 Olympus microscope or a SteREO Discovery V12 Zeiss microscope.

Different soaking approaches were followed depending on the tested CORM. For ALF850, a few milligrams of the compound were dissolved in distilled water and were added to the crystallization drops. Due to its partial water solubility, the final concentration of the CORM in the drops is not known. After 24 hours, the soaked crystals were flash frozen with the harvesting buffer supplemented with 30% (v/v) glycerol as a cryo-protectant. Using synchrotron radiation (beamline Proxima 1 at Soleil, Paris, France), the crystals diffracted beyond the 1.50 Å resolution and a complete data set was collected.

The compounds ALF475, 486 and 487 were dissolved in a harvesting buffer solution containing 12% (w/v) NaCl up to a final concentration of 50 mM. After 24 hours of soaking, the crystals were harvested and flash frozen using a similar cryo-protectant. Different datasets were

collected up to 1.67 Å resolution in beamlines ID14-1 and ID14-2 at the European Synchrotron Radiation Facility – ESRF (Grenoble, France).

The compound ALF_MS1 was dissolved in a harvesting buffer solution containing 12% (w/v) NaCl up to a final concentration of 10 mM. A 4 μl drop was prepared and some native HEWL were transferred into it. The soaking was prolonged for 24 hours. The best crystals were afterwards flash frozen using the mentioned cryo-protectant and different datasets were collected up to 1.1 Å in beamline P14 at PetraIII (Hamburg, Germany).

The collected datasets were integrated with the programs Mosflm or XDS and scaled with Aimless from the CCP4 suite of programs.[281,282,283] The structures were solved by Molecular Replacement (using PDB entry 193L as a model)[284] with Phaser[285] and the refinement was performed using Refmac5[286] followed by visual inspection of the model and electron density maps in COOT.[287] The quality of the model was attended using the validation tools of COOT and PDB_REDO.[288]

2.2.1.2.2 – Results and Discussion

This section will be divided into three different parts according to the used CORMs in order to make it more readable and comprehensible.

2.2.1.2.2.1 – ALF850

The complex $[Ru(CO)_3Cl_2(1,3\text{-thiazole})]$, herein named ALF850 (Figure 2.3), was originally synthesized by Cini and collaborators not to investigate its potential CO releasing properties but to study its biological activity while a ruthenium complex.[289] Lately, it has been shown that ALF850 interacts with the human β-amyloid peptides 1-28 and 1-42 (Aβ28 and Aβ42, respectively) which are related to the Alzheimer's disease.[290]

Both CORM-3 and ALF850 have a similar general formula – $[Ru(CO)_3L_3]^{2+}$ – and ALF850 was compared with CORM-3 in order to assign potential differences in terms of their reactivity towards proteins.[291]

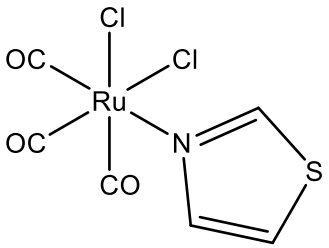

Figure 2.3 – Structure of ALF850 complex, $[Ru(CO)_3Cl_2(1,3\text{-thiazole})]$.

The CO stretching region of the FTIR spectrum of solid ALF850 in KBr pellets was previously characterized showing a sharp peak at 2139 cm^{-1} and a broad, very strong peak at 2052 cm^{-1} with some shoulder features at 2077, 2063 and 2017 cm^{-1}. It was also shown by FTIR that the compound is labile in water: new peaks were assigned signaling the disappearance of fac-$[Ru(CO)_3]^{2+}$ and the formation of cis-$[Ru(CO_2)]^{2+}$ fragments.[291]

As demonstrated with CORM-3, it is also very probable that ALF850 interacts with plasma proteins.[274] In order to better understand the putative reactivity towards proteins, the interaction of ALF850 with HEWL was studied by incubating the complex with the protein for one hour. The protein was then separated from the soluble compounds by dialysis and the isolated fraction was lyophilized. Its FTIR spectrum (KBr pellet, Figure 2.4) shows four peaks in the CO stretching region: 2070, 2025, 1974 and 1943 cm^{-1} indicating that more than one Ru–CO containing species remain coordinated to HEWL. Most likely these are two cis-$Ru(CO)_2$ adducts, the most populated corresponding to the stronger peaks, 2025 and 1943 cm^{-1}. A similar experiment with CORM-3 has produced two sets of vibrations compatible with cis-$Ru(CO)_2$ adducts one of which has values similar to those above: 2038 and 1950 cm^{-1}.

Figure 2.4 – FTIR spectrum of lyophilized dialysate of the adduct of ALF850 with HEWL, in KBr pellet. This is the spectrum of the solid obtained by lyophilization of the protein-containing fraction obtained through dialysis of the solution resulting from the incubation of ALF850 with HEWL for 1 hour. The small peak to the left has a maximum at 2070 cm^{-1}.

The mentioned FTIR experiment proves the ability of the compound to react with proteins. Therefore, it would be ideal to characterize the interactions between serum albumin, the dominant plasma protein, and ALF850. Tests like circular dichroism or isothermal titration calorimetry are not very informative due to the large number of species present in the solution after ALF850 is dissolved. Conversely, crystallographic analysis gives very important information allowing the characterization of the fragments that are formed and their interaction with protein residues. However, for crystallographic characterization, the use of albumin crystals for soaking is usually not an option

because suitable crystals are not robust, diffract to medium resolution and are difficult to obtain. This well-known difficulty with albumin crystals is even amplified in these studies due to the fact that CORMs decompose during soaking experiments and cause inherent loss of resolution.

Therefore, as pointed, it was decided to use the robust and highly diffracting crystals of lysozyme for the soaking experiments with ALF850 as previously successfully done with CORM-3. After 24 hours, soaked crystals were yellowish as shown in Figure 2.5.

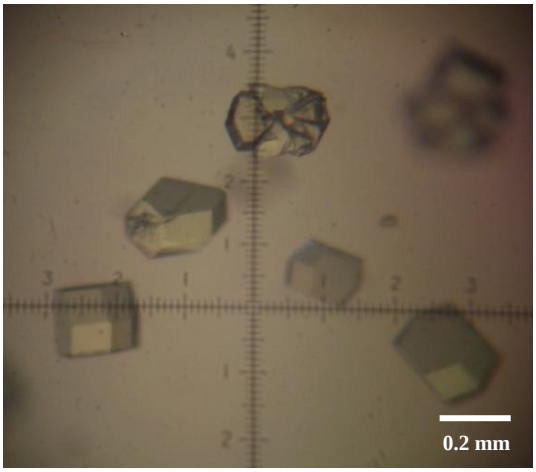

Figure 2.5 – HEWL crystals with ALF850 after 24 hours of soaking. Yellowish ≈ 0.2×0.2×0.1 mm^3 crystals were obtained. In addition to the color change, some crystals are slightly cracked which could indicate the success of the soaking experiment.

The best soaked HEWL crystal diffracted up to 1.5 Å resolution at beamline Proxima 1, Soleil (Figure 2.6) and the data were processed in $P4_32_12$ space group (a=b=78.79, c=37.32 Å). Molecular Replacement was used to solve the structure. Data collection and refinement statistics are summarized in Table 2.1.

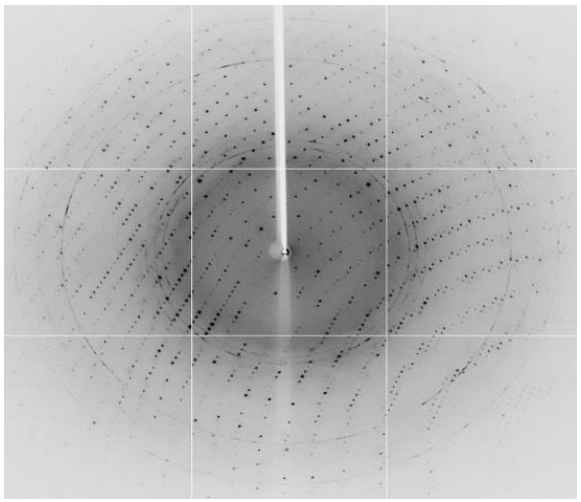

Figure 2.6 – Diffraction pattern of the HEWL•ALF850 crystal. Resolution at the edge is 1.5 Å.

Table 2.1 – Data collection and refinement statistics for HEWL•ALF850 adduct crystal. Values in parentheses correspond to the highest resolution shell.

X-ray source	Proxima 1 (Soleil)
Crystal data	
Space group	$P4_32_12$
Unit cell parameters (Å, º)	$a = b = 78.79$, $c = 37.32$ $\alpha = \beta = \gamma = 90$
Molecules per ASU	1
Matthews coefficient (Å^3/Da)	2.01
Solvent content (%)	39
Data collection	
Wavelength (Å)	0.992
Resolution range (Å)	39.40–1.50 (1.58–1.50)
<I/σI>	22.7 (3.5)
Multiplicity	11.7 (3.8)
Number of observed reflections	219414 (8584)
Number of unique reflections	18731 (2262)
R_{pim} (%)	1.7 (17.7)
Completeness (%)	96.9 (83.5)
Refinement	
Resolution range (Å)	39.40–1.50
R_{work} (%)	18.5
R_{free} (%)	21.3
RMSD bond length (Å)	0.026
RMSD bond angle (º)	2.21
Ramachandran plot (%)	
Residues in favored regions	99.2
Residues in additionally allowed regions	0.8
Residues in disallowed regions	0

$R_{pim} = \Sigma_{hkl} [1/(N-1)]^{1/2} \Sigma_i|I_i(hkl) - \langle I(hkl)\rangle|/\Sigma_{hkl} \Sigma_i I_i(hkl)$, where N is the multiplicity measured.

$R_{work} = \Sigma ||F_{calc}|-|F_{obs}|| / \Sigma|F_{obs}| \times 100$, where F_{calc} and F_{obs} are the calculated and observed structure factor amplitudes, respectively.

R_{free} is calculated for a randomly chosen 5% of the reflections for each dataset.

With one molecule in the asymmetric unit (Matthews coefficient of 2.01 Å^3/Da and solvent content of 39%), the overall structure of HEWL•ALF850 is very similar to that of the native protein as well as to the HEWL•CORM-3 structure obtained previously (PDB entry 2XJW).[274]

As in the other published models, chloride and sodium ions from the crystallization conditions are found interacting with the protein. In addition, the electron density map shows that Ru fragments of ALF850 are bound to HEWL at four different sites: the unique histidine residue (His15) and also three aspartate residues (Asp18, Asp101 and Asp119) as depicted in Figure 2.7.

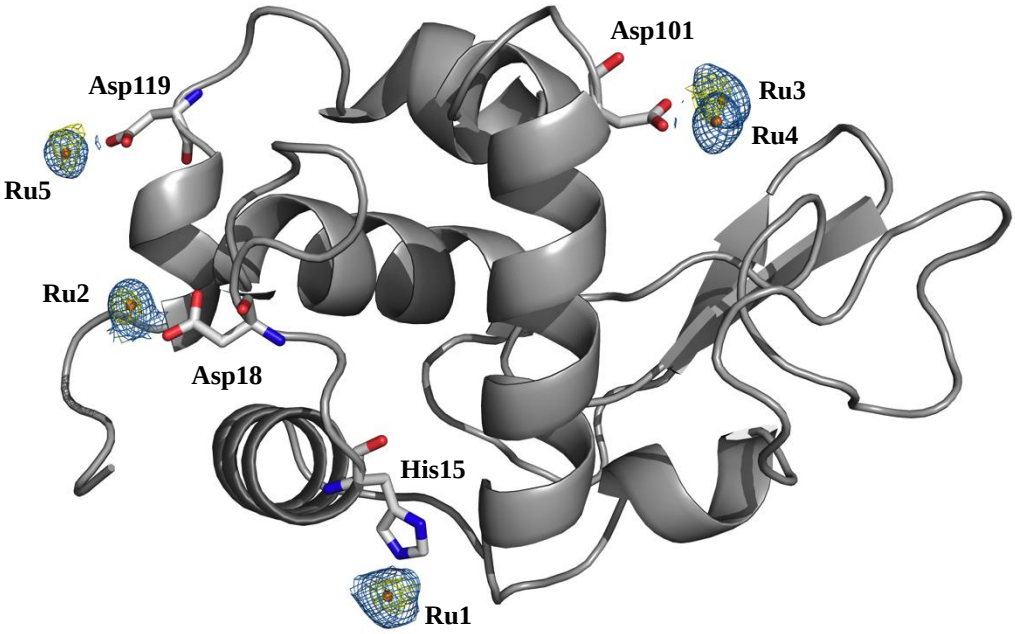

Figure 2.7 – Overall structure of HEWL bound to Ru fragments derived from ALF850. Four residues (His15, Asp18, Asp101 and Asp119) interact with five ruthenium atoms. Electron density map with a contour of 1.0 σ. Picture has been prepared using Pymol.

As observed for the HEWL•CORM-3 structure, His15 has the higher binding affinity for ALF850 and, even though the MCC occupancy is only 0.65 (Table 2.2), the six ligands of the metal could be properly fitted in the electron density maps (both chloride and 1,3-thiazole moieties are absent in the adduct with the protein). Due to a lower occupancy of the Ru atom in the remaining aspartate sites, the octahedral geometry expected for these adducts is not observed and only part of the ligands were included in the final model.

Table 2.2 – Occupancy and B factors of ruthenium atoms in the HEWL•ALF850 model. For comparison, polypeptide chain, water molecules and whole model have B factors of 19.81, 31.22 and 21.50 Å^2, respectively.

Ruthenium atom	Associated residue	Occupancy	B factor (Å^2)
Ru1	His15	0.65	45.29
Ru2	Asp18	0.35	32.23
Ru3	Asp101	0.30	41.61
Ru4	Asp101	0.30	34.58
Ru5	Asp119	0.30	31.00

Several lysozyme structures accessible in the PDB exhibit transition metals bound to histidine 15.[274,277,278,279,280] As in those cases, the Ru–protein adduct shows a covalent bond between the metal and the Nε2 of the imidazole ring of the histidine side chain. Besides His15, Ru is also bound to one CO molecule and four water molecules (Figure 2.8). This preferred bonding of Ru–carbonyl fragments of ALF850 to histidine, had also been observed by Valensin and co-workers.[290] However, in the

present case only one Ru-CO bond is left in the HEWL•ALF850 adduct instead of the three Ru-CO bonds identified in the adduct of ALF850 with Aβ42 peptide.

The ruthenium atom is at 1.97 Å from the carbon atom of CO, in the range of the expected values for these types of complexes. The Ru–C–O angle of nearly 139° reveals an end-on coordination of CO to the metal. Finally, the distances between Ru and the four water molecules range between 2.33 and 3.24 Å – similar values to those observed in HEWL•CORM-3 structure.[274]

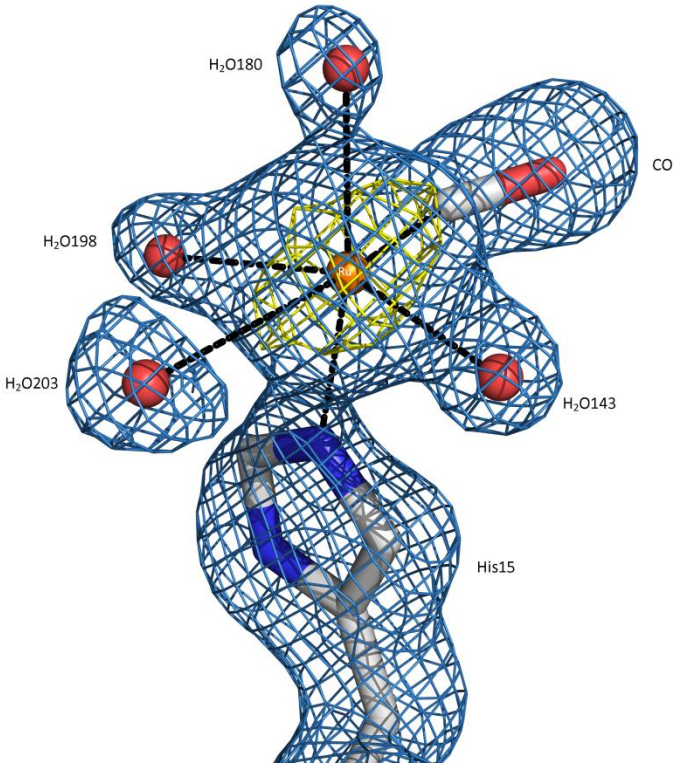

Figure 2.8 – Structural representation of Ru•His15 adduct. The ruthenium moiety interacts with six ligands – one CO, four water molecules and the Nε2 of His15 – in an octahedral geometry. Electron density maps: 2Fo–Fc (blue, 0.8 σ) and anomalous (yellow, 3.0 σ); carbon in gray, nitrogen in blue, oxygen in red and ruthenium in orange. Picture has been prepared using Pymol.

Even though the interpretation of the electron density maps in the other binding sites is ambiguous, it is clear that both the Asp18 and the Asp119 sites are coordinating mono-carbonylated Ru–CO fragments. Disorder might be the reason why the binding mode between the metal and CO is not done in an end-on but in a bent conformation. Such orientation has been described in a structure of a Ru complex deposited in the CSD (Cambridge Structural Database) with the code PADQAM.[292]

A remarkable difference, however, is observed for the binding of Asp101 to ALF850. In this case, the carboxylate of Asp101 is acting as a bridging ligand between two Ru atoms, Ru3 and Ru4. This feature is observed in Figure 2.7 where two strong blobs of electron density are found both in the experimental and in the anomalous electron density maps.

Taking into account the results obtained with CORM-3, the formation of HEWL•$Ru(CO)_2$ adducts was expected. Surprisingly, the adduct formed between HEWL and ALF850 only contains one Ru-CO bond (Figure 2.9). It seems that in the conditions of this particular experiment, the

HEWL•$Ru(CO)_2$ adducts initially formed, and characterized by IR, decomposed to lose CO, most likely through a ligand substitution reaction. In fact, this crystallographic observation is nothing but a snapshot taken along the decarbonylation pathway of ALF850 that only reveals the viability of several fragments to effectively release CO, without information on the rate or mechanism of their formation. Beyond the identification of the preferred binding sites of the protein, the important point to concentrate upon is that, after its interaction with the protein, the initially formed $Ru(CO)_2$ fragment is able to decay and lose CO within a relatively short time and under mild conditions.

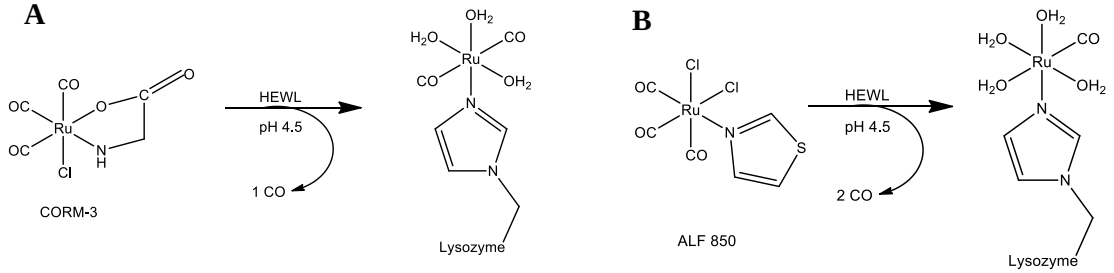

Figure 2.9 – Schematic representation of adducts formed between the histidine residue of HEWL and CORM-3 (A) and ALF850 (B). Both compounds release CO molecules due to reactions with HEWL. However, the obtained crystal structures show that, at His15 site, CORM-3 releases only one CO while ALF850 releases two out of three CO molecules. Schemes have been prepared using ChemDraw.

Although lysozyme is only a model for the plasma proteins, and there are no *in vivo* data for ALF850, this finding provides an important circumstantial support to the earlier proposal on the mechanism by which CORM-3 and its analogues deliver CO *in vivo*.[274]

We propose that, after entering the blood, these CORMs react rapidly with the plasma proteins losing one equivalent of CO and forming protein•$Ru(CO)_2$ adducts which are carried throughout the body in the circulation. During this process, they slowly decay with a stepwise loss of CO. At high CORM concentrations, one may expect that a constant, extended release of CO takes place until the metallated protein is removed from circulation. This slow distribution of CO throughout the organism is also consistent with the intriguingly broad range of therapeutic activity of CORM-3, which has been reported efficacious for many diseases in different organs and tissues. A slow delivery of CO through the blood via the protein adducts, but not through COHb transportation, would be consistent with the observed therapeutic versatility and could become a useful strategy for therapeutic CO delivery *in vivo*.

2.2.1.2.2.2 – ALF475, ALF486 and ALF487

The described results obtained with ALF850 led to new investigations in order to improve the understanding of the chemistry of $[Ru^{II}(CO)_3]$ derived complexes under biological conditions and, by that, contribute to the design of compounds equipped with drug-like properties.

The team of Alfama has synthesized a series of $[Ru(CO)_3Cl_2L]$ complexes where the variation of the nature of L is intended to provide information on the influence of the inner coordination sphere on different pharmacologically relevant properties of the complexes.[293]

Different compounds were used in soaking experiments but only three of them produce useful X-ray diffraction data: ALF475, ALF486 and ALF487 (Figure 2.10). The methionine oxide (ALF475) was selected to improve the biocompatibility and aqueous solubility. The pyridine ligands (ALFs486 and 487) represent biologically meaningful N-heterocyclic ligands imparting the solubility through the sulfonate functionality.

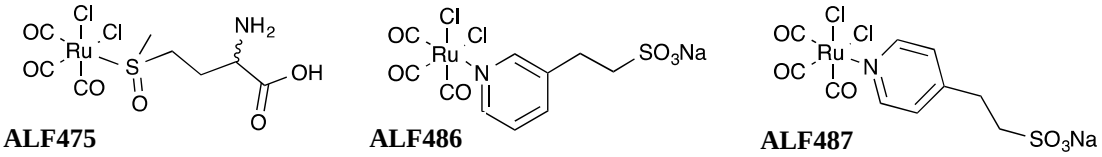

Figure 2.10 – Structures of ALF475 (left), ALF486 (center) and ALF487 (right) complexes. Schemes have been prepared using ChemDraw.

Using a similar approach to the one used with ALF850, crystals of HEWL previously soaked (24 hours) with the three mentioned complexes were measured and complete datasets were collected at high resolution up to 1.67 Å, 1.77 Å and 1.78 Å resolution (ALF475, ALF486 and ALF487, respectively) at beamlines ID14-1 and ID14-2, ESRF.

The structures were solved by MR using the native protein as the reference model (PDB code 193L) and refined with all residues in the allowed regions of the Ramachandran plot. Data collection and refinement statistics are summarized in Table 2.3.

As expected the three obtained models are highly similar to each other and to the native protein. Common to the three structures is the presence of Ru species bound to the histidine residue (His15) in an octahedral geometry (Figure 2.11) as previously observed for HEWL•CORM-3 and HEWL•ALF850 complex models.

More ruthenium ions are also found at the surface of the protein bound to aspartate residues, which in some cases bridge two metal ions (Table 2.4). In the obtained structures, not all the Ru atoms and the ligand atoms are fully occupied due to disorder at the ruthenium binding sites. Nevertheless, it is clear from the electron density that in the three protein•CORM complexes obtained, one or two of the initial CO ligands as well as the ancillary ligands are absent and have been replaced by water molecules.

Table 2.3 – Data collection and refinement statistics for HEWL•ALF475, HEWL•ALF486 and HEWL•ALF487 adduct crystals. Values in parentheses correspond to the highest resolution shell.

	HEWL·ALF475	HEWL·ALF486	HEWL·ALF487
X-ray source	ID14-1 (ESRF)	ID14-2 (ESRF)	ID14-2 (ESRF)
Crystal data			
Space group	$P4_32_12$	$P4_32_12$	$P4_32_12$
Unit cell parameters (Å, º)	a = b = 79.93, c = 36.89 $\alpha = \beta = \gamma = 90$	a = b = 78.66, c = 37.00 $\alpha = \beta = \gamma = 90$	a = b = 80.22, c = 37.16 $\alpha = \beta = \gamma = 90$
Molecules per ASU	1	1	1
Mosaicity (°)	0.25	0.35	0.31
Matthews coefficient (Å^3/Da)	2.03	1.97	2.06
Solvent content (%)	39.50	37.71	40.37
Data collection			
Wavelength (Å)	0.933	0.933	0.933
Resolution range (Å)	30.89–1.67 (1.76–1.67)	27.81–1.78 (1.87–1.78)	28.36–1.77 (1.86–1.77)
<I/σI>	19.3 (5.1)	42.07 (19.6)	29.3 (10.3)
Multiplicity	7.0 (6.8)	13.8 (13.2)	13.8 (13.2)
Number of observed reflections	100389 (14122)	161272 (21868)	171634(23241)
Number of unique reflections	14435 (2064)	11707 (1655)	12 432 (1757)
R_{pim} (%)	2.2 (14.8)	1.4 (4.4)	1.6 (6.3)
Completeness (%)	99.9 (100)	100 (100)	100 (99.9)
Refinement			
Resolution range (Å)	30.89–1.67	27.81–1.78	28.36–1.77
R_{work} (%)	16.57	16.13	18.30
R_{free} (%)	21.15	19.52	22.20
RMSD bond length (Å)	0.013	0.010	0.019
RMSD bond angle (º)	1.53	1.29	1.81
Ramachandran plot (%)			
Residues in favored regions	96.06	96.06	95.28
Residues in additionally allowed regions	3.94	3.94	4.72
Residues in disallowed regions	0	0	0
PDB code	4UWN	4UWU	4UWV

$R_{pim} = \Sigma_{hkl} [1/(N-1)]^{1/2} \Sigma_i|I_i(hkl) - \langle I(hkl)\rangle|/\Sigma_{hkl} \Sigma_i I_i(hkl)$, where N is the multiplicity measured.

$R_{work} = \Sigma ||F_{calc}|-|F_{obs}|| / \Sigma|F_{obs}| \times 100$, where F_{calc} and F_{obs} are the calculated and observed structure factor amplitudes, respectively.

R_{free} is calculated for a randomly chosen 5% of the reflections for each dataset.

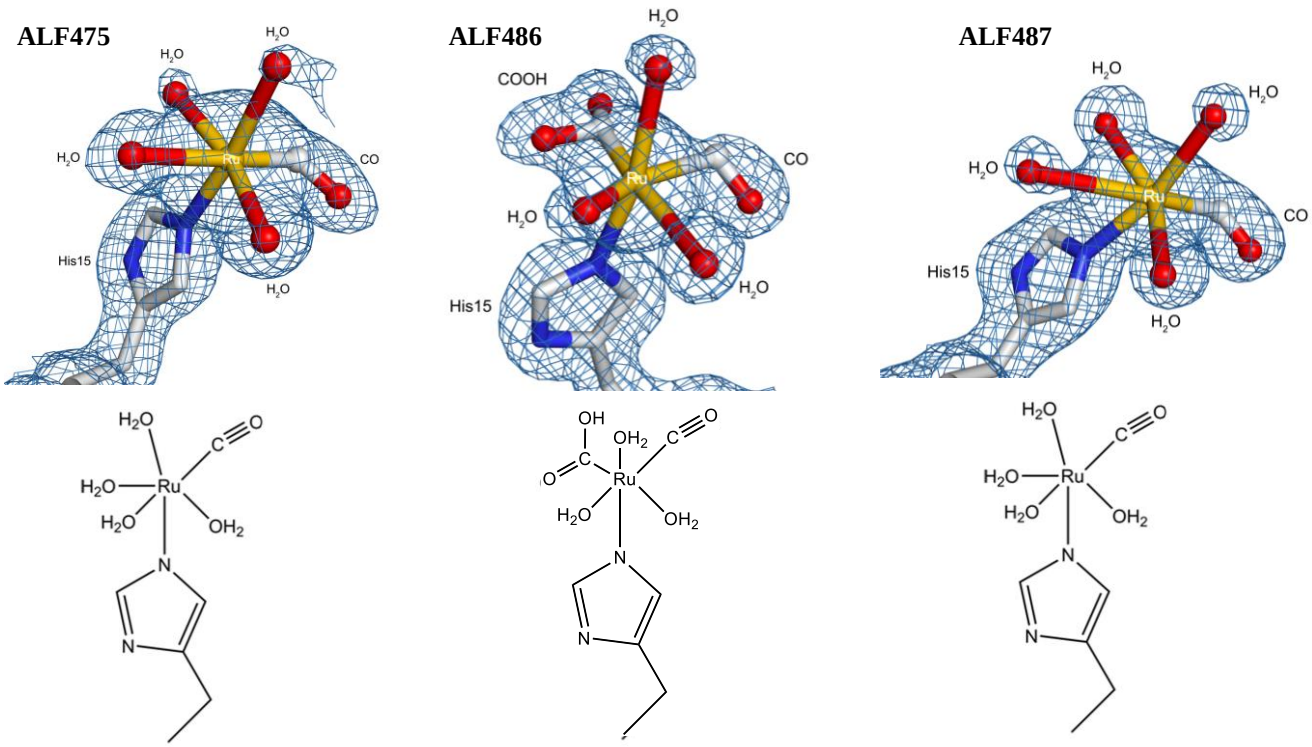

Figure 2.11 – Structural representation of HEWL•CORM complexes at the site with the highest Ru occupation, obtained by soaking HEWL crystals with ALF 475 (left), ALF486 (center) and ALF487 (right). In the top, the experimentally observed electronic density map 2Fo–Fc at the His15 site (map contoured at 1 σ) is shown; carbon in gray, nitrogen in blue, oxygen in red and ruthenium in orange. In the bottom, a schematic representation of the referred adducts is depicted. The three adducts complexes present an octahedral geometry at the Ru atom: in addition to the histidine residue, the metal coordination sphere is completed with CO, COOH and H_2O molecules depending on the compound the HEWL crystals were treated with. Picture has been prepared using Pymol and ChemDraw.

In the crystal structure of the HEWL•ALF486 complex, a less common electron density is observed in the coordination sphere of Ru at the His15 binding site. This electron density has been interpreted as a metallacarboxylate with a covalent Ru–C bond. Thus, the interaction of the tricarbonyl complex ALF486 with HEWL crystals led to the formation of a $[Ru(CO)(COOH)(H_2O)_3]^+$ species, which is coordinated to the protein by the imidazole group of His15 (Figure 2.11). Such species is formed through the addition of HO^- to the dicationic fragment $[Ru\text{-}(CO)_2(H_2O)_3]^{2+}$.

This finding illustrates a specific step of the decarbonylation pathway of CORMs being the first time that such step is shown by X-ray crystallography. This result, taken together with other studies, strongly suggest that the chemistry of the $[Ru(CO)_3]^{2+}$ complexes in aqueous solution is initiated by the first step of the pH dependent water-gas shift reaction sequence as depicted in Equation 2.1.

$$[Ru(CO)_3Cl_2L] \underset{H^+}{\overset{HO^-}{\rightleftharpoons}} [Ru(CO)_2(COOH)Cl_2L] \qquad \textbf{Equation 2.1}$$

Table 2.4 – Metal binding sites found in the crystal structures of HEWL soaked with ALF475, ALF486 and ALF487, describing the ligands at each Ru binding site. Values in parentheses correspond to the occupancy of the ruthenium.

CORM·HEWL adduct ligands	HEWL·ALF475	HEWL·ALF486	HEWL·ALF487
His15 site	Ru (1) CO 4 H_2O	Ru (0.8) CO $COOH^-$ 3 H_2O	Ru (0.7) CO 4 H_2O
Asp18 site	Ru (0.65) CO 3 H_2O	Ru-Ru (0.5) 8 H_2O	–
Asp52 site	Ru (0.5) 3 H_2O	Ru (0.4) CO 2 H_2O	–
Asp101 site	–	Ru-Ru (0.7) 6 H_2O	Ru-Ru (0.5) 5 H_2O
Asp119 site	Ru (0.5) 3 H_2O	Ru (0.7) CO 4 H_2O	–

DFT (Density Functional Theory) calculations were also performed by Professor Luís Veiros (*Instituto Superior Técnico, Universidade de Lisboa*) modeling the reaction of fac-$[RuCl_2(CO)_3(MeIm)]$ (MeIm = methylimidazole) with HO^- in the presence of H_2O. The mechanism occurs in an essentially barrierless single step, with HO^- attacking the C-atom of one CO ligand and yielding a $COOH^-$ ligand bonded to the metal in the final product. It was also shown that HO^- addition is much faster than halide displacement: the putative substitution of chloride by hydroxide was also modeled by DFT calculations indicating that this substitution reaction is considerably less favorable than HO^- attack on coordinated CO.

Therefore, the results above strongly suggest that aqueous chemistry of $Ru(CO)_3Cl_2L$ complexes effectively takes place from $[Ru\text{-}(COOH)Cl_2(CO)_2L]^-$ and species of this kind are the ones that actually interact with the proteins and other biological entities soon after incubation starts. Nevertheless, from the data gathered in this work, it seems that halides and other ligands L are easily displaced because they are absent in all the protein•organometallic complexes identified using X-ray crystallography.

With the already discussed results, it is plausible to admit that once dissolved in aqueous medium, the chemistry of the compounds $[Ru^{II}\text{-}(CO)_3Cl_2L]$ is governed by the reactivity of the metallacarboxylate species $[Ru^{II}(CO)_2(COOH)Cl_2L]^-$. Under biological conditions, with a pH much higher than 3, the equilibrium of Equation 2.1 is strongly driven to the right and the $Ru(CO)_3$ fragment is completely absent in solution as shown by FTIR in the cases of CORM-3 and ALF850.[274,291] It is under these conditions that it becomes important to establish the stability of the metallacarboxylate

intermediate. If it is stable for a time span compatible with the time scale of the biological experiment, it is possible that it behaves as a stable prodrug with a recognizable and quantifiable pharmacokinetic profile. When the metallacarboxylate species ages in solution, it decomposes irreversibly generating CO2, metal hydrides, hydroxyl radicals and other species (Figure 2.12).

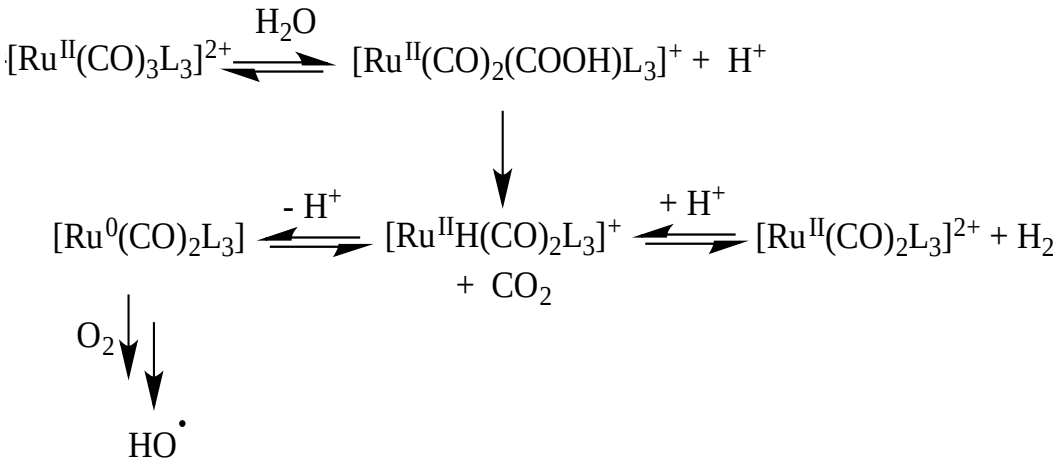

Figure 2.12 – Reactivity of $[Ru^{II}(CO)_3L_3]^{2+}$ CORMs in aqueous, aerobic solutions. All types of species presented have been identified for at least one CORM.

When this complicated chemistry takes place under biological conditions, two situations may happen: it takes place independently of the biological species present which may then react with the reaction/decomposition products or the presence of the biological molecules modulates the decomposition process. It is not possible to ascertain the role (if any) of HEWL in the decomposition of the $Ru(CO)_3Cl_2L$ complexes and formation of the HEWL•$Ru(CO)_x$ but, very likely, the protein accelerates the first loss of CO and other ligands.

The results obtained show that $Ru(CO)_x$ fragments bind several residues of the HEWL protein (Table 2.4) but the adduct with His15 residue is the one that systematically presents the highest occupancy. As depicted in Figure 2.11 both complexes ALF475 and ALF487 generated the fragment $Ru^{II}(CO)(H_2O)_4$ bound to His15 as found in similar experiments with ALF850. As indicated, the chloride ligands are absent in the final adduct, attesting their lability. The ultimate fate of the initial $Ru(CO)_3Cl_2L$ complex is the loss of two CO ligands, the two Cl^- ligands and the ancillary ligand L: methionine oxide (ALF475) and pyridine (ALF487).

It was previously identified a cis-$Ru(CO)_2(H_2O)_3$ fragment bound to the His15 residue in similar experiments with CORM-3 – one CO and all other ligands were lost following the first addition of HO^- to the $Ru(CO)_3$ fragment.[274] Quite interestingly, the soaking of HEWL with ALF486 led to the identification of the metallacarboxylate intermediate [His15•$Ru^{II}(COOH)(CO)(H_2O)^3$] derived from the addition of HO^- to the dicarbonyl dication cis-$[Ru(CO)_2(H_2O)_3]^{2+}$. Crystallographic resolution does not allow distinguishing the metallacarboxylate from the corresponding Ru(η1-CO_2) species but, at pH 4.5, we favor the presence of the Ru–COOH fragment.

It is now obvious that the use of HEWL has allowed to capture a series of snapshots along the pathway of the decomposition of $[Ru(CO)_3Cl_2L]$ complexes in aqueous medium. Moreover, the obtained results allow also hypothesizing a mechanism by which these labile CORMs deliver CO to cells and elicit CO dependent biological responses. If the metallacarboxylate lasts long enough in the biological medium, it gets to cells where it can exchange its added HO^- with any other ROH (transesterification) or RNH_2 (transamidoylation) terminal group present at the surface of the cells, thus anchoring the Ru complexes as adducts of the formula $[(cell\text{-}Y\text{-}CO)Ru(CO)_2L_3]$ and $[(cell\text{-}Y)Ru(CO)_2(H_2O)_3]$ (Y = O, NH) at a later stage following CO_2 loss (Figure 2.13).

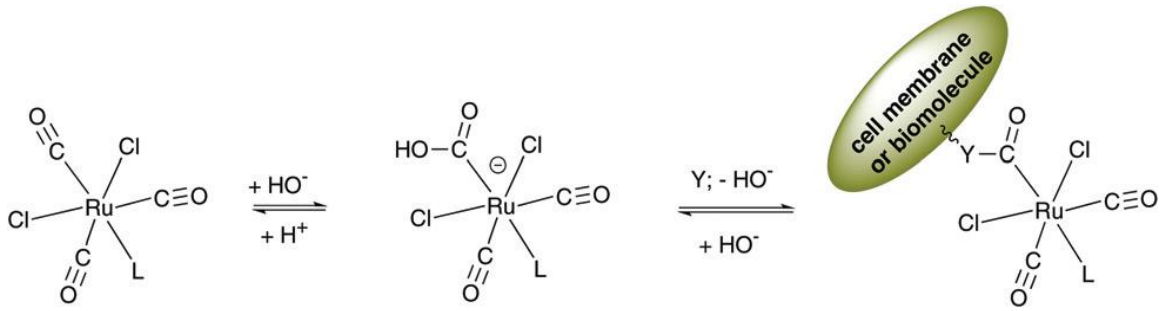

Figure 2.13 – Proposed mechanism for the interaction of $[Ru^{II}\text{-}(CO)_3Cl_2L]$ with cells or biomolecules.

In this way, these CORMs can accumulate efficiently at the surface of cells and actually move from cell to cell by means of reversible exchanges with carrier molecules in the intercellular medium. This anchoring of the CORM to the cell surface enables decomposition or internalization of the Ru scaffold to take place at or inside the cell. In both cases, CO will be readily available to the cell and its internal targets, e.g. mitochondria. In the case of internalization, the amount of CO delivered to the cell can be much higher than that usually achieved by dissolved free CO, which rapidly diffuses across membranes.

Finally, it should be pointed that the very rich and complex chemistry of $Ru^{II}(CO)_3$ based CORMs, summarized in Figure 2.12, may also contribute to some of their biological effects. The formation of ROS species downstream of the water-gas shift reaction may be relevant in some cases, since these species are strongly involved in signaling processes, including those involving CO. Some of these possibilities have been raised and discussed elsewhere but the present data do not provide any evidence favoring or disfavoring them.[294,295]

It should be highlighted that, as mentioned in the first lines of this section, the structural results herein discussed are included in a detailed study of several $[Ru(CO)_3Cl_2L]$ complexes. Different characteristics, including the solubility, stability, reactivity, CO release profile, cytotoxicity and anti-inflammatory activity of the complexes, were evaluated by a vast multidisciplinary team and the complete discussion can be found in the respective paper.[293]

2.2.1.2.2.3 – ALF_MS1

Following the results described in the previous sections, despite the problems occurred during its synthesis, ALF_MS1 was also used in some soaking experiments with HEWL (Figure 2.14) in order to have more evidences to support the presented conclusions.

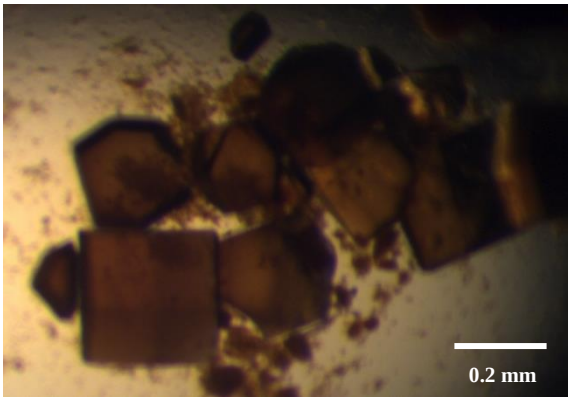

Figure 2.14 – HEWL crystals with ALF_MS1 after 24 hours of soaking. Brownish ≈ 0.2×0.2×0.2 mm^3 crystals were obtained.

HEWL crystals were soaked (24 hours) with ALF_MS1 (10 mM) and a complete dataset was collected at high resolution up to 1.05 Å at beamline P14, PetraIII. The structure was once again solved by Molecular Replacement. Table 2.5 shows the data collection and refinement statistics.

The structure is still under refinement but it is clear the presence of an adduct next to His15 similarly to those obtained for the other tested CORMs. A density blob was also found next to Asp18 residue: the anomalous map hints that a ruthenium moiety (with low occupancy) should be located there but it was not modeled yet.

At the current refinement stage, the adduct was modeled with an occupancy of 0.75 and none of the initial chloride ancillary ligands remain in the adduct, as expected. The ruthenium-ligand distances calculated are also in the expected range of values. However, some considerable differences were found in this Ru•His15 adduct comparing with the previous obtained models (Figure 2.15).

The characteristic octahedral geometry, often obtained in these structural studies, is not observed. The sixth ligand, presumably a water molecule, in the apical position is absent although a disordered molecule should not be completely ruled out. Another remarkable difference is the coordination of the adduct by a nitrogen atom of the near arginine residue (Arg14).

The unique CO ligand of the complex was found in the metal-protein adduct. More likely, the obtained structure corresponds to a snapshot prior of the described reactions initiated by the addition of HO^-. Nevertheless, the adduct revealed in the structure corroborates the previous findings of the putative use of plasma proteins as carriers.

Table 2.5 – Data collection and current refinement statistics for HEWL•ALF_MS1 adduct crystal. Values in parentheses correspond to the highest resolution shell.

X-ray source	P14 (PetraIII)
Crystal data	
Space group	$P4_32_12$
Unit cell parameters (Å, º)	$a = b = 78.72$, $c = 37.00$ $\alpha = \beta = \gamma = 90$
Molecules per ASU	1
Matthews coefficient (Å³/Da)	1.98
Solvent content (%)	37.81
Data collection	
Wavelength (Å)	0.976
Resolution range (Å)	39.36–1.05 (1.07–1.05)
<I/σI>	27.5 (2.5)
Multiplicity	13.6 (11.1)
Number of observed reflections	739852 (28712)
Number of unique reflections	54588 (2581)
R_{pim} (%)	1.8 (47.3)
Completeness (%)	99.7 (97.2)
Current refinement	
Resolution range (Å)	39.36–1.05
R_{work} (%)	19.4
R_{free} (%)	21.4
RMSD bond length (Å)	0.025
RMSD bond angle (º)	2.16
Ramachandran plot (%)	
Residues in favored regions	96.85
Residues in additionally allowed regions	3.15
Residues in disallowed regions	0

$R_{pim} = \Sigma_{hkl} [1/(N-1)]^{1/2} \Sigma_i|I_i(hkl) - \langle I(hkl)\rangle|/\Sigma_{hkl} \Sigma_i I_i(hkl)$, where N is the multiplicity measured.

$R_{work} = \Sigma ||F_{calc}|-|F_{obs}|| / \Sigma|F_{obs}| \times 100$, where F_{calc} and F_{obs} are the calculated and observed structure factor amplitudes, respectively.

R_{free} is calculated for a randomly chosen 5% of the reflections for each dataset.

Once the structure refinement is completed, a more accurate description will be obtained. The displacement of the ancillary ligands is one of the points to be explored. In fact, as systematically observed in the other obtained crystallographic structures, it appears that the ancillary ligands are released prior the CO molecule upon protein interaction. A proper characterization of the structure can be useful to further understand the chemistry of the Ru-based complexes.

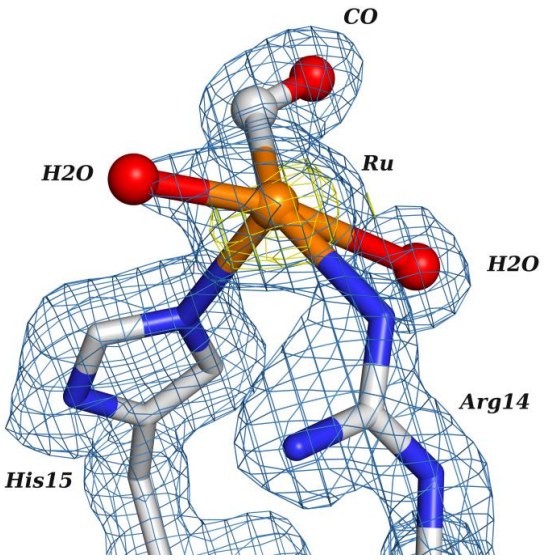

Figure 2.15 – Structural representation of the Ru•His15 adduct obtained by soaking HEWL crystals with ALF_MS1. The analysis of the density maps doesn't reveal the presence of a sixth ligand to complete the octahedral geometry. Moreover, differently from the previous obtained HEWL•CORM structures, Arg14 appears to be also bonded to Ru through a nitrogen atom. The electronic density map 2Fo–Fc (blue) is contoured at 1 σ while anomalous density (yellow) is contoured at 3 σ. Color code: carbon in gray, nitrogen in blue, oxygen in red and ruthenium in orange. Picture has been prepared using Pymol.

2.2.1.3 – Interactions with Bovine Hemoglobin

As mentioned, COHb is widely seen as a reliable parameter to evaluate the potential toxicity of CO-based therapeutic approaches. Even if CORMs are designed to act only in the affected tissues, it is useful to know their potential interactions with hemoglobin. Moreover, their pharmacokinetics depends also on the interactions with the red blood cells, which bring us again to the importance of such interactions.

Three ruthenium CORMs have been selected for these studies: the well-known CORM-3, ALF475 (also characterized with HEWL) and ALF_MS1. However, the hemoglobin crystals soaked with ALF_MS1 diffracted poorly not allowing a proper structural characterization. Thus, only the obtained results with the first two CORMs will be addressed herein.

2.2.1.3.1 – Materials and Methods

The complexes CORM-3 and ALF475 were synthesized by the team of Alfama. Hemoglobin was purified from bovine blood according to the literature.[296,297]

Polyethylene glycol 4K (PEG4K), ammonium chloride (NH_4Cl) and ammonium iodide (NH_4I) were purchased from Sigma-Aldrich, Riedel-de Haën and Merck, respectively. Tris (Trizma, Tris-(hydroxymethyl)-aminomethane) buffer were purchased from Sigma-Aldrich.

- **X-ray crystallography – Crystallization, data collection, structure solution and structure refinement**

Bovine hemoglobin at 60 mg/ml in 20 mM Tris-HCl buffer pH 8.2 was crystallized using two different conditions: 20% (w/v) PEG4K, 0.2 M NH_4Cl and 20% (w/v) PEG4K, 0.2 M NH_4I. Hanging drops were prepared at 20°C using the vapor diffusion method (2+2 and 2+3 drops with 700 µl of the precipitant solution in the reservoir) in 24-well plates from Molecular Dimensions.

Crystals of approximately 0.1×0.1×0.05 mm^3 appeared within 24-48 hours and were stabilized with a harvesting buffer containing 25% (w/v) PEG 4K. Crystals were observed either with a SZH10 Olympus microscope or a SteREO Discovery V12 Zeiss microscope.

The compounds CORM-3 and ALF475 were dissolved in a harvesting buffer solution up to a final concentration of 50 mM. After 24 hours, the soaked crystals were flash frozen with the harvesting buffer supplemented with 30% (v/v) glycerol as a cryo-protectant. Two datasets were collected up to approximately 2 Å resolution in beamlines ID14-1 and ID23-1 at the European Synchrotron Radiation Facility – ESRF (Grenoble, France).

The dataset integration and structure resolution, refinement and validation were carried out similarly to what has been described for HEWL. The structures were solved by Molecular Replacement using PDB entry 2QSS as a model.[298]

2.2.1.3.2 – Results and Discussion

Bovine hemoglobin crystallization conditions have been determined previously. Two conditions using 20% PEG4K with 0.2 M of an ammonium salt (chloride or iodide) were identified as those giving the best crystals. Nevertheless, individual crystals are hard to be obtained. Instead, some crystal "clusters" are often formed as illustrated in Figure 2.16. Such clusters are usable in the subsequent soaking experiments although it is necessary to break them before being flash frozen in liquid nitrogen.

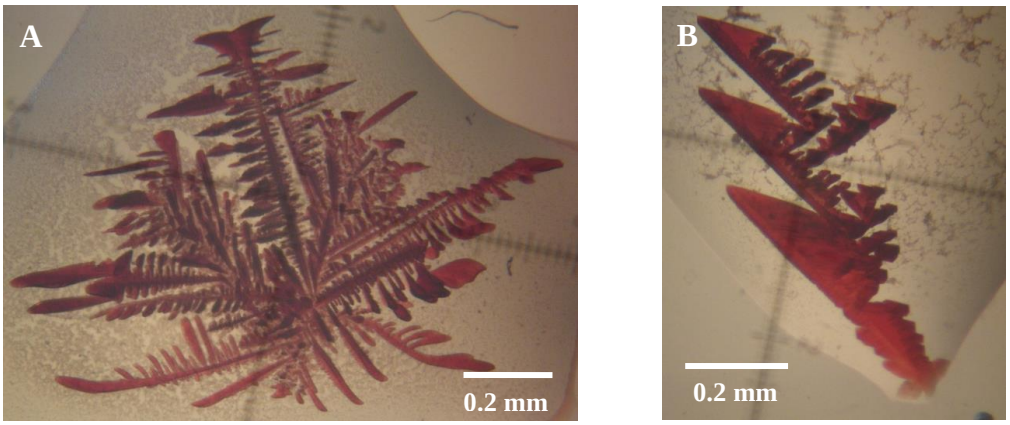

Figure 2.16 – Native bovine hemoglobin crystals obtaining with PEG4K and NH_4Cl (A) and NH_4I (B). The use of the mentioned crystallization conditions leads to different crystal morphologies but, often, clusters such those represented are obtained.

Using the crystals obtained with the described crystallization conditions, soaking experiments with CORM-3 and ALF475 were performed. After 24 hours, soaked crystals do not present significant visible differences when compared to the native ones.

The best soaked bovine hemoglobin crystals diffracted up to, approximately, 1.9 Å resolution at beamlines ID14-1 and ID23-1, ESRF (Figure 2.17) and the data were processed in $P2_12_12_1$ space group. Molecular Replacement was used to solve the structure (PDB entry 2QSS as a model). Data collection and refinement statistics are summarized in Table 2.6.

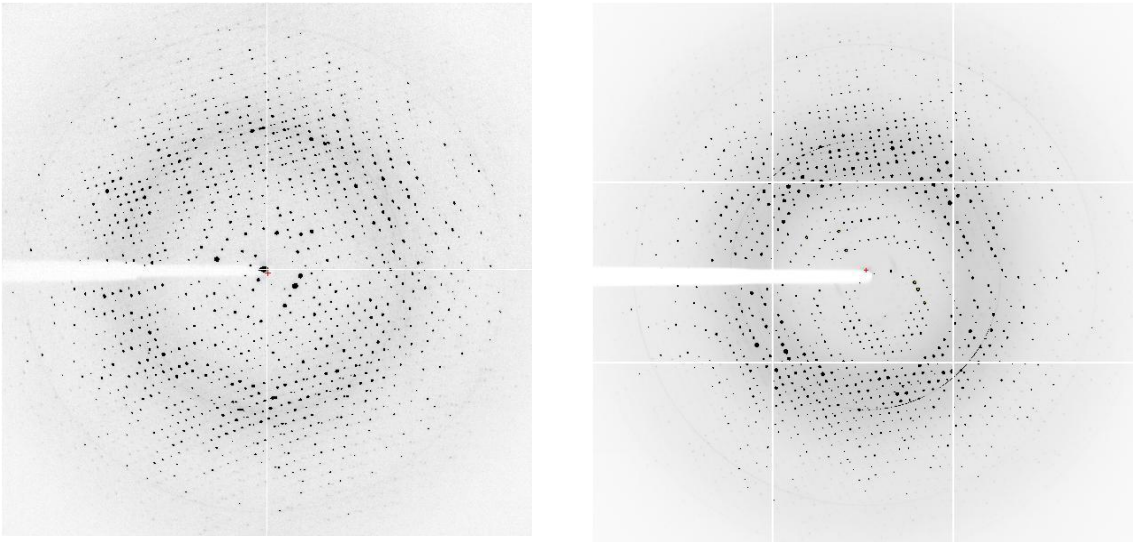

Figure 2.17 – Diffraction pattern of hemoglobin•CORM-3 (left) and hemoglobin•ALF475 (right) crystals. Resolution at the edge is 1.97 and 1.92 Å, respectively.

Both structures are still under refinement but some conclusions have been already obtained. In the first refinement cycles, only the polypeptide chain was present and, by visual inspection of the electron density maps, several ligands were added to the models.

In the hemoglobin•CORM-3 model, analysis of the $2F_o$-F_c and the F_o-F_c maps shows a Ru ion at the surface of the protein (Figure 2.18).

The mentioned ruthenium is coordinated to two histidine side chains in the equatorial plane and two water molecules. The other coordination position is occupied with a CO at ca 2.35 Å from the metal. No other extra density is observed to complete the octahedral geometry characteristic of this type of complexes. The two histidines are at the surface of the protein in two different chains: His76D and His89A from the neighboring hemoglobin molecule of the crystal lattice (Figure 2.19).

Coordinating the iron ion of heme A, the one closer to the $Ru(CO)(H_2O)_3(His)_2$ adduct, is a diatomic molecule with clear electron density peaks. Analysis of the temperature factors suggests that O_2 is bound to the metal although CO cannot be ruled out. Apart from this heme, all other heme molecules are coordinated to water molecules which is in agreement with the experimental evidences where low COHb levels are detected when CORM-3 is administrated.[174,299]

Table 2.6 – Data collection and refinement statistics for hemoglobin•CORM-3 and hemoglobin•ALF475 adduct crystals. Values in parentheses correspond to the highest resolution shell.

	Hemoglobin·CORM-3	Hemoglobin·ALF475
X-ray source	ID14-1 (ESRF)	ID23-1 (ESRF)
Crystal data		
Space group	$P2_12_12_1$	$P2_12_12_1$
Unit cell parameters (Å, º)	a = 65.36, b = 78.79, c = 109.68; $\alpha = \beta = \gamma = 90$	a = 65.13, b = 78.22, c = 109.63; $\alpha = \beta = \gamma = 90$
Molecules per ASU	1	1
Mosaicity (°)	0.27	0.20
Matthews coefficient (Å^3/Da)	2.19	2.16
Solvent content (%)	43.85	43.22
Data collection		
Wavelength (Å)	0.933	0.975
Resolution range (Å)	45.72–1.97 (2.02–1.97)	45.53–1.92 (1.97–1.92)
<I/σI>	16.7 (2.9)	45.01 (15.9)
Multiplicity	7.0 (4.7)	13.7 (11.1)
Number of observed reflections	284103 (12972)	591832 (31913)
Number of unique reflections	40743 (2763)	43226 (2879)
R_{pim} (%)	4.3 (32.9)	1.7 (5.0)
Completeness (%)	99.8 (98.0)	99.4 (99.9)
Current refinement		
Resolution range (Å)	45.72–1.97	45.53–1.92
R_{work} (%)	23.78	20.16
R_{free} (%)	28.63	25.41
RMSD bond length (Å)	0.016	0.018
RMSD bond angle (º)	1.64	1.90
Ramachandran plot (%)		
Residues in favored regions	96.65	96.01
Residues in additionally allowed regions	3.35	3.99
Residues in disallowed regions	0	0

$R_{pim} = \Sigma_{hkl} [1/(N-1)]^{1/2} \Sigma_i|I_i(hkl) - \langle I(hkl)\rangle|/\Sigma_{hkl} \Sigma_i I_i(hkl)$, where N is the multiplicity measured.

$R_{work} = \Sigma ||F_{calc}|-|F_{obs}|| / \Sigma|F_{obs}| \times 100$, where F_{calc} and F_{obs} are the calculated and observed structure factor amplitudes, respectively.

R_{free} is calculated for a randomly chosen 5% of the reflections for each dataset.

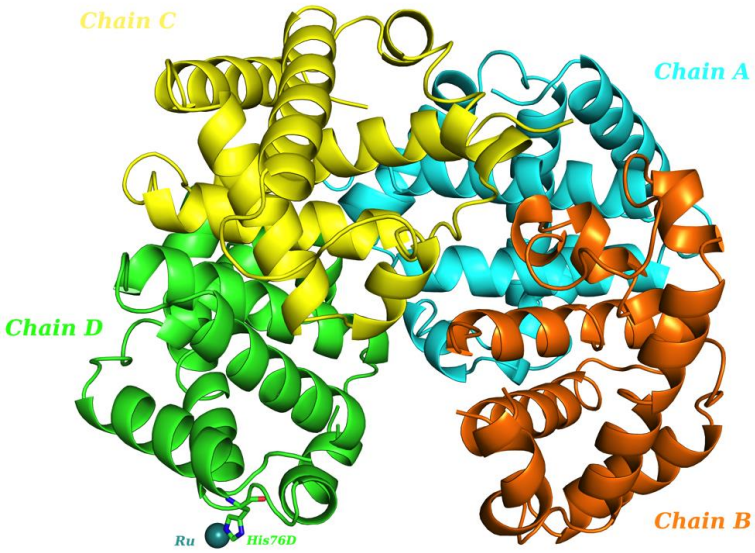

Figure 2.18 – Overall structure of hemoglobin•CORM-3 model. The four protein chains are depicted as well as the ruthenium moiety found next to a histidine residue in chain D (His76D). His89A residue from the symmetry molecule is not represented. Picture has been prepared using Pymol.

Close to His72C some electron density is also present bridging the imidazole ring of the histidine and the carboxylic acid of Asp51B from a symmetry related molecule. This electron density is not very strong and is most likely derived from a disordered and low occupied ruthenium ion. Interestingly the same extra electron density is found in the $2F_o$-F_c and the F_o-F_c maps of hemoglobin crystals with another Ru containing CORM (unpublished data).

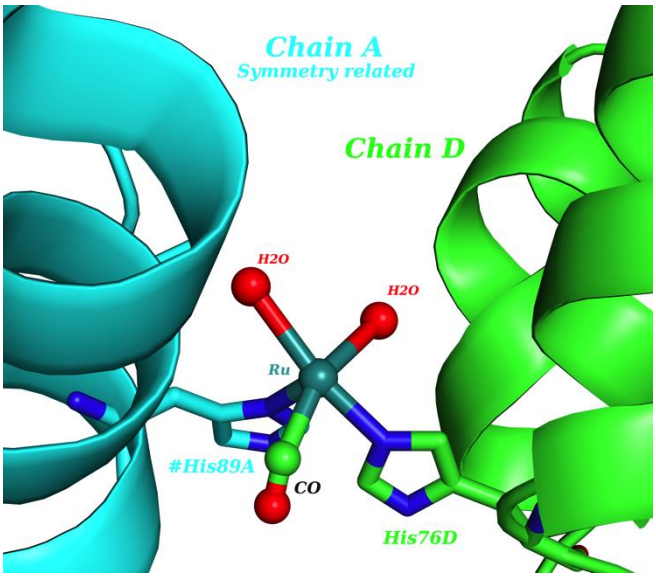

Figure 2.19 – Structural representation of the Ru adduct obtained in the hemoglobin•CORM-3 model. Ruthenium was modeled with an occupancy of 0.5. Chain D and the respective symmetry related chain A are depicted. An incomplete octahedral geometry is observed and the adduct contains one CO molecule. Picture has been prepared using Pymol.

Differently from the previous structure, the crystal of hemoglobin soaked with ALF475 was obtained using NH_4I as a precipitating agent. Several I^- ions were found at the surface of the protein making electrostatic interactions with positively charged side chains. Moreover, two distinct ruthenium moieties were also found as illustrated in Figure 2.20.

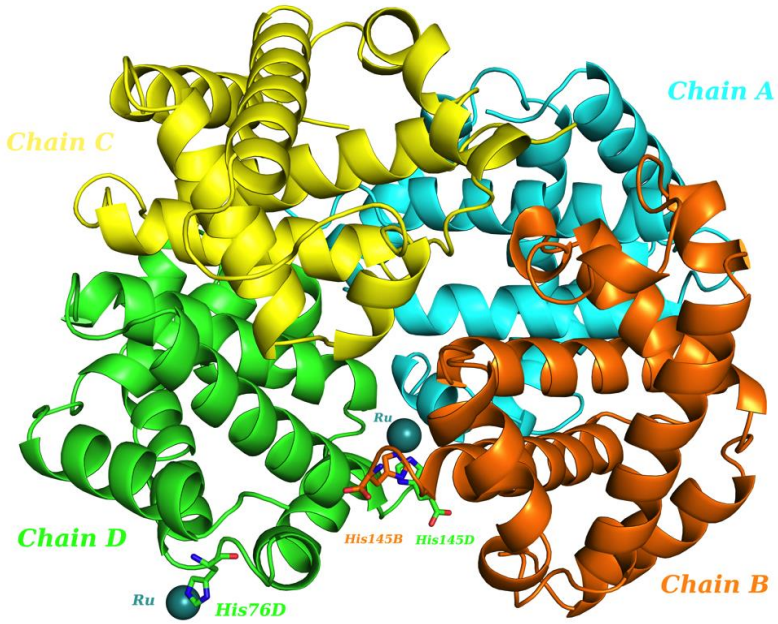

Figure 2.20 – Overall structure of hemoglobin•ALF475 model. The two Ru adducts positions are indicated: next to His76D (similar to CORM-3) and also at the interface of chains B and D (His145B and His145D, respectively). Picture has been prepared using Pymol.

The structure obtained shows a Ru ion coordinated to His89A(#) and His76D. In this case, the CO molecules have been released and the octahedral geometry is achieved with the binding of two water molecules and two iodide ions.

A second Ru-protein adduct coordinated to two I^-, one water molecule and to His145B and His145D was also found at the interface between chains B and D (no sixth ligand was identified). As before, the imidazole rings of the histidine residues are in the equatorial plane while the iodide ions sit in apical positions (Figure 2.21). This region appears to be significantly disordered – proven by the poor density maps obtained – but the presence of a strong anomalous signal – for both ruthenium and iodide moieties – allows to confirm the nature of the adduct. Commonly to the first adduct, no CO moiety was identified.

Interestingly, comparison with other structures deposited in the PDB shows that this metal complex is sitting very close to the 2,3-biphosphoglycerate (BPG) binding site of the human hemoglobin structure (PDB code: 1B86).[300] This molecule is an allosteric effector reducing the affinity of hemoglobin for oxygen. At the current stage of the refinement, however, it is not possible to confirm if the presence of this metal complex has an implication on the conformational changes observed upon BPG binding or if it is a crystallographic artifact due to the use of NH_4I in crystallization conditions.

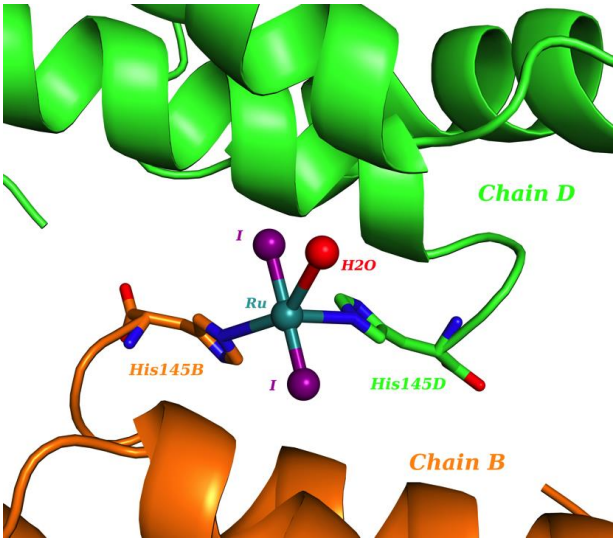

Figure 2.21 – Structural representation of the Ru adduct obtained at the interface of chains B and D in the hemoglobin•ALF475 model. Ruthenium was modeled with an occupancy of 0.35 and two iodide ions from the crystallization conditions were also added. No CO molecules were found in the adduct. Picture has been prepared using Pymol.

Finally, from the ongoing refinement, it appears that hemes A, B and C are coordinated to water molecules while heme D has a diatomic molecule, corresponding to O_2 or CO.

In fact, the analysis of the two structures clearly reveals that both CORM-3 and ALF475 adducts have released partially or fully their CO molecules but it is not clear if such molecules are bound to the heme moieties of the protein. The elucidation of this point can be very important to the use of these complexes as viable drugs. If a significant amount of CO is captured by the protein, two drawbacks should be considered: in addition to a reduced capacity on the CO delivery, the formation of COHb can lead to its well-known toxic effects. Once the structure refinement is completed, a more definitive description will be obtained (namely on the nature of the ligands of the heme moieties) and further hypotheses can be discussed.

2.2.2 – Iridium- and platinum-based CORMs

As shown in the last chapter, ruthenium-based CORMs are perhaps the most extensively studied MCCs. Nevertheless, some other metal-based complexes are also progressively being used in this field.[85]

Iridium is known by its inertness which explains its use as a therapeutic agent.[301,302] A relatively recent paper is available on the usage of complexes based on tetrachlorocarbonyliridate(III) as CORMs suggesting a poor back-donation from the metal to the bound CO's which could facilitate the CO release. Moreover, it has been shown that chloride ligands are labile and can be substituted by other ligands (particularly the chloride trans to the CO moiety). The inertness of Ir(III) compounds

will contribute to a low toxicity of the complex, which is clear advantage of this class of compounds.[303]

Regarding platinum, its use in several metal-based drugs – particularly cisplatin, as indicated in the Introduction – suggests that it could be also useful in the CO releasing context.

In this section, the synthesis of an iridium-based and a platinum-based CORM was carried out. Moreover, a second iridium-based CORM was also purchased to be analyzed. The three different potential CORMs have been used in structural studies by X-ray crystallography similar to those described in the previous section. Results with HEWL, albumin and transferrin will be presented next.

2.2.2.1 – Synthesis of $Cs_2[Ir(CO)Cl_5]$ complex (ALF_MS2) and $Cs[Pt(CO)Br_3]$ complex (ALF_MS3)

Two different compounds were synthesized: an iridium-based CORM – cesium pentachlorocarbonyliridate (III), $Cs_2[Ir(CO)Cl_5]$ named ALF_MS2 – and a platinum-based CORM – cesium tribromocarbonylplatinate, $Cs[Pt(CO)Br_3]$ named ALF_MS3.

2.2.2.1.1 – Materials and Methods

Sodium hexachloroiridate(III) and potassium hexabromoplatinate(IV) were purchased from Strem Chemicals. Hydrochloric acid and formic acid were purchased from Sigma-Aldrich. Hydrobromic acid was obtained from Fluka. Cesium chloride was purchased from Alfa Aesar.

The synthesis was carried out under a nitrogen atmosphere, using standard schlenk techniques, being based in the procedure described by Cleare and Griffith.[276]

Sodium hexachloroiridate(III) (0.35 g) was dissolved in a mixture (1:1 v/v) of 37% of hydrochloric acid and 90% of formic acid (3.5+3.5 ml). The solution was boiled at 110ºC for 5 minutes until it assumed an orange color. Cesium chloride (0.245 g) was then added to the filtered solution and, upon cooling, a pale orange powder was obtained.

Potassium hexabromoplatinate(IV) (0.35 g) was refluxed with a mixture of 90% formic acid (5.25 ml) and 48% hydrobromic acid (1.75 ml) at 110ºC until the original red color changed to yellowish/orange (approximately 5 hours). The obtained solution was filtered and cesium chloride (0.175 g) was then added. The resulting solution was evaporated and a yellowish/orange powder was obtained.

For both compounds, an infrared spectrum was traced in an IFS66/S FTIR spectrophotometer (Bruker) using KBr pellets (potassium bromide from Sigma-Aldrich).

2.2.2.1.2 – Results and Discussion

The synthesis of both ALF_MS2 and ALF_MS3 was conducted according to the literature (Figure 2.22). Both complexes gave an orange powder with high purity and relatively high yields: 0.335 g and 0.301 g for ALF_MS2 and ALF_MS3, respectively.

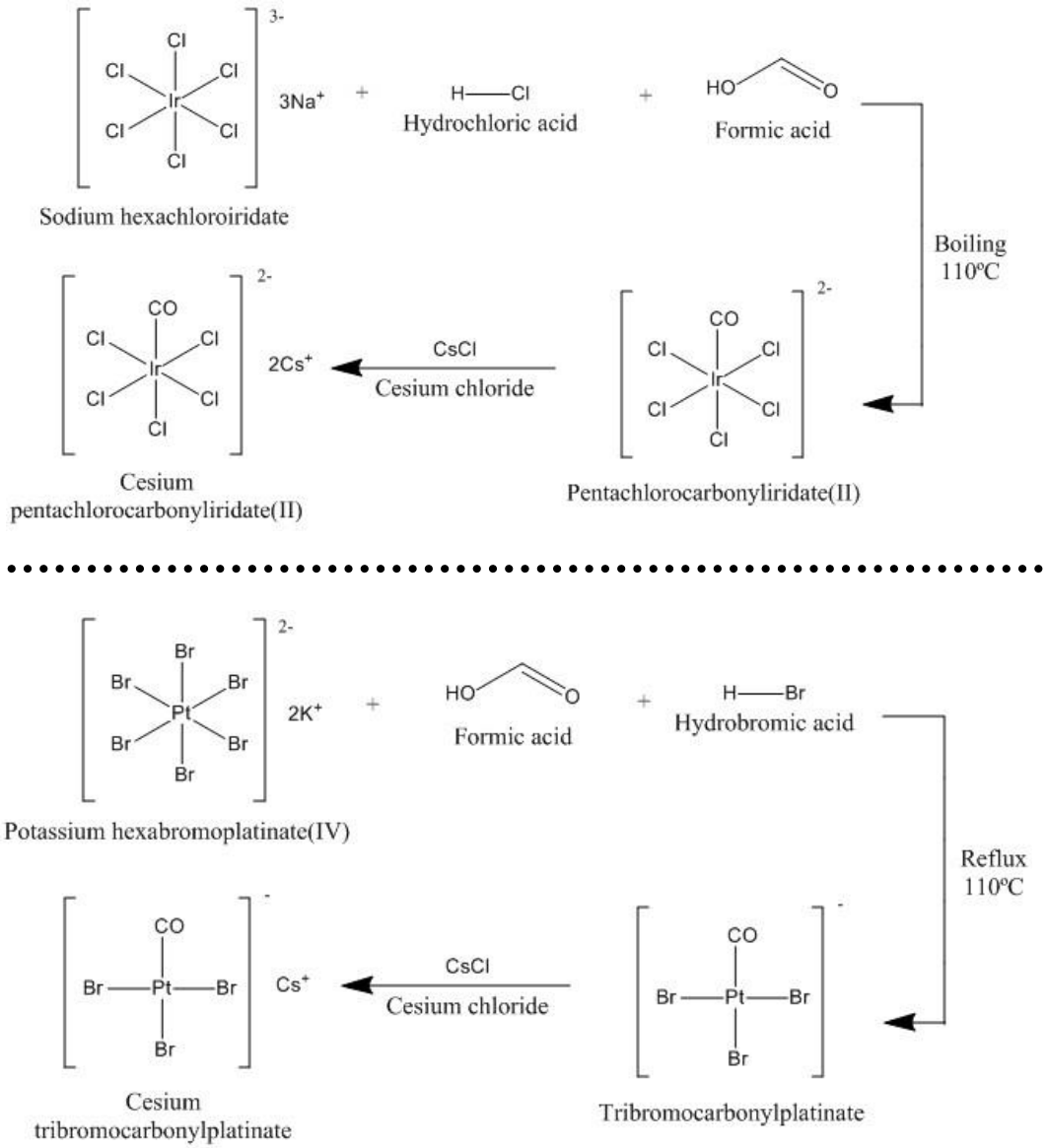

Figure 2.22 – Reaction scheme of the synthesis of the compounds ALF_MS2 (top) and ALF_MS3 (bottom) according the followed experimental procedure. Similarly to ALF_MS1, the addition of cesium chloride allows the precipitation of the final salt.

Once again, in order to characterize the synthesized compounds, FTIR spectroscopy was used. KBr pellets of ALF_MS2 and ALF_MS3 were analyzed and the respective spectra are shown in Figure 2.23.

Regarding ALF_MS2, a distinct peak is located at 2065 cm^{-1} which is close to the reported value in literature (2060 cm^{-1}). Regarding ALF_MS3, two adjacent sharp peaks are found at 2123 and

2100 cm^1; such values are also related to those previously reported – 2120 and 2101 cm^1 – in agreement with the values found in terminal carbonyls of transition metal complexes.[276]

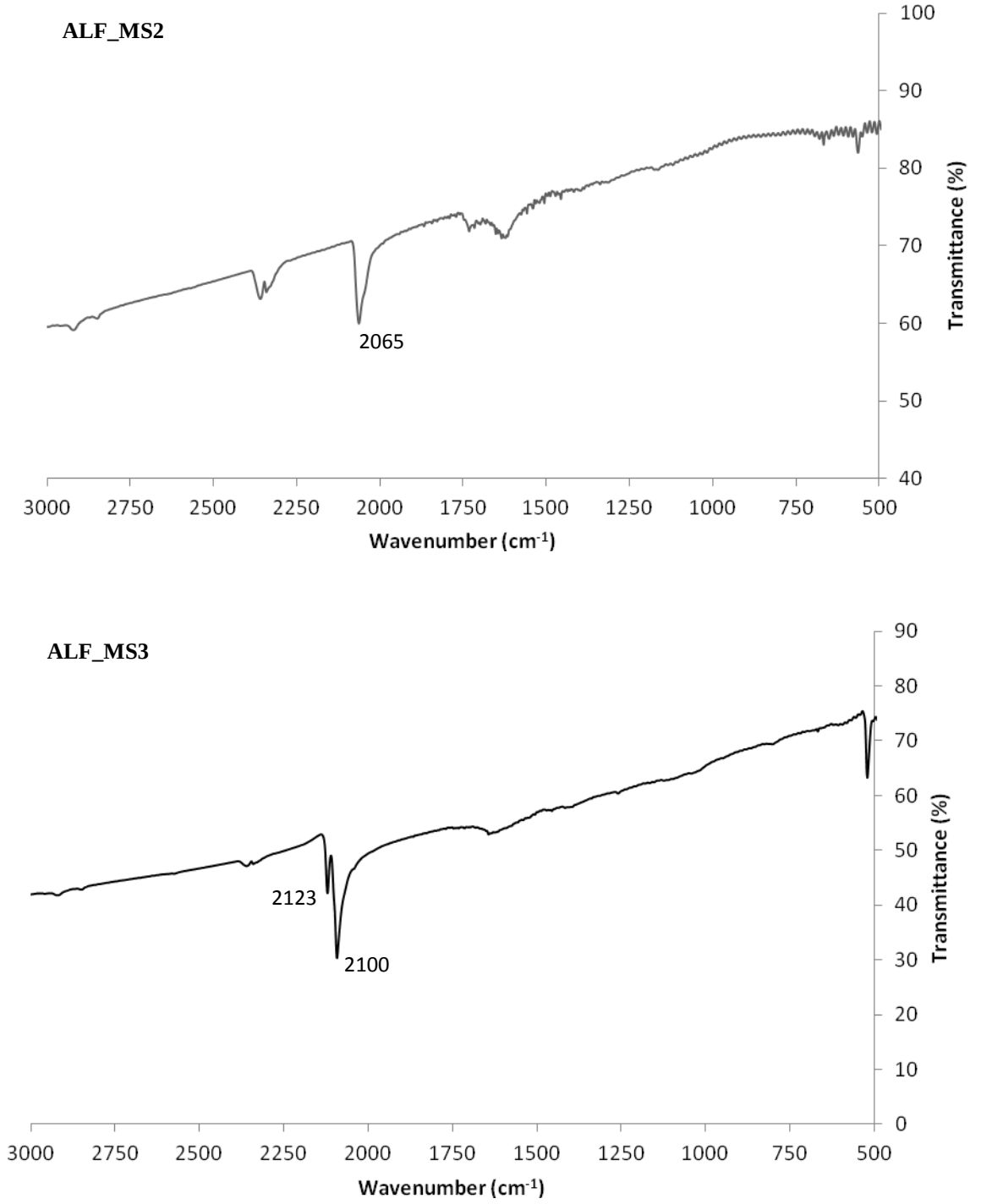

Figure 2.23 – FTIR spectra of solid ALF_MS2 (top) and ALF_MS3 (bottom) in KBr pellets. The peaks identified in both experimental obtained spectra correspond to the reported values in the literature pointing the success of the synthesis.

The analysis of the mentioned wavenumber values strongly suggests that the synthesized complexes ALF_MS2 and ALF_MS3 correspond to the desired iridium- and platinum-based compounds: $Cs_2[Ir(CO)Cl_5]$ and $Cs[Pt(CO)Br_3]$, respectively. Similarly to what has been discussed for ALF_MS1, elemental analysis is currently under way.

Differently from the ruthenium-based CORMs, none of these iridium- and platinum-based CORMs were tested in order to evaluate their potential CO release properties. Interestingly, both ALF_MS2 and ALF_MS3 just have one CO molecule in their structure rather the three CO molecules found in the studied ruthenium-based CORMs. This could lead to differences in their potential CO release properties and it will be one of the aspects to carefully be analyzed soon by our team. Nevertheless, the compounds were used in some structural studies in order to understand its potential reactivity towards proteins as described in the following sections.

2.2.2.2 – Interactions with Hen Egg White Lysozyme

Following a similar approach to the described for the ruthenium-CORMs, HEWL was also selected to be used in the proposed structural studies by X-ray crystallography with iridium- and platinum-based CORMs.

2.2.2.2.1 – Materials and Methods

ALF_MS2 and ALF_MS3 were synthesized as described in the chapter 2.2.2.1. Other iridium-based CORM – acetylacetonatodicarbonyliridium(I) herein named ALF_MS4 – was purchased from Sigma-Aldrich. HEWL, sodium acetate buffer and glycerol were purchased from Sigma-Aldrich. Sodium chloride was acquired from Scharlay.

- **Infrared Spectroscopy**

The interaction of ALF_MS2, ALF_MS3 and ALF_MS4 with HEWL was studied by incubating the protein with the three complexes for 1 hour (ratio 1:10). The samples were then passed through a PD-10 MiniTrap G-25 column (GE Healthcare) in order to remove the unbound compound and the isolated fractions were lyophilized. The same procedure was repeated with a sample of native HEWL (10 mM) without any incubation. FTIR spectra were traced in a Perkin Elmer Spectrum1000 spectrophotometer using KBr pellets.

- **X-ray crystallography – Crystallization, data collection, structure solution and structure refinement**

HEWL was crystallized similarly to the described in chapter 2.2.1.2.1: 6-8% (w/v) NaCl and 0.1 M acetate buffer at pH 4.5 using the vapor diffusion method at 20ºC.

The three ALFs (MS2, MS3 and MS4) were dissolved in a harvesting buffer solution containing 12% (w/v) NaCl up to a final concentration of 10 mM. Native HEWL crystals were transferred into 4 µl drops of harvesting buffer with each of the ALFs for soaking experiments during

1 and 7 days. The best crystals were flash frozen using the harvesting buffer solution supplemented with 30% (v/v) glycerol as cryo-protectant and different datasets were collected up to 1.2 Å in beamlines P14 at PetraIII (Hamburg, Germany), I02 at Diamond Light Source (Didcot, Oxfordshire, United Kingdom) and ID23-1 at the ESRF (Grenoble, France).

The dataset integration and structure determination, refinement and validation were carried out similarly to what has been earlier described (PDB entry 193L as a model in MR).[284]

2.2.2.2.2 – Results and Discussion

Following a similar strategy to that previously explained, the three iridium- and platinum-based CORMs were used in soaking experiments with HEWL in order to characterize their interactions with this model protein at the atomic level.

HEWL crystals were soaked with ALF_MS2, ALF_MS3 and ALF_MS4 (10 mM) for 24 hours after which the crystals became slight colored. Different crystals were tested using Synchrotron radiation but no clear protein•CORM adducts were observed in the three cases although some dubious small density blobs were found in both 2Fo–Fc and Fo–Fc maps. However, the absence of anomalous signal in those blobs suggested that protein•CORM adducts were not formed.

In order to try to obtain such adducts, longer soaking experiments were carried out. A golden/yellowish coloration was particularly noticed in the drops soaked with ALF_MS3 and ALF_MS4 (Figure 2.24).

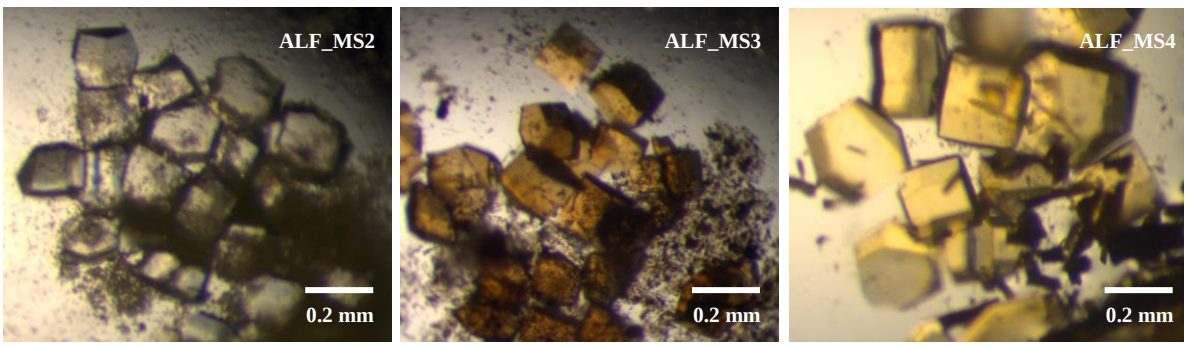

Figure 2.24 – HEWL crystals with ALF_MS2 (left), ALF_MS3 (center) and ALF_MS4 (right) after 24 hours of soaking. Different colored ≈ 0.2×0.2×0.2 mm^3 crystals were obtained.

The best soaked HEWL crystals diffracted up to 1.2 Å resolution at different beamlines and, similarly to the previous examples, the data were processed in $P4_32_12$ space group. The structures were, once again solved by Molecular Replacement. Data collection and refinement statistics are summarized in Table 2.7.

Table 2.7 – Data collection and refinement statistics for HEWL•ALF_MS2, HEWL• ALF_MS3 and HEWL• ALF_MS2 adduct crystals. Values in parentheses correspond to the highest resolution shell.

	HEWL·ALF_MS2	HEWL·ALF_MS3	HEWL·ALF_MS4
X-ray source	P14 (PetraIII)	I02 (Diamond)	ID23-1 (ESRF)
Crystal data			
Space group	$P4_32_12$	$P4_32_12$	$P4_32_12$
Unit cell parameters (Å, º)	a = b = 77.97, c = 37.46 $\alpha = \beta = \gamma = 90$	a = b = 78.54, c = 37.04 $\alpha = \beta = \gamma = 90$	a = b = 78.94, c = 37.02 $\alpha = \beta = \gamma = 90$
Molecules per ASU	1	1	1
Mosaicity (°)	0.05	0.60	0.53
Matthews coefficient (Å³/Da)	1.96	1.98	1.99
Solvent content (%)	37.38	37.88	38.36
Data collection			
Wavelength (Å)	0.976	0.979	0.954
Resolution range (Å)	38.98–1.18 (1.20–1.18)	37.06–1.40 (1.42–1.40)	35.34–1.44 (1.46–1.44)
<I/σI>	29.4 (3.3)	20.8 (2.3)	10.7 (2.1)
Multiplicity	14.1 (12.6)	12.4 (12.9)	9.5 (9.5)
Number of observed reflections	542321 (23700)	291900 (14987)	207071 (10003)
Number of unique reflections	38473 (1882)	23561 (1164)	21840 (1048)
R_{pim} (%)	1.5 (37.5)	2.4 (53.3)	4.8 (67.1)
Completeness (%)	99.8 (96.3)	100 (100)	100 (100)
Refinement			
Resolution range (Å)	38.98–1.18	37.06–1.40	35.34–1.44
R_{work} (%)	22.81	16.90	17.40
R_{free} (%)	25.55	19.80	20.20
RMSD bond length (Å)	0.023	0.023	0.024
RMSD bond angle (º)	1.96	2.26	2.19
Ramachandran plot (%)			
Residues in favored regions	98.43	96.8	96.8
Residues in additionally allowed regions	1.57	3.2	3.2
Residues in disallowed regions	0	0	0

$R_{pim} = \Sigma_{hkl} [1/(N-1)]^{1/2} \Sigma_i |I_i(hkl) - \langle I(hkl) \rangle| / \Sigma_{hkl} \Sigma_i I_i(hkl)$, where N is the multiplicity measured.

$R_{work} = \Sigma \; ||F_{calc}| - |F_{obs}|| \; / \; \Sigma |F_{obs}| \times 100$, where F_{calc} and F_{obs} are the calculated and observed structure factor amplitudes, respectively.

R_{free} is calculated for a randomly chosen 5% of the reflections for each dataset.

The refinement of the three structures is not finished yet but, at the current refinement stage, some features are already observable including the clear formation of protein•CORM adducts contrasting with the results obtained in the previous experiments with a shorter soaking time. Similarly to the previous reported protein•CORM structures, the most relevant adducts are located next to the histidine residue (His15).

The binding of ALF_MS4 to His15 is closely related with the structures previously obtained using different ruthenium-based CORMs. In this case, an octahedral geometry is observed at the metal site, where Ir is found coordinating one of the nitrogen atoms of His15, one CO and four water molecules (Figure 2.25). The adduct was modeled with an occupancy of 0.65 (the iridium atom has a B-factor of 40.8 $Å^2$).

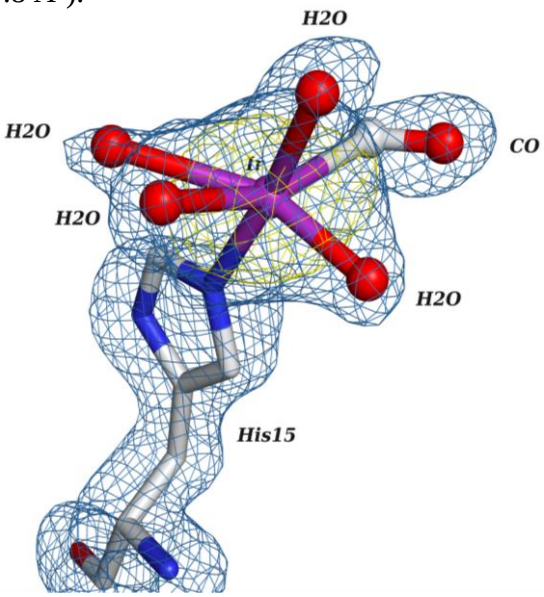

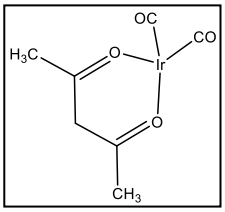

Figure 2.25 – Structural representation of the HEWL•ALF_MS4 adduct. The iridium moiety interacts with six ligands – one CO, four water molecules and a nitrogen atom of His15 – in an octahedral geometry. Electron density maps: 2Fo–Fc (blue, 1.0 σ) and anomalous (yellow, 3.0 σ); carbon in gray, nitrogen in blue, oxygen in red and iridium in purple. Picture has been prepared using Pymol. In the insert, the original structure of ALF_MS4 is shown.

ALF_MS4 is a dicarbonyl complex but only one CO was detected in the adduct suggesting a decarbonylation pathway similarly to those found for the $[Ru(CO)_3L_3]$ CORMs ALF850, ALF475, ALF487 and CORM-3 . The results here obtained for the reactivity of this $Ir(CO)_2L_2$ CORM are encouraging and prompt further in-vitro studies to attend its putative biologic activity.

In the HEWL•ALF_MS2 structure, a distorted octahedral geometry was also found for the His15 binding site (Figure 2.26). The single CO molecule of ALF_MS2 is observed in the protein-CORM adduct suggesting a putative slow CO releasing profile for this $IrCO_2L$ complex. Similarly to ALF_MS1, Arg14 appears to be interacting with the iridium moiety. Three water molecules and the Nε2 of the imidazole ring of His15 complete the six coordination sphere.

With an occupancy of 0.65, the observed bond distance between the iridium atom and the carbon atom of CO, 2.01 Å, is in the range of the values determined in the previous complexes.

Differently from the past examples, the obtained adduct kept the CO moiety existing in the parent CORM, suggesting a higher stability of the complex upon CO release compared with the other tested compounds. Most likely, this CO will be released according to the mechanism explained before. If the release doesn't occur, the use of this compound as a viable CORM will be compromised. However, if ALF-MS2 proves to be, in fact, a CORM, such stability could be quite beneficial, increasing the life-time of the complex in circulation. Moreover, a CORM with a single CO can simplify pharmacokinetic characterization and *in-vitro* and *in-vivo* studies that are very challenging for multi-CO CORMs due to the inherent instability of the pro-drugs. The high resolution structure here obtained is a good starting point for future studies of this $IrCOL_3$ complex and our first step will be the detection of the CO release using CG or/and UV-visible spectrophotometry using heme-binding proteins or fluorescent probes as COP-1.[170]

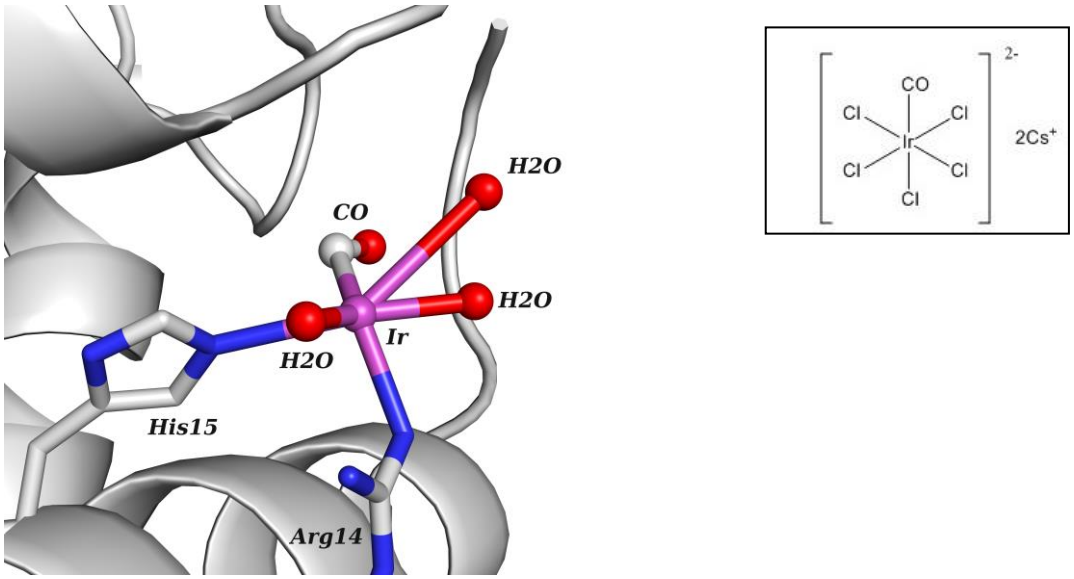

Figure 2.26 – Structural representation of the HEWL•ALF_MS2 adduct. The iridium moiety interacts with six ligands – one CO, three water molecules and two nitrogen atoms of Arg14 and His15 – in a distorted octahedral geometry; carbon in gray, nitrogen in blue, oxygen in red and iridium in purple. Picture has been prepared using Pymol. In the insert, the original structure of ALF_MS2 is shown.

In the HEWL•ALF_MS2 structure, some disordered or low occupancy metal moieties were also found in other binding sites as confirmed by the anomalous signal. In addition to the expected aspartate residues (in this case, Asp18), a significant electron density blob was found next to a tryptophan residue (Trp62). Trp62 is disordered – as proved by its poorly defined density – but our current analysis shows that the iridium is interacting with the aromatic nitrogen atom and some water molecules could be added to the adduct even if the presence of a CO molecule should be not completely discarded. Up to now, this is the first time that a clear interaction between a CORM and a Trp residue is observed. This unspecific binding is of great importance and cannot be neglected since many studies reported in the literature only take into account histidines as CO vehicles. In fact, it is very tempting for many scientists to admit that the number of CORMs bound to a biological molecule

corresponds to the number of histidine residues present, even though we have shown that Asp and, now, Trp, are active players in this process. These details can hardly be obtained by any other technique and this is why we believe an atomic-detail characterization of the interaction between a given CORM and target/model proteins is of utmost importance for the scientific progress of the field.

Moving to the platinum-based CORM, the HEWL•ALF_MS3 structure presents a distinct geometry when compared with the large majority of the previous determined structures. The platinum moiety was modeled (occupancy of 0.60) with four ligands: one CO, two bromide ions and a nitrogen atom of His15 (Figure 2.27).

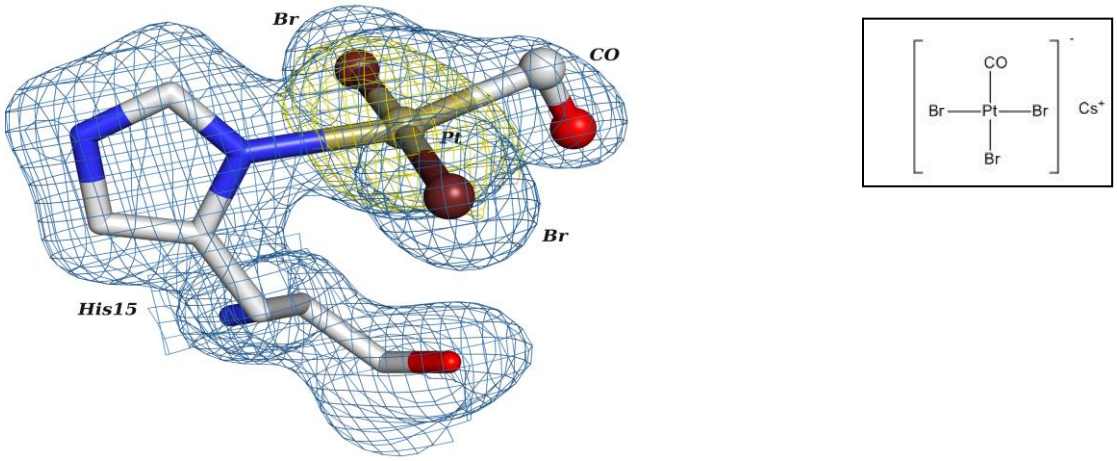

Figure 2.27 – Structural representation of the HEWL•ALF_MS3 adduct. The platinum moiety interacts with four ligands: one CO, two bromine moieties and a nitrogen atom of His15. Electron density maps: 2Fo–Fc (blue, 1.0 σ) and anomalous (yellow, 3.0 σ); carbon in gray, nitrogen in blue, oxygen in red and platinum in olive. Picture has been prepared using Pymol. In the insert, the original structure of ALF_MS3 is shown.

Moreover, a remarkable difference when compared with the other structures is observable. Two out of the initial three bromine moieties remain in the adduct rather thzan their substitution by water molecules as so frequently registered with chloride in the previous HEWL•CORM structures (water molecules were initially modeled but significant positive blobs of electron density appear in the Fo-Fc maps excluding their presence). The effect of the electronegativity of the ancillary ligands is known to affect the stability of the complexes and consequently, the CO releasing profile. In this case, the single CO moiety of ALF_MS3 is observed in the crystal structure of the protein-CORM adduct. This is actually in agreement with the discussed DFT data by which the CO is released prior the displacement of the other ancillary ligands.

Similarly to HEWL•ALF_MS2, the found adduct in HEWL•ALF_MS3 model also kept the CO molecule existing in the original CORM. Therefore, an identical hypothesis could be formulated. By one hand, an excessive stability could lead to the ineffectiveness of the application of ALF_MS3 as a CO releasing molecule. By the other hand, such stability could increase the life-time of the complex in circulation improving its therapeutic application. Once again, further studies are required in order to confirm the behavior of the complex.

As observed with CORM-3 and ALF850, FTIR experiments were useful to show the presence of Ru–CO species bound to HEWL. Therefore, a similar strategy was followed with these three complexes attempting to confirm the X-ray crystallography results.

A spectrum for a native HEWL sample was firstly prepared – the protein was prepared similarly to those incubated with the complexes. It was not possible to lyophilize the HEWL•ALF_MS2 sample due to poor handling, making it impossible to perform the respective FTIR measurement. However, HEWL•ALF_MS3 and HEWL•ALF_MS4 samples were properly lyophilized and FTIR spectra were traced.

Analyzing the obtained results (Figure 2.28), it is possible to observe that the three spectra are very similar to each other. Moreover, contrasting with the spectrum of ALF_MS3 (Figure 2.23) and ALF_MS4 (data not shown), no peaks are observable in the CO stretching region: such result is expected in the native sample but its occurrence in the HEWL•ALF_MS3 and HEWL•ALF_MS4 samples means that no metal–CO containing species remain coordinated to HEWL.

These results suggest that both ALF_MS3 and ALF_MS4 are labile enough to release CO as result of the interaction with the protein and be considered as biological active CORM. This appears to be in agreement with the crystallographic HEWL•ALF_MS4 model in which a release of one (out of two) CO was detected. However, in the crystallographic HEWL•ALF_MS3 model, the unique CO was kept in the adduct in a long-time soaking experiment (seven days); it is plausible to speculate that the incubation of the protein with the compound and its *in-crystallo* behavior lead to a different CO release profile in solution. On the other hand, an ineffective incubation cannot be discarded; ICP-AES (Inductively Coupled Plasma-Atomic Emission Spectrometry) will be hereafter used to detect the presence of metal clusters bound to protein confirming the success of the incubation step.

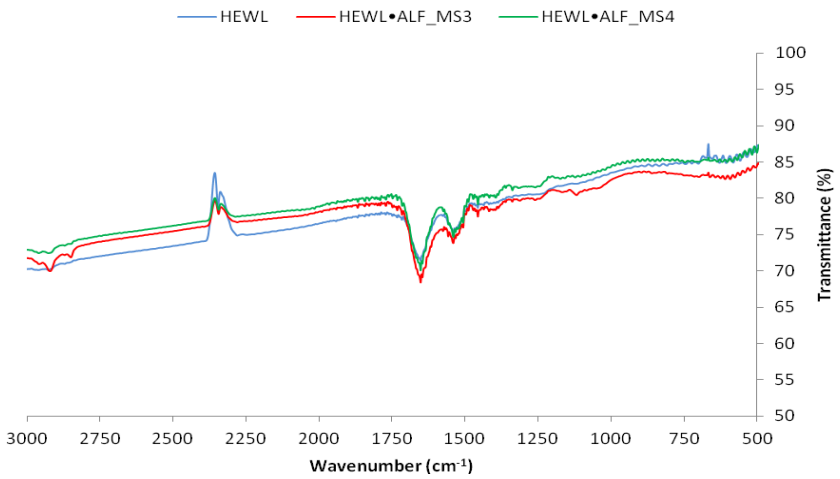

Figure 2.28 – FTIR spectra of solid native HEWL (blue), HEWL•ALF_MS3 (red) and HEWL•ALF_MS4 (green) in KBr pellets. The three spectra are quite similar pointing that only HEWL is contributing for the obtained results. Also importantly, no peaks were identified in the CO stretching region revealing the absence of CO moieties bound to the protein.

2.2.2.3 – Interactions with Human and Bovine Serum Albumin

It was previously mentioned that, from a crystallographic point of view, the use of albumin to study CO releasing molecules is a significant challenge due to the low/medium resolution obtained. Notwithstanding, it is also evident that albumin is the most abundant protein in plasma capable of transport several drugs largely controlling their distribution and, consequently, their pharmacokinetics.

Considering the previous paragraph, different approaches have been tried in order to crystallize the protein for similar structural studies to those described with HEWL. Two different types of serum albumin – HSA (human) and BSA (bovine) – have been used due to their high (76%) sequence identity (Figure 2.29).

```
HSA       DAHKSEVAHRFKDLGEENFKALVLIAFAQYLQQCPFEDHVKLVNEVTEFAKTCVADESAE
BSA       DTHKSEIAHRFKDLGEEHFKGLVLIAFSQYLQQCPFDEHVKLVNELTEFAKTCVADESHA
          *:****:**********.**.******:********::*******:************

HSA       NCDKSLHTLFGDKLCTVATLRETYGEMADCCAKQEPERNECFLQHKDDNPNLPRLVRPEV
BSA       GCEKSLHTLFGDELCKVASLRETYGDMADCCEKQEPERNECFLSHKDDSPDLPKL-KPDP
           *:*********:**.**:******:***** **********.****.*:**:* :*:

HSA       DVMCTAFHDNEETFLKKYLYEIARRHPYFYAPELLFFAKRYKAAFTECCQAADKAACLLP
BSA       NTLCDEFKADEKKFWGKYLYEIARRHPYFYAPELLYYANKYNGVFQECCQAEDKGACLLP
          :.:*  *: :*:.*  ********************::*::*:.* ***** **.*****

HSA       KLDELRDEGKASSAKQRLKCASLQKFGERAFKAWAVARLSQRFPKAEFAEVSKLVTDLTK
BSA       KIETMREKVLASSARQRLRCASIQKFGERALKAWSVARLSQKFPKAEFVEVTKLVTDLTK
          *:: :*::  ****:***:***:*******:***:******:******.**:********

HSA       VHTECCHGDLLECADDRADLAKYICENQDSISSKLKECCEKPLLEKSHCIAEVENDEMPA
BSA       VHKECCHGDLLECADDRADLAKYICDNQDTISSKLKECCDKPLLEKSHCIAEVEKDAIPE
          **.**********************:***:*********:***************:* :*

HSA       DLPSLAADFVESKDVCKNYAEAKDVFLGMFLYEYARRHPDYSVVLLLRLAKTYETTLEKC
BSA       NLPPLTADFAEDKDVCKNYQEAKDAFLGSFLYEYSRRHPEYAVSVLLRLAKEYEATLEEC
          :** *:***.*.******* ****.*** *****:****:*:* :****** **:***:*

HSA       CAAADPHECYAKVFDEFKPLVEEPQNLIKQNCELFEQLGEYKFQNALLVRYTKKVPQVST
BSA       CAKDDPHACYSTVFDKLKHLVDEPQNLIKQNCDQFEKLGEYGFQNALIVRYTRKVPQVST
          **  *** **:.***::* **:**********: **:**** *****:****:*******

HSA       PTLVEVSRNLGKVGSKCCKHPEAKRMPCAEDYLSVVLNQLCVLHEKTPVSDRVTKCCTES
BSA       PTLVEVSRSLGKVGTRCCTKPESERMPCTEDYLSLILNRLCVLHEKTPVSEKVTKCCTES
          ********.*****::**.:**::****:*****::**:***********::********

HSA       LVNRRPCFSALEVDETYVPKEFNAETFTFHADICTLSEKERQIKKQTALVELVKHKPKAT
BSA       LVNRRPCFSALTPDETYVPKAFDEKLFTFHADICTLPDTEKQIKKQTALVELLKHKPKAT
          ***********  ******* *: : ********** :.*:***********:*******

HSA       KEQLKAVMDDFAAFVEKCCKADDKETCFAEEGKKLVAASQAALGL
BSA       EEQLKTVMENFVAFVDKCCAADDKEACFAVEGPKLVVSTQTALA-
          :****:**::*.***:*** *****:*** ** ***.::*:**.
```

Figure 2.29 – Comparison of the amino acid sequence of human serum albumin (UniProt entry: P02768) and bovine serum albumin (UniProt entry: P02769). Alignment results were obtained with CLUSTAL Omega multiple sequence alignment program available in the EMBL-EBI web server; an "*" (asterisk) indicates positions which have a single, fully conserved residue, a ":" (colon) indicates conservation between groups of strongly similar properties and a "." (period) indicates conservation between groups of weakly similar properties.

2.2.2.3.1 – Materials and Methods

ALF_MS2 and ALF_MS3 were synthesized as described in the chapter 2.2.2.1. Acetylacetonatodicarbonyliridium(I) – ALF_MS4 – was purchased from Sigma-Aldrich. HSA (Recombumin®) and BSA (Fraction V, Fatty Acid-Free) were purchased from Novozymes and Calbiochem, respectively. Gel filtration chromatography was performed using both Superdex 75 10/300 GL and Superdex 200 prep grade columns (GE Healthcare) coupled to a FPLC system (AKTA Prime Plus, GE Healthcare). Samples were concentrated with 10 kDa Centricon Vivaspin Turbo concentrators from Sartorius. The final concentration was confirmed by A_{280} using a spectrophotometer Ultrospec 2100 Pro (Amersham Bioscienses). Nanocrystallization setups were performed in an Oryx8 protein crystallization robot (Douglas Instruments).

PEG 4K, PEG5000 MME, monobasic potassium phosphate, dibasic potassium phosphate, ammonium chloride, cadmium sulfate, HEPES (4-(2-hydroxyethyl)-1-piperazineethanesulfonic acid), Tris (Trizma, Tris-(hydroxymethyl)-aminomethane) and glycerol were purchased from Sigma-Aldrich. Sodium chloride and sodium acetate was acquired from Scharlay. Calcium acetate was purchased from Merck.

- **Protein purification – Gel filtration chromatography**

The initial purification of HSA was carried out based in the procedure available in the literature.[304] The protein sample (500 µl, 50 mg/ml) was purified on a Superdex S75 gel filtration column using 50 mM potassium phosphate pH 7.5 and 150 mM sodium chloride as a running buffer. The eluted fractions containing HSA (1 ml) were confirmed by SDS-PAGE (10% acrylamide) electrophoresis (200 mA, variable voltage, 45 minutes). The described purification was not totally efficient and it was repeated using a Superdex S200 gel filtration column (sample: 2 ml, 75 mg/ml). The selected fractions were pooled together and concentrated to 100 mg/ml in the same buffer.

BSA was also purified according previously published protocols.[305,306] The protein sample was dissolved in a buffer (2 ml, 75 mg/ml) containing 10 mM Tris-HCl pH 7.5 and 150 mM NaCl followed by its purification using a Superdex S200 gel filtration column. The eluted fractions of BSA (1 ml), confirmed by SDS-PAGE electrophoresis, were pooled together and concentrated to 10 and 40 mg/ml in the referred buffer.

- **Crystallization trials and X-ray diffraction experiments**

Both HSA and BSA, before and after a purification step, have been used in different crystallization trials in order to get suitable crystals to pursuit the structural characterization of protein•CORM adducts.

HSA (100 mg/ml) was initially tested with the published crystallization conditions: 25-30% (w/v) PEG4K and 50 mM potassium phosphate pH 7.5.[304] The sitting drop vapor diffusion method (drops: 1+1 and 2+2 with 1000 µl of precipitant solution in the well) was carried out at 4ºC and 20ºC.

Several initial screens were also tested – Structure 1 and 2 (from Molecular Dimensions) and an *in-house* sparse matrix screen (80!) indicated in Appendix 1, Appendix 2 and Appendix 3, respectively – using the crystallization robot. These setups were carried out at 20ºC with 0.5 µl of protein plus 0.5 µl of precipitant solution on 96-well crystallization plates (Douglas Instruments). A promising condition was found containing 1 M sodium acetate, 0.05 M cadmium sulfate and 0.1 M HEPES pH 7.5, and it was optimized as further discussed. Microseeding was also tried. Several native datasets were analyzed using Synchrotron radiation but the vast majority presents a low resolution (ca 3-4 Å) or it was not possible to process them.

The protein was also incubated with ALF_MS2, ALF_MS3 and ALF_MS4 (1:10) for one hour and overnight, prior to crystallization trials. However, no good diffracting crystals were obtained using this co-crystallization approach.

Two different published crystallization conditions were also tested with BSA (10 and 40 mg/ml): 20% PEG5000 MME, 0.25M ammonium chloride, 0.1M MES pH 6.5 (condition 1) and 0.2 M calcium acetate, 20% PEG4K, 0.1 M Tris-HCl pH 6.5 (condition 2).[305,306] For both conditions, hanging drop vapor diffusion method (drops: 1+1 and 2+2 with 700 µl of precipitant solution in the well) was attempted at 20ºC.

Needle-like crystals (approximately 0.3×0.05×0.05 mm^3) were obtained with the second condition after 3-4 days of crystallization set-up, and the crystals were flash frozen with a harvesting buffer supplemented with 30% (v/v) glycerol as a cryo-protectant. A soaking experiment with ALF_MS3 (10 mM) was also performed. Using synchrotron radiation (beamline ID23-1 at the ESRF, Grenoble, France), the best native crystal diffracted beyond 3.3 Å resolution and a complete data set was collected.

2.2.2.3.2 – Results and Discussion

Both HSA and BSA used in these studies were commercially purchased and, for such reason, an elevated purity is expected. Nevertheless, commercial proteins often come with impurities that can prevent their crystallization. Moreover, mammalian albumins are known to form dimers due to an unpaired cysteine.[305] A heterogeneous sample – with a simultaneous composition of monomers and dimers – can be a significant impediment to achieve a successful crystallization. Keeping this in mind, an additional step of protein purification – size exclusion chromatography – to remove protein dimers could be strongly advantageous.

2.2.2.3.2.1 – Human serum Albumin

Following the available procedure, a gel filtration chromatography was performed using a Superdex S75 column. The results are shown in Figure 2.30.

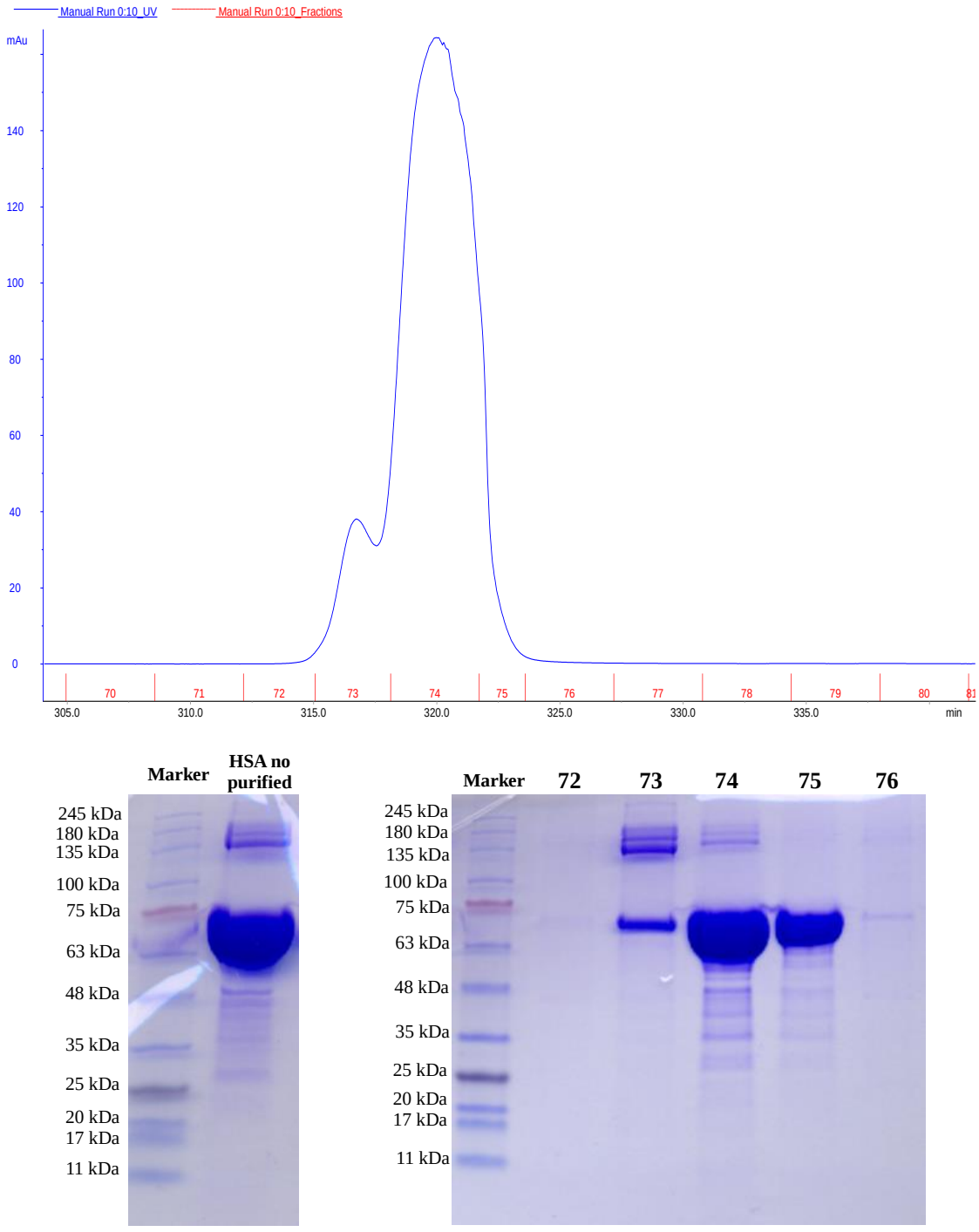

Figure 2.30 – Purification of human serum albumin by gel filtration chromatography using a Superdex S75 column. Top: Elution profile obtained from the gel filtration column being visible two distinctive peaks corresponding to the dimeric and monomeric forms (smaller and larger peaks, respectively). Bottom: SDS-PAGE (10% acrylamide) analysis of the different fractions obtained from the gel filtration (fractions were identified according to the numeration of the chromatogram) as well as a sample of unpurified HSA.

Analyzing the gel lane corresponding to the unpurified HSA sample, it is possible to verify a very intense band (approximately 66 kDa) corresponding to the expected monomeric form of the protein (66.5 kDa). However, bands of smaller molecular weight are also observable, likely corresponding to some proteolysis, in addition to some bands of the dimeric HSA (approximately 135 kDa). As registered in the chromatogram, the gel filtration chromatography reveals the existence of two peaks, which were interpreted as the dimeric and monomeric forms of the protein (firstly and secondly eluted, respectively).

Since Superdex S75 has a separation range for molecules with molecular weights between 3 and 70 kDa and HSA has a molecular weight close to the mentioned upper limit a new similar gel filtration chromatography was performed using a Superdex S200 which has a separation range for molecules with molecular weights between 10 and 600 kDa. The results are shown in Figure 2.31.

Similarly to the described, the obtained chromatogram shows a smaller peak firstly eluted (dimer) immediately followed by a larger peak (monomer). Importantly, the bands of the gel corresponding to proteolysis, with smaller molecular weight, were significantly reduced, making this a better preparation for crystallization.

Fractions 18, 19 and 20 were pooled together and concentrated to 100 mg/ml in 50 mM potassium phosphate pH 7.5 and 150 mM sodium chloride. This purified HSA sample was used in the next explained crystallization trials along with samples not subjected to extra purification steps. No significant improvements in the morphology of the crystals and in the respective diffraction quality were registered when the purified protein was used. Nevertheless, the removal of the dimers and proteolysis products by the described purification protocol should be considered in the next studies involving this protein.

The crystallization conditions available in the literature – 25-30% (w/v) PEG4K and 50 mM potassium phosphate pH 7.5 – and small variations on PEG concentration and pH – failed to produce crystals. Consequently, using a crystallization robot, some initial screens were also tested in order to find a suitable crystallization condition.

Combining the three mentioned screens, 176 conditions were tested. From all these conditions, only one (condition 16 of Structure 2 screen – 1 M sodium acetate, 0.05 M cadmium sulfate and 0.1 M HEPES pH 7.5) was identified as a potential hit with several multiple bidimensional plates (Figure 2.32). The condition was then further optimized considering the precipitant agent, the salt and the pH value of the buffer as summarized in Table 2.8. The best crystals resulting from such optimization (Figure 2.32) were found in the following condition: 0.4 M sodium acetate, 0.11 M cadmium sulfate and 0.1 M HEPES pH 7.8 (12.5% pH 7 and 87.5% pH 8). Using

some crystals previously obtained in this optimized condition, microseeding was tried but no significant improvements were achieved.

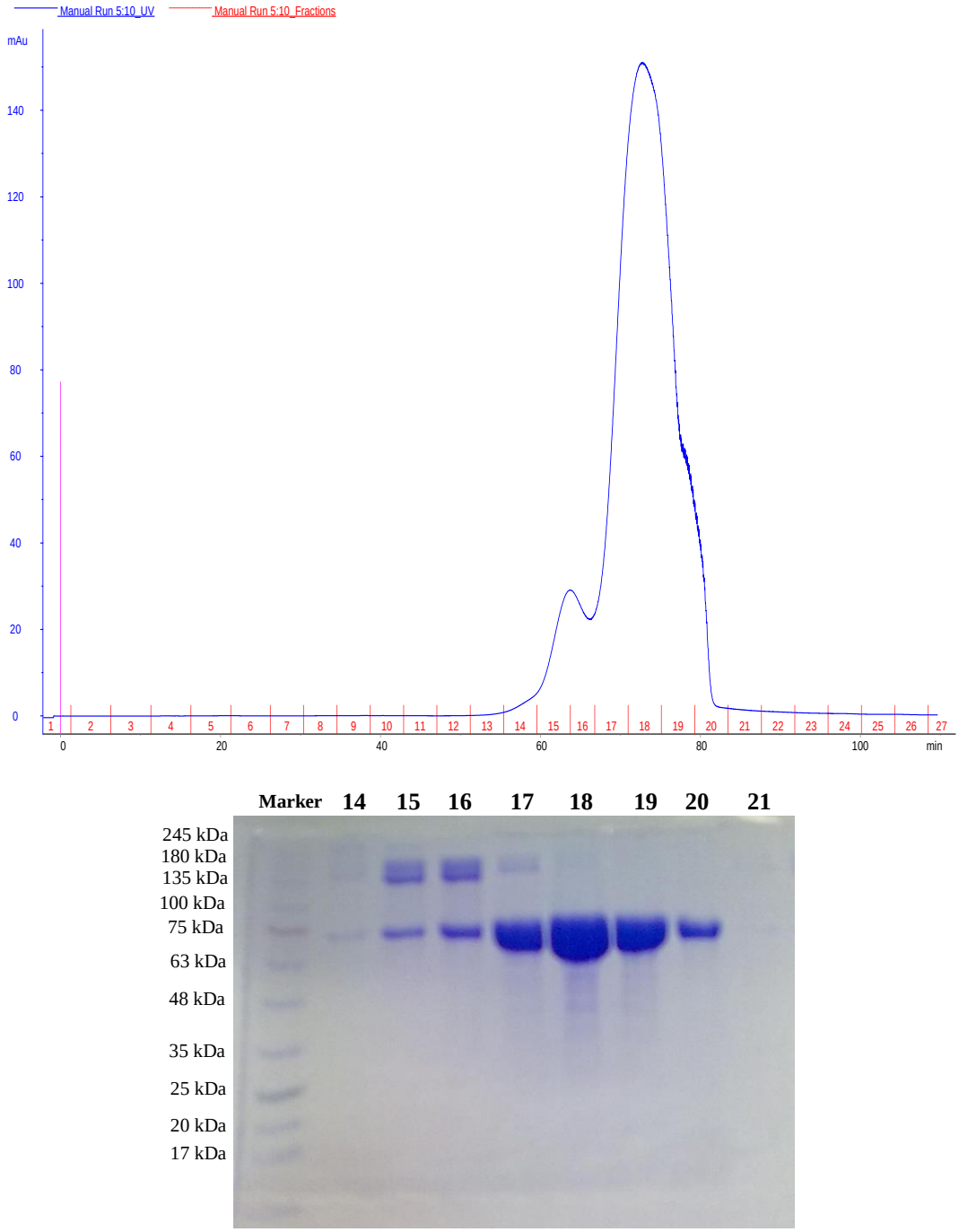

Figure 2.31 – Purification of human serum albumin by gel filtration chromatography using a Superdex S200 column. Top: Elution profile obtained from the gel filtration column being visible two peaks corresponding to the dimeric and monomeric forms (smaller and larger peaks, respectively). Bottom: SDS-PAGE (10% acrylamide) analysis of the different fractions obtained from the gel filtration (fractions were identified according to the numeration of the chromatogram).

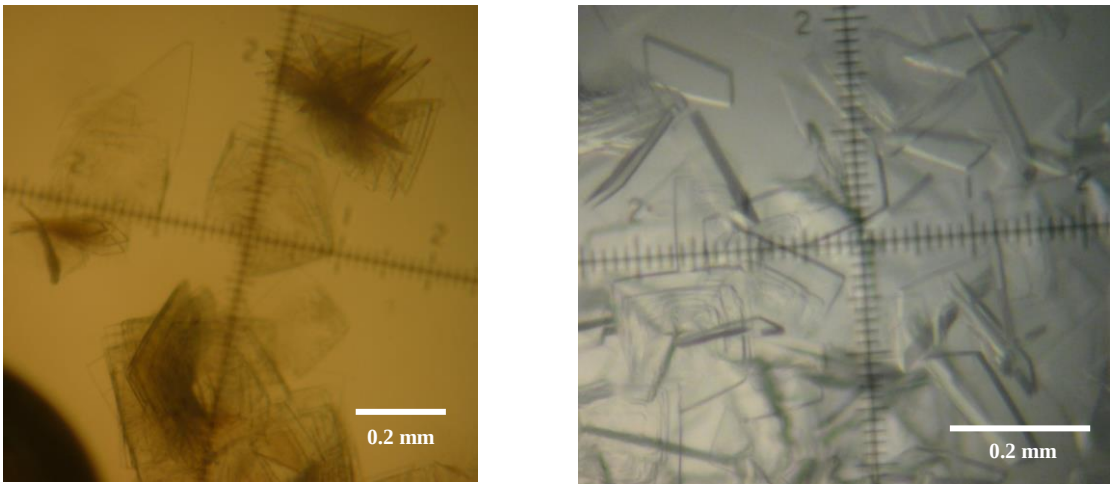

Figure 2.32 – Native HSA crystals obtained before and after the optimization of the found crystallization hit (left and right, respectively). The performed optimization allowed to select some tridimensional crystals for the diffraction experiments rather than the initial 2D plates.

Different crystals obtained with the mentioned condition were tested using Synchrotron radiation but no useful datasets were collected. Most of the tested crystals diffract poorly (6 to 7 Å) or present a high anisotropy not allowing their structure determination. Nevertheless, different space groups (namely P1, P4 and C121) and associated cell constants have been obtained similarly to those reported in the PDB; as a representative example, a monoclinic (C121) 3.5 Å resolution dataset was collected at beamline I03 (Diamond) with the following cell constants: a=190.22 Å, b=38.97 Å, c=96.24 Å, α=γ=90° and β=105.75°.

Table 2.8 – Optimization of the crystallization condition of HSA. Different parameters were tested namely the precipitant agent (four different concentrations), salt (six different concentrations) and pH (range of values: 7-8).

Sodium acetate (M)	Cadmium sulfate (M)	% of 0.1 M HEPES	
		pH 7	**pH 8**
		100	0
	0.03	87.5	12.5
0.2	0.07	75	25
0.4	0.09	62.5	37.5
0.6	0.11	50	50
	0.13	37.5	62.5
	0.15	25	75
		12.5	87.5
		0	100

Using the determined condition, some co-crystallization trials with the iridium- and platinum-based CORMs were also performed. However, no suitable crystals have been obtained. Therefore, it was not possible to study the interactions established between this protein and different CORMs. New attempts to obtain suitable crystals are planned and will be further addressed in the last chapter of this thesis.

2.2.2.3.2.2 – Bovine serum Albumin

Similarly to HSA, a gel filtration chromatography was performed using a Superdex S200 column with BSA in order to separate the monomeric and dimeric forms of the protein. The results are shown in Appendix 4. The obtained chromatogram is quite related with the ones obtained with HSA and a smaller peak (corresponding to the dimer) and a larger peak (corresponding to the monomer) were found.

The fractions were concentrated to 10 and 40 mg/ml in 10 mM Tris-HCl pH 7.5 and 150 mM NaCl to be further used in crystallization trials.

The structure of BSA was not solved and published in the PDB until 2012. Since then, four entries are available: two native structures (3V03 and 4F5S) and two structures complexed with different ligands (4JK4 and 4OR0). These four crystal structures were obtained using two distinct crystallization conditions: 20-24% PEG5000 MME, 0.15-0.3 M ammonium chloride, 0.1M MES pH 6.5 (condition 1) and 0.2 M calcium acetate, 20% PEG4K, 0.1 M Tris-HCl pH 6.5 (condition 2).

Both conditions were tried in addition to a slight variation in the precipitant agent of the second condition (16-24% PEG4K). However, all the tested conditions originate similar results: needle-like crystals as illustrated in Figure 2.33.

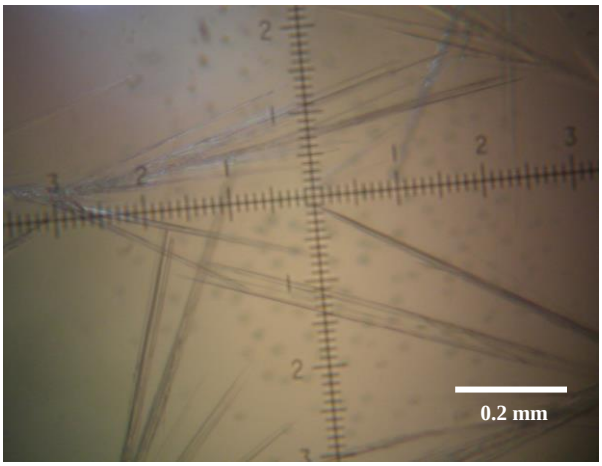

Figure 2.33 – Native BSA crystals obtained with 0.2 M calcium acetate, 20% PEG4K, 0.1 M Tris-HCl pH 6.5 (condition 2). Needle-like crystals were obtained in the generality of the tested crystallization conditions and some of them present dimensions (approximately 0.3×0.05×0.05 mm^3) compatible with their use in further diffraction trials.

A soaking experiment with ALF_MS3 (10 mM) was also performed and both native and soaked crystals were tested using synchrotron radiation (beamline ID23-1 at the ESRF, Grenoble, France). However, only one native crystal diffracted beyond 3.3 Å resolution. The structure was not solved due to low resolution but it was possible to determine the space group (C121) and the cell constants (a=218.91 Å, b=45.02 Å, c=154.39 Å, α= γ=90° and β=110.08°) which are in agreement with the reported values in the PDB.

Further optimization trials are required in order to get suitable crystals for a more detail comprehension of the BSA•CORMs interactions.

2.2.2.4 – Interactions with Human Serum Transferrin

The term "transferrin" is used to refer a family of glycoproteins – mainly comprising serum transferrin, lactoferrin and ovotransferrin – with an approximate molecular mass of 80 kDa (with two homologous lobes: N- and C-terminal) which play an important role in the iron transport and homeostasis. The protein can adopt a closed (holo-transferrin) or an open (apo-transferrin) conformation if it is iron-loaded or iron-free, respectively.[307,308,309]

Serum transferrin is particularly important for Fe^{3+} transport (one ion binding at each lobe) but there are evidences that the protein is also able to transport some other alternative metals making it a suitable candidate for metal-based compounds carrier.[78,310]

CORMs are not exception and, as metal-based complexes, their interactions with human serum apo-transferrin (hs-apoTF) are potentially involved in their respective pharmacokinetics. Consequently, hs-apoTF was also used in the structural studies herein presented.

2.2.2.4.1 – Materials and Methods

ALF_MS2 and ALF_MS3 were synthesized as described in the chapter 2.2.2.1. Acetylacetonatodicarbonyliridium(I) – ALF_MS4 – was purchased from Sigma-Aldrich. Human serum apo-transferrin, PEG 4K, glycerol, ammonium citrate, Tris (Trizma, tris-(hydroxymethyl)-aminomethane) and sodium carbonate (Na_2CO_3) were also purchased from Sigma-Aldrich. Sodium chloride was acquired from Scharlay.

- **X-ray crystallography – Crystallization, data collection, structure solution and structure refinement**

A sample of hs-apoTF was prepared at 30 mg/ml in 20 mM Tris-HCl pH 8, 20 mM sodium carbonate and 200 mM sodium chloride and crystallized using the condition described in the literature: 15% glycerol, 20% PEG 4K, 0.2 M ammonium citrate pH 7; hanging drops were prepared at 20°C

using the vapor diffusion method (drops between 4 and 12 μl with equal volumes of protein and precipitant solution and 700 μl of the precipitant solution in the reservoir) in 24-well plates from Molecular Dimensions.[311] Crystals were observed either with a SZH10 Olympus microscope or a SteREO Discovery V12 Zeiss microscope.

This condition was further optimized varying the concentration of glycerol (9-21%) and PEG 4K (7.5-25%) as well as the pH (a range between 6 and 7). The optimization was carried out at 20 and 4 ºC with 0.5 μl of protein plus 0.5 μl of precipitant solution on 96-well crystallization plates (Douglas Instruments).

Once the best crystallization condition was found (13% glycerol, 17.5% PEG 4K, 0.2 M ammonium citrate pH 6.73), microseeding was used (nanodrops with 0.5 μl of protein, 0.4 μl of precipitant solution and 0.1 μl seeds). Moreover, different post-crystallization treatments were also tried: dehydration – transfer of the drop with the crystals into a new reservoir containing a dehydrating solution (with 30% PEG4K) during 16 hours – and incubation at 35 ºC for 15 minutes prior the crystallization setups.[312,313,314]

The best crystals (approximately 0.3×0.2×0.2 mm^3) appeared within 48 hours and several native datasets were analyzed using Synchrotron radiation.

Some of the best obtained crystals were then used in soaking experiments. The compound ALF_MS2 was dissolved in a harvesting buffer solution containing 25% (w/v) PEG 4K up to a final concentration of 10 mM and 2 μl of this solution was added to the drop. After 24 hours of soaking, the crystals were harvested and flash frozen with the harvesting buffer supplemented with 30% (v/v) glycerol as a cryo-protectant. A dataset with maximum resolution of 2.70 Å resolution was collected in beamline ID29 at the European Synchrotron Radiation Facility – ESRF (Grenoble, France).

The dataset integration and structure resolution, refinement and validation were carried out similarly to what has been earlier described in the section dedicated to HEWL and ruthenium-based CORMs (PDB entry 2HAV was used as model in MR).[311]

The protein was also incubated with ALF_MS2, ALF_MS3 and ALF_MS4 (in a 10-fold excess) for 1 hour prior the crystallization trials (using the optimized condition both in 24- and 96-well plates) but no good diffracting crystals have been obtained.

2.2.2.4.2 – Results and Discussion

The first crystallization setups were carried out reproducing the previous determined condition: 15% glycerol, 20% PEG 4K, 0.2 M ammonium citrate pH 7 (hs-apoTF at 30 mg/ml) using drops with 2 μl of protein and 2 μl of precipitant solution. Multiple crystals were obtained (Figure 2.34A) and tested in Proxima 1 (Soleil, France) but all of them did not diffract or diffracted very poorly, below 6 Å resolution. Other proportions of the drop were tested (up to 6 μl of protein and a

similar volume of the precipitant solution) and better crystals were obtained as illustrated in Figure 2.34B but no significant diffraction improvement was registered.

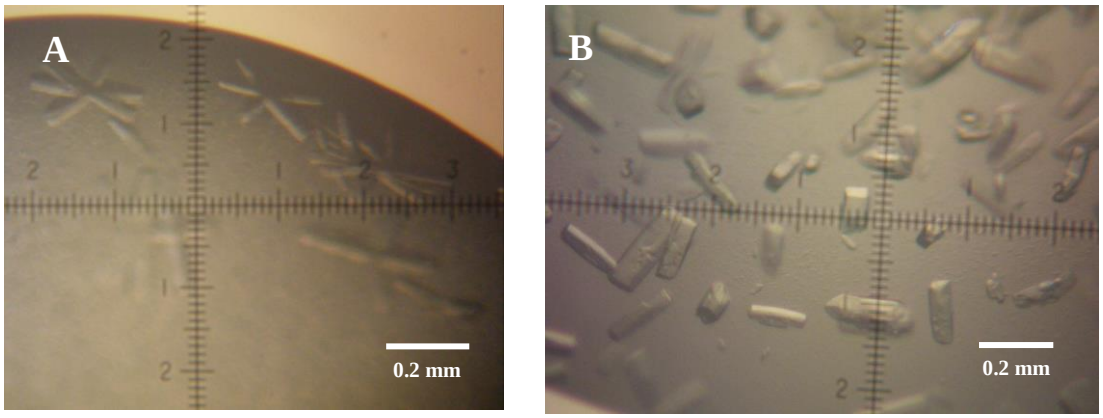

Figure 2.34 – Native hs-apoTF crystals obtained with 15% glycerol, 20% PEG 4K, 0.2 M ammonium citrate pH 7. A – Drop with 2 µl of protein and 2 µl of precipitant solution; B – Drop with 6 µl of protein and 6 µl of precipitant solution.

The condition was then further optimized considering the concentrations of PEG 4K and glycerol as well as the pH value of the buffer as summarized in Table 2.9 using the crystallization robot. The best crystals resulting from such optimization (Figure 2.35) were found in the following condition: 13%(V/V) glycerol, 17.5% PEG 4K, 0.2 M ammonium citrate pH 6.73 (prepared by combining 25% pH 6 and 75% pH 7).

Table 2.9 – Optimization of the crystallization condition of hs-apoTF. Different parameters were tested: PEG 4K (eight different concentrations), glycerol (seven different concentrations) and the pH range (6-7).

PEG 4K (%)	Glycerol (%V/V)	% of 0.2 M Ammonium citrate	
		pH 6	**pH 7**
7.5	9	100	0
10	11	87.5	12.5
12.5	13	75	25
15	15	62.5	37.5
17.5	17	50	50
20	19	37.5	62.5
22.5	21	25	75
25		12.5	87.5
		0	100

Diffraction experiments showed that a considerable improvement was achieved with the described optimization. Although the crystals appearance did not change much, a *ca* 3 Å resolution

was obtained for most of the tested crystals. This range of resolution is still very poor for a detailed atomic characterization of the CORM-protein interaction, as desired.

Microseeding was then used with the optimized crystallization but no significant differences were verified either in the morphology of crystals or in their resulting diffraction. A similar situation occurred with the two post-crystallization treatments applied: the decrease of the solvent content (dehydration) as well as the removal of eventual precipitated protein aggregates by gentile heating (35 ºC) failed to improve the crystals.

After the described optimization steps, using a similar strategy to that previously explained, ALF_MS2 (10 mM) was soaked into hs-apoTF crystals. The soaking was prolonged for 24 hours and no detectable changes were visible in the crystals (Figure 2.36). Different crystals were tested using Synchrotron radiation and the best soaked hs-apo-TF•ALF_MS2 crystal diffracted up to 2.7 Å resolution (ID29, ESRF, Grenoble). The data were processed in $P2_12_12_1$ space group and the structure was solved by Molecular Replacement. Data collection and refinement statistics are summarized in Table 2.10.

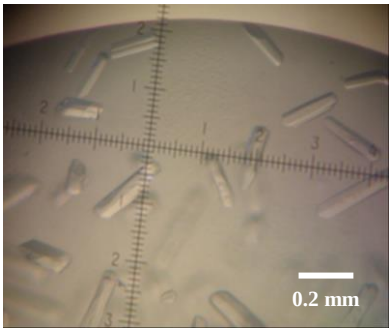

Figure 2.35 – Native hs-apoTF crystals obtained with 13% glycerol, 17.5% PEG 4K, 0.2 M ammonium citrate pH 6.73.

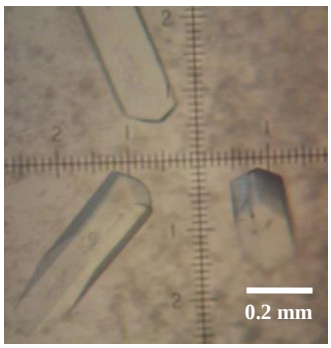

Figure 2.36 – Soaked hs-apoTF crystals with ALF_MS2. Large crystals (some of them larger than 0.3×0.2×0.1 mm^3) were obtained.

The refinement of the structure is not finished yet but is possible to discuss some relevant aspects. In each iron binding site – comprising two tyrosine, one aspartate and one histidine residues (Tyr95, Tyr188, Asp63, His249 and Tyr392, Tyr426, Asp517, His585 depending on the considered lobe) – a small density blob was found in both 2Fo–Fc and Fo–Fc maps. The blobs were not modeled but their shape as well as the absence of anomalous signal suggest that such blobs don't correspond to a protein•CORM adduct. Most likely, molecules from the crystallization condition are occupying these positions: glycerol or citrate.

Nevertheless, a 2Fo–Fc and Fo–Fc blob, with a significant anomalous signal, was found at the surface of N-terminal lobe next to a histidine residue (His578), which is not present in native crystals. An iridium moiety was modeled with an occupancy of 0.70 with a temperature factor of 96.2 $Å^2$ which, despite its high value, is in the range of values found for the polypeptide chain (Figure 2.37).

Table 2.10 – Data collection and refinement statistics for hs-apo-TF•ALF_MS2 adduct crystal. Values in parentheses correspond to the highest resolution shell.

X-ray source	ID29 (ESRF)
Crystal data	
Space group	$P2_12_12_1$
Unit cell parameters (Å, º)	a = 85.06, b = 102.03, c = 199.48 $\alpha = \beta = \gamma = 90$
Molecules per ASU	2
Matthews coefficient (Å^3/Da)	2.79
Solvent content (%)	55.98
Data collection	
Wavelength (Å)	0.972
Resolution range (Å)	46.60–2.70 (2.79–2.70)
<I/σI>	15.3 (2.0)
Multiplicity	4.9 (5.0)
Number of observed reflections	235475 (22005)
Number of unique reflections	48374 (4385)
R_{pim} (%)	1.7 (17.7)
Completeness (%)	99.8 (99.9)
Refinement	
Resolution range (Å)	46.60–2.70
R_{work} (%)	23.4
R_{free} (%)	28.8
RMSD bond length (Å)	0.011
RMSD bond angle (º)	1.56
Ramachandran plot (%)	
Residues in favored regions	88.65
Residues in additionally allowed regions	7.49
Residues in disallowed regions	3.86

$R_{pim} = \Sigma_{hkl} [1/(N-1)]^{1/2} \Sigma_i|I_i(hkl) - \langle I(hkl)\rangle|/\Sigma_{hkl} \Sigma_i I_i(hkl)$, where N is the multiplicity measured.

$R_{work} = \Sigma ||F_{calc}|-|F_{obs}|| / \Sigma|F_{obs}| \times 100$, where F_{calc} and F_{obs} are the calculated and observed structure factor amplitudes, respectively.

R_{free} is calculated for a randomly chosen 5% of the reflections for each dataset.

Probably this high value is also reflected in the disorder of the adduct and it was not possible to further model it. Moreover, the Nε2 of the imidazole ring of His578 is located 4.39 Å apart from the iridium moiety which is far away from the usual values for a covalent binding. Interestingly, a second nitrogen atom was found nearby belonging to the Lys280 residue of a neighbor symmetry molecule similarly to the verified in the HEWL•ALF_MS2 structure where a nitrogen atom from Arg14 appears to be interacting with the iridium moiety. However, the determined distance between the lysine and iridium (4.45 Å) is in the same range than the His578-Ir distance.

Therefore, the data, at the current refinement stage, is not informative about the presence or absence of a CO in the adduct. On the other hand, it is also mandatory to understand if the adduct is effectively covalently bound to the protein or weakly interacting with residues at the surface. Nonetheless, the obtained results indicate the potential ability of hs-apoTF to transport CORMs along the blood stream in different locations than the iron binding site suggesting that the protein could be able to transport such molecules even when is loaded with iron.

Such finding implies that the totality of serum transferrin – both in apo- and holo-form – is potentially available for this purpose. Consequently, the pharmacological profile – namely the pharmacokinetic profile – of these compounds will be affected: a given lower concentration of CORM could be enough to produce the desired beneficial effect since it might be efficiently delivered in the target tissue by transferrin. Further studies are required to corroborate such hypothesis.

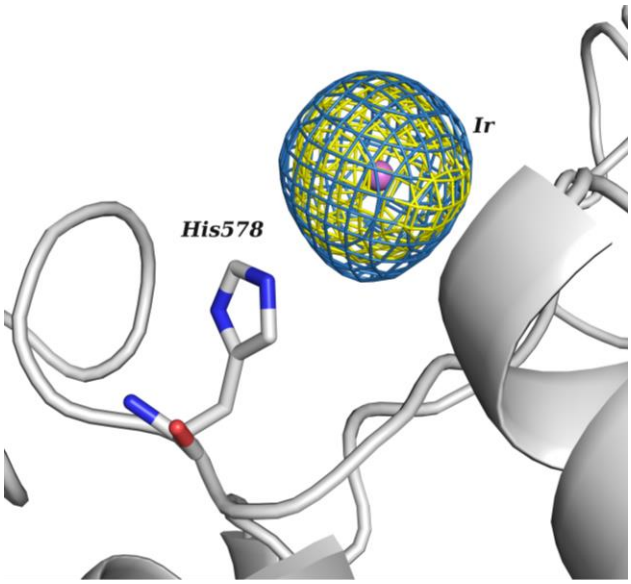

Figure 2.37 – Structural representation of the iridium moiety found at the surface of the N-terminal lobe of hs-apoTF. A strong anomalous signal is clearly visible. Histidine578 is also depicted but, at the current stage of refinement, it is not clear if the residue is bound to iridium. Electron density maps: 2Fo–Fc (blue, 1.0 σ) and anomalous (yellow, 3.0 σ); carbon in gray, nitrogen in blue, oxygen in red and iridium in purple. Picture has been prepared using Pymol.

2.2.3 – Other metal-based CORMs

The majority of the work concerning proteins and CO Releasing Molecules has been developed using ruthenium-, iridium- and platinum-based CORMs as described in the two previous chapters.

Nonetheless, some other metal-based compounds were also preliminary tested in several soaking and posterior X-ray diffraction experiments with different proteins – HEWL, bovine hemoglobin and hs-apoTF – and the obtained results will be addressed herein.

Five CORMs have been used: one manganese-based compound (ALF21), two iron-based compounds (ALF58 and ALF153) and two molybdenum-based compounds (ALF73 and ALF157). None of the molecular and structural formulas can be revealed due to intellectual property issues.

2.2.3.1 – Materials and Methods

The five CORMs – ALF21, ALF58, ALF73, ALF153 and ALF157 – were synthesized by the group of Professor Carlos Romão (ITQB-UNL). All the other reagents were obtained as previously mentioned.

HEWL and bovine hemoglobin was crystallized as described in chapters 2.2.1.2 and 2.2.1.3, respectively. For both proteins, the soaking was tried by sprinkle a small quantity of powder of the compounds on the drops with the crystals letting it to diffuse into the crystallization drop and, concomitantly, into the crystal solvent channels for 24 hours. The best soaked crystals were flash frozen (cryo-protected similar to the previously reported). Using synchrotron radiation (beamline PXIII at SLS, Villigen, Switzerland), the crystals diffracted to medium to high resolutions and several datasets were collected.

Regarding hs-apoTF, a co-crystallization methodology was followed. The protein (60 mg/ml) was incubated with the mentioned compounds in a 10-fold excess and for 1 hour and then passed through a PD-10 MiniTrap G-25 column (GE Healthcare) in order to remove the unbound compound prior the crystallization trials (with the protein at 30 mg/ml). The crystallization was carried out at 20 ^{o}C with 0.5 µl of protein, 0.4 µl of precipitant solution and 0.1 µl of seeds on 96-well crystallization plates (Douglas Instruments) using the following condition: 13% glycerol, 17.5% PEG 4K, 0.2 M ammonium citrate pH 6.73. Different datasets were collected at low resolution in beamline I04 at Diamond Light Source (Didcot, Oxfordshire, United Kingdom).

The dataset integration and structure resolution, refinement and validation were carried out similarly to the previously explained for the three proteins.

2.2.3.2 – Results and Discussion

HEWL crystals were soaked with ALF21, ALF58, ALF73, ALF153 and ALF157 for 24 hours after which the crystals remain intact as shown in Figure 2.38. Two of the compounds – ALF21 and ALF73 – reveal to be water insoluble contrasting with the other three ALFs as particularly visible in the soaked crystals with ALF153 which became strongly colored.

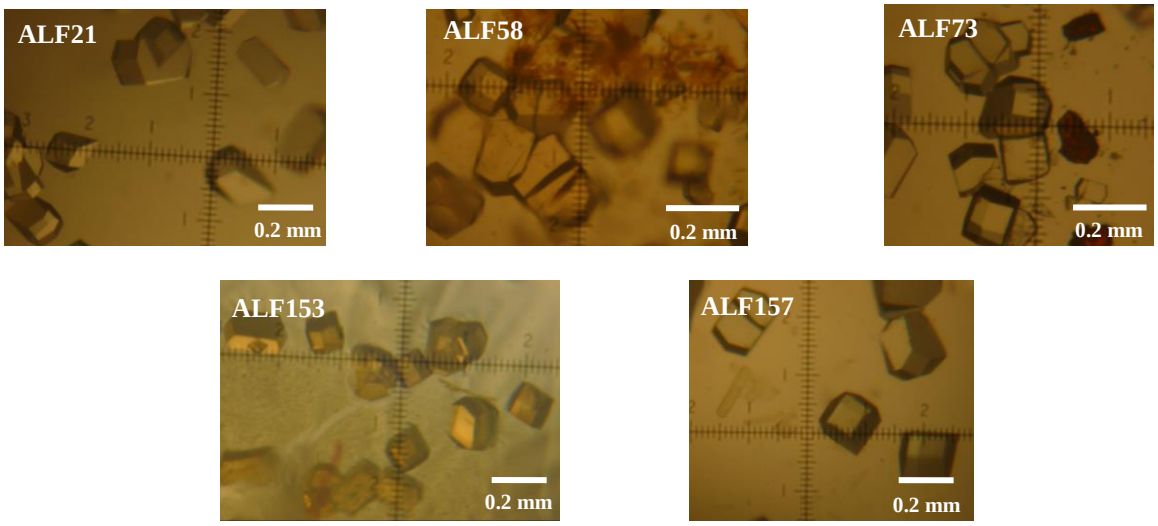

Figure 2.38 – HEWL crystals with the tested manganese-, iron- and molybdenum-based CORMs after 24 hours of soaking.

A similar procedure was adopted with bovine hemoglobin and the obtained crystals are reproduced in Figure 2.39. As expected, the compounds present a similar behavior regarding their water solubility and no color changes were observed in the crystals.

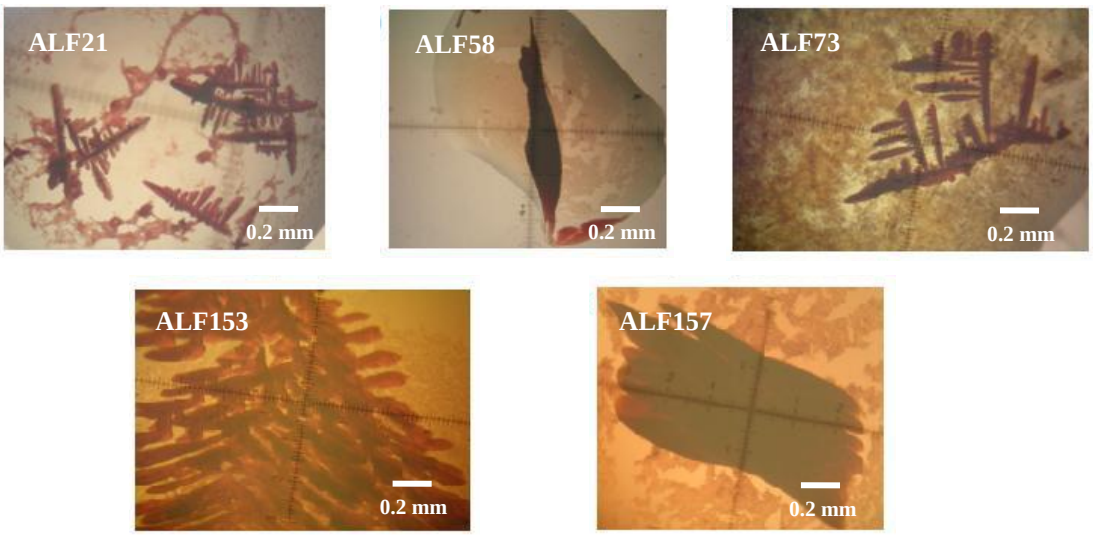

Figure 2.39 – Bovine hemoglobin crystals with the tested manganese-, iron- and molybdenum-based CORMs after 24 hours of soaking.

Several soaked HEWL and hemoglobin crystals were exposed to an incident X-ray beam using Synchrotron sources. Table 2.11 summarizes the best measured crystals.

Table 2.11 – X-ray diffraction results obtained with the soaked HEWL and bovine hemoglobin crystals with ALF21, ALF58, ALF73, ALF153 and ALF157.

Soaked crystal	Obtained resolution	Beamline (Synchrotron)
HEWL•ALF21	1.7 Å	PXIII (SLS)
HEWL•ALF58	1.3 Å	
HEWL•ALF73	1.4 Å	
HEWL•ALF153	1.3 Å	
HEWL•ALF157	1.3 Å	
Hemoglobin•ALF21	2.7 Å	
Hemoglobin•ALF58	2.3 Å	
Hemoglobin•ALF73	1.9 Å	
Hemoglobin•ALF153	2.0 Å	
Hemoglobin•ALF157	1.6 Å	

The ten crystal structures were solved but, after analyzing the respective electron density maps, no protein•CORM adducts were identified in any of them. These results suggest that the used soaking approach was not successfully applied and increasing the time of soaking is a possibility to be considered similarly to the decided for the soaking of HEWL with ALF_MS2, ALF_MS3 and ALF_MS4. Highly disordered or low occupied adducts that are eventually present in these structures could be then properly determined and modeled.

The low water solubility of compounds ALF21 and ALF73 should be also considered as one of the reasons explaining the unsuccessful soaking. In fact, ICP-AES (Inductively Coupled Plasma-Atomic Emission Spectrometry) results (data not shown) indicate that these two complexes bind to both HEWL and hemoglobin in a much less extend than the ALF58, ALF153 and ALF157.

Moreover, the obtained results with FTIR spectroscopy (data not shown) are also not conclusive on the presence of CO moieties bound to the protein (both in solution- and crystal-form).

Therefore, it was not possible to conclude on the potential interactions established by these metal-based CORMs with HEWL and bovine hemoglobin. The planned long soaking experiment could be a useful test to clarify such aspect.

Regarding transferrin, similar ICP-AES results have been obtained showing a much more pronounced interaction between the protein and water soluble complexes when compared with the water insoluble CORMs (data not shown).

Nevertheless, all the five CORMs were used in different co-crystallization trials with hs-apoTF and crystals have been obtained not being significantly different from those represented in Figures 2.34 and 2.35. Several crystals were tested using Synchrotron radiation and the best measured crystals are summarized in Table 2.12.

Table 2.12 – X-ray diffraction results obtained with the soaked hs-apoTF crystals with ALF21, ALF58, ALF73, ALF153 and ALF157.

Soaked crystal	Obtained resolution	Beamline (Synchrotron)
hs-apoTF•ALF21	3.0 Å	I04 (Diamond Light Source)
hs-apoTF•ALF58	3.5 Å	
hs-apoTF•ALF73	3.5 Å	
hs-apoTF•ALF153	3.5 Å	
hs-apoTF•ALF157	3.5 Å	

These datasets indicate low resolution crystal structures that will not provide the atomic detail we are looking for. New crystals, with a higher resolution, are mandatory to further investigations on the subject.

CHAPTER 3

INTERACTION OF PROTEINS WITH VANADIUM COMPOUNDS

3.1 – Introduction and objectives

As mentioned in the respective introductory chapter, multiple roles are attributed to vanadium and inorganic or organic vanadium-based compounds. Particularly relevant, the involvement of such complexes in several medical applications is progressively growing in the last years. Corroborating this fact, a similar growing number of scientific papers, reviews, book chapters and books have been published some of which are indicated in the introduction of this thesis.

Nevertheless, there are still several questions without a definitive answer. As example, serum transferrin has been implicated in the transport of vanadium complexes in the blood stream. Such results are incredibly important keeping in mind the role of plasma proteins on the pharmacokinetic profile of potential drugs. However, the exact mechanism by which vanadium is transported is still dubious. Moreover, some other proteins have been also proposed to be involved in this process.[210] Once again, combined with other biophysical methodologies, X-ray crystallography could be a very important technique to address such questions revealing details of the interactions above mentioned.

Therefore, the principal aim of the experimental work described in this chapter was to characterize the interactions established between several vanadium compounds and a set of proteins: HEWL, bovine trypsin and human serum transferrin.

Our first goal was to determine if, upon binding of vanadium complexes, apo-transferrin adopts a closed conformation similar to that exhibited by holo-transferrin or if it remains in an open conformation. X-ray crystallography was proposed to elucidate this point but, due to difficulties in obtaining good quality diffracting crystals, the interactions with transferrin was also characterized by urea gel electrophoresis and by SAXS (Small Angle X-ray Scattering).

Simultaneously, applying the same principle followed with CORMs, HEWL was used as a crystallographic model in order to obtain significant structural data on these interactions. The obtained results with one vanadium picolinate-complex led to a new goal of the work involving the determination of the potential role of such compounds as protein inhibitors. Bovine trypsin was also used for such purpose as a member of the proteases family.

3.2 – Structural and Functional studies of vanadium complexes with proteins

The work herein presented results from a collaboration with Professor João da Costa Pessoa (*Instituto Superior Técnico, Universidade de Lisboa*).

3.2.1 – Human Serum Transferrin

As mentioned in the chapter 2.2.2.4, serum transferrin has an approximate molecular mass of 80 kDa presenting two homologous lobes: N- and C-terminal. The protein has a high binding affinity towards Fe^{III} ions but it is also able to bind other metal ions such as Bi^{III}, Ga^{III}, In^{III}, Al^{III}, Cu^{II}, Mn^{II}, Zn^{II}, Ni^{II} and Ru^{III}. Conformational changes occurring in transferrin are associated with Fe^{III} binding or release. When iron is bound, each domain moves to form, what is designated by, the closed conformation. Similarly, upon release of iron, the metal-binding domains move apart and the protein adopts the open conformation. The Fe^{III} bound form can be recognized by the hTF-cell receptors and internalized by the cell through a process known as receptor-mediated endocytosis.[307,308,309,310,315]

Therefore, the determination of the conformation of transferrin upon vanadium binding is important in order to understand its cell uptake mechanism.

3.2.1.1 – Materials and Methods

The vanadium compounds – $VOSO_4$ (vanadyl sulfate tetrahydrate, 235 g/mol) and $NaVO_3$ (sodium metavanadate, 121.9 g/mol) – and the respective ligands – maltol (3-hydroxy-2-methyl-4H-pyran-4-one, 126.11 g/mol), Hdhp (1,2-dimethyl-3-hydroxy-4-pyridinone, 139.15 g/mol), Hpic (picolinic acid, 123.11 g/mol) and H_2dipic (dipicolinic acid, 167.12 g/mol) – were prepared by the group of Professor João da Costa Pessoa (*Instituto Superior Técnico, Universidade de Lisboa*).

Human serum apo-transferrin, human serum holo-transferrin, PEG 4K, glycerol, ammonium citrate, Tris (Trizma, tris-(hydroxymethyl)-aminomethane), sodium carbonate (Na_2CO_3), FicollR Type 400, urea and bromophenol blue were purchased from Sigma-Aldrich. Sodium chloride and boric acid were purchased from Scharlay and Riedel-de-Haën, respectively.

- **X-ray crystallography – Crystallization and data collection**

A sample of hs-apoTF was prepared at 30 mg/ml in 20 mM Tris-HCl pH 8, 20 mM sodium carbonate and 200 mM sodium chloride and crystallized using the best conditions described in the chapter 2.2.2.4.1: 13% glycerol, 17.5% PEG 4K, 0.2 M ammonium citrate pH 6.73 using both 24-well plates (drops with 6 µl of protein and 6 µl of precipitant solution) and 96-well plates (nanodrops with 0.5 µl of protein and 0.5 µl of precipitant solution) at 20ºC. Nanocrystallization setups were performed in an Oryx8 protein crystallization robot (Douglas Instruments) and the crystals were observed either with a SZH10 Olympus microscope or a SteREO Discovery V12 Zeiss microscope.

A co-crystallization approach was also tried. The protein (60 mg/ml) was incubated with the indicated vanadium-ligand complexes in a 10- and 30-fold excess, respectively, for 1 hour. The samples were then passed through a PD-10 MiniTrap G-25 column (GE Healthcare) to a final protein

concentration of 30 mg/ml in order to remove the unbound compound prior the crystallization trials using the described conditions. Different crystals were flash frozen using a harvesting buffer with 30% (v/v) glycerol as a cryoprotector.

Several datasets were tested and collected using different Synchrotron beamlines: BM14 at the ESRF (Grenoble, France) and I02 at Diamond (Didcot, Oxfordshire, United Kingdom).

- **Protein conformation by urea gel electrophoresis**

The solutions were prepared by adding 10 times molar equivalent excess of metal salt or complex to an hs-apoTF solution (~50 μM in 100 mM Tris-HCl 7.4). Solutions of ligands (~500 μM) and $VOSO_4$ (~100 μM) were mixed in 1 ml of milli-Q water to prepare $V^{IV}O$:ligand solutions of 1:2.5 ratio (in the case of dipicolinic acid the ratio was 1:2). Then 50 μl of these V^{IV}-ligand solutions were added to 500 μl of the 50 μM hs-apoTF solution to prepare hs-apoTF:V^{IV}-complex (maltol, Hdhp, Hpic and H_2dipic) solutions of 1:10 molar ratios. These solutions were allowed to equilibrate for 30 min. Up to this point all manipulations were carried out in the absence of O_2 in an anaerobic chamber (1200/780, MBraun), but the following steps were carried out allowing contact with air. A similar sample was prepared but using $NaVO_3$ instead of $VOSO_4$, and not adding the carrier ligands, for comparison purposes. Moreover, controls samples (native hs-apoTF and native hs-holoTF) were also prepared.

Urea gel electrophoresis was performed using a Novex 6% Tris-TBE urea minigel and a XCell SureLock™ Mini-Cell system (Invitrogen). Running (5X, 89 mM Tris base and 89 mM boric acid) and sample (2X, 45 mM Tris base and 45 mM boric acid, 6% FicollR Type 400, 3.5 urea and 0.005% bromophenol blue) buffers used were similar to the Novex commercial buffers with the exception that EDTA was not added (running buffer was diluted for 1X prior its use). 5 μl of each sample was mixed with 5 μl of the sample buffer and loaded in the gel. The electrophoresis was carried out for 3 hours at 180 V voltage and 40 mA current. The protein bands were visualized by staining with Coomassie blue.

- **SAXS (Small Angle X-ray Scattering) experiments**

A sample of hs-apoTF (60 mg/ml) was prepared in the same buffer used in the crystallization trials and incubated with $VOSO_4$ and Hpic in a 10- and 30-fold excess, respectively, for 1 hour. The sample was then passed through a PD-10 MiniTrap G-25 column (GE Healthcare) to a final protein concentration of 30 mg/ml. A similar experiment was also performed using a sample of the native protein.

SAXS data were collected in beamline BM29 at the ESRF (Grenoble, France) using a robotic sample changer.[316] The two protein samples were measured at 4ºC using different protein concentrations (range from 0.23 to 30 mg/ml) and covering the range of momentum transfer $0.02 < s < 6$ nm^{-1} ($s = 4\pi \sin\theta/\lambda$, where 2θ is the scattering angle). Ten frames of 2 seconds each were collected,

normalized to the transmitted intensity, and subsequently averaged using the image analysis software BsxCuBE (Biosaxs Customized Beamline Environment).[316]

The data were processed in collaboration with Dr. Márcia Correia (UCIBIO@REQUIMTE, FCT/UNL) with the ATSAS package using standard procedures, corrected for buffer contribution and extrapolated to infinite dilution using the program PRIMUS.[317,318] The forward scattering [I(0)] and the radii of gyration (R_g) were evaluated using the Guinier approximation assuming that at very small angles ($s < 1.3/R_g$) the intensity is represented as $I(s)=I(0).\exp(-1/3.R_g^2s^2)$. These parameters were also computed from the entire scattering pattern using the indirect transform package GNOM which also provides the maximum dimension of the particle (D_{max}) and the distance distribution function [P(r)].[319]

Low resolution shape analysis was performed using the *ab initio* program DAMMIN.[320] Multiple runs were carried out to verify the stability of the solution, and the most typical reconstructions were selected using the program DAMAVER.[321] The scattering from the atomic models was calculated using the program CRYSOL which either predicts theoretical scattering patterns or fits the experimental data by adjusting the excluded volume and the contrast of the hydration layer.[322] SUPCOMB was used to superimpose the obtained SAXS models with the available X-ray structures in PDB (open and closed conformations).[323]

3.2.1.2 – Results and Discussion

3.2.1.2.1 – Crystallization and preliminary X-ray diffraction analysis

Using the best crystallization conditions previously mentioned (chapter 2.2.2.4), several co-crystallization trials were performed with different vanadium compounds. This approach was selected rather than soaking as the goal of the experiment is to determine potential conformational changes due to the presence of such compounds.

On the other hand, the use of different carrier ligands is justified by the fact that coordinated ligands should be able to improve the absorption and possibly the transport and uptake of vanadium to the cells, reducing the dose necessary for producing an equivalent effect. In fact, several vanadium complexes have been found to have higher insulin enhancing activity than inorganic V^V or V^{IV} salts probably related with the improvement of the bioavailability. The four used ligands (Figure 3.1) have been previously investigated showing positive results in different studies.[237,315,324,325,326]

Different hs-apoTF crystals soaked with the different ligands have been obtained without remarkable differences in their morphology compared with the native crystals shown in Figure 2.35. Several of those crystals were tested using synchrotron radiation. However, none of them diffracted satisfactorily and only 3.5 to 4 Å resolution datasets could be collected. At such resolutions, an accurate interpretation of the electron density is hard to achieve and no definitive conclusions could be obtained.

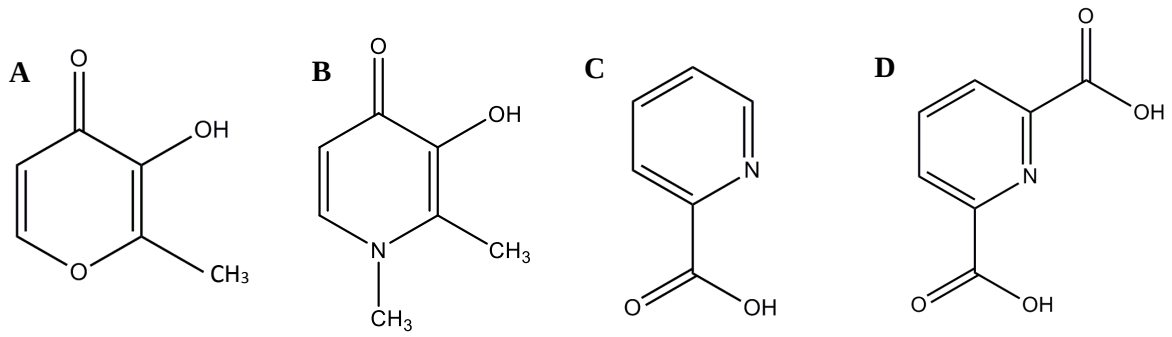

Figure 3.1 – Molecular formulas of maltol (A), Hdhp (B), picolinic acid (C) and dipicolinic acid (D). All the carrier ligands are shown in their protonated forms. The structures were prepared in ChemDraw.

Nevertheless, some of these structures were solved by Molecular Replacement using as a model a structure in the open conformation (PDB code: 2HAV). Particularly relevant, the crystal of the apo-protein soaked with V^{IV}-Hpic diffracted beyond 3.6 Å resolution and an electron density blob was found in the iron binding site of the N-lobe. However, no anomalous signal was detected in that position contradicting the presence of the V in the metal binding site. As discussed before, glycerol or citrate molecules are suitable candidates to be positioned in the mentioned blob as verified in the 2HAV model structure. No anomalous blobs were found in any other position of the structure, suggesting the absence of adducts.

Therefore, the crystallographic experiments with hs-apoTF were not conclusive and the conformation of the protein upon interaction with the different ligands was not properly characterized. Consequently, this question was addressed by other techniques as described in the following sections.

3.2.1.2.2 – Conformation determination by urea gel electrophoresis

To determine the effect of binding of $V^{IV}O$ and $V^{IV}O$-complexes on the conformation of hs-apoTF, gel electrophoresis experiments were carried out using a TBE urea gel system. It must be emphasized that the sample and running buffers used were similar to the commercial buffers with the exception that EDTA was not added: in the presence of EDTA, the obtained gel differ from the one herein discussed because $V^{IV}O$ is sequestered (data not shown).

Several groups reported that polyacylamide gel electrophoresis in the presence of urea can resolve bands corresponding to apo-transferrin, the two mono-ferric forms – (Fe)C-hTF and (Fe)N-hTF corresponding, respectively, to the C- and N-terminal – and di-ferric transferrin (holo-transferrin – hs-holoTF). Migration through these gels is influenced by the pH, time and temperature of the experiment together with shape, charge, and disulfide bond content of the two lobes of the protein.[327,328] It was observed that hs-holoTF, which is the most compact form of the protein, migrates the farthest through the gel before being denatured by the urea. The least compact apo-form, where both lobes are open, is denatured soon after exposure to the 6 M urea, and hence stays near the top of

the gel. The two mono-ferric species migrate at differing intermediate positions. Importantly, as mentioned, the closed form of di-ferric transferrin is the one that is recognized by the cell transferrin receptors and thus may be up-taken by receptor-mediated endocytosis.[329]

Figure 3.2 shows a gel picture where seven different samples were prepared with hs-apoTF, hs-holoTF, $V^{IV}O$ and the carrier ligands: maltol, Hdhp, picolinate and dipicolinate.

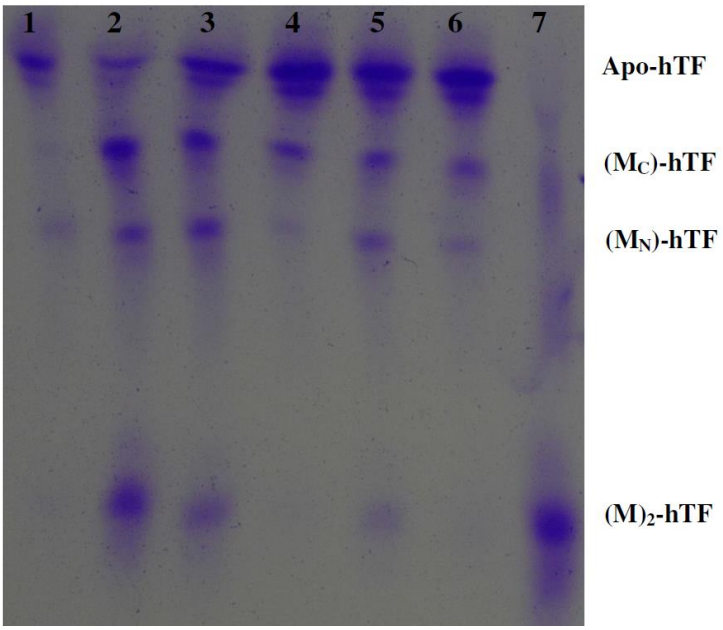

Figure 3.2 – Urea-polyacrylamide gel electrophoresis of: 1) hs-apoTF, 2) hs-apoTF+$V^{IV}O$, 3) hs-apoTF+$V^{IV}O$+Maltol, 4) hs-apoTF+$V^{IV}O$+Hdhp, 5) hs-apoTF+$V^{IV}O$+Hpic, 6) hs-apoTF+$V^{IV}O$+H_2dipic and 7) hs-holoTF. All samples applied to the gel were first desalted by passing them through a size-exclusion PD-10 minitrap G-25 column.

Apart from small changes in the intensity of bands probably due to slight differences in the amount/concentration of hs-apoTF applied to each well, in Figure 3.2 it is observed that at least for lanes 2, 3 and 5 (inorganic $VOSO_4$, maltol and Hpic, respectively) spots corresponding to the closed form of transferrin are visible, while in lanes 4 (Hdhp) and 6 (H_2dipic) this closed form is not detected.

Thus, these results suggest that $V^{IV}O$ binding with hs-apoTF, and at least some of the $V^{IV}O$–carrier complexes, may involve the change of conformation of transferrin to the closed form as is the case of hs-holoTF (lane 7). It should be emphasized that the results here obtained by electrophoresis suggest that the formation of $(V^{IV}O)_2$-hTF possibly occurs with closing of the transferrin conformation, but at this stage it cannot be concluded that the same happens in the presence of the carrier ligands. Although the bands detected in lanes 3 and 5 could suggest this, partial hydrolysis of the $V^{IV}O$–hTF-carrier species might have taken place during the electrophoretic experiment, yielding $V^{IV}O$–hTF species and allowing the detection of $(V^{IV}O)_2$-hTF in the mentioned lanes.[315]

On the other hand, it is clear that the relative ratio of the amounts of $(M)_C$-hTF, $(M)_N$-hTF and $(M)_2$-hTF (where M corresponds to V^{IV} or Fe^{III}) differs for $V^{IV}O$ and Fe^{III}, reflecting the much higher formation constant of $(Fe^{III})_2$-hTF when compared with the $(V^{IV}O)_2$–hTF species formed.

In similar experiments with a solution of hs-apoTF and sodium vanadate ($NaVO_3$), it was found that the pattern of the electrophoretic bands is exactly the same as for hs-apoTF alone (data not shown) suggesting that although V^V binds to hs-apoTF, this occurs without the formation of the closed conformation.[330]

3.2.1.2.3 – Conformation determination by SAXS

In order to complement the results of the urea-polyacrylamide gel electrophoresis previously discussed, SAXS (Small Angle X-ray Scattering) experiments were also carried out to determine the conformation of transferrin in solution upon interaction with vanadium.

For such purpose, synchrotron radiation has been used and only one of the studied carriers – Hpic – has been selected for a first trial. In addition, a sample of the native hs-apoTF was also analyzed in order to compare the respective results. Importantly, both samples were passed through a PD-10 MiniTrap G-25 column a couple of days prior the data collection (beamline BM29, ESRF). Data collection parameters are indicated in Table 3.1.

Table 3.1 – SAXS data collection and scattering-derived parameters of native hs-apoTF and hs-apoTF+$V^{IV}O$+Hpic samples. † Reported for 0.23 mg/ml measurement.

	Native hs-apoTF	hs-apoTF+$V^{IV}O$+Hpic
Data-collection parameters		
Beamline (Synchrotron)	BM29 (ESRF)	
Wavelength (Å)	0.99	
s range (nm^{-1})	0.2-6	
Concentration range (mg/ml)	0.2-30	
Temperature (ºC)	4	
Structural parameters		
I(0) [from Guinier] †	85.66	69.38
R_g (nm) [from Guinier] †	3.44	3.65
I(0) (nm) [from P(r)]	89.3	65.1
R_g (nm) [from P(r)]	3.5	3.3
D_{max} (nm) [from P(r)]	12.8	10.9
Porod volume estimate ($Å^3$)	125.0	120.9
Molecular mass determination (kDa)		
Molecular mass M_r [from I(0)] †	85.8	69.5
Molecular mass M_r (from Porod volume)	75.0	72.5
Calculated monomeric M_r (from sequence)	77.5	77.5

The scattering profiles of both protein samples – native and incubated with the carrier – are shown in Figure 3.3. The structural parameters, including the radius of gyration (R_g), the maximum particle dimension (D_{max}) and the excluded (Porod) volume of the hydrated particle, were computed from the experimental scattering patterns (Table 3.1 and Figure 3.3). Furthermore, the Kratky plot of the two samples displays a gaussian behavior, indicating the well folded nature of the protein (Figure 3.3).

The distance distribution function – P(r) – also suggests a compact and globular structure (Figure 3.3). The relative molecular mass estimated from I(0) of native hs-apoTF and vanadium-picolinate-bound hs-apoTF yielded a molecular weight of 85.8 kDa and 69.5 kDa respectively through BSA calibration. From the Porod volume, the relative molecular mass estimated was 75.0 kDa and 72.5 kDa respectively, confirming the monomeric state of hTF in solution (Table 3.1).

Using the program CRYSOL, the experimental SAXS data were fitted to the scattering profiles calculated from two different transferrin crystal structures deposited in the PDB – 2HAV (apo-transferrin, open conformation) and 3V83 (holo-transferrin, closed conformation) as represented in Figure 3.4.[311,331]

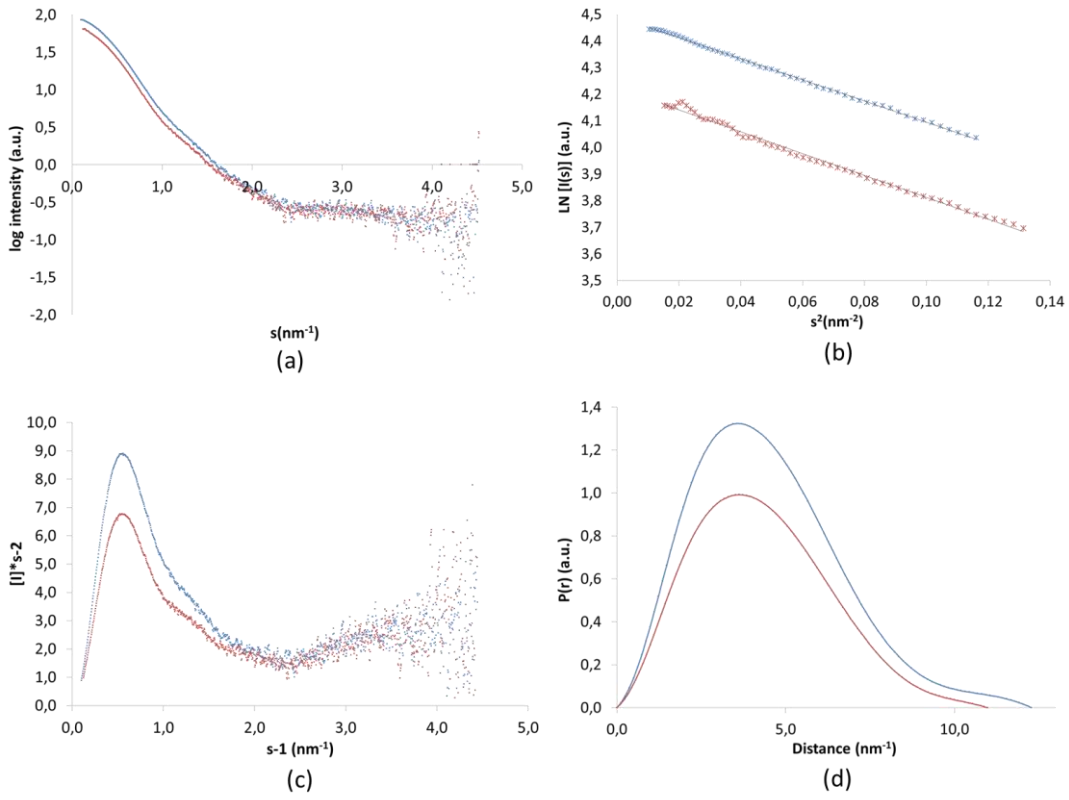

Figure 3.3 – Experimental SAXS data of native hs-apoTF (blue) and hs-apoTF+$V^{IV}O$+Hpic (red). Section (a) corresponds to the scattering profiles. Section (b) corresponds to the Guinier plot. Section (c) corresponds to the Kratky plot. Section (d) corresponds to the distance distribution function – P(r) – computed from the scattering patterns using the program GNOM.

As expected, regarding the native hs-apoTF sample, a better fit was obtained when the corresponding crystallographic model (2HAV) was used. Nevertheless, the fitting is not perfect as proved by the high value of χ^2 indicating that the structure of the crystalline form presents some differences when compared with the solution form being, probably, more compact. Interestingly, the sample incubated with $VOSO_4$ and Hpic follows a similar behavior and the best fit – although not perfect – was also obtained when the same model in the open conformation was used (χ^2 of 2.026).

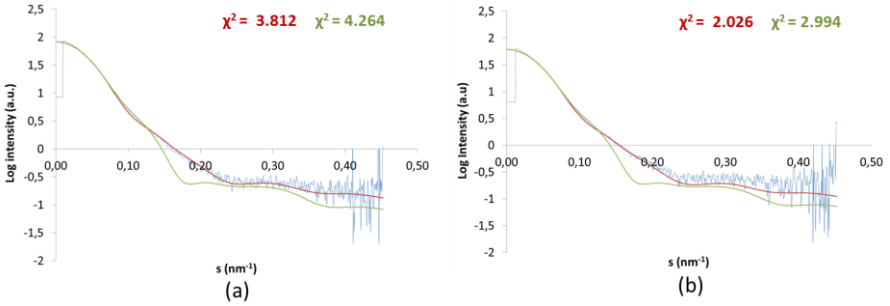

Figure 3.4 – Scattering profiles generated by CRYSOL from transferrin crystal structures 2HAV and 3V83 and respective comparison with the scattering profiles of the native hs-apoTF (a) and hs-apoTF+$V^{IV}O$+Hpic (b) samples. Experimental data are shown in blue. Red fit is computed from the crystal structure of the open form (2HAV) and the green fit for the closed form (3V83).

The overall molecular envelope of the two samples was calculated using the *ab initio* program DAMMIN from the respective scattering profile. The 20 final independent models obtained were aligned using DAMAVER giving Normalized Spatial Discrepancy (NSD, a measure of quantitative similarity between sets of three-dimensional points) values of 1.299 and 1.269 for native hs-apoTF and vanadium-bound hs-apoTF, respectively.

Finally, the two calculated molecular envelopes were superimposed with the crystallographic structure 2HAV using SUPCOMB (Figure 3.5). A reasonable match was obtained suggesting that the open conformation is the predominant form found in solution even in the presence of vanadium and the respective carrier. Most likely, such result is in agreement with the one obtained for the picolinate carrier by urea-polyacrylamide gel electrophoresis: an equilibrium in solution between both forms – open and closed – with a predominance of the open conformation. This could also contribute for the deviations found between the SAXS experimental profile and the simulated profile from the crystallographic structure.

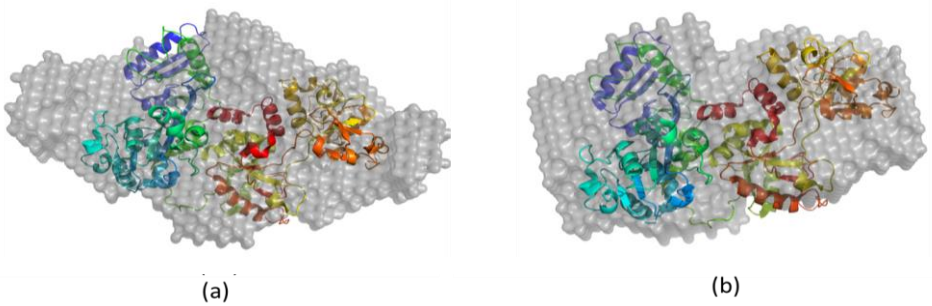

Figure 3.5 – Superposition of the calculated most likely molecular envelope of native hs-apoTF (a) and hs-apoTF+$V^{IV}O$+Hpic (b) samples with the X-ray structure 2HAV. Molecular envelopes are represented by the grey beads while the crystallographic model is represented in cartoon and colored from N-(blue) to C-terminal (red).

Therefore, the results obtained by SAXS indicate the apo-protien adopts the open conformation upon vanadium-picolinate interaction. However, some important points should be taken into account in such interpretation. As mentioned, the samples were prepared a couple of days prior the data collection and two major phenomena could be verified: the dissociation of the putative adduct or the oxidation of the vanadium atom which, ultimately, can also mask the results.

In order to overcome these potential problems, a double strategy was followed (Figure 3.6). In the first strategy, the experiment herein described was repeated preparing the samples in the laboratory considerably some time before the data collection (designated by "long incubation"). In the second strategy, the samples were prepared in the beamline immediately before the data collection (designated by "short incubation"). In these experiments, the four carriers were tested as well as the inorganic salts of V^{IV} and V^{V}. Moreover, native samples of holo-transferrin were also measured in order to obtain the respective experimental scattering profile for further comparison. The data collection was also conducted in BM29 at the ESRF.

The referred data are still under treatment in collaboration with Dr. James Doutch (Diamond Light Source) and no final results could be presented at this point. Nevertheless, some aspects could be briefly mentioned. As expected, the scattering profiles of apo- and holo-transferrin are significant different. Moreover, the fit of the scattering profiles calculated from the respective PDB structure to the experimental SAXS data was also poor confirming the differences of the protein in the two states. Regarding the "long incubations", the obtained scattering profiles were very similar to that obtained for the apo form. Some differences have been found in "short incubations" mainly related with the values of R_g or D_{max} but further analysis is required prior to any assumption on the subject.

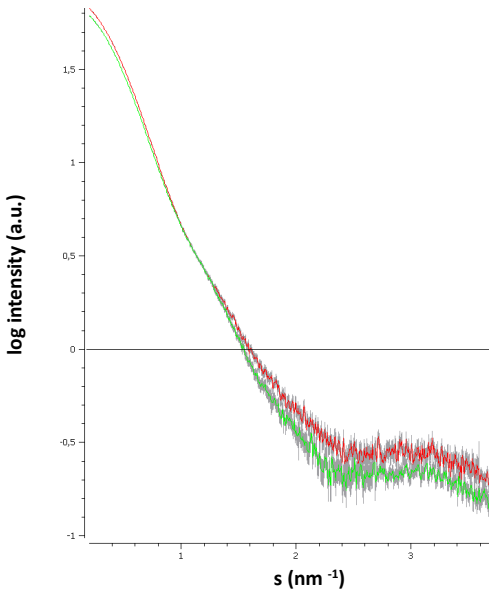

Figure 3.6 – Experimental SAXS scattering profiles of hs-apoTF+$V^{IV}O$+Hpic obtained by long incubation (red) and short incubation (green). The differences in the profiles suggest that the time of incubation is an important parameter that should be taken into account in the study. As mentioned in the text, the data obtained by both long and short incubation are currently under treatment.

3.2.2 – Hen Egg White Lysozyme

As previously covered, the crystallographic results obtained with hs-apoTF did not allow determining the conformation of the protein upon interaction with the different vanadium complexes. In addition to the conformation, a proper characterization of the potentially formed protein-ligand adducts would be also important for the study on this subject, for example, to elucidate if the carriers remain bound to the central vanadium upon interaction.

Taking advantage on its remarkable diffraction quality, HEWL was once again selected as a crystallographic model in the studies presented in the next sections.

3.2.2.1 – Materials and Methods

The vanadium compounds – $VOSO_4$, $NaVO_3$ and $VO(acac)_2$ (vanadyl acetylacetonate, 265.2 g/mol) – and the respective ligands – maltol, Hdhp, Hpic, H_2dipic, 1,10-phen (phenanthroline, 180.2 g/mol) and bipy (2,2'-bipyridine, 156.2 g/mol) – were prepared by the group of João da Costa Pessoa (*Instituto Superior Técnico, Universidade de Lisboa*).

HEWL, sodium acetate buffer, glycerol and salicylic acid were purchased from Sigma-Aldrich. Sodium chloride and proline were acquired from Scharlay and Fluka, respectively.

X-ray crystallography – Crystallization, data collection, structure solution and structure refinement

HEWL was crystallized using 4-8% (w/v) NaCl in 0.1 M acetate buffer pH 4.5 (protein stock concentration of 50 mg/ml in the same buffer). The crystallization process was carried out at 20ºC using the hanging drop vapor diffusion method (2 µl of protein and 2 µl of reservoir solution with 700 µl of the precipitant solution in the reservoir) in 24-well plates from Molecular Dimensions. Crystals of approximately 0.2×0.2×0.2 mm^3 appeared within 24 hours and were stabilized with a harvesting buffer containing 12% (w/v) NaCl. Crystals were observed either with a SZH10 Olympus microscope or a SteREO Discovery V12 Zeiss microscope.

$VOSO_4$, $NaVO_3$ and $VO(acac)_2$ solutions were prepared in the harvesting buffer up to a final concentration of 10 mM. Similarly, different solutions of $VOSO_4$:ligand (maltol, Hdhp, Hpic, H_2dipic, 1,10-phen, bipy, salicylic acid and proline) with a molar ratio of 1:3 were also prepared ($VOSO_4$ concentration: 10 mM). A 4 µl drop was prepared and some native HEWL crystals were transferred into it. The soaking was prolonged during 24 hours after which the crystals were flash frozen using harvesting buffer with 30% (v/v) glycerol as a cryoprotector and several high resolution datasets were collected using different Synchrotron beamlines namely ID29 and ID23-2 (ESRF, Grenoble, France), Proxima1 (Soleil, Paris, France) and PXIII (SLS, Villigen, Switzerland).

The collected datasets were integrated with the programs Mosflm or XDS and scaled with Aimless from the CCP4 suite of programs.[281,282,283] The structures were solved by Molecular Replacement (using PDB entry 193L as a model)[284] with Phaser[285] and the refinement was performed using Refmac5[286] followed by visual inspection of the model and electron density maps in COOT.[287] The quality of the model was attended using the validation tools of COOT and PDB_REDO.[288]

3.2.2.2 – Results and Discussion

Using a similar strategy to that followed with CORMs, HEWL crystals were used in different soaking experiments with the compounds previously used with hs-apoTF: the inorganic salts of V^{IV} and V^{V} and the four carriers (maltol, Hdhp, Hpic and H_2dipic) complexed with $VOSO_4$.

Interestingly, the majority of the soaked crystals remain colorless except the crystal soaked with Hdhp, which clear exhibits a purple color (Figure 3.7). In addition, the crystal soaked with $NaVO_3$ appears to exhibit a slight yellowish color which could indicate the formation of decavanadate species.[194,195]

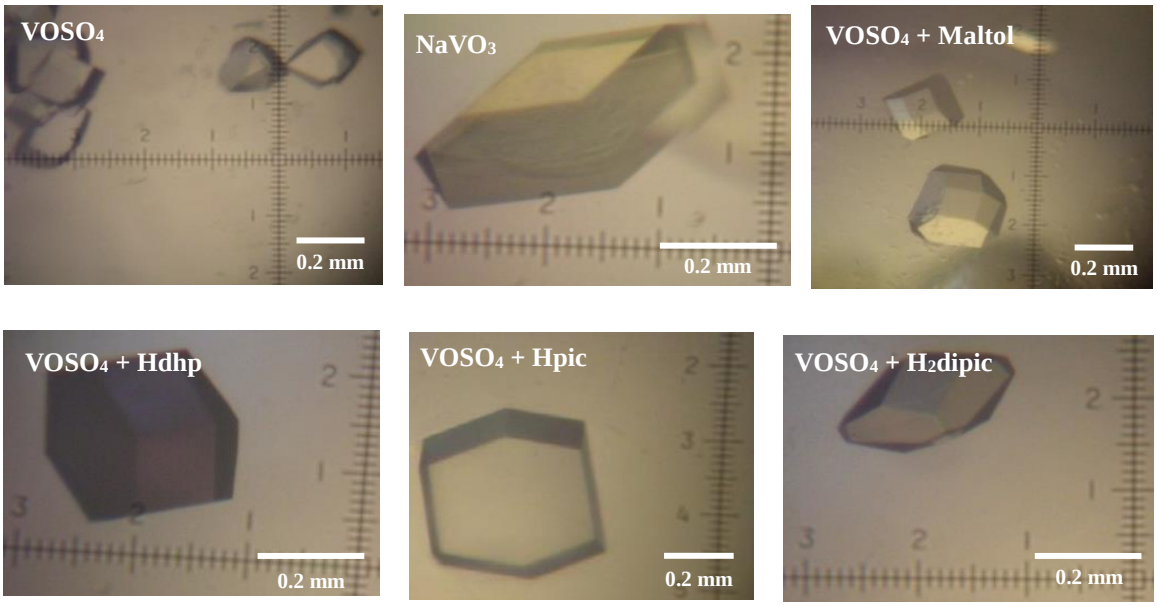

Figure 3.7 – HEWL crystals with different vanadium complexes after 24 hours of soaking. Several ≈ 0.2×0.2×0.2 mm^3 crystals were obtained.

Using synchrotron radiation, the best soaked HEWL crystals diffracted up to 1.2 Å resolution (Table 3.2) and, similarly to the previous examples, the data were processed in $P4_32_12$ space group.

All the structures were solved by Molecular Replacement and the respective density maps were carefully inspected in order to find any potential adducts with the used vanadium complexes. Nevertheless, only the structure corresponding to the HEWL•$VOSO_4$•Hpic crystal shows unambiguously the presence of a blob of extra density.

In fact, more soaking experiments with the mentioned compounds have been tried (data not shown) but no different results have been obtained: the formation of adducts occurs merely in the HEWL•$VOSO_4$•Hpic crystals. Consequently, the focus of the study was centered in this complex.

Table 3.2 – X-ray diffraction results obtained with the best HEWL crystals soaked with different vanadium complexes.

Soaked crystal	Obtained resolution	Beamline (Synchrotron)
HEWL•$VOSO_4$	1.2 Å	ID29 (ESRF)
HEWL•$NaVO_3$	1.4 Å	
HEWL•$VOSO_4$•Maltol	1.4 Å	
HEWL•$VOSO_4$•Hdhp	1.2 Å	
HEWL•$VOSO_4$•Hpic	1.3 Å	
HEWL•$VOSO_4$•H_2dipic	1.2 Å	

3.2.2.2.1 – HEWL and vanadium-picolinate complex

The data collection and refinement statistics of the HEWL•$VOSO_4$•Hpic crystal are summarized in Table 3.3.[332]

As mentioned, an extra density blob was found in the structure but, unlike the presented structures soaked with the different CORMs, not located next to the His15 site. In fact, the analysis of the electron density map of the HEWL structure revealed a strong peak at the active site of the enzyme, close to the Asp52 residue, at which a $V^{IV}O(pic)_2$ moiety could be modeled with an occupancy of 0.65. An anomalous electron density map was also calculated and a strong peak was clearly observed (Figure 3.8).

Vanadium adopts a distorted octahedral geometry covalently bound to Asp52, with a bidentate coordination to two pic^- anions and an O_{oxido} atom (Figure 3.8). The V^{IV}=O bonds typically vary between 1.57 and 1.65 Å.[333] Interestingly, in the present case, the V^{IV}=O bond length determined by X-ray analysis is quite long (1.82 Å) whereas that of V^{IV}–O (Asp52) is relatively short (1.89 Å).

An asparagine residue (Asn46) is found close to the complex, and it interacts with the O_{oxido} atom through a hydrogen bond. This interaction could be responsible for the anomalous distance observed. However, X-ray-induced reduction owing to the very intense beam used for data collection is a more plausible explanation. Partial reduction of the metal from the +4 oxidation state to the +3 oxidation state, which occurs during radiation exposure, may explain the large distance between V and O_{oxido}.

Table 3.3 – Data collection and refinement statistics for HEWL•$VOSO_4$•Hpic adduct crystal. Values in parentheses correspond to the highest resolution shell.

X-ray source	ID29 (ESRF)
Crystal data	
Space group	$P4_32_12$
Unit cell parameters (Å, º)	$a = b = 78.12$, $c = 37.32$ $\alpha = \beta = \gamma = 90$
Molecules per ASU	1
Matthews coefficient (Å^3/Da)	1.96
Solvent content (%)	37.30
Data collection	
Wavelength (Å)	1.04
Resolution range (Å)	33.67–1.28 (1.30–1.28)
<I/σI>	7.3 (2.2)
Multiplicity	6.4 (6.1)
Number of observed reflections	193174 (9006)
Number of unique reflections	30287 (1478)
R_{pim} (%)	7.1 (45.3)
Completeness (%)	99.8 (100)
$CC_{1/2}$	0.989 (0.796)
Refinement	
Resolution range (Å)	33.67–1.28
R_{work} (%)	14.45
R_{free} (%)	17.49
RMSD bond length (Å)	0.01
RMSD bond angle (º)	1.58
Ramachandran plot (%)	
Residues in favored regions	96.2
Residues in additionally allowed regions	3.8
Residues in disallowed regions	0
PDB code	4C3W

$R_{pim} = \Sigma_{hkl} [1/(N-1)]^{1/2} \Sigma_i|I_i(hkl) - \langle I(hkl)\rangle|/\Sigma_{hkl} \Sigma_i I_i(hkl)$, where N is the multiplicity measured.

$R_{work} = \Sigma ||F_{calc}|-|F_{obs}|| / \Sigma|F_{obs}| \times 100$, where F_{calc} and F_{obs} are the calculated and observed structure factor amplitudes, respectively.

R_{free} is calculated for a randomly chosen 5% of the reflections for each dataset.

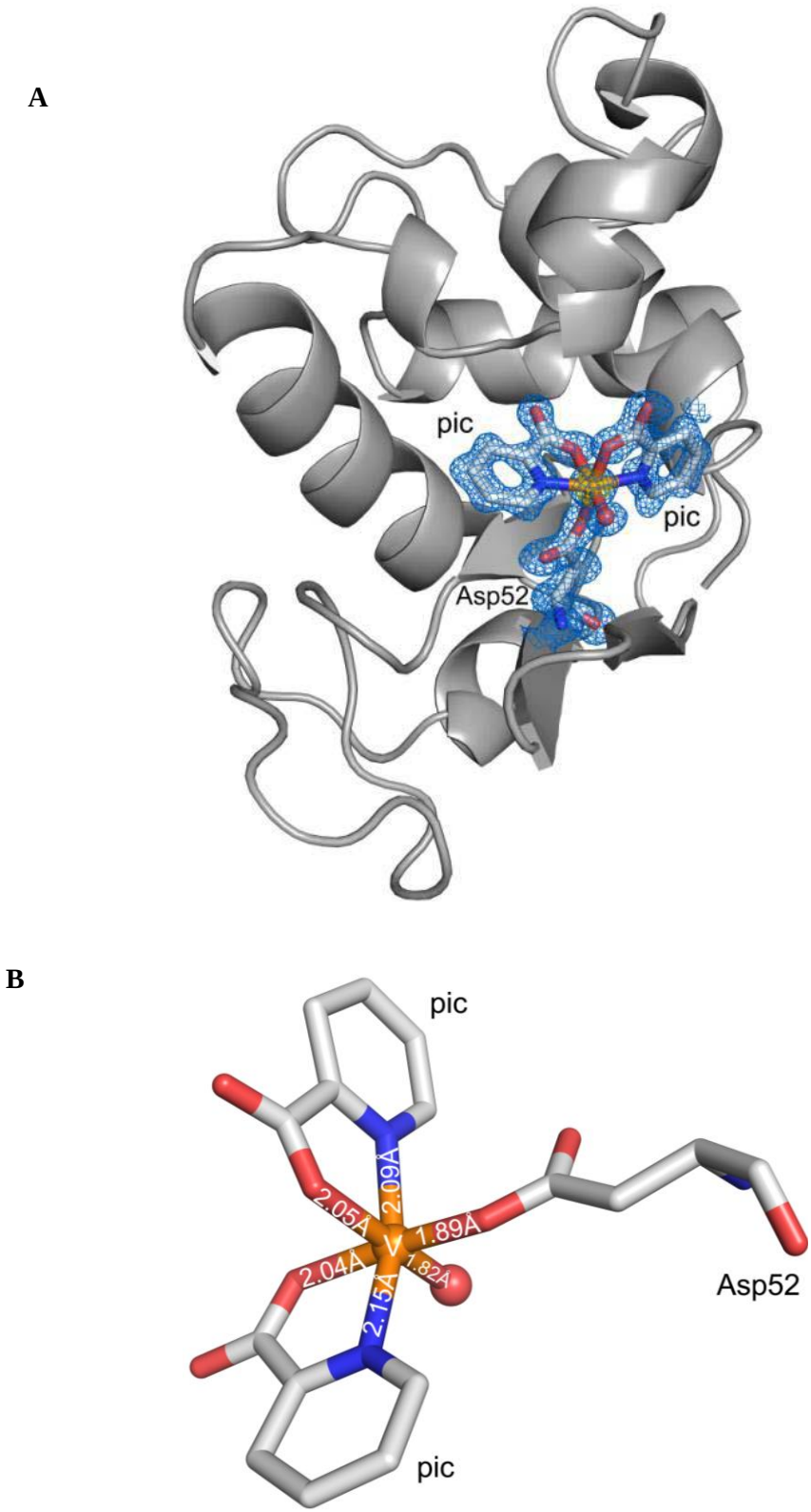

Figure 3.8 – Overall representation of HEWL with the $V^{IV}O(pic)_2$ complex close to the Asp52 residue at the enzyme active site (A) and the detailed structural representation of the respective $V^{IV}O(pic)_2$–Asp52 fragment (B). Electron density maps – 2Fo-Fc (blue) and anomalous (yellow) – are contoured at 1 and 4 σ, respectively. Vanadium is shown in orange. Bond lengths between V and the donor atoms are indicated (see also text).

This type of phenomenon has been reported for metalloenzymes[334,335] and, in the present case, it would correspond to a progressive change during radiation exposure from a V^{IV}=O bond to a V^{III}–O bond with concomitant elongation of the bond length.

To test this hypothesis, model refinement was conducted using different slices of the collected data for further comparison with the final model. Table 3.4 shows the measured distances between V and all donor atoms in different cases: for the complete data set, for the first 350 images, for the first 500 images and also for the last 500 images collected.

Table 3.4 – Distance between V and the coordinating ligands for the complete data set, the first 350 images, the first 500 images and the last 500 images collected.

Bond	Distance [Å]			
	Images 1-1000	**Images 1-350**	**Images 1-500**	**Images 501-1000**
V=O	1.82	1.76	1.78	1.85
V–Asp52	1.89	1.91	1.90	1.93
V–N (pic1)	2.09	2.13	2.11	2.10
V–O (pic1)	2.05	2.05	2.03	2.07
V–N (pic2)	2.15	2.16	2.19	2.11
V–O (pic2)	2.04	2.02	2.01	2.04

Even though the completeness of each of the studied subsets is not ideal (Table 3.5), it is clear that pronounced changes occur during data collection, especially for the V^{IV}=O bond. Hence, whereas in the early stages of data collection (initial 35% of the dataset used) the distance between the metal and the O_{oxido} ligand is 1.76 Å, this value increases by the end of the data collection (final 50% of the data used) up to 1.85 Å.

Table 3.5 – Data collection statistics for HEWL•$VOSO_4$•Hpic sub-sets: images 1-350, images 1-500 and images 501-1000. Values in parentheses correspond to the highest resolution shell.

	Images 1-350	**Images 1-500**	**Images 501-1000**
Wavelength (Å)	1.04	1.04	1.04
Resolution range (Å)	27.62-1.28 (1.30-1.28)	27.62-1.28 (1.30-1.28)	33.67-1.28 (1.30-1.28)
<I/σI>	8.8 (3.9)	8.6 (3.1)	9.3 (1.9)
Multiplicity	2.7 (2.7)	3.6 (3.4)	3.2 (3.1)
Number of observed reflections	67017 (3147)	96200 (4513)	96042 (4454)
Number of unique reflections	24664 (1179)	26453 (1341)	29958 (1457)
R_{pim} (%)	6.4 (18.3)	6.2 (24.3)	4.4 (28.7)
Completeness (%)	82.2 (80.7)	87.9 (91.4)	99.0 (98.8)
$CC_{1/2}$	0.983 (0.910)	0.986 (0.858)	0.992 (0.859)

These differences corroborate the idea that V is reduced during data collection. Large distances previously obtained for V^{V}=O bonds in other vanadium–protein studies may have also resulted from reduction induced by radiation.[219]

To further confirm the oxidation state of V, electron paramagnetic resonance (EPR) experiments of the HEWL•$VOSO_4$•Hpic adduct crystals were undertaken by Dr. Isabel Correia (*Instituto Superior Técnico, Universidade de Lisboa*). The spectra obtained at room temperature with a suspension of unmeasured crystals in buffer and for the same suspension frozen at 77 K confirm the presence of a monomeric $V^{IV}O$-bound species.[332]

Moreover, to confirm that the V^{IV} species responsible for the EPR signal is the bound complex and not the free one in solution, the spectrum at room temperature was measured again 10 days after the first measurement with the same sample of crystals kept at ~6 ºC during this period. The intensity of all EPR spectra was roughly the same indicating that the EPR signal is due to protein bound $V^{IV}O(pic)_2$–Asp52. On the other hand, this also proves that this complex species, if bound to the protein in the crystals, is quite stable to hydrolysis and to oxidation: in the absence of any interaction with HEWL, the oxidation of $V^{IV}O(pic)_2(H_2O)$ would be relatively fast at the used pH.[333,336]

In addition, DFT (Density Functional Theory) calculations were also conducted by Professor Eugenio Garribba (*Università di Sassari*, Italy) in order to elucidate the oxidation state of V. Given that the critical point was the V^{IV}=O distance (1.82 Å), an optimization of the position of O_{oxido} was performed by freezing the positions of all other atoms with the COO group of Asp52 in the deprotonated form and a distance of 1.601 Å for V^{IV}=O was obtained. Moreover, the simulated EPR parameters also corroborate the presence of a V^{IV}=O bond.[332]

Therefore, these results indicate that, in the crystal, the V^{IV}=O bond of the adduct has its usual length. The long V=O bond obtained from the X-ray data is thus due to partial reduction induced by the intense X-ray radiation used during the data collection as already discussed. Low dose data collection should be considered to fully elucidate the real bond distances found in the crystal. In fact, this strategy allows to minimizing the radiation damage caused by the X-ray beam namely the putative reduction of vanadium.

$V^{IV}O$ carrier–protein adducts might form with transferrin, albumin or other proteins such as membrane or cytosolic proteins. We proved herein that $V^{IV}O$ carriers can bind strongly to proteins, as observed for HEWL, but more data is required to better understand the interaction of $V^{IV}O$ carrier compounds with serum proteins as discussed in the previous chapter.

3.2.2.2.2 – HEWL and other vanadium compounds

The interesting results obtained with picolinate led to hypothesize that related complexes could also be used for the same purposes forming $VO(ligand)_2$ adducts. In this sense, salicylic acid and proline have been selected due to their structural similarity to the picolinate carrier (Figure 3.9).

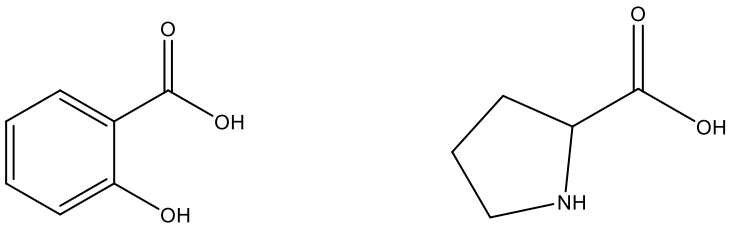

Figure 3.9 – Molecular formulas of salicylic acid (left) and proline (right). Both ligands are shown in their protonated forms. The structures were prepared in ChemDraw.

Similar experiments were performed and different soaked HEWL crystals (Figure 3.10) have been collected up to 1.3 Å at different beamlines namely ID23-2 (ESRF), PXIII (SLS) and Proxima 1 (Soleil). Different soaking times have been tested – 3 and 24 hours – and the datasets are still under analysis. Nevertheless, considering the already treated data, no adducts have been found in the active site of the protein (data not shown) despite the color of the soaked crystals particularly visible when salicylic acid was used. Most likely, the formation of the complex with V^{IV} was not achieved and different higher proportions of the ligand should be tested in order to favor it.

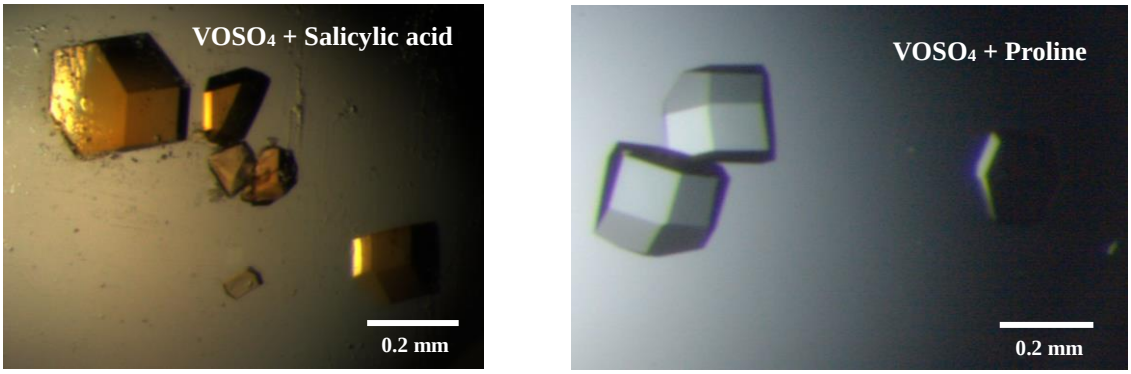

Figure 3.10 – HEWL crystals soaked (24 hours) with $VOSO_4$ and salicylic acid (left) and proline (right). Several ≈ 0.2×0.2×0.2 mm^3 crystals were obtained.

Simultaneously, three other compounds (Figure 3.11) have been tested – $VO(acac)_2$ (vanadyl acetylacetonate) and the carriers phenanthroline and 2,2'-bipyridine (1,10-phen and bipy, respectively) – which have been also implicated in different therapeutic actions namely insulin-mimetic and anti-cancer activity.[337,338,339,340,341]

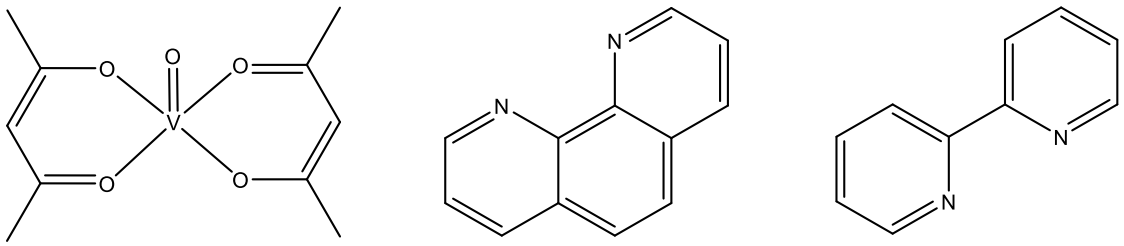

Figure 3.11 – Molecular formulas of $VO(acac)_2$ (left), 1,10-phen (center) and bipy (right). The structures were prepared in ChemDraw.

Once again, different soaking experiments have been tried and different greenish colored crystals were obtained (Figure 3.12). In addition to the color, most of the soaked crystals present a cracked aspect, which could indicate the diffusion of the compounds through the respective solvent channels. Subsequently, several of those crystals, with different times of soaking, have been collected up to 1.2 Å using synchrotron sources: beamlines ID23-2 (ESRF) and Proxima1 (Soleil).

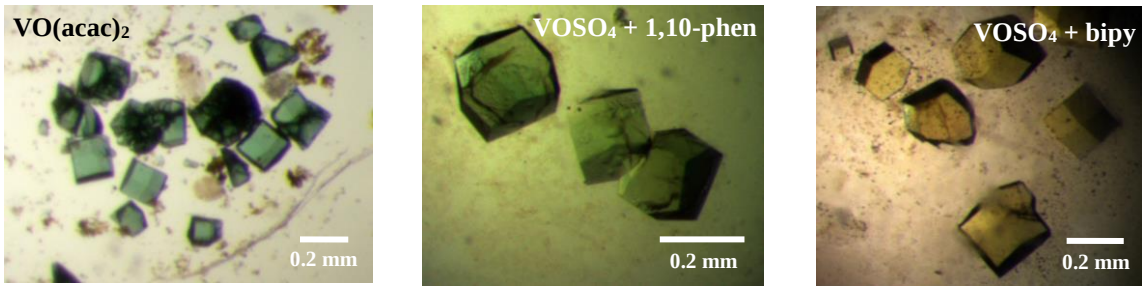

Figure 3.12 – HEWL crystals soaked (24 hours) with different vanadium complexes: $VO(acac)_2$ (left), $VOSO_4$+1,10-phen (center) and $VOSO_4$+bipy (right). Different colored ≈ 0.2×0.2×0.2 mm^3 crystals were obtained.

Analogously to the described for the soaking experiments with salicylic acid and proline, the vast majority of the collected datasets were not still analyzed and no definitive conclusions on the presence or absence of the respective adducts is available.

Notwithstanding, a 1.26 Å resolution structure of HEWL•$VOSO_4$•bipy (24 hours of soaking) was already solved. Currently under refinement, a preliminary analysis of the structure could be done and the respective current data collection and refinement statistics are summarized in Table 3.6.

As for the previous case, the analysis of the electron density maps of the HEWL structure revealed a strong peak next to Asp52 residue in the active site of the enzyme which is corroborated by the detected anomalous signal. However, some remarkable differences have been found when compared with the adduct formed by picolinate as depicted in Figure 3.13. More importantly, a $V^{IV}O(bipy)_2$ adduct is not observed and only one bipy moiety could be properly modeled with an occupancy of 0.60. The two nitrogen atoms of bipy appear to be bound to the central vanadium moiety. Interestingly, the determined V^{IV}–O (Asp52) bond length is longer than the one previously found (1.97 Å).

In the HEWL•$VOSO_4$•Hpic structure the Asn46 residue, at 2.04 Å from the metal coordinates the metal, binding in the equatorial position. An O_{oxido} atom was also modeled as an axial ligand at 2.08 Å. It is possible that the long distance results from the reduction of vanadium during the data collection as explained and a refinement using different slices of the collected data for should be also considered. A water molecule was added to complete the octahedral geometry but further refinement cycles are required to confirm its presence.

Table 3.6 – Data collection and refinement statistics for HEWL•$VOSO_4$•bipy adduct crystal. Values in parentheses correspond to the highest resolution shell.

X-ray source	Proxima1 (Soleil)
Crystal data	
Space group	$P4_32_12$
Unit cell parameters (Å, º)	$a = b = 77.90$, $c = 37.53$ $\alpha = \beta = \gamma = 90$
Molecules per ASU	1
Matthews coefficient (Å^3/Da)	1.96
Solvent content (%)	37.40
Data collection	
Wavelength (Å)	0.976
Resolution range (Å)	38.95–1.26 (1.28–1.26)
<I/σI>	16.0 (5.0)
Multiplicity	8.3 (6.8)
Number of observed reflections	265395 (10545)
Number of unique reflections	31813 (1547)
R_{pim} (%)	3.2 (14.3)
Completeness (%)	100 (99.9)
$CC_{1/2}$	0.995 (0.937)
Refinement	
Resolution range (Å)	38.95–1.26
R_{work} (%)	19.73
R_{free} (%)	22.85
RMSD bond length (Å)	0.027
RMSD bond angle (º)	2.26
Ramachandran plot (%)	
Residues in favored regions	96.06
Residues in additionally allowed regions	3.94
Residues in disallowed regions	0

$R_{pim} = \Sigma_{hkl} [1/(N-1)]^{1/2} \Sigma_i|I_i(hkl) - \langle I(hkl)\rangle|/\Sigma_{hkl} \Sigma_i I_i(hkl)$, where N is the multiplicity measured.

$R_{work} = \Sigma ||F_{calc}|-|F_{obs}|| / \Sigma|F_{obs}| \times 100$, where F_{calc} and F_{obs} are the calculated and observed structure factor amplitudes, respectively.

R_{free} is calculated for a randomly chosen 5% of the reflections for each dataset.

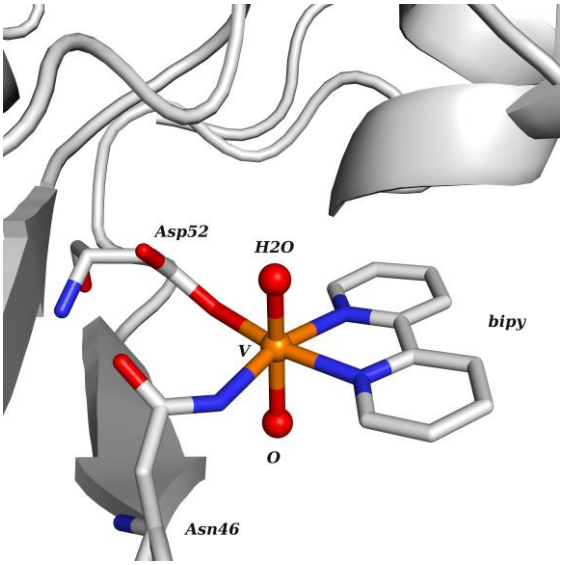

Figure 3.13 – Preliminary structural representation of the adduct observed in the HEWL•$VOSO_4$•bipy structure. At the current point of the refinement, the observed electron density (not shown in the figure) indicates an octahedral geometry with the presence of only one bipy moiety. Differently from the structure with picolinate, Asn46 appears to be also bound to vanadium (shown is orange).

As mentioned, the HEWL•$VOSO_4$•bipy structure is still under refinement and further analysis is necessary prior its correct characterization. However, both structures obtained – with pic and bipy – clear indicate that vanadium complexes are able to bind to the active site of the protein. HEWL is widely used in studies on the formation of amyloid fibrils being also known that the presence of small molecules could decrease the rate of such formation by stabilizing the native state of the proteins.[342,343,344,345] Therefore, it might be possible that vanadium compounds may act as anti-aggregation agents but there is still a long way to go for testing this hypothesis. Some very preliminary results suggest that the activity of HEWL, when incubated with V^{IV} and picolinate, significantly decreases (data not shown). Nevertheless, the conditions of the assay should be optimized – namely the concentration of the protein and inhibitor, the temperature and the time of incubation – before any statement on the use of vanadium complexes for such purpose can be considered. These results should be considered as good evidences of the putative side effects that this class of drugs can have upon administration. More studies are required to draw a clearer picture of the eventual use of vanadium complexes in medicine.

3.2.3 – Bovine Trypsin

The results described in the last chapter on the interactions of vanadium complexes with HEWL clearly suggest that the tested complexes are able to bind to the active site of the protein. Such observation led us to a simple question: a similar behavior is observed using some other classes of

proteins? In fact, as mentioned in the respective introductory section, different vanadium complexes have been used as substrate analogue or inhibitor.[210]

Among the different families of proteins, proteases have been selected to confirm this hypothesis. Proteases hydrolyze peptide bonds and are classified according to the catalytic mechanism into different groups: metallo, serine, cysteine, threonine and aspartic proteases. Particular attention has been given to serine proteases which are involved in numerous biological processes such as digestion, apoptosis and different signal transduction pathways (as example, the ones involved in blood coagulation could be cited).[346,347,348] Abnormal levels or mutations of such enzymes are implicated in several diseases and a lot of effort has been given to the design of efficient and selective inhibitors.[349]

Moreover, corroborating the feasibility of such approach, a 1.5 Å resolution structure of bovine chymotrypsin, a serine protease, complexed with vanadate and benzohydroxamic acid (PDB code: 2P8O) was reported. The complex is located in the active center and the V-atom is covalently bound to the O-atom of Ser195. The V-atom presents a distorted octahedral geometry with six ligands: the mentioned serine, the carbonyl and hydroxyl oxygen atoms of the benzohydroxamate and three O-atoms, one of which is hydrogen bonded to the backbone N-atom of Gly193 and Ser195 residues (the so-called oxyanion hole).[350]

Trypsin, widely used as a model in the investigations on serine proteases, has been used in the current study. This digestive enzyme cleaves peptide bonds at the carboxyl side of lysine and arginine (positively charged residues). Importantly, trypsin presents the so-called catalytic triad encompassing three residues – Ser195, His57 and Asp102 – which are hydrogen-bonded. An aspartate residue – Asp189 – is also relevant by stabilizing the positively charged side chains of the lysine and arginine residues and, by that, contributing for the specificity of the protein.[351,352]

3.2.3.1 – Materials and Methods

The vanadium compounds – $VOSO_4$, $NaVO_3$ and $VO(acac)_2$ – and the respective ligands – maltol, Hdhp, Hpic, H_2dipic, 1,10-phen and bipy – were prepared by the group of João da Costa Pessoa (*Instituto Superior Técnico, Universidade de Lisboa*).

Trypsin from bovine pancreas was purchased from Panreac/AppliChem. PEG 4K, sodium cacodilate, calcium chloride and salicylic acid were purchased from Sigma-Aldrich. Ammonium sulfate and proline was acquired from Panreac and Fluka, respectively.

X-ray crystallography – Crystallization, data collection, structure solution and structure refinement

A sample of bovine trypsin was prepared at 30 mg/ml in 25 mM HEPES pH 7.5 and 10 mM calcium chloride and crystallized using two different conditions: 1) – 0.1 M sodium acetate tri-hydrate pH 4.6, 0.2 M ammonium sulfate, 25% PEG4K and 2) – 0.2 M ammonium sulfate, 30% PEG4K. Both conditions were carried out at 20ºC using the hanging drop vapor diffusion method (2 µl of protein and 2 µl of reservoir solution with 700 µl of the precipitant solution in the reservoir) in 24-well plates from Molecular Dimensions. Crystals appeared within 24-48 hours and were stabilized with a harvesting buffer containing an increased percentage of PEG4K – 30% and 35% (w/v), respectively. Crystals were observed either with a SZH10 Olympus microscope or a SteREO Discovery V12 Zeiss microscope.

Different soaking experiments were carried out using a similar procedure to that described for HEWL. $VOSO_4$, $NaVO_3$ and $VO(acac)_2$ solutions were prepared in the harvesting buffer up to a final concentration of 10 mM and different solutions of $VOSO_4$:ligand (maltol, Hdhp, Hpic, H_2dipic, 1,10-phen, bipy, salicylic acid and proline) with a molar ratio of 1:3 were also prepared ($VOSO_4$ concentration: 10 mM). A 4 µl drop was prepared and some native trypsin crystals were transferred into it. The soaking was prolonged during 24 hours.

A co-crystallization approach was also tried. The protein was prepared as described and incubated with the several vanadium compounds and vanadium-ligand complexes in a 10- and 30-fold excess, respectively, for one hour. The mentioned crystallization conditions were then used. Different crystals were flash frozen using a harvesting buffer with 30% (v/v) glycerol as a cryoprotector.

For both soaking and co-crystallization experiments, crystals were flash frozen using harvesting buffer with 30% (v/v) glycerol as a cryoprotector and several high resolution datasets were collected using different Synchrotron beamlines namely ID29 (ESRF, Grenoble, France), Proxima1 (Soleil, Paris, France) and PXIII (SLS, Villigen, Switzerland).

The dataset integration and structure resolution, refinement and validation were carried out similarly to what has been described for HEWL. The structures were solved by Molecular Replacement using PDB entry 1S0Q as a model.

3.2.3.2 – Results and Discussion

The first experiments with bovine trypsin were performed using the initial compounds tested with HEWL namely the inorganic salts of V^{IV} and V^{V} and the four carriers (maltol, Hdhp, Hpic and H_2dipic) complexed with $VOSO_4$.

As observed in Figure 3.14, the crystals survived the prolonged soaking (24 hours) without serious visible damages. Moreover, some of the soaked crystals became colored. However, the co-crystallization approach failed to produce suitable crystals except when the protein was incubated with V^{IV} and picolinate: colorless crystals similar to the native ones have been obtained.

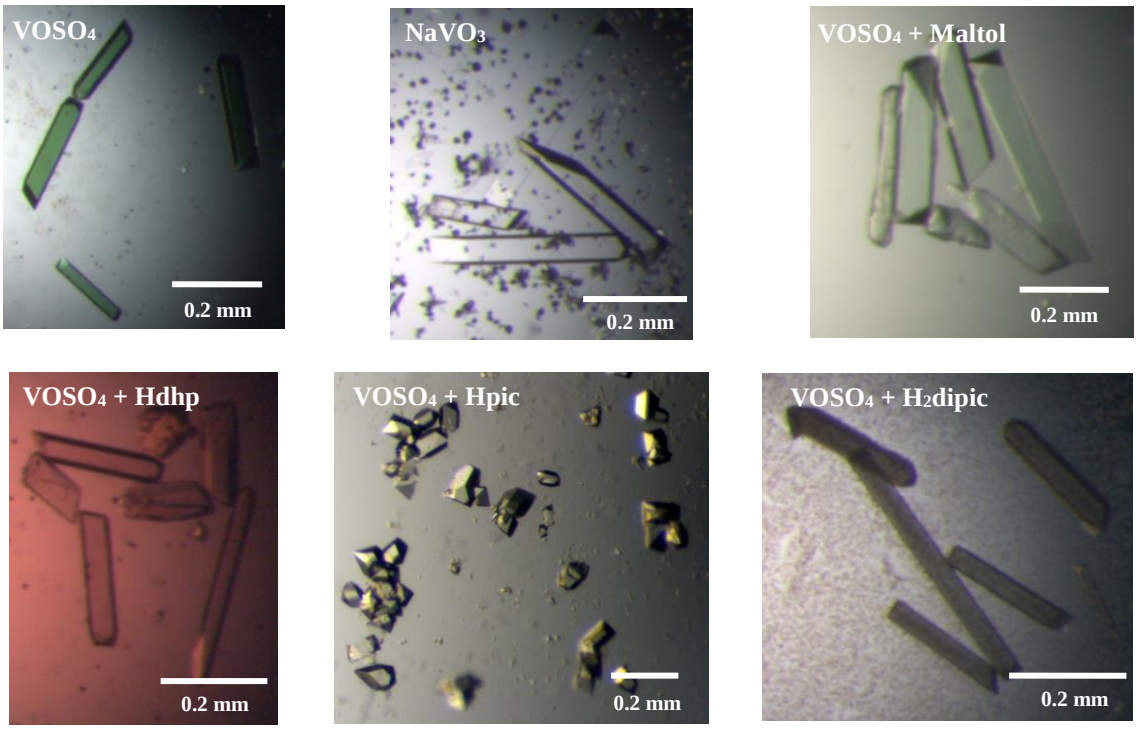

Figure 3.14 – Bovine trypsin crystals with different vanadium complexes after 24 hours of soaking. Several crystals with different sizes, forms and colors were obtained.

Several soaked and co-crystallized trypsin crystals were analyzed using synchrotron radiation in different facilities (ESRF and Soleil) and high resolutions data sets were obtained. The best results are indicated in Table 3.7.

All of these datasets were processed in two different space groups: $P2_12_12_1$ (orthorhombic, used for the crystals obtained by soaking) or $P3_121$ (trigonal, used in the single crystal obtained by co-crystallization).

The structures were solved by Molecular Replacement using PDB entry 1S0Q as a model. Nevertheless, taking into account the results obtained with HEWL, the structure corresponding to the trypsin•$VOSO_4$•Hpic crystal was selected to be firstly analyzed in order to find the expected adducts. The remaining five structures were not yet evaluated although they are expected to be soon analyzed.

Table 3.7 – X-ray diffraction results obtained with the best bovine trypsin crystals soaked and co-crystallized with different vanadium complexes.

Crystal (technique)	Obtained resolution	Beamline (Synchrotron)
Trypsin•$VOSO_4$ (soaking)	1.2 Å	ID29 (ESRF)
Trypsin•$NaVO_3$ (soaking)	1.1 Å	ID29 (ESRF)
Trypsin•$VOSO_4$•Maltol (soaking)	1.1 Å	ID29 (ESRF)
Trypsin•$VOSO_4$•Hdhp (soaking)	1.2 Å	ID29 (ESRF)
Trypsin•$VOSO_4$•Hpic (co-crystallization)	1.1 Å	Proxima1 (Soleil)
Trypsin•$VOSO_4$•H_2dipic (soaking)	1.1 Å	ID29 (ESRF)

The refinement of the trypsin•$VOSO_4$•Hpic structure is quite advanced although not completely finished since some of the validation steps are not yet complete (namely, several water molecules should be confirmed). However, at this current stage, valuable information could be already obtained and different features have been observed in the structure.

The data collection and refinement statistics of the trypsin•$VOSO_4$•Hpic crystal are summarized in Table 3.8.

Several moieties corresponding to different reagents used in the crystallization and cryo-protection steps were modeled namely five molecules of glycerol and one sulfate ion. Moreover, a calcium ion was also found in the so-called calcium-binding site; the ion contributes for the protein stability exhibiting an octahedral coordination with four different residues – Glu70, Asn72, Val75 and Glu80 – and two conserved water molecules.[353]

The structure presents the two characteristic β-barrels and an extra ligand was found next to the serine residue of the active site. This corresponds to a $V^{IV}O(pic)_2$ moiety modeled with an occupancy of 0.80 (Figure 3.15).

The modeled adduct exhibits a remarkable similarity with what was described for HEWL•vanadium adduct, adopting a distorted octahedral geometry covalently bound to Ser195, with a bidentate coordination to two pic^- anions and an O_{oxido} atom (Figure 3.16).

Table 3.8 – Data collection and refinement statistics for trypsin•$VOSO_4$•Hpic adduct crystal. Values in parentheses correspond to the highest resolution shell.

X-ray source	Proxima1 (Soleil)
Crystal data	
Space group	$P3_121$
Unit cell parameters (Å, º)	$a = b = 54.52$, $c = 108.20$ $\alpha = \beta = 90$, $\gamma = 120$
Molecules per ASU	1
Matthews coefficient ($Å^3$/Da)	1.98
Solvent content (%)	37.78
Data collection	
Wavelength (Å)	1.04
Resolution range (Å)	41.22–1.09 (1.11–1.09)
<I/σI>	8.2 (2.2)
Multiplicity	5.4 (5.1)
Number of observed reflections	423729 (19569)
Number of unique reflections	78462 (3802)
R_{pim} (%)	6.1 (43.7)
Completeness (%)	100 (100)
$CC_{1/2}$	0.995 (0.761)
Refinement	
Resolution range (Å)	41.22–1.09
R_{work} (%)	11.14
R_{free} (%)	13.62
RMSD bond length (Å)	0.015
RMSD bond angle (º)	1.81
Ramachandran plot (%)	
Residues in favored regions	96.35
Residues in additionally allowed regions	3.65
Residues in disallowed regions	0

$R_{pim} = \Sigma_{hkl} [1/(N-1)]^{1/2} \Sigma_i|I_i(hkl) - \langle I(hkl)\rangle|/\Sigma_{hkl} \Sigma_i I_i(hkl)$, where N is the multiplicity measured.

$R_{work} = \Sigma ||F_{calc}|-|F_{obs}|| / \Sigma|F_{obs}| \times 100$, where F_{calc} and F_{obs} are the calculated and observed structure factor amplitudes, respectively.

R_{free} is calculated for a randomly chosen 5% of the reflections for each dataset.

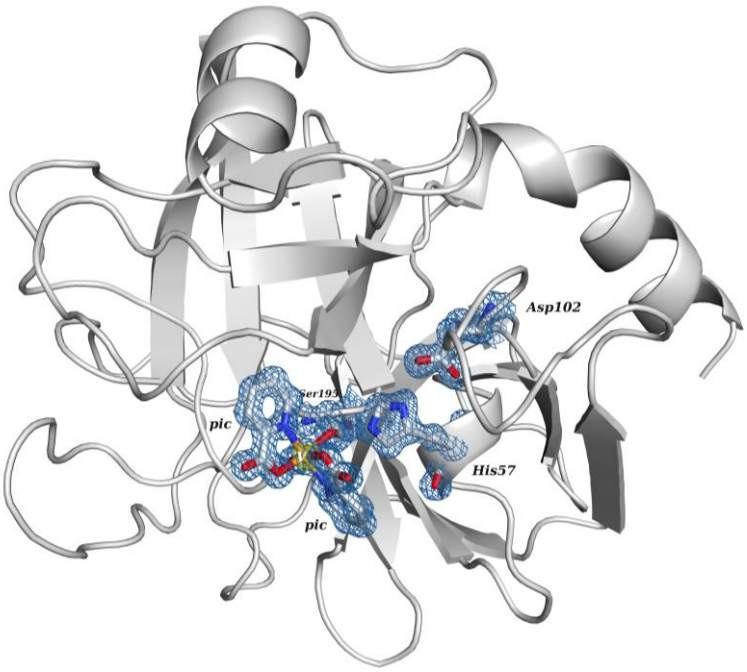

Figure 3.15 – Overall representation of bovine trypsin with the $V^{IV}O(pic)_2$ complex close to the Ser195 residue. The other two residues of the catalytic triad – His57 and Asp102 – are also shown. Electron density maps – 2Fo-Fc (blue) and anomalous (yellow) – are contoured at 1 and 3 σ, respectively. Vanadium is shown in orange.

Nevertheless, some differences are also found namely in the length of the V^{IV}=O bond which was determined to be 1.70 Å significantly lower than the length determined in the structure of HEWL (1.82 Å). This length bond is still slightly higher than the reported usual values (1.57 to 1.65 Å) and, as described previously, a partial reduction of the metal due to the radiation exposure should be considered. Similarly to the discussed with HEWL, low dose data collection can be used to further address such point but, at the current stage, the data suggest the presence of V^{IV} in the structure.

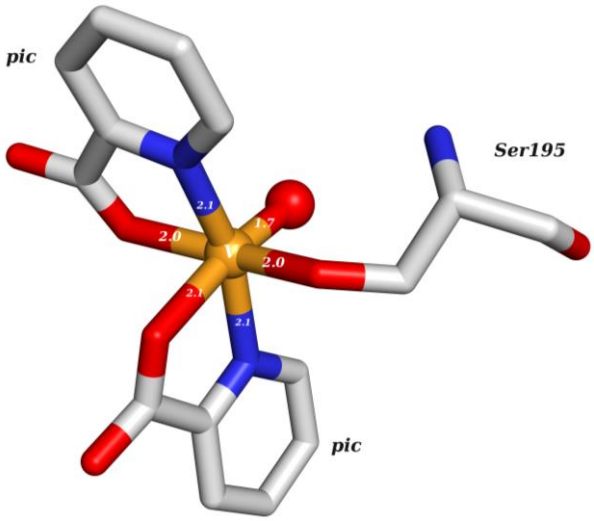

Figure 3.16 – Structural representation of $V^{IV}O(pic)_2$-Ser195 adduct. Vanadium is shown in orange. Bond lengths between V and the donor atoms are indicated (in Å). The length of the bond with Ser195 is longer than the one determined in the structure of HEWL while the bonds with both pic moieties remain nearly unchanged. The length of the bond V^{IV}=O is discussed more detailed in the text above.

The crystal structure here presented shows that this type of V complexes can occupy the active site of serine proteases, binding to the catalytic serine residue. The mentioned Asp189 is not implicated in the modeled adduct even though the complex fills the substrate pocket. The adduct will be carefully analyzed once the refinement is completed in order to confirm the existence of other interactions with the protein. Nevertheless, at the current refinement stage, it appears that, unlike the vanadium complex found in the PDB structure 2P8O, the picolinate moieties are not hydrogen bonded to the oxyanion hole.

Based on the success of the described experiment, some other related complexes have also been used similar to the tests done with HEWL. Both soaking and co-crystallization were tried but, so far, only the first approach produced suitable crystals (Figure 3.17).

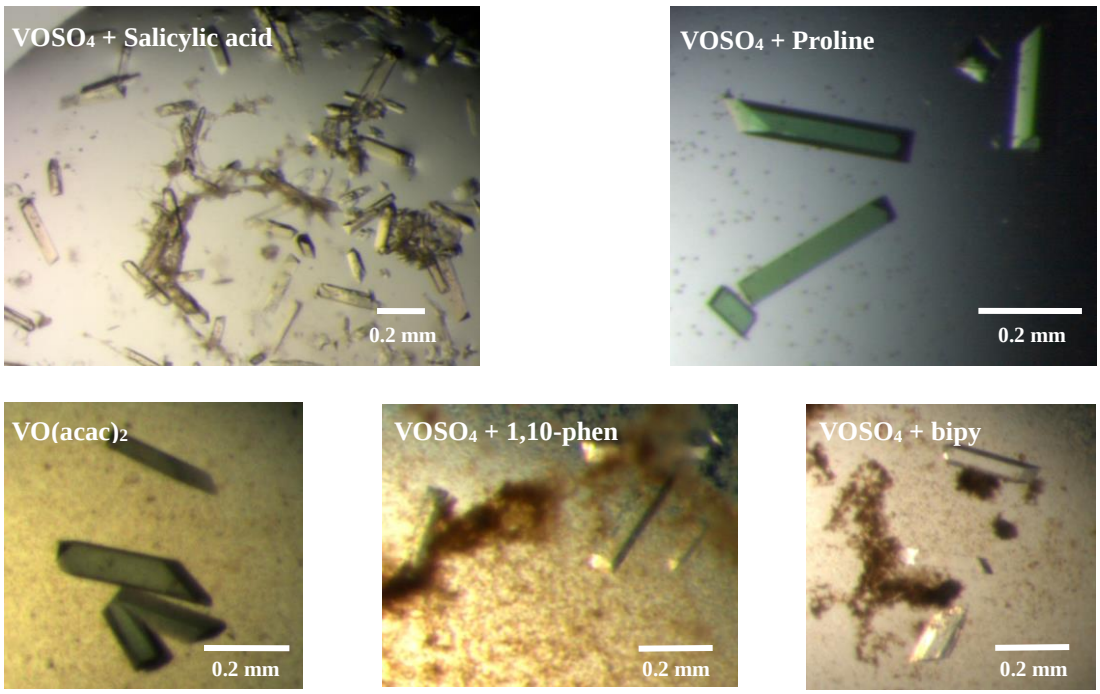

Figure 3.17 – Bovine trypsin crystals soaked with different vanadium complexes: $VOSO_4$+salicylic acid (left, top), $VOSO_4$+proline (right, top), $VO(acac)_2$ (bottom, left), $VOSO_4$+1,10-phen (bottom, center) and $VOSO_4$+bipy (bottom, right). Some of the soaked crystals became colored after 24 hours.

Different soaked crystals were then analyzed using different synchrotron sources (ESRF and SLS) and the best results are indicated in Table 3.9. All of these datasets will be soon solved in order to confirm if similar adducts are found in the respective crystal structures.

Nevertheless, the already obtained results with picolinate clear support the hypothesis of the binding of this type of vanadium complexes to the active site of other proteins than glycoside hydrolases (represented by HEWL). In parallel, this finding led us to speculate the potential role of such complexes as inhibitors of proteases for either future development of a new class of inhibitors or simply to attest putative side effects upon administration.

Table 3.9 – X-ray diffraction results obtained with the best bovine trypsin crystals soaked with different vanadium complexes related to picolinate.

Crystal	Obtained resolution	Beamline (Synchrotron)
Trypsin•$VOSO_4$•Salicylic acid	1.1 Å	PXIII (SLS)
Trypsin•$VOSO_4$•Proline	1.1 Å	ID29 (ESRF)
Trypsin•$VO(acac)_2$	1.1 Å	ID29 (ESRF)
Trypsin•$VOSO_4$•1,10-phen	1.2 Å	ID29 (ESRF)
Trypsin•$VOSO_4$•bipy	1.2 Å	ID29 (ESRF)

In order to confirm it, kinetic enzymatic assays should be performed being, currently, under preparation. A chromogenic substrate – BApNA (Nα-Benzoyl-DL-arginine-p-nitroanilide) – was selected allowing to follow its enzymatic conversion to the respective yellow product (p-nitroanilide) at 410 nm by UV-vis spectroscopy. Moreover, benzamidine is also planned to be used in order to compare the eventual inhibitory properties of the vanadium-picolinate complex with the results of a well-known inhibitor of trypsin. So far, preliminary experiments allowed the optimization of some of the conditions – namely the protein and the substrate concentrations (data not shown) – but further optimization is required in order to properly characterize the reaction (the concentration of the inhibitor should be particularly considered).

On the other hand, keeping in mind that trypsin was used as a protease model, the use of this type of complexes with other similar proteins should be also considered.[354]

CHAPTER 4

GENERAL CONCLUSIONS AND FUTURE PERSPECTIVES

Nowadays, our quality of life is massively affected by innumerous scientific and technologic progresses and it is not inaccurate to say that, globally, the world is changing. Very likely, or surely, to the question "what are the major advances achieved by mankind", multiple answers will be collected. Perhaps the improvement of the transports – by air, rail, road or water – will be cited by a significant number of people. The incredible simplicity to access information – namely by the "boom" of smartphones and similar devices – will be not forgotten by many others. Nevertheless, as important as the previous findings, the development of new and more potent drugs is a remarkable achievement with a major impact in the contemporary societies. As example, according the database Pordata, the life expectancy at birth in Portugal significantly increases from 67.1 years in 1970 to 80.2 years in 2013 and one of the reasons was certainly the progressive access to a larger range of new and more effective drugs.

Therefore, considerable efforts have been taken in the drug design and development field. In fact, several entities – both academic and industrial – are involved in the process implying not only a noteworthy monetary investment but also the establishment of multidisciplinary work teams. This last item is crucial for a successful strategy due to the multiple aspects that should be considered in the process. X-ray crystallography is, indubitably, one of the crucial techniques used in the investigation of new drugs providing valuable information at an atomic level namely in the analysis of different protein-ligand interactions.

In this Dissertation, X-ray crystallography, complemented by some other biochemical and biophysical procedures, was used as the main methodology to study two distinct drug design projects involving metal-based compounds: CO-Releasing Molecules and vanadium complexes. In both projects, the main focus was given to the characterization of putative interactions established between several organometallic compounds and different blood proteins using also some model proteins. In the next paragraphs, the principal conclusions of the different steps of the work as well as some future perspectives will be presented starting with the results concerning the project of CO-Releasing Molecules.

Formerly known as a toxic substance, carbon monoxide is nowadays also recognized as an agent with biological effects and different approaches to its therapeutic use have been proposed. The use of CORMs, molecules capable of transport CO in the blood delivering it at the damaged tissues, is one of such approaches but, being a relatively recent field, a lot of questions are yet to answer.

Nevertheless, it seems clear that the pharmacokinetic profile of this class of complexes strongly depends on the interactions established with plasma proteins as usually observed for most of the available drugs. Consequently, a proper characterization of such interactions is crucial for the development of CORMs as a viable methodology for CO delivery.

A vast majority of the known CORMs are metal carbonyl complexes. In this study, different metals have been tested but the most relevant results have been obtained with ruthenium-based CORMs. Sharing a similar general formula with the previously analyzed CORM-3, the complex

$[Ru(CO)_3Cl_2(1,3\text{-thiazole})]$ – named ALF850 – was firstly studied with HEWL and the resulting FTIR spectrum shows four peaks in the CO stretching region (2070, 2025, 1974 and 1943 cm^{-1}) indicating the presence of $Ru(CO)_2$ species coordinated to the protein.

In fact, ALF850 is rather labile in aqueous media following a reactivity pattern similar to that of CORM-3. As shown by X-ray crystallography, the soaking of ALF850 with HEWL resulted in the metallation of several residues of the protein, the most important one being the coordination of a $[Ru(CO)(H_2O)_4]^{2+}$ fragment to the His15 site in a octahedral geometry. However, lower occupancy adducts were also found next to different aspartate residues. Based on these results, we suggest that the compounds react rapidly with plasma proteins with the concomitant formation of protein•$Ru(CO)_2$ adducts which are carried throughout the body in the circulation. Taken together with the similar data available for CORM-3, where a $[Ru(CO)_2(H_2O)_3]^{2+}$ adduct was observed, we propose that the stepwise decay of the fac-$[Ru(CO)_3]^{2+}$ fragment in the presence of proteins is a rather plausible mechanism for the therapeutic delivery of CO *in vivo* from fac-$[Ru(CO)_3]^{2+}$ based CORMs.

To further investigate such hypothesis, some other different $[Ru(CO)_3Cl_2L]$ complexes – ALF475, ALF486 and ALF487 – have been used. The soaked HEWL crystals were collected up to, approximately, 1.7 Å resolution. The results obtained show that $Ru(CO)_x$ fragments bind several residues of the protein but the adduct with His15 residue is the one that systematically presents the highest occupancy. In both HEWL•ALF475 and HEWL•ALF487 crystal structures, a similar fragment to the one discussed for ALF850 – $[Ru(CO)(H_2O)_4]^{2+}$ – was found.

Remarkably, HEWL•ALF486 structure exhibits a feature observed for the first time in this type of studies: the adduct $[His15•Ru^{II}(COOH)(CO)(H_2O)_3]$ corresponding to a metallacarboxylate intermediate of the decarbonylation pathway of the CORM. This result suggests that the chemistry of $[Ru(CO)_3]^{2+}$ complexes in aqueous solution is initiated by the addition of a HO^- group in a pH dependent water-gas shift reaction as further confirmed by DFT calculations. Moreover, the stability of such intermediates could be also important for the delivery of CO to the cells as suggested in the text.

The mentioned findings with HEWL led us to interrogate if ruthenium-based CORMs present a similar decomposition behaviour in the presence of other proteins. Using bovine hemoglobin, soaking experiments with CORM-3 and ALF475 were performed and, in both 1.9 Å crystal resolution structures, ruthenium adducts were found at the surface of the protein.

The hemoglobin•CORM-3 structure presents a Ru adduct, next to two histidine residues, in which a CO molecule was also modeled. The hemoglobin•ALF475 structure exhibits two distinct adducts: the first one corresponds to the localization previously mentioned and the second one sits next to His145B and His145D; in both adducts, CO moieties are absence but iodide ions were identified in the last one. Both structures seem to corroborate the conclusions presented for HEWL by which proteins can favor the decomposition of CORMs since all the found adducts have released, partially or totally, the respective CO moieties.

Moreover, interesting points were also raised by the studies with iridium- and platinum-based CORMs. All the three compounds tested with HEWL exhibit the expected adducts next to His15 but, in two of them, CO release was not detected. Both ALF_MS2 and ALF_MS3 possess only one CO molecule in their composition and should be regarded as simple experimental CORMs to be used in fundamental/basic science.

All together, the mentioned results clearly indicate that HEWL is a robust model for this kind of studies, providing valuable information on the behavior of the complexes upon interaction with proteins and should be considered for preliminary tests with new classes of CORMs. In addition, it will be also interesting to further understand the fate of the CO molecules in the structures of hemoglobin since our data show that only the hemes closer to the metal complex are coordinating a diatomic molecule that can be modeled as a CO. This is in agreement with the low carboxy-hemoglobin levels, consistently observed. Although counter intuitive and yet to be disclosed, this result encourages the use of CORM in CO therapy, discarding gas poisoning events.[355]

Serum albumin – both human and bovine – has been also considered for similar experiments but no suitable crystals have been obtained and no further findings could be achieved. New initial screens as well as different additives should be tested to eventually find more promising crystallization conditions. Moreover, in a near future, we also intend to incubate HSA with sodium myristate prior the co-crystallization experiments with different CORMs in order to improve the already obtained crystals. Such approach is widely used and some examples are available in the literature.[304,356,357,358] If better HSA crystals are obtained, a similar methodology can be applied to BSA, a good and cheaper model of HSA.

Human serum apo-transferrin was also tested in the present work. Despite the multiple attempts to improve the quality of crystals, it was not possible to find a procedure to systematically obtain good diffracting crystals. Notwithstanding, due to the mentioned efforts, a transferrin•CORM structure was determined for the first time corresponding to a 2.7 Å resolution structure soaked with ALF_MS2. A suspicious blob was found at the surface of the N-terminal lobe, next to His578 but, apart from an iridium moiety, no other putative elements of the adduct could be modeled. Even so, the obtained results appear to indicate the ability of the protein to transport this type of complexes in some additional sites than the two iron binding sites. Consequently, in addition to the improvement of the described crystals of apo-transferrin, the use of holo-transferrin is also planned as future work. The iron-loaded form of the protein has been also crystallized at 2.1 Å resolution (PDB code: 4V83) and, if similar or better resolutions could be achieved, significant insights on the transport of CORMs along the blood stream and the respective repercussions on their pharmacokinetic profile, can be further obtained.[331]

As widely referred in the text, the main focus of the developed experimental work was given to blood proteins. Nevertheless, the study could be extended to some other proteins. The use

of ferritin, an iron-storage protein, as a system capable of store several CORMs molecules and simultaneously acting as a delivery carrier is particularly tempting as the uptake of the desired molecules by the cells could be facilitated by the existence of cell surface receptors for the protein.[359] Some preliminary soaking experiments with the iridium- and platinum-based CORMs have been already performed for bovine ferritin crystals but a more systematic approach using different CORMs is planned for the future.

In conclusion, albeit the lack of determination of a structure of albumin complexed with CORMs, the presented work provided significant insights on the mechanisms by which these organometallic compounds interact with proteins leading to the release of carbon monoxide. Nevertheless, confirming the potentialities of the project, there are still a lot of questions to be answered and further explored.

Regarding the second project, vanadium is recognized as an agent with biological properties (interacting with several proteins) and putative therapeutic actions (insulin-enhancer, anti-cancer and anti-parasitic). Importantly, different metal-ion carriers are used in order to improve absorption, transport and uptake of vanadium. Similarly to the described for CORMs, transferrin has been proposed as a putative physiological carrier of vanadium allowing its transport in the blood and also controlling the pharmacokinetic profile of such complexes.

However, the mechanisms by which the transport is achieved are not fully understood namely the conformation adopted by transferrin upon vanadium binding. X-ray crystallography was used to further address this point but no suitable crystals have been obtained. Therefore, it was studied by some alternative techniques. $V^{IV}O$ and different carrier ligands – maltol, Hdhp, picolinate and dipicolinate – were incubated with transferrin and analyzed by urea gel electrophoresis. The migrating pattern of the closed and open conformations is clear although not so easy to correlate with the presence of the complexes and, in the case of maltol and Hpic, a simultaneous presence of the open and closed forms is observed.

A hs-apoTF+$V^{IV}O$+Hpic sample was also tested by SAXS. A preliminary analysis reveals that the respective scattering profile shows a better fit using the crystallographic model corresponding to the open conformation. However, such fit is not perfect suggesting that, putatively, an equilibrium is observed in solution with the simultaneous presence of both forms – open and closed – of the protein which is also in agreement with the observed in the urea gel electrophoresis. As discussed in the text, in order to overcome the potential oxidation of the complexes to V^{V} before the data collection, a more systematic strategy was adopted using two different times of incubation. The analysis of the described SAXS data is one of the tasks to be done in a near future. Hopefully, these results will provide significant insights on the elucidation of the conformation of transferrin upon vanadium binding.

Following a similar approach to the one used with CORMs, HEWL was also used as a crystallographic model. Different soaking experiments were tried with the four previously mentioned

carrier ligands and the interaction of $V^{IV}O(pic)_2$ with HEWL was characterized: the V^{IV} ion of $V^{IV}O(pic)_2$ can covalently bind to the COO^- group of the Asp52 residue of HEWL by substituting the equatorial water molecule; this is the first example of V^{IV}–protein binding confirmed by single-crystal X-ray diffraction. For the HEWL–$V^{IV}O(pic)_2$ adduct, a relatively strong EPR signal was observed confirming the presence of $V^{IV}O$ species; DFT results allowed the binding of the carboxylate of the Asp52 residue of HEWL to the $V^{IV}O(pic)_2$ moiety to be confirmed and allowed for the prediction that the V^{IV}=O bond is in fact ≈1.60 Å in the soaked crystals. However, in the refined crystallographic structure a relatively long bond was found between the metal and the O_{oxido} donor (1.82 Å). As explained in the text, the reduction of V^{IV} to V^{III} during the beam exposure was corroborated by analysis of subsets of the diffraction images. This is a relevant finding, as similar reduction might explain anomalous structural data previously reported in V^V-containing proteins. Low dose data collection should corroborate these findings and provide more accurate values for the bond distances of V-protein adducts.

Some other carrier ligands were also tested with HEWL and the most relevant result was obtained for 2,2'-bipyridine (bipy). An adduct was found also sitting in the active site of the protein next to Asp52 residue and, even if the structure is still under refinement, some differences are visible when compared to the HEWL–$V^{IV}O(pic)_2$ adduct. Most notable, only one bipy molecule could be properly modeled and Asn46 is also implicated in the adduct.

Furthermore, the mentioned experiments with HEWL led to hypothesize the potential use of these vanadium complexes as protein inhibitors. HEWL represent the class of glycoside hydrolases but it is clear that the study could be extended to some other classes. In this sense, proteases have been chosen to be part of the study and different soaking and co-crystallization trials were performed using bovine trypsin, a serine protease. Remarkably, a 1.1 Å resolution trypsin•$VOSO_4$•Hpic structure was obtained showing a $V^{IV}O(pic)_2$ adduct bound to Ser195 in the active site very similar to the one found in the HEWL structure. This finding suggests the feasibility of the use of the compound as a protease inhibitor, but, as previously discussed, kinetic enzymatic assays are required to confirm it.

In addition to the already mentioned future tasks to be developed, two more proteins are planned to be used in the investigation: ferritin and hemoglobin. The inclusion of ferritin is justified by similar reasons to those explained in the section dedicated to CORMs being related to the putative ability of the protein to act as a storage and delivery system. A small number of structures – soaked with inorganic V^{IV} – have been already obtained but, so far, it was not possible to confirm if the detected anomalous density blobs correspond to vanadium or to cadmium which is present in the protein buffer. New experiments with different carriers are expected to be helpful to elucidate such aspect.

On the other hand, red cells have been also implicated in the transport of vanadium complexes and hemoglobin, as the most abundant protein existing in erythrocytes, is very likely responsible for such interactions. Therefore, the putative protein-adducts determined by X-ray crystallography can be

an excellent complement to the already available EPR and DFT studies in order to obtain new insights on the subject namely the identification of the residues involved in the binding process as well as the number of vanadium complexes loaded by the protein.[360,361]

In conclusion, although the existence of multiple vanadium-containing structures, the vast majority of them corresponds to proteins, which require such element for their function or to proteins in which vanadium has been used as phosphate analogue or inhibitor. The work herein presented provides significant new structural insights on the transport of vanadium. Most notable, the ability of vanadium carriers to bind to different proteins has been demonstrated allowing not only further studies on the topic but also to expand them to some new goals such as their use as protein inhibitors.

Therefore, the results obtained over the time of this thesis for both projects illustrate nicely the potentialities of the use of X-ray crystallography in the drug design field. In fact, the use of this technique, combined with some other complementary methodologies, reveals to be extremely useful allowing the elucidation of several molecular details which, in turn, contribute to propose different mechanisms of action or, alternatively, prompt to new experiments and objectives.

Nevertheless, in parallel with its numerous advantages, it is also undeniable that X-ray crystallography is a very challenging technique. The lack of good diffracting crystals, the low success rate of soaking and co-crystallization trials and the limited access to appropriate X-ray radiation are just some representative examples of such challenges and difficulties. Even if some of them are expected to continue to be part of the quotidian of the crystallographers, some others tend to diminish thanks to the efforts of a large community. The continuous improvements of both Synchrotron beamlines and crystallographic softwares are some examples of such efforts.

Moreover, despite the regular access to different European synchrotron facilities – ESRF, Soleil, Diamond, SLS and, more lately, PetraIII – in the last four years, the recent acquisition of an in-house X-ray diffractometer (Bruker D8 Venture) by the X-ray Crystallography group at FCT/UNL is expected to largely contribute to the development of the mentioned projects. Although it will not replace the use of synchrotron radiation, this equipment will allow not only to distinguish salt crystals from protein crystals (often found during the crystallization of albumin) but also to rapidly test a great range of experiments – as example, combining different concentrations of the desired ligand with different soaking times – allowing a more systematic and rational selection of the crystals to be analyzed at the synchrotron.

As general conclusion, the results herein discussed provide valuable insights towards a better understanding of relevant aspects in the development of these metal-based drugs. New findings, together with the already achieved results, will be essential for the future use of this class of molecules as viable and safe therapeutic agents fighting several world-spread diseases and, by that, helping to improve the conditions of life of a significant percentage of the population.

CHAPTER 5

REFERENCES

1. Michael D. Rawlins, Cutting the cost of drug development?, *Nature Reviews Drug Discovery* **2004**, *3*, 360-364.

2. Roy Berggren, Martin Møller, Rachel Moss, Pawel Poda, Katarzyna Smietana, Outlook for the next 5 years in drug innovation, *Nature Reviews Drug Discovery* **2012**, *11*, 435-436.

3. Graham L. Patrick, *An Introduction to Medicinal Chemistry*, Oxford University Press, 5th edition, **2013**, 1-13.

4. Gareth Thomas, *Medicinal Chemistry: An Introduction*, John Wiley & Sons Ltd, 2nd edition, **2007**, 1-35.

5. Enrique Raviña, *The Evolution of Drug Discovery: From Traditional Medicines to Modern Drugs*, Wiley-VCH Verlag GmbH & Co. KGaA, 1st edition, **2011**, 1-22.

6. Joseph A. DiMasi, Ronald W. Hansen, Henry G. Grabowski, The price of innovation: new estimates of drug development costs, *Journal of Health Economics* **2003**, *22*, 151-185.

7. Walter Sneader, *Drug Discovery: A History*, John Wiley & Sons Ltd, 1st edition, **2005**, 8-31.

8. Alan L. Harvey, Natural products in drug discovery, *Drug Discovery Today* **2008**, *13(19/20)*, 894-901.

9. José Francisco Meirinhas, Avatares da antiga atribuição de obras a Pedro Hispano/João XXI: Parte II – Os séculos XV-XIX, *Revista Portuguesa de História do Livro* **2009**, *24*, 437-501.

10. Ivo Álvares Furtado, O Médico Pedro Hispano Portucalense (1205 – 1277), *Acta Médica Portuguesa* **2012**, *25(1)*, 2-3.

11. Palmira Fontes da Costa, Teresa Nobre-Carvalho, Between East and West: Garcia de Orta's Colloquies and the Circulation of Medical Knowledge in the Sixteenth Century, *Asclepio. Revista de Historia de la Medicina y de la Ciencia* **2013** *65(1)*, p008.

12. Ana Sofia Pina, Abid Hussain, Ana Cecília A. Roque, An Historical Overview of Drug Discovery *in Ligand-Macromolecular Interactions in Drug Discovery – Methods and Protocols* edited by Ana Cecília A. Roque, Humana Press, 1st edition, **2010**, 3-12.

13. Jürgen Drews, Drug Discovery: A Historical Perspective, *Science* **2000**, *287*, 1960-1964.

14. Bernard Munos, Lessons from 60 years of pharmaceutical innovation, *Nature Reviews Drug Discovery* **2009**, *8*, 959-968.

15. Janice M. Reichert, Trends in Development and Approval Times for New Therapeutics in the United States, *Nature Reviews Drug Discovery* **2003**, *2*, 695-702.

16. Jeffrey A. Kramer, John E. Sagartz, Dale L. Morris, The application of discovery toxicology and pathology towards the design of safer pharmaceutical lead candidates, *Nature Reviews Drug Discovery* **2007**, *6*, 636-649.

17. Solomon Nwaka, Robert G. Ridley, Virtual drug discovery and development for neglected diseases through public–private partnerships, *Nature Reviews Drug Discovery* **2003**, *2*, 919-928.

18. James P. Hughes, Stephen Rees, S. Barrett Kalindjian, Karen L. Philpott, Principles of early drug discovery, *British Journal of Pharmacology* **2011**, *162*, 1239-1249.

19. Peter Imming, Christian Sinning, Achim Meyer, Drugs, their targets and the nature and number of drug targets, *Nature Reviews Drug Discovery* **2006**, *6*, 821-834.

20. Isabella Gashaw, Peter Ellinghaus, Anette Sommer, Khusru Asadullah, What makes a good drug target?, *Drug Discovery Today* **2011**, *16(23-24)*, 1037-1043.

21. Tala M. Bakheet, Andrew J. Doig, Properties and identification of human protein drug targets, *Bioinformatics* **2009**, *25(4)*, 451-457.

22. Michael S. Kinch, Denton Hoyer, Eric Patridge, Mark Plummer, Target selection for FDA-approved medicines, Target discovery from data mining approaches, *Drug Discovery Today* **2015**, *20(7)*, 784-789.

23. Monica Schenone, Vlado Dančík, Bridget K Wagner, Paul A Clemons, Target identification and mechanism of action in chemical biology and drug discovery, *Nature Chemical Biology* **2013**, *9*, 232-240.

24. Yongliang Yang, S. James Adelstein, Amin I. Kassis, Target discovery from data mining approaches, *Drug Discovery Today* **2012**, *17S*, S16-S23.

25. Konrad H. Bleicher, Hans-Joachim Böhm, Klaus Müller, Alexander I. Alanine, Hit and lead generation: beyond high-throughput screening, *Nature Reviews Drug Discovery* **2003**, *2*, 369-378.

26. Keith Moore, Stephen Rees, Cell-based Versus Isolated Target Screening: How Lucky Do You Feel?, *Journal of Biomolecular Screening* **2001**, *6(2)*, 69-74.

27. Lorenz M Mayr, Dejan Bojanic, Novel trends in high-throughput screening, *Current Opinion in Pharmacology* **2009**, *9*, 580-588.

28. Ge Wu, Stephen K. Doberstein, HTS technologies in biopharmaceutical discovery, *Drug Discovery Today* **2006**, *11*, 718-724.

29. Ricardo Macarron, Martyn N. Banks, Dejan Bojanic, David J. Burns, Dragan A. Cirovic, Tina Garyantes, Darren V. S. Green, Robert P. Hertzberg, William P. Janzen, Jeff W. Paslay, Ulrich Schopfer, G. Sitta Sittampalam, Impact of high-throughput screening in biomedical research, *Nature Reviews Drug Discovery* **2011**, *10*, 188-195.

30. Duncan E. Scott, Anthony G. Coyne, Sean A. Hudson, Chris Abell, Fragment-Based Approaches in Drug Discovery and Chemical Biology, *Biochemistry* **2012**, *51*, 4990-5003.

31. Richard Law, Oliver Barker, John J. Barker, Thomas Hesterkamp, Robert Godemann, Ole Andersen, Tara Fryatt, Steve Courtney, Dave Hallett, Mark Whittaker, The multiple roles of computational chemistry in fragment-based drug design, *Journal of Computer-Aided Molecular Design* **2009**, *23*, 459-473.

32. György M. Keserű, Gergely M. Makara, Hit discovery and hit-to-lead approaches, *Drug Discovery Today* **2006**, *11*, 741-748.

33. Ismail Kola, John Landis, Can the pharmaceutical industry reduce attrition rates?, *Nature Reviews Drug Discovery* **2004**, *3*, 711-715.

34. Michael J. Waring, John Arrowsmith, Andrew R. Leach, Paul D. Leeson, Sam Mandrell, Robert M. Owen, Garry Pairaudeau, William D. Pennie, Stephen D. Pickett, Jibo Wang, Owen Wallace, Alex Weir, An analysis of the attrition of drug candidates from four major pharmaceutical companies, *Nature Reviews Drug Discovery* **2015**, *14*, 475-486.

35. Paul D. Leeson, Brian Springthorpe, The influence of drug-like concepts on decision-making in medicinal chemistry, *Nature Reviews Drug Discovery* **2007**, *6*, 881-890.

36. David J. Newman, Gordon M. Cragg, Natural Products as Sources of New Drugs over the 30 Years from 1981 to 2010, *Journal of Natural Products* **2012**, *75*, 311-335.

37. Alan L. Harvey, RuAngelie Edrada-Ebel, Ronald J. Quinn, The re‐emergence of natural products for drug discovery in the genomics era, *Nature Reviews Drug Discovery* **2015**, *14*, 111-129.

38. Christopher A. Lipinski, Franco Lombardo, Beryl W. Dominy, Paul J. Feeney, Experimental and computational approaches to estimate solubility and permeability in drug discovery and development settings, *Advanced Drug Delivery Reviews* **1997**, *23*, 3-25.

39. Christopher A. Lipinski, Franco Lombardo, Beryl W. Dominy, Paul J. Feeney, Experimental and computational approaches to estimate solubility and permeability in drug discovery and development settings, *Advanced Drug Delivery Reviews* **2001**, *46*, 3-26.

40. Christopher A. Lipinski, Lead- and drug-like compounds: the rule-of-five revolution, *Drug Discovery Today: Technologies* **2004**, *1(4)*, 337-341.

41. Ming-Qiang Zhang, Barrie Wilkinson, Drug discovery beyond the 'rule-of-five', *Current Opinion in Biotechnology* **2007**, *18*, 478-488.

42. Hongyu Zhao, Lead optimization in the nondrug-like space, *Drug Discovery Today* **2011**, *16*, 158-163.

43. Paul Leeson, Chemical beauty contest, *Nature* **2012**, *481*, 455-456.

44. Blessy M, Ruchi D. Patel, Prajesh N. Prajapati, Y .K. Agrawal, Development of forced degradation and stability indicating studies of drugs – A review, *Journal of Pharmaceutical Analysis* **2014**, *4(3)*, 159-165.

45. Jarkko Rautio, Hanna Kumpulainen, Tycho Heimbach, Reza Oliyai, Dooman Oh, Tomi Järvinen, Jouko Savolainen, Prodrugs: design and clinical applications, *Nature Reviews Drug Discovery* **2008**, *7*, 255-270.

46. Bernard Testa, Prodrugs: bridging pharmacodynamic/pharmacokinetic gaps, *Current Opinion in Chemical Biology* **2009**, *13*, 338-344.

47. Valentino J. Stella, Prodrugs: Some Thoughts and Current Issues, *Journal of Pharmaceutical Sciences* **2010**, *99(12)*, 4755-4765.

48. Jolanta B. Zawilska, Jakub Wojcieszak, Agnieszka B. Olejniczak, Prodrugs: A challenge for the drug development, *Pharmacological Reports* **2013**, *65*, 1-14.

49. Jonathan McConathy, Michael J. Owens, Stereochemistry in Drug Action, *Journal of Clinical Psychiatry* **2003**, *5*, 70-73.

50. Janine R. Cossy, The Importance of Chirality in Drugs and Agrochemicals *in Comprehensive Chirality* edited by Erick M. Carreira and Hisashi Yamamoto, Elsevier, **2012**,1-7.

51. Margherita Strolin Benedetti, Rhys Whomsley, Italo Poggesi, Willi Cawello, François-Xavier Mathy, Marie-Laure Delporte, Peggy Papeleu, Jean-Baptiste Watelet, Drug metabolism and pharmacokinetics, *Drug Metabolism Reviews* **2009**, *41(3)*, 344-390.

52. Ana Ruiz-Garcia, Marival Bermejo, Aaron Moss, Vicente G. Casabo, Pharmacokinetics in Drug Discovery, *Journal of Pharmaceutical Sciences* **2008**, *97*, 654-690.

53. Andrew S. Jarrell, Rachel M. Kruer, Dachelle Johnson, Pamela A. Lipsett, Antimicrobial Pharmacokinetics and Pharmacodynamics, *Surgical Infections* **2015**, *16(4)*, 375-379.

54. Jianghong Fan, Inés A.M. de Lannoy, Pharmacokinetics, *Biochemical Pharmacology* **2014**, *87(1)*, 93-120.

55. Han van de Waterbeemd, Eric Gifford, ADMET in silico modelling: Towards prediction paradise?, *Nature Reviews Drug Discovery* **2003**, *2*, 192-204.

56. S. A. Shaikh, T. Jain, G. Sandhu, N. Latha, B. Jayaram, From Drug Target to Leads-Sketching A Physicochemical Pathway for Lead Molecule Design In Silico, *Current Pharmaceutical Design* **2007**, *13*, 3454-3470.

57. George L Trainor, The importance of plasma protein binding in drug discovery, *Expert Opinion on Drug Discovery* **2007**, *2(1)*, 51-64.

58. Stephan Schmidt, Daniel Gonzalez, Hartmut Derendorf, Significance of Protein Binding in Pharmacokinetics and Pharmacodynamics, *Journal of Pharmaceutical Sciences* **2010**, *99(3)*, 1107-1122.

59. Tonika Bohnert, Liang-Shang Gan, Plasma Protein Binding: From Discovery to Development, *Journal of Pharmaceutical Sciences* **2013**, *102(9)*, 2953-2994.

60. Iain L. O. Buxton, Leslie Z. Benet, Pharmacokinetics: The Dynamics of Drug Absorption, Distribution, Metabolism, and Elimination *in Goodman and Gilman's – The Pharmacological Basis of Therapeutics* edited by Laurence L. Brunton, McGraw-Hill, 12th edition, **2011**, 17-40.

61. Maciej J. Zamek-Gliszczynski, Keith A. Hoffmaster, Ken-ichi Nezasa, Melanie N. Tallman, Kim L.R. Brouwer, Integration of hepatic drug transporters and phase II metabolizing enzymes: Mechanisms of hepatic excretion of sulfate, glucuronide, and glutathione metabolites, *European Journal of Pharmaceutical Sciences* **2006**, *27*, 447-486.

62. Ulrich M. Zanger, Miia Turpeinen, Kathrin Klein, Matthias Schwab, Functional pharmacogenetics/genomics of human cytochromes P450 involved in drug biotransformation, *Analytical and Bioanalytical Chemistry* **2008**, *392*, 1093-1108.

63. Ulrich M. Zanger, Matthias Schwab, Cytochrome P450 enzymes in drug metabolism: Regulation of gene expression, enzyme activities, and impact of genetic variation, *Pharmacology & Therapeutics* **2013**, *38*, 103-141.

64. R. Scott Obach, Phuong Huynh, Mary C. Allen, Christine Beedham, Human Liver Aldehyde Oxidase: Inhibition by 239 Drugs, *The Journal of Clinical Pharmacology* **2004**, *44*, 7-19.

65. Enrico Garattini and Mineko Terao, Increasing recognition of the importance of aldehyde oxidase in drug development and discovery, *Drug Metabolism Reviews* **2011**, *43(3)*, 374-386.

66. Catarina Coelho, Alessandro Foti, Tobias Hartmann, Teresa Santos-Silva, Silke Leimkühler, Maria João Romão, Structural insights into xenobiotic and inhibitor binding to human aldehyde oxidase, *Nature Chemical Biology* **2015**, *11*, 779-783.

67. Palleria Caterina, Di Paolo Antonello, Giofrè Chiara, Caglioti Chiara, Leuzzi Giacomo, Siniscalchi Antonio, De Sarro Giovambattista, Gallelli Luca, Pharmacokinetic drug−drug interaction and their implication in clinical management, *Journal of Research in Medical Sciences* **2013**, *18*, 600-609.

68. C. Frank Shaw III, Metal-based Drugs *in Encyclopedia of Inorganic and Bioinorganic Chemistry*, John Wiley & Sons, **2011**, 1-29.

69. Declan Gaynora, Darren M. Griffith, The prevalence of metal-based drugs as therapeutic or diagnostic agents: beyond platinum, *Dalton Transactions* **2012**, *41*, 13239-13257.

70. Nicolas P. E. Barry, Peter J. Sadler, Exploration of the medical periodic table: towards new targets, *Chemical Communications* **2013**, *49*, 5106-5131.

71. Gianni Colotti, Andrea Ilari, Alberto Boffi, Veronica Morea, Metals and Metal Derivatives in Medicine, *Mini-Reviews in Medicinal Chemistry* **2013**, *13*, 211-221.

72. Linus Chiang, Michael R. Jones, Cara L. Ferreira, Tim Storr, Multifunctional Ligands in Medicinal Inorganic Chemistry – Current Trends and Future Directions, *Current Topics in Medicinal Chemistry* **2012**, *12*, 122-144.

73. Hoi-Ling Seng, Edward R.T Tiekink, Main-Group Medicinal Chemistry Including Li and Bi *in Comprehensive Inorganic Chemistry II* edited by Jan Reedijk and Kenneth Poeppelmeier, Elsevier, 2nd edition, **2013**, 951-974.

74. Raymond Wai-Yin Sun, Dik-Lung Ma, Ella Lai-Ming Wong and Chi-Ming Che, Some uses of transition metal complexes as anti-cancer and anti-HIV agents, *Dalton Transactions* **2007**, *43*, 4884-4892.

75. Serenella Medici, Massimiliano Peana, Valeria Marina Nurchi, Joanna I. Lachowicz,Guido Crisponi, Maria Antonietta Zoroddu, Noble metals in medicine: Latest advances, *Coordination Chemistry Reviews* **2015**, *284*, 329-350.

76. Angela Casini, Exploring the mechanisms of metal-based pharmacological agents via an integrated approach, *Journal of Inorganic Biochemistry* **2012**, *109*, 97-106.

77. Isolda Romero-Cenelón, Peter J. Sadler, Next-Generation Metal Anticancer Complexes: Multitargeting via Redox Modulation, *Inorganic Chemistry* **2013**, *52(21)*, 12276-12291.

78. Ingo Ott, Biodistribution of Metals and Metallodrugs *in Comprehensive Inorganic Chemistry II* edited by Jan Reedijk and Kenneth Poeppelmeier, Elsevier, 2nd edition, **2013**, 933-949.

79. Jürgen Bierhals, Carbon Monoxide *in Ullmann's Encyclopedia of Industrial Chemistry*, John Wiley and Sons, **2001**, 679-693.

80. Heinz-Wolfgang Häring, Hydrogen and Carbon Monoxide: Synthesis Gases *in Industrial Gases Processing*, Wiley-VCH Verlag GmbH & Co. KGaA, **2008**, 135-184.

81. Stefan W. Ryter, Jawed Alam, Augustine M. K. Choi, Heme Oxygenase-1/Carbon Monoxide: From Basic Science to Therapeutic Applications, *Physiological Reviews* **2006**, *86(2)*, 583-650.

82. Inge Bauer, Benedikt H.J. Pannen, Bench-to-bedside review: Carbon monoxide - from mitochondrial poisoning to therapeutic use, *Critical Care* **2009**, *13(4)*, 220.

83. Lingyun Wu, Rui Wang, Carbon Monoxide: Endogenous Production, Physiological Functions, and Pharmacological Applications, *Pharmacological Reviews* **2005**, *57(4)*, 585-630.

84. Shin Miyakawa, Hiroto Yamanashi, Kensei Kobayashi, H. James Cleaves, Stanley L. Miller, Prebiotic synthesis from CO atmospheres: Implications for the origins of life, *Proceedings of the National Academy of Sciences* **2002**, *99(23)*, 14628-14631.

85. Brian E. Mann, Signaling Molecule Delivery (CO) *in Comprehensive Inorganic Chemistry II* edited by Jan Reedijk and Kenneth Poeppelmeier, Elsevier, 2nd edition, **2013**, 857-876.

86. Kelly S. Davidge, Roberto Motterlini, Brian E. Mann, Jayne Louise Wilson, Robert K. Poole, Carbon Monoxide in Biology and Microbiology: Surprising Roles for the "Detroit Perfume", *Advances in Microbial Physiology* **2009**, *56*, 85-167.

87. Louise W. Kao, Kristine A. Nañagas, Toxicity Associated with Carbon Monoxide, *Clinics in Laboratory Medicine* **2006**, *26*, 99-125.

88. Leon D. Prockop, Rossitza I. Chichkova, Carbon monoxide intoxication: An updated review, *Journal of the Neurological Sciences* **2007**, *262*, 122-130.

89. Peter Tilney, Carbon Monoxide Poisoning in a 55-Year-Old Man after a Suicide Attempt, *Air Medical Journal* **2011**,*30*, 112-115.

90. Roberta Foresti, Mohamed G. Bani-Hani, Roberto Motterlini, Use of carbon monoxide as a therapeutic agent: promises and challenges, *Intensive Care Medicine* **2008**, *34*, 649-658.

91. Carlos C. Romão, Walter A. Blättler, João D. Seixas, Gonçalo J. L. Bernardes, Developing drug molecules for therapy with carbon monoxide, *Chemical Society Reviews* **2012**, *41*, 3571-3583.

92. Józef Dulak, Alicja Józkowicz, Carbon monoxide – a "new" gaseous modulator of gene expression, *Acta Biochimica Polonica* **2003**, *50*, 31-47.

93. Roberto Motterlini, Leo E. Otterbein, The therapeutic potential of carbon monoxide, *Nature Reviews Drug Discovery* **2010,** *9(9)*, 728-743.

94. Stefan H. Heinemann, Toshinori Hoshi, Matthias Westerhausen, Alexander Schiller, Carbon monoxide – physiology, detection and controlled release, *Chemical Communications* **2014**, *50*, 3644-3660.

95. Toshitaka Matsui, Mari Iwasaki, Ryota Sugiyama, Masaki Unno, Masao Ikeda-Saito, Dioxygen Activation for the Self-Degradation of Heme: Reaction Mechanism and Regulation of Heme Oxygenase, *Inorganic Chemistry* **2010**, *49*, 3602-3609.

96. Nader G. Abraham, Attallah Kappas, Pharmacological and Clinical Aspects of Heme Oxygenase, *Pharmacological Reviews* **2008**, *60*, 79-127.

97. Stefan W. Ryter, Leo E. Otterbein, Danielle Morse, Augustine M.K. Choi, Heme oxygenase/carbon monoxide signaling pathways: Regulation and functional significance, *Molecular and Cellular Biochemistry* **2002**, *234/235*, 249-263.

98. David J. Schuller, Angela Wilks, Paul R. Ortiz de Montellano, Thomas L. Poulos, Crystal structure of human heme oxygenase-1, *Nature Structural Biology* **2009**, *6(9)*, 860-867.

99. Latesh Lad, David J. Schuller, Hideaki Shimizu, Jonathan Friedman, Huiying Li, Paul R. Ortiz de Montellano, Thomas L. Poulos, Comparison of the Heme-free and -bound Crystal Structures of Human Heme Oxygenase-1, *The Journal of Biological Chemistry* **2003**, *10(7)*, 7834-7843.

100. Christopher M. Bianchetti, Li Yi, Stephen W. Ragsdale, George N. Phillips Jr., Comparison of Apo- and Heme-bound Crystal Structures of a Truncated Human Heme Oxygenase-2, *The Journal of Biological Chemistry* **2007**, *282(52)*, 37624-37631.

101. Stefan W. Ryter, Augustine M. K. Choi, Heme Oxygenase-1/Carbon Monoxide – From Metabolism to Molecular Therapy, *American Journal of Respiratory Cell and Molecular Biology* **2009**, *41*, 251-260.

102. Stefan W. Ryter, Leo E. Otterbein, Carbon monoxide in biology and medicine, *BioEssays* **2004**, *26*, 270-280.

103. Leo E. Otterbein, The Evolution of Carbon Monoxide Into Medicine, *Respiratory Care* **2009**, *54(7)*, 925-932.

104. Csaba Szabo, Medicinal Chemistry and Therapeutic Applications of the Gasotransmitters NO, CO, and H_2S and their Prodrugs *in Burger's Medicinal Chemistry, Drug Discovery and Development* edited by Donald J. Abraham and David P. Rotella, John Wiley and Sons, Inc., 7th edition, **2010**, 265-367.

105. Csaba Szabo, Hydrogen sulphide and its therapeutic potential, *Nature Reviews Drug Discovery* **2007**, *6*, 917-935.

106. Jon M. Fukuto, Samantha J. Carrington, Dean J. Tantillo, Jason G. Harrison, Louis J. Ignarro, Bruce A. Freeman, Andrew Chen, David A. Wink, Small Molecule Signaling Agents: The Integrated Chemistry and Biochemistry of Nitrogen Oxides, Oxides of Carbon, Dioxygen, Hydrogen Sulfide, and Their Derived Species, *Chemical Research in Toxicology* **2012**, *25*, 769-793.

107. Stefan W. Ryter, Augustine M. K. Choi, Carbon monoxide: present and future indications for a medical gas, Korean Journal of Internal Medicine **2013**, *28*, 123-140.

108. Kenneth D. Bloch, Fumito Ichinose, Jesse D. Roberts Jr., Warren M. Zapol, Inhaled NO as a therapeutic agent, *Cardiovascular Research* **2007**, *75*, 339-348.

109. Ulrich Förstermann, William C. Sessa, Nitric oxide synthases: regulation and function, *European Heart Journal* **2012**, *33*, 829-837.

110. Rui Wang, Physiological Implications of Hydrogen Sulfide: a Whiff Exploration that Blossomed, *Physiological Reviews* **2012**, *92*, 791-896.

111. Carlos C. Romão, Helena L.A. Vieira, Metal Carbonyl Prodrugs: CO Delivery and Beyond *in Bioorganometallic Chemistry: Applications in Drug Discovery Biocatalysis, and Imaging* edited by Gérard Jaouen and Michèle Salmain, Wiley-VCH Verlag GmbH & Co. KGaA, 1st edition, **2015**, 165-202.

112. Xiaolei Ma, Nazish Sayed, Annie Beuve, Focco van den Akker, NO and CO differentially activate soluble guanylyl cyclase via a heme pivot-bend mechanism, *The EMBO Journal* **2007**, *26*, 578-588.

113. Mohammed Ibrahim, Emily R. Derbyshire, Alexandra V. Soldatova, Michael A. Marletta, Thomas G. Spiro, Soluble Guanylate Cyclase Is Activated Differently by Excess NO and by YC-1: Resonance Raman Spectroscopic Evidence, *Biochemistry* **2010**, *49*, 4864-4871.

114. Mohammed Ibrahim, Emily R. Derbyshire, Michael A. Marletta, Thomas G. Spiro, Probing Soluble Guanylate Cyclase Activation by CO and YC-1 Using Resonance Raman Spectroscopy, *Biochemistry* **2010**, *49*, 3815-3823.

115. Hong Pyo Kim, StefanW. Ryter, Augustine M.K. Choi, CO as a cellular signaling molecule, *The Annual Review of Pharmacology and Toxicology* **2006**, *46*, 411-449.

116. Stephen P.L. Cary, Michael A. Marletta, The case of CO signaling: why the jury is still out, *The Journal of Clinical Investigation* **2001**, *107(9)*, 1071-1073.

117. Mitsuhiro Fukao, Helen S. Mason, Fiona C. Britton, James L. Kenyon, Burton Horowitz, Kathleen D. Keef, Cyclic GMP-dependent Protein Kinase Activates Cloned BK_{Ca} Channels Expressed in Mammalian Cells by Direct Phosphorylation at Serine 1072, *The Journal of Biological Chemistry* **1999**, *274(16)*, 10927-10935.

118. M. Nara, P. D. K. Dhulipala, G. J. Ji, U. R. Kamasani, Y.-X. Wang, S. Matalon, M. I. Kotlikoff, Guanylyl cyclase stimulatory coupling to KCa channels, *The American Journal of Physiology - Cell Physiology* **2000**, *279*, C1938-C1945.

119. Jessie English, Gray Pearson, Julie Wilsbacher, Jennifer Swantek, Mahesh Karandikar, Shuichan Xu, Melanie H. Cobb, New Insights into the Control of MAP Kinase Pathways, *Experimental Cell Research* **1999**, *253*, 255-270.

120. Melanie H. Cobb, MAP kinase pathways, *Progress in Biophysics & Molecular Biology* **1999**, *71*, 479-500.

121. Lufen Chang, Michael Kari, Mammalian MAP kinase signalling cascades, *Nature* **2001**, *410*, 37-40.

122. Richard J. Orton, Oliver E. Sturm, Vladislav Vyshemirsky, Muffy Calder, David R. Gilbert, Walter Kolch, Computational modelling of the receptor-tyrosine-kinase-activated MAPK pathway, *Biochemical Journal* **2005**, *392*, 249-261.

123. Kunio Kondoh, Eisuke Nishida, Regulation of MAP kinases by MAP kinase phosphatases, *Biochimica et Biophysica Acta* **2007**, *1773*, 1227-1237.

124. James A. McCubrey, Linda S. Steelman, William H. Chappell, Stephen L. Abrams, Ellis W.T. Wong, Fumin Chang, Brian Lehmann, David M. Terrian, Michele Milella, Agostino Tafuri, Franca Stivala, Massimo Libra, Jorg Basecke, Camilla Evangelisti, Alberto M. Martelli, Richard A. Franklin, Roles of the Raf/MEK/ERK pathway in cell growth, malignant transformation and drug resistance, *Biochimica et Biophysica Acta* **2007**, *1773*, 1263-1284.

125. Carl Nathan, Points of control in inflammation, *Nature* **2002**, *420*, 846-852.

126. Kevin J. Tracey, The inflammatory reflex, *Nature* **2002**, *420*, 853-859.

127. Lisa M. Coussens, Zena Werb, Inflammation and cancer, *Nature* **2002**, *420*, 860-867.

128. Peter Libby, Inflammation in atherosclerosis, *Nature* **2002**, *420*, 868-874.

129. Stefan W. Ryter, Danielle Morse, Augustine M. K. Choi, Carbon Monoxide and Bilirubin: Potential Therapies for Pulmonary/Vascular Injury and Disease, *American Journal of Respiratory Cell and Molecular Biology* **2007**, *36*, 175-182.

130. Martin Bilban, Arvand Haschemi, Barbara Wegiel, Beek Y. Chin, Oswald Wagner, Leo E. Otterbein, Heme oxygenase and carbon monoxide initiate homeostatic signaling, *Journal of Molecular Medicine* **2008**, *86*, 267-279.

131. Susan Elmore, Apoptosis: A Review of Programmed Cell Death, *Toxicologic Pathology* **2007**, *35*, 495-516.

132. Atsunori Nakao, Augustine M. K. Choi, Noriko Murase, Protective effect of carbon monoxide in transplantation, *Journal of Cellular and Molecular Medicine* **2006**, *10(3)*, 650-671.

133. Yorihiro Akamatsu, Manabu Haga, Shivraj Tyagi, Kenichiro Yamashita, Aurelio Vicente Graça-Souza, Robert Ollinger, Eva Czismadia, G. Aaron May, Emeka Ifedigbo, Leo E. Otterbein, Fritz H. Bach, Miguel P. Soares, Heme oxygenase-1-derived carbon monoxide protects hearts from transplant associated ischemia reperfusion injury, *FASEB Journal* **2004**, *18*, 771-772.

134. Junichi Kohmoto, Atsunori Nakao, Takashi Kaizu, Allan Tsung, Atsushi Ikeda, Koji Tomiyama, Timothy R. Billiar, Augustine M.K. Choi, Noriko Murase, Kenneth R. McCurry, Low-dose carbon monoxide inhalation prevents ischemia/reperfusion injury of transplanted rat lung grafts, *Surgery* **2006**, *140(2)*, 178-185.

135. Farin Amersi, Xiu-Da Shen, Dean Anselmo, Judy Melinek, Suhasani Iyer, Daniel J. Southard, Masamichi Katori, Hans-Dieter Volk, Ronald W. Busuttil, Roland Buelow, Jerzy W. Kupiec-Weglinski, Ex Vivo Exposure to Carbon Monoxide Prevents Hepatic Ischemia/Reperfusion Injury Through p38 MAP Kinase Pathway, *Hepatology* **2002**, *35(4)*, 815-823.

136. Atsunori Nakao, Kei Kimizuka, Donna B. Stolz, Joao Seda Neto, Takashi Kaizu, Augustine M.K. Choi, Takashi Uchiyama, Brian S. Zuckerbraun, Anthony J. Bauer, Michael A. Nalesnik, Leo E. Otterbein, David A. Geller, Noriko Murase, Protective effect of carbon monoxide inhalation for cold-preserved small intestinal grafts, *Surgery* **2003**, *134(2)*, 285-292.

137. Atsunori Nakao, Joao Seda Neto, Shinichi Kanno, Donna B. Stolz, Kei Kimizukaa, Fang Liu, Fritz H. Bach, Timothy R. Billiar, Augustine MK. Choi, Leo E. Otterbein, Noriko Murase, Protection Against Ischemia/Reperfusion Injury in Cardiac and Renal Transplantation with Carbon Monoxide, Biliverdin and Both, *American Journal of Transplantation* **2005**, *5*, 282-291.

138. Koichiro Sato, Jozsef Balla, Leo Otterbein, R. Neal Smith, Sophie Brouard, Yuan Lin, Eva Csizmadia, Jean Sevigny, Simon C. Robson, Gregory Vercellotti, Augustine M. Choi, Fritz H. Bach, Miguel P. Soares, Carbon Monoxide Generated by Heme Oxygenase-1 Suppresses the Rejection of Mouse-to-Rat Cardiac Transplants, *The Journal of Immunology* **2001**, *166*, 4185-4194.

139. Sophie Brouard, Leo E. Otterbein, Josef Anrather, Edda Tobiasch, Fritz H. Bach, Augustine M.K. Choi, Miguel P. Soares, Carbon Monoxide Generated by Heme Oxygenase 1 Suppresses Endothelial Cell Apoptosis, *The Journal of Experimental Medicine* **2000**, *192(7)*, 1015-1025.

140. Xuchen Zhang, Peiying Shan, Jawed Alam, Xin-Yuan Fu, Patty J. Lee, Carbon Monoxide Differentially Modulates STAT1 and STAT3 and Inhibits Apoptosis via a Phosphatidylinositol 3-Kinase/Akt and p38 Kinase-dependent STAT3 Pathway during Anoxia-Reoxygenation Injury, *The Journal of Biological Chemistry* **2005**, *280(10)*, 8714-8721.

141. Xiao-ming Liu, Gary B. Chapman, Kelly J. Peyton, Andrew I. Schafer, William Durant, Carbon monoxide inhibits apoptosis in vascular smooth muscle cells, *Cardiovascular Research* **2002**, *55*, 396-405.

142. Leo E. Otterbein, Brian S. Zuckerbraun, Manabu Haga, Fang Liu, Ruiping Song, Anny Usheva, Christina Stachulak, Natalya Bodyak, R. Neal Smith, Eva Csizmadia, Shivraj Tyagi, Yorihiro Akamatsu, Richard J. Flavell, Timothy R. Billiar, Edith Tzeng, Fritz H. Bach, Augustine M. K. Choi, Miguel P. Soares, Carbon monoxide suppresses arteriosclerotic lesions associated with chronic graft rejection and with balloon injury, *Nature Medicine* **2003**, *9(2)*, 183-190.

143. Barbara Wegiel, Beek Y. Chin, Leo E. Otterbein, Inhale to survive, cycle or die? – Carbon monoxide and cellular proliferation, *Cell Cycle* **2008**, *7(10)*, 1379-1384.

144. Ruiping Song, Raja S. Mahidhara, Fang Liu, Wen Ning, Leo E. Otterbein, Augustine M. K. Choi, Carbon Monoxide Inhibits Human Airway Smooth Muscle Cell Proliferation via Mitogen-Activated Protein Kinase Pathway, *American Journal of Respiratory Cell and Molecular Biology* **2002**, *27*, 603-610.

145. Ruiping Song, Raja S. Mahidhara, Zhihong Zhou, Rosemary A. Hoffman, Dai-Wu Seol, Richard A. Flavell, Timothy R. Billiar, Leo E. Otterbein, Augustine M. K. Choi, Carbon Monoxide Inhibits T Lymphocyte Proliferation via Caspase-Dependent Pathway, *The Journal of Immunology* **2004**, *172*, 1220-1226.

146. Fabio Zobi, CO and CO-releasing molecules in medicinal chemistry, *Future Medicinal Chemistry* **2013**, *5(2)*, 175-188.

147. Takeshi Shinohara, Takeshi Kaneko, Yoji Nagashima, Atsuhisa Ueda, Akihiro Tagawa, Yoshiaki Ishigatsubo, Adenovirus-Mediated Transfer and Overexpression of Heme Oxygenase 1 cDNA in Lungs Attenuates Elastase-Induced Pulmonary Emphysema in Mice, *Human Gene Therapy* **2005**, *16*, 318-327.

148. Jean-Marc Hyvelin, Blandine Maurel, Rustem Uzbekov, Roberto Motterlini, Patrick Lermusiaux, Hemin prevents in-stent stenosis in rat and rabbit models by inducing heme-oxygenase-1, *Journal of Vascular Surgery* **2010**, *51(2)*, 417-428.

149. Ulrich Schatzschneider, Novel lead structures and activation mechanisms for CO-releasing molecules (CORMs), *British Journal of Pharmacology*, **2015**, *172*, 1638-1650.

150. Gabriele Sass, Stefan Seyfried, Miguel Parreira Soares, Kenichiro Yamashita, Elzbieta Kaczmarek, Winfried L. Neuhuber, Gisa Tiegs, Cooperative Effect of Biliverdin and Carbon Monoxide on Survival of Mice in Immune-Mediated Liver Injury, *Hepatology* **2004**, *40(5)*, 1128-1135.

151. Christine Chauveau, Delphine Bouchet, Jean-Christian Roussel, Patrick Mathieu, Cécile Braudeau, Karine Renaudin, Laurent Tesson, Jean-Paul Soulillou, Suhasini Iyer, Roland Buelow, Ignacio Anegon, Gene Transfer of Heme Oxygenase-1 and Carbon Monoxide Delivery Inhibit Chronic Rejection, *American Journal of Transplantation* **2002**, *2*, 581-592.

152. Roberto A. Motterlini, Brian E. Mann, Preparation of Metal Complexes for Therapeutic Delivery of Carbon Monoxide, WO 2002/092075, 20020515, **2002**.

153. Werner Haas, Carlos Romão, Beatriz Royo, Ana Cristina Fernandes, Isabel Gonçalves, Method for Treating a Mammal by Administration of a Compound having the Ability to Release CO, Compounds having the Ability to Release CO and Pharmaceutical Compositions Thereof, WO 2003/066067, 20030203, **2003**.

154. Roberto Motterlini, James E. Clark, Roberta Foresti, Padmini Sarathchandra, Brian E. Mann, Colin J. Green, Carbon Monoxide-Releasing Molecules: Characterization of Biochemical and Vascular Activities, *Circulation Research* **2002**, *90*, e17-e24.

155. Roberto Motterlini, Brian E. Mann, Roberta Foresti, Therapeutic applications of carbon monoxide-releasing molecules, *Expert Opinion on Investigational Drugs* **2005**, *14(11)*,1305-1318.

156. Brian E. Mann, Carbon Monoxide: An Essential Signalling Molecule, *Topics in Organometallic Chemistry* **2010**, *32*, 247-285.

157. Teresa Santos-Silva, Abhik Mukhopadhyay, João D. Seixas, Gonçalo J.L. Bernardes, Carlos C. Romão, Maria J. Romão, Towards Improved Therapeutic CORMs: Understanding the Reactivity of CORM-3 with Proteins, *Current Medicinal Chemistry* **2011**, *18*, 3361-3366.

158. Lovely Angel Panamparambil Antony, Tomáš Slanina, Peter Šebej, Tomáš Šolomek, Petr Klán, Fluorescein Analogue Xanthene-9- Carboxylic Acid: A Transition-Metal-Free CO Releasing Molecule Activated by Green Light, *Organic Letters* **2013**, *15(17)*, 4552-4555.

159. Ping Peng, Chaoming Wang, Zheng Shi, Valentine K. Johns, Liyuan Ma, Jeremiah Oyer, Alicja Copik, Robert Igarashi Yi Liao, Visible-light activatable organic CO-releasing molecules (PhotoCORMs) that simultaneously generate fluorophores, *Organic & Biomolecular Chemistry* **2013**, *11*, 6671-6674.

160. Tony R. Johnson, Brian E. Mann, James E. Clark, Roberta Foresti, Colin J. Green, Roberto Motterlini, Metal Carbonyls: A New Class of Pharmaceuticals?, *Angewandte Chemie International Edition* **2003**, *42*, 3722-3729.

161. Roger Alberto, Roberto Motterlini, Chemistry and biological activities of CO-releasing molecules (CORMs) and transition metal complexes, *Dalton Transactions* **2007**, 1651-1660.

162. Margarita A. Gonzalez, Nicole L. Fry, Richard Burt, Riddhi Davda, Adrian Hobbs, Pradip K. Mascharak, Designed Iron Carbonyls as Carbon Monoxide (CO) Releasing Molecules: Rapid CO Release and Delivery to Myoglobin in Aqueous Buffer, and Vasorelaxation of Mouse Aorta, *Inorganic Chemistry* **2011**, *50*, 3127-3134.

163. Fabio Zobi, Alois Degonda, Marcus C. Schaub, Anna Yu. Bogdanova, CO Releasing Properties and Cytoprotective Effect of cis-trans- $[Re^{II}(CO)_2Br_2L_2]^n$ Complexes, *Inorganic Chemistry* **2010**, *49*, 7313-7322.

164. Steffen Romanski, Birgit Kraus, Ulrich Schatzschneider, Jörg-Martin Neudörfl, Sabine Amslinger, Hans-Günther Schmalz, Acyloxybutadiene Iron Tricarbonyl Complexes as Enzyme-Triggered CO-Releasing Molecules (ET-CORMs), *Angewandte Chemie International Edition* **2011**, *50*, 2392-2396.

165. Steffen Romanski, Hannelore Rücker, Eleni Stamellou, Miguel Guttentag, Jörg-Martin Neudörfl, Roger Alberto, Sabine Amslinger, Benito Yard, Hans-Günther Schmalz, Iron Dienylphosphate Tricarbonyl Complexes as Water-Soluble Enzyme-Triggered CO-Releasing Molecules (ET-CORMs), *Organometallics* **2012**, *31*, 5800-5809.

166. Brian C. Wilson, Michael S. Patterson, The physics, biophysics and technology of photodynamic therapy, *Physics in Medicine and Biology* **2008**, *53*, R61–R109.

167. Margarita A. Gonzales, Pradip K. Mascharak, Photoactive metal carbonyl complexes as potential agents for targeted CO delivery, *Journal of Inorganic Biochemistry* **2014**, *133*, 127-135.

168. Indranil Chakraborty, Samantha J. Carrington, Pradip K. Mascharak, Design Strategies To Improve the Sensitivity of Photoactive Metal Carbonyl Complexes (photoCORMs) to Visible Light and Their Potential as CO-Donors to Biological Targets, *Accounts of Chemical Research* **2014**, *47(8)*, 2603-2611.

169. Samantha McLean, Brian E. Mannb, Robert K. Poole, Sulfite species enhance carbon monoxide release from CO-releasing molecules: Implications for the deoxymyoglobin assay of activity, *Analytical Biochemistry* **2012**, *427*, 36-40.

170. Brian W. Michel, Alexander R. Lippert, Christopher J. Chang, A Reaction-Based Fluorescent Probe for Selective Imaging of Carbon Monoxide in Living Cells Using a Palladium-Mediated Carbonylation, *The Journal of the American Chemical Society* **2012**, *134(38)*, 15668-15671.

171. Roberto Motterlini, Carbon monoxide-releasing molecules (CO-RMs): vasodilatory, anti-ischaemic and anti-inflammatory activities, *Biochemical Society Transactions* **2007**, *35(5)*, 1142-1146.

172. Philip Sawle, Roberta Foresti, Brian E. Mann, Tony R. Johnson, Colin J. Green, Roberto Motterlini, Carbon monoxide-releasing molecules (CO-RMs) attenuate the inflammatory response elicited by lipopolysaccharide in RAW264.7 murine macrophages, *British Journal of Pharmacology* **2005**, *145*, 800-810.

173. Yunwei Wei, Ping Chen, Marco de Bruyn, Weihui Zhang, Edwin Bremer, Wijnand Helfrich, Carbon monoxide-Releasing Molecule-2 (CORM-2) attenuates acute hepatic ischemia reperfusion injury in rats, *Gastroenterology* **2010**, *10*, 42.

174. James E. Clark, Patrick Naughton, Sandra Shurey, Colin J. Green, Tony R. Johnson, Brian E. Mann, Roberta Foresti and Roberto Motterlini, Cardioprotective Actions by a Water-Soluble Carbon Monoxide–Releasing Molecule, *Circulation Research* **2003**, *93*, e2-e8.

175. Ashraf Sandouka, Barry J. Fuller, Brian E. Mann, Colin J. Green, Roberta Foresti, Roberto Motterlini, Treatment with CO-RMs during cold storage improves renal function at reperfusion, *Kidney International* **2006**, *69*, 239-247.

176. Roberto Motterlini, Philip Sawle, Jehad Hammad, Sandip Bains, Roger Alberto, Roberta Foresti, Colin J. Green, CORM-A1: a new pharmacologically active carbon monoxide-releasing molecule, *The FASEB Journal* **2005**, *19(2)*, 284-286.

177. Ana R. Marques, Kukas Kromer, David J. Gallo, Nuno Penacho, Sandra S. Rodrigues, João D. Seixas, Gonçalo J. L. Bernardes, Patrícia M. Reis, Sherrie L. Otterbein, Rachel A. Ruggieri, Ana S. G. Gonçalves, Ana M. L. Gonçalves, Marta N. de Matos, Isabel Bento, Leo E. Otterbein, Walter A. Blattler, Carlos C. Romão, Generation of Carbon Monoxide Releasing Molecules (CO-RMs) as Drug Candidates for the Treatment of Acute Liver Injury: Targeting of CO-RMs to the Liver, *Organometallics* **2012**, *31*, 5810-5822.

178. Biswajit Mukherjee, Balaram Patra, Sushmita Mahapatra, Pratik Banerjee, Amit Tiwari, Malay Chatterjee, Vanadium – an element of atypical biological significance, *Toxicology Letters* **2004**, *150*, 135-143.

179. Dieter Rehder, Introduction and Background *in Bioinorganic Vanadium Chemistry*, John Wiley & Sons, Ltd, 1st edition, **2008**, 1-11.

180. Debbie C. Crans, Pabitra B. Chatterjee, Vanadium Biochemistry *in Comprehensive Inorganic Chemistry II* edited by Jan Reedijk and Kenneth Poeppelmeier, Elsevier, 2nd edition, **2013**, 323-342.

181. Dieter Rehder, A possible role for extraterrestrial vanadium in the encounter of life, *Coordination Chemistry Reviews* **2011**, *255*, 2227-2231.

182. Lyman R. Caswell, Andrés del Rio, Alexander von Humboldt, and the twice-discovered element, *Bulletin for the History of Chemistry* **2003**, *28(1)*, 35-41.

183. Pedro Cintas, The Road to Chemical Names and Eponyms: Discovery, Priority, and Credit, *Angewandte Chemie International Edition* **2004**, *43*, 5888-5894.

184. Dieter Rehder, The future of/for vanadium, *Dalton Transactions* **2013**, *42*, 11749-11761.

185. João Costa Pessoa, Thirty years through vanadium chemistry, *Journal of Inorganic Biochemistry* **2015**, *147*, 4-24.

186. R.R. Moskalyk, Akram M. Alfantazi, Processing of vanadium: a review, *Minerals Engineering* **2003**, *16*, 793-805.

187. Mannar R. Maurya, Amit Kumar, J. Costa Pessoa, Vanadium complexes immobilized on solid supports and their use as catalysts for oxidation and functionalization of alkanes and alkenes, *Coordination Chemistry Reviews* **2011**, *255*, 2315-2344.

188. Israel E. Wachs, Catalysis science of supported vanadium oxide catalysts, *Dalton Transactions* **2013**, *42*, 11762-11769.

189. Liyu Li, Soowhan Kim, Wei Wang, M. Vijayakumar, Zimin Nie, Baowei Chen, Jianlu Zhang, Guanguang Xia, Jianzhi Hu, Gordon Graff, Jun Liu, Zhenguo Yang, A Stable Vanadium Redox-Flow Battery with High Energy Density for Large-Scale Energy Storage, *Advanced Energy Materials* **2011**, *1*, 394-400.

190. Katherine H. Thompson, Chris Orvig, Vanadium in diabetes: 100 years from Phase 0 to Phase I, *Journal of Inorganic Biochemistry* **2006**, *100*, 1925-1935.

191. Dieter Rehder, Inorganic and Coordination Compounds of Vanadium *in Bioinorganic Vanadium Chemistry*, John Wiley & Sons, Ltd, 1st edition, **2008**, 13-51.

192. Debbie C. Crans, Alan S. Tracey, The Chemistry of Vanadium in Aqueous and Nonaqueous Solution *in Vanadium Compounds – Chemistry, Biochemistry, and Therapeutic Applications* edited by Alan S. Tracey and Debbie C. Crans, American Chemical Society, 1st edition, **1998**, 2-29.

193. Kan Kanamori, Kiyoshi Tsuge, Inorganic Chemistry of Vanadium *in Vanadium: Biochemical and Molecular Biological Approaches* edited by Hitoshi Michibata, Springer, 1st edition, **2012**, 3-31.

194. Manuel Aureliano, Recent perspectives into biochemistry of decavanadate, *World Journal of Biological Chemistry* **2011**, *2(10)*, 215-225.

195. Manuel Aureliano, C. André Ohlin, Decavanadate in vitro and in vivo effects: facts and opinions, *Journal of Inorganic Biochemistry* **2014**, *137*, 123-130.

196. Eugenio Garribba, Daniele Sanna, Vanadium *in Binding, Transport and Storage of Metal Ions in Biological Cells* edited by Wolfgang Maret and Anthony Wedd, The Royal Society of Chemistry, 1st edition, **2014**, 153-187.

197. Forrest H. Nielsen, The Nutritional Essentiality and Physiological Metabolism of Vanadium in Higher Animals *in Vanadium Compounds – Chemistry, Biochemistry, and Therapeutic Applications* edited by Alan S. Tracey and Debbie C. Crans, American Chemical Society, 1st edition, **1998**, 297-307.

198. João Costa Pessoa, Susana Etcheverry, Dinorah Gambino, Vanadium compounds in medicine, *Coordination Chemistry Reviews* **2015**, *301–302*, 24-48.

199. Mitchell D. Cohen, Toxicity of Vanadium Compounds: Pulmonary and Immune System Targets *in Vanadium: The Versatile Metal* edited by Kenneth Kustin, João Costa Pessoa and Debbie C. Crans, ACS Symposium Series 974, American Chemical Society, 1st edition, **2007**, 217-239.

200. Veronika A. Ehrlich, Armen K. Nersesyan, Christine Hoelzl, Franziska Ferk, Julia Bichler, Eva Valic, Andreas Schaffer, Rolf Schulte-Hermann, Michael Fenech, Karl-Heinz Wagner, Siegfried Knasmüller, Inhalative Exposure to Vanadium Pentoxide Causes DNA Damage in Workers: Results of a Multiple End Point Study, *Environmental Health Perspectives* **2008**, *116(12)*, 1689-1693.

201. Farida Louise Assem, Leonard Stephen Levy, Inhalation Toxicity of Vanadium *in Vanadium: Biochemical and Molecular Biological Approaches* edited by Hitoshi Michibata, Springer, 1st edition, **2012**, 209-224.

202. Susana B. Etcheverry, Ana L. Di Virgilio, Daniel A. Barrio, Vanadium Effects on Bone Metabolism *in Vanadium: Biochemical and Molecular Biological Approaches* edited by Hitoshi Michibata, Springer, 1st edition, **2012**, 145-162.

203. Debbie C. Crans, Jason J. Smee, Ernestas Gaidamauskas, Luqin Yang, The Chemistry and Biochemistry of Vanadium and the Biological Activities Exerted by Vanadium Compounds, *Chemical Reviews* **2004**, *104*, 849-902.

204. Dieter Rehder, The potentiality of vanadium in medicinal applications, *Future Medicinal Chemistry* **2012**, *4(14)*, 1823-1837.

205. Dieter Rehder, Biological Activities of V and Cr *in Comprehensive Inorganic Chemistry II* edited by Jan Reedijk and Kenneth Poeppelmeier, Elsevier, 2nd edition, **2013**, 819-834.

206. Dieter Rehder, Vanadium. Its Role for Humans *in Interrelations between Essential Metal Ions and Human Diseases* edited by Astrid Sigel, Helmut Sigel, and Roland K.O. Sigel, Springer, 1st edition, **2013**, 139-169.

207. Dieter Rehder, The role of vanadium in biology, *Metallomics* **2015**, *7*, 730-742.

208. Dieter Rehder, Naturally Occurring Vanadium Compounds *in Bioinorganic Vanadium Chemistry*, John Wiley & Sons, Ltd, 1st edition, **2008**, 87-155.

209. Dieter Rehder, Influence of Vanadium Compounds on Cellular Functions *in Bioinorganic Vanadium Chemistry*, John Wiley & Sons, Ltd, 1st edition, **2008**, 157-201.

210. João Costa Pessoa, Eugenio Garribba, Marino F.A. Santos, Teresa Santos-Silva, Vanadium and proteins: Uptake, transport, structure, activity and function, *Coordination Chemistry Reviews* **2015**, *301–302*, 49-86.

211. Sabine R. Akabayov, Barak Akabayov, Vanadate in structural biology, *Inorganica Chimica Acta* **2014**, *420*, 16-23.

212. Daniele Fattorini, Francesco Regoli, Hyper-Accumulation of Vanadium in Polychaetes *in Vanadium: Biochemical and Molecular Biological Approaches* edited by Hitoshi Michibata, Springer, 1st edition, **2012**, 73-92.

213. José A.L. da Silva, João J.R. Fraústo da Silva, Armando J.L. Pombeiro, Amavadine, a Vanadium Compound in Amanita Fungi *in Vanadium: Biochemical and Molecular Biological Approaches* edited by Hitoshi Michibata, Springer, 1st edition, **2012**, 35-49.

214. Hitoshi Michibata, Tatsuya Ueki, High Levels of Vanadium in Ascidians *in Vanadium: Biochemical and Molecular Biological Approaches* edited by Hitoshi Michibata, Springer, 1st edition, **2012**, 51-71.

215. Tatsuya Ueki, Hitoshi Michibata, Molecular mechanism of the transport and reduction pathway of vanadium in ascidians, *Coordination Chemistry Reviews* **2011**, *255*, 2249-2257.

216. Hiroki Kitayama, Sohei Yamamoto, Hitoshi Michibata, Tatsuya Ueki, Metal ion selectivity of the vanadium(V)-reductase Vanabin2, *Dalton Transactions* **2013**, *42*, 11921-11925.

217. Toshiyuki Hamada, Miwako Asanuma, Tatsuya Ueki, Fumiaki Hayashi, Naohiro Kobayashi, Shigeyuki Yokoyama, Hitoshi Michibata, Hiroshi Hirota, Solution Structure of Vanabin2, a Vanadium(IV)-Binding Protein from the Vanadium-Rich Ascidian Ascidia sydneiensis samea, *The Journal of American Chemical Society* **2005**, *127*, 4216-4222.

218. Albrecht Messerschmidt, Ron Wever, X-ray structure of a vanadium-containing enzyme: Chloroperoxidase from the fungus Curvularia inaequalis, *Proceedings of the National Academy of Sciences* **1996**, *93*, 392-396.

219. Albrecht Messerschmidt, Lars Prade, Ron Wever, Implications for the Catalytic Mechanism of the Vanadium-Containing Enzyme Chloroperoxidase from the Fungus Curvularia inaequalis by X-Ray Structures of the Native and Peroxide Form, *Biological Chemistry* **1997**, *378*, 309-315.

220. Tiago A. S. Brandão, Alvan C. Hengge, Sean J. Johnson, Insights into the Reaction of Protein-tyrosine Phosphatase 1B: Crystal Structures for Transition State Analogs of both Catalytic Steps, *The Journal of Biological Chemistry* **2010**, *285(21)*, 15874-15883.

221. Douglas R. Davies, Adeel Mushtaq, Heidrun Interthal, James J. Champoux, Wim G. J. Hol, The Structure of the Transition State of the Heterodimeric Topoisomerase I of Leishmania donovani as a Vanadate Complex with Nicked DNA, *Journal of Molecular Biology* **2006**, *357*, 1202-1210.

222. Jane E. Ladner, Brian D. Wladkowski, L. Anders Svensson, Lennart Sjolin, Gary L. Gilliland, X-ray Structure of a Ribonuclease A-Uridine Vanadate Complex at 1.3Å Resolution, *Acta Crystallographica* **1997**, *D53*, 290-301.

223. Tamás Jakusch, João Costa Pessoa, Tamás Kiss, The speciation of vanadium in human serum, *Coordination Chemistry Reviews* **2011**, *255*, 2218-2226.

224. Daniele Sanna, Maria Serra, Giovanni Micera, Eugenio Garribba, Interaction of Antidiabetic Vanadium Compounds with Hemoglobin and Red Blood Cells and Their Distribution between Plasma and Erythrocytes, *Inorganic Chemistry* **2014**, *53*, 1449-1464.

225. Tony Scully, Diabetes in Numbers, *Nature* **2012**, *485*, S2-S3.

226. Jacek Zajac, Anil Shrestha, Parini Patel, Leonid Poretsky, The Main Events in the History of Diabetes Mellitus *in Principles of Diabetes Mellitus* edited by Leonid Poretsky, Springer, 2nd edition, **2010**, 3-16.

227. Ketan Laud, Uri Shabto, Diabetic Retinopathy *in Principles of Diabetes Mellitus* edited by Leonid Poretsky, Springer, 2nd edition, **2010**, 331-346.

228. Jennifer K. Svahn, Jeffrey S. Kirk, Omar H. Llaguna, Nancy Habib, Peripheral Vascular Disease in Diabetes *in Principles of Diabetes Mellitus* edited by Leonid Poretsky, Springer, 2nd edition, **2010**, 371-379.

229. Dennis Shavelson, John S. Steinberg, Bradley W. Bakotic, The Diabetic Foot *in Principles of Diabetes Mellitus* edited by Leonid Poretsky, Springer, 2nd edition, **2010**, 381-399.

230. Omar Ali, Type 1 Diabetes Mellitus: Epidemiology, Genetics, Pathogenesis, and Clinical Manifestations *in Principles of Diabetes Mellitus* edited by Leonid Poretsky, Springer, 2nd edition, **2010**, 181-201.

231. Vivian Fonseca, Jennifer John-Kalarickal, Type 2 Diabetes Mellitus: Epidemiology, Genetics, Pathogenesis, and Clinical Manifestations *in Principles of Diabetes Mellitus* edited by Leonid Poretsky, Springer, 2nd edition, **2010**, 381-399.

232. Theodore P. Ciaraldi, Cellular Mechanisms of Insulin Action *in Principles of Diabetes Mellitus* edited by Leonid Poretsky, Springer, 2nd edition, **2010**, 75-87.

233. Giovanna Scapin, Structural Chemistry and Molecular Modeling in the Design of DPP4 Inhibitors *in Multifaceted Roles of Crystallography in Modern Drug Discovery* edited by Giovanna Scapin, Disha Patel and Eddy Arnold, Springer, 1st edition, **2015**, 53-67.

234. Clayton E. Heyliger, Arun G. Tahiliani, John H. Mcneill, Effect of Vanadate on Elevated Blood Glucose and Depressed Cardiac Performance of Diabetic Rats, *Science* **1984**, *227*, 1474-1477.

235. Joseph Meyerovitch, Zvi Farfelsn, Joseph Sack, Yoram Shechter, Oral Administration of Vanadate Normalizes Blood Glucose Levels in Streptozotocin-treated Rats – Characterization and mode of action, *The Journal of Biological Chemistry* **1987**, *262(14)*, 6658-6662.

236. John H. McNeill, Violet G. Yuen, Soter Dai and Chris Orvig, Increased potency of vanadium using organic ligands, *Molecular and Cellular Biochemistry* **1995**, *153*, 175-180.

237. Katherine H. Thompson, Barry D. Liboiron, Yan Sun, Karycia D.D. Bellman, Ika A. Setyawati, Brian O. Patrick, Veranja Karunaratne, Gulnar Rawji, Jeffrey Wheeler, Kymberley Sutton, Sanjay Bhanot, Carrie Cassidy, John H. McNeill, Violet G. Yuen, Chris Orvig, Preparation and characterization of vanadyl complexes with bidentate maltol-type ligands; in vivo comparisons of anti-diabetic therapeutic potential, *Journal of Biological Inorganic Chemistry* **2003**, *8*, 66-74.

238. Katherine H. Thompson, Jay Lichter, Carl LeBel, Michael C. Scaife, John H. McNeill, Chris Orvig, Vanadium treatment of type 2 diabetes: A view to the future, *Journal of Inorganic Biochemistry* **2009**, *103*, 554-558.

239. Subhadeep Das, Mary Chatterjee, Muthumani Janarthan, Hari Ramachandran, Malay Chatterjee, Vanadium in Cancer Prevention *in Vanadium: Biochemical and Molecular Biological Approaches* edited by Hitoshi Michibata, Springer, 1st edition, **2012**, 163-185.

240. Osmond J. D'Cruz, Fatih M. Uckun, Metvan: a novel oxovanadium(IV) complex with broad spectrum anticancer activity, *Expert Opinion on Investigational Drugs* **2002**, *11(12)*, 1829-1836.

241. Iduna Fichtner, James Claffey, Anthony Deally, Brendan Gleeson, Megan Hogan, Maria Rivera Markelova, Helge Müller-Bunz, Holger Weber, Matthias Tacke, Antitumor activity of vanadocene Y and its selenocyanate derivative in xenografted caki-1 tumors in mice, *Journal of Organometallic Chemistry* **2010**, *695*, 1175-1181.

242. Luciana G. Naso, Evelina G. Ferrer, Nataliya Butenko, Isabel Cavaco, Luis Lezama, Teófilo Rojo, Susana B. Etcheverry, Patricia A. M. Williams, Antioxidant, DNA cleavage, and cellular effects of silibinin and a new oxovanadium(IV)/silibinin complex, *Journal of Biological Inorganic Chemistry* **2011**, *16*, 653-668.

243. Dinorah Gambino, Potentiality of vanadium compounds as anti-parasitic agents, *Coordination Chemistry Reviews* **2011**, *255*, 2193-2203.

244. http://www.rcsb.org/pdb/static.do?p=general_information/pdb_statistics/index.html (31st July 2016)

245. Michelle Montoya, Alberto Moscatelli, Andrea Taroni, Crystallography, *Nature Milestones* **2014**, 4-21, DOI:10.1038/nature13348

246. Maria João Romão, Teresa Santos-Silva, Isabel Bento, Filipe Freire, Marino F. A. Santos, Ana Luísa Carvalho, Marcos Históricos em Cristalografia, *Química - Boletim da Sociedade Portuguesa de Química* **2015**, *136*, 21-30.

247. Mariusz Jaskolski, Zbigniew Dauter, Alexander Wlodawer, A brief history of macromolecular crystallography, illustrated by a family tree and its Nobel fruits, *FEBS Journal* **2014**, *281*, 3985-4009.

248. Yigong Shi, A Glimpse of Structural Biology through X-Ray Crystallography, *Cell* **2014**, *159*, 995-1014.

249. Celebrating structural biology, *Nature Structural & Molecular Biology* **2011**, *18(12)*, 1304-1316, DOI:10.1038/nsmb1211-1304

250. Helen M. Berman, Peter W. Rose, Shuchismita Dutta, Christine Zardecki, Andreas Prlic, The Protein Data Bank: Overview and Tools for Drug Discovery *in Multifaceted Roles of Crystallography in Modern Drug Discovery* edited by Giovanna Scapin, Disha Patel and Eddy Arnold, Springer, 1st edition, **2015**, 93-106.

251. Bernhard Rupp, *Biomolecular Crystallography – Principles, Practice and Application to Structural Biology*, Garland Science Taylor & Francis Group, 1st edition, **2010**.

252 Gale Rhodes, *Crystallography Made Crystal Clear - A Guide for Users of Macromolecular Models*, Academic Press, 3rd edition, **2006**.

253. Ana Luísa Carvalho, José Trincão, Maria João Romão, X-Ray Crystallography in Drug Discovery *in Ligand-Macromolecular Interactions in Drug Discovery – Methods and Protocols* edited by Ana Cecília A. Roque, Humana Press, 1st edition, **2010**, 31-56.

254. Alexander Wlodawer, Wladek Minor, Zbigniew Dauter, Mariusz Jaskolski, Protein crystallography for non-crystallographers, or how to get the best (but not more) from published macromolecular structures, *FEBS Journal* **2008**, *275(1)*, 1-21.

255. Alexander Wlodawer, Wladek Minor, Zbigniew Dauter, Mariusz Jaskolski, Protein crystallography for aspiring crystallographers or how to avoid pitfalls and traps in macromolecular structure determination, *FEBS Journal* **2013**, *280*, 5705-5736.

256. Andrea Ilari, Carmelinda Savino, Protein Structure Determination by X-Ray Crystallography *in Bioinformatics: Data, Sequence Analysis and Evolution* edited by Jonathan M. Keith, Humana Press, 1st edition, **2008**, 63-87.

257. Audrey L. Lamb, T. Joseph Kappock, Nicholas R. Silvaggi, You are lost without a map: Navigating the sea of protein structures, *Biochimica et Biophysica Acta* **2015**, *1854*, 258-268.

258. Zbigniew Dauter, Mariusz Jaskolski, How to read (and understand) Volume A of International Tables for Crystallography: an introduction for nonspecialists, *Journal of Applied Crystallography* **2010**, *43*, 1150-1171.

259. Patricia C. Weber, Overview of Protein Crystallization Methods, *Methods in Enzymology* **1997**, *276*, 13-22.

260. Joseph R. Luft, George T. Detitra, Kinetic Aspects of Macromolecular Crystallization, *Methods in Enzymology* **1997**, *276*, 110-131.

261. Naomi E. Chayen, Emmanuel Saridakis, Protein crystallization: from purified protein to diffraction-quality crystal, *Nature Methods* **2008**, *5(2)*, 147-153.

262. Mei Li, Wen-rui Chang, Protein crystallization, *Photosynthesis Research* **2009**, *102(2-3)*, 223-229.

263. Alexander McPherson, Jose A. Gavira, Introduction to protein crystallization, *Acta Crystallographica* **2014**, *F70*, 2-20.

264. Marc L. Pusey, Zhi-Jie Liu, Wolfram Tempel, Jeremy Praissman, Dawei Lin, Bi-Cheng Wang, José A. Gavira, Joseph D. Ng, Life in the fast lane for protein crystallization and X-ray crystallography, *Progress in Biophysics and Molecular Biology* **2005**, *88*, 359-386.

265. Magdalena A. Bukowska, Markus G. Grutter, New concepts and aids to facilitate crystallization, *Current Opinion in Structural Biology* **2013**, *23*, 409-416.

266. Catarina Coelho, José Trincão, Maria João Romão, The use of ionic liquids as crystallization additives allowed to overcome nanodrop scaling up problems:A success case for producing diffraction-quality crystals of a nitrate reductase, *Journal of Crystal Growth* **2010**, *312*, 714-719.

267. Antonella Balerna, Settimio Mobilio, Introduction to Synchrotron Radiation *in Synchrotron Radiation – Basics, Methods and Applications* edited by Settimio Mobilio, Federico Boscherini and Carlo Meneghini, Springer, 1st edition, **2015**, 3-28.

268. Elspeth Garman, Macromolecular Cryo-crystallography *in Evolving Methods for Macromolecular Crystallography* edited by Randy J. Read and Joel L. Sussman, Springer, 1st edition, **2007**, 25-40.

269. Garry Taylor, The phase problem, *Acta Crystallographica* **2003**, *D59*, 1881-1890.

270. Garry L. Taylor, Introduction to phasing, *Acta Crystallographica* **2010**, *D66*, 325-338.

271. Philip R. Evans, An introduction to stereochemical restraints, *Acta Crystallographica* **2007**, *D63*, 58-61.

272. Roman A. Laskowski, Malcolm W. Macarthur, David S. Moss, Janet M. Thornton, PROCHECK: a program to check the stereochemical quality of protein structures, *Journal of Applied Crystallography* **1993**, *26*, 283-291.

273. Ian W. Davis, Laura Weston Murray, Jane S. Richardson, David C. Richardson, MOLPROBITY: structure validation and all-atom contact analysis for nucleic acids and their complexes, *Nucleic Acids Research* **2004**, *32*, W615-W619.

274. Teresa Santos-Silva, AbhiknMukhopadhyay, João D. Seixas, Gonçalo J. L. Bernardes, Carlos C. Romão, Maria J. Romão, CORM-3 Reactivity toward Proteins: The Crystal Structure of a Ru(II) Dicarbonyl-Lysozyme Complex, *Journal of the American Chemical Society* **2011**, *133*, 1192-1195.

275. João D. Seixas, Abhik Mukhopadhyay, Teresa Santos-Silva, Leo E. Otterbein, David J. Gallo, Sandra S. Rodrigues, Bruno H. Guerreiro, Ana M. L. Gonçalves, Nuno Penacho, Ana R. Marques, Ana C. Coelho, Patrícia M. Reis, Maria J. Romão, Carlos C. Romão, Characterization of a versatile organometallic pro-drug (CORM) for experimental CO based therapeutics, *Dalton Transactions* **2013**, *42*, 5985-5998.

276. M. J. Cleare, W. P. Griffith,Halogeno-carbonyl and -nitrosyl Complexes of the Platinum Metals, and their Vibrational Spectra, *Journal of the Chemical Society A* **1969**, 372-380.

277. Iain W. McNae, Katy Fishburne, Abraha Habtemariam, Tina M. Hunter, Michael Melchart, Fuyi Wang, Malcolm D. Walkinshaw, Peter J. Sadler, Half-sandwich arene ruthenium(II)–enzyme complex, *Chemical Communications* **2004**, 1786-1787.

278. Mathieu Razavet, Vincent Artero, Christine Cavazza, Yohan Oudart, Colette Lebrun, Juan Carlos Fontecilla-Camps, Marc Fontecave, Tricarbonylmanganese(I)–lysozyme complex: a structurally characterized organometallic protein, *Chemical Communications* **2007**, 2805-2807.

279. Angela Casini, Guido Mastrobuoni, Claudia Temperini, Chiara Gabbiani, Simona Francese, Gloriano Moneti, Claudiu T. Supuran, Andrea Scozzafava, Luigi Messori, ESI mass spectrometry and X-ray diffraction studies of adducts between anticancer platinum drugs and hen egg white lysozyme, *Chemical Communications* **2007**, 156-158.

280. Sarah L. Binkley, Christopher J. Ziegler, Richard S. Herrick, Roger S. Rowlett, Specific derivatization of lysozyme in aqueous solution with $Re(CO)_3(H_2O)_3^+$, *Chemical Communications* **2007**, *46*, 1203-1205.

281. A. G. W. Leslie, Harold R. Powell, Processing Diffraction Data with Mosflm *in Evolving Methods for Macromolecular Crystallography* edited by Randy J. Read and Joel L. Sussman, Springer, 1st edition, **2007**, 41-51.

282. Wolfgang Kabsch, XDS, *Acta Crystallographica* **2010**, *D66*, 125-132.

283. Philip R. Evans, An introduction to data reduction: space-group determination, scaling and intensity statistics, *Acta Crystallographica* **2011**, *D67*, 282-292.

284. Marie-Christine Vaney, Sébastien Maignan, Madeleine Ries-Kautt, Arnaud Ducruix, High-Resolution Structure (1.33Å) of a HEW Lysozyme Tetragonal Crystal Grown in the APCF Apparatus. Data and Structural Comparison with a Crystal Grown under Microgravity from SpaceHab-01 Mission, *Acta Crystallographica* **1996**, *D52*, 505-517.

285. Airlie J. McCoy, Ralf W. Grosse-Kunstleve, Paul D. Adams, Martyn D. Winn, Laurent C. Storonia, Randy J. Read, Phaser crystallographic software, *Journal of Applied Crystallography* **2007**, *40*, 658-674.

286. Garib N. Murshudov, Alexei A. Vagin, Eleanor J. Dodson, Refinement of Macromolecular Structures by the Maximum-Likelihood Method, *Acta Crystallographica* **1997**, *D53*, 240-225.

287. Paul Emsley, Kevin Cowtan, Coot: model-building tools for molecular graphics, *Acta Crystallographica* **2004**, *D60*, 2126-2132.

288. Robbie P. Joosten, Krista Joosten, Garib N. Murshudov, Anastassis Perrakis, PDB_REDO: constructive validation, more than just looking for errors, *Acta Crystallographica* **2012**, *D68*, 484-496.

289. Renzo Cini, Sandra Defazio, Gabriella Tamasi, Mario Casolaro, Luigi Messori, Angela Casini, Margherita Morpurgo, Michael Hursthouse, fac-$(Ru(CO)_3)^{2+}$-Core Complexes and Design of Metal-Based Drugs. Synthesis, Structure, and Reactivity of Ru-Thiazole Derivative with Serum Proteins and Absorption-Release Studies with Acryloyl and Silica Hydrogels as Carriers in Physiological Media, *Inorganic Chemistry* **2007**, *46*, 79-92.

290. Daniela Valensin, Paolo Anzini, Elena Gaggelli, Nicola Gaggelli, Gabriella Tamasi, Renzo Cini, Chiara Gabbiani, Elena Michelucci, Luigi Messori, Henryk Kozlowski, Gianni Valensin,
fac-$(Ru(CO)_3)^{2+}$ Selectively Targets the Histidine Residues of the β-Amyloid Peptide 1-28. Implications for New Alzheimer's Disease Treatments Based on Ruthenium Complexes, *Inorganic Chemistry* **2010**, *49*, 4720–4722.

291. Marino F. A. Santos, João D. Seixas, Abhik Mukhopadhyay, Patrícia M. Reis, Maria J. Romão, Carlos C. Romão, Teresa Santos-Silva, New insights into the chemistry of fac-$[Ru(CO)_3]^{2+}$ fragments in biologically relevant conditions: The CO releasing activity of $[Ru(CO)_3Cl_2(1,3\text{-thiazole})]$, and the X-ray crystal structure of its adduct with lysozyme, *Journal of Inorganic Biochemistry* **2012**, *117*, 285-291.

292. George R. Clark, Warren R. Roper, L. James Wright, V. Patricia D. Yap, Acid-Base Control of a Migratory Insertion Reaction: p-Aminophenyl Derivatives of Ruthenium(II) and the Crystal Structure of $Ru(\eta^2\text{-}C[O]C_6H_4NH_2\text{-}4)Cl(CO)(PPh_3)_2$, *Organometallics* **1997**, *16*, 5135-5136.

293. João D. Seixas, Marino F. A. Santos, Abhik Mukhopadhyay, Ana C. Coelho, Patrícia M. Reis, Luís F. Veiros, Ana R. Marques, Nuno Penacho, Ana M. L. Gonçalves, Maria J. Romão, Gonçalo J. L. Bernardes, Teresa Santos-Silva, Carlos C. Romão, A contribution to the rational design of $Ru(CO)_3Cl_2L$ complexes for in vivo delivery of CO, *Dalton Transactions* **2015**, *44*, 5058-5075.

294. Antonia Marazioti, Mariarosaria Bucci, Ciro Coletta, Valentina Vellecco, Padmamalini Baskaran, Csaba Szabó, Giuseppe Cirino, Ana Rita Marques, Bruno Guerreiro, Ana M.L. Gonçalves, João D. Seixas, Annie Beuve, Carlos C. Romão, Andreas Papapetropoulos, Inhibition of Nitric Oxide–Stimulated Vasorelaxation by Carbon Monoxide-Releasing Molecules, *Arteriosclerosis, Thrombosis, and Vascular Biology* **2011**, *31*, 2570-2576.

295. Ana Filipa N. Tavares, Miguel Teixeira, Carlos C. Romão, João D. Seixas, Lígia S. Nobre, Lígia M. Saraiva, Reactive Oxygen Species Mediate Bactericidal Killing Elicited by Carbon Monoxide-releasing Molecules, *Journal of Biological Chemistry* **2011**, *286(30)*, 26708-26717.

296. Max F. Perutz, Preparation of Haemoglobin Crystals, *Journal of Crystal Growth* **1968**, *2*, 54-56.

297. Guoyong Sun, Andre F. Palmer, Preparation of ultrapure bovine and human hemoglobin by anion exchange chromatography, *Journal of Chromatography B* **2008**, *867*, 1-7.

298. Roman Aranda IV, He Cai, Chad E. Worley, Elena J. Levin, Rong Li, John S. Olson, George N. Phillips Jr, Mark P. Richards, Structural analysis of fish versus mammalian hemoglobins: Effect of the heme pocket environment on autooxidation and hemin loss, *Proteins: Structure, Function, and Bioinformatics* **2009**, *75(1)*, 217-230.

299. Trinity Vera, Jeffery R. Henegar, Heather A. Drummond, John M. Rimoldi, David E. Stec, Protective Effect of Carbon Monoxide–Releasing Compounds in Ischemia-Induced Acute Renal Failure, *Journal of American Society of Nephrology* **2005**, *16*, 950-958.

300. V. Richard, G.G. Dodson, Y. Mauguen, Human Deoxyhaemoglobin-2,3-Diphosphoglycerate Complex Low-Salt Structure at 2.5 Å Resolution, *Journal of Molecular Biology* **1993**, *233(2)*, 270-274.

301. Luigi Messori, Giordana Marcon, Pierluigi Orioli, Marco Fontani, Piero Zanello, Alberta Bergamoc, Gianni Savac, Pasquale Mura, Molecular structure, solution chemistry and biological properties of the novel [ImH][trans-$IrCl_4$(Im)(DMSO)], (I) and of the orange form of [$(DMSO)_2$H][trans-$IrCl_4(DMSO)_2$], (II), complexes, *Journal of Inorganic Biochemistry* **2003**, *95*, 37-46.

302. Francisca M. Albertí, Juan J. Fiol, Angel García-Raso, Marta Torres, A. Terrón, Miquel Barceló-Oliver, María J. Prieto, Virtudes Moreno, Elies Molins, Ruthenium(III) and iridium(III) complexes with nicotine, *Polyhedron* **2010**, *29*, 34-41.

303. Damian E. Bikiel, Estefanía González Solveyra, Florencia Di Salvo, Humberto M. S. Milagre, Marcos N. Eberlin, Rodrigo S. Corrêa, Javier Ellena, Darío A. Estrin, Fabio Doctorovich, Tetrachlorocarbonyliridates: Water-Soluble Carbon Monoxide Releasing Molecules Rate-Modulated by the Sixth Ligand, *Inorganic Chemistry* **2011**, *50(6)*, 2334-2345.

304. Stephen Curry, Hendrik Mandelkow, Peter Brick, Nick Franks, Crystal structure of human serum albumin complexed with fatty acid reveals an asymmetric distribution of binding sites, *Nature Structural & Molecular Biology* **1998**, *5*, 827-835.

305. Anna Bujacz, Structures of bovine, equine and leporine serum albumin, *Acta Crystallographica* **2012**, *D68*, 1278-1289.

306. Karolina A. Majorek, Przemyslaw J. Porebski, Arjun Dayal, Matthew D. Zimmerman, Kamila Jablonska, Alan J. Stewart, Maksymilian Chruszcz, Wladek Minor, Structural and immunologic characterization of bovine, horse, and rabbit serum albumins, *Molecular Immunology* **2012**, *52*, 174-182.

307. Peter J. Sargent, Sebastien Farnaud, Robert W. Evans, Structure/Function Overview of Proteins Involved in Iron Storage and Transport, *Current Medicinal Chemistry* **2005**, *12*, 2683-2693.

308. Peter F. Lindley, Transferrins in *Handbook of Metalloproteins Volume 3* edited by Albrecht Messerschhmidt, Wolfram Bode and Mirek Cygler, John Wiley & Sons, Ltd, **2006**, 1-19.

309. Konstantinos Gkouvatsos, George Papanikolaou, Kostas Pantopoulos, Regulation of iron transport and the role of transferrin, *Biochimica et Biophysica Acta* **2012**, *1820*, 188-202.

310. John B. Vincent, Sharifa Love, The binding and transport of alternative metals by transferrin, *Biochimica et Biophysica Acta* **2012**, *1820*, 362-378.

311. Jeremy Wally, Peter J. Halbrooks, Clemens Vonrhein, Mark A. Rould, Stephen J. Everse, Anne B. Mason, Susan K. Buchanan, The Crystal Structure of Iron-free Human Serum Transferrin Provides Insight into Inter-lobe Communication and Receptor Binding, *The Journal of Biological Chemistry* **2006**, *281(34)*, 24934–24944.

312. Begoña Heras, Jennifer L. Martin, Post-crystallization treatments for improving diffraction quality of protein crystals, *Acta Crystallographica* **2005**, *D61*, 1173-1180.

313. Janet Newman, A review of techniques for maximizing diffraction from a protein crystal in stilla, *Acta Crystallographica* **2006**, *D62*, 27-31.

314. Marc L. Pusey, Zhi-Jie Liu, Wolfram Tempel, Jeremy Praissman, Dawei Lin, Bi-Cheng Wang, José A. Gavira, Joseph D. Ng, Life in the fast lane for protein crystallization and X-ray crystallography, *Progress in Biophysics and Molecular Biology* **2005**, *88*, 359-386.

315. Sameena Mehtab, Gisela Gonçalves, Somnath Roy, Ana Isabel Tomaz, Teresa Santos-Silva, Marino F.A. Santos, Maria J. Romão, Tamás Jakusch, Tamás Kiss, João Costa Pessoa, Interaction of vanadium(IV) with human serum apo-transferrin, *Journal of Inorganic Biochemistry* **2013**, *121*, 187-195.

316. Petra Pernot, Adam Round, Ray Barrett, Alejandro De Maria Antolinos, Alexandre Gobbo, Elspeth Gordon, Julien Huet, Jerôme Kieffer, Mario Lentini, Muriel Mattenet, Christian Morawe, Christoph Mueller-Dieckmann, Staffan Ohlsson, Werner Schmid, John Surr, Pascal Theveneau, Louiza Zerrada, Sean McSweeney, Upgraded ESRF BM29 beamline for SAXS on macromolecules in solution, *Journal of Synchrotron Radiation* **2013**, *20*, 660-664.

317. Maxim V. Petoukhov, Peter V. Konarev, Alexey G. Kikhneya, Dmitri I. Svergun, ATSAS 2.1 – towards automated and web supported small-angle scattering data analysis, *Journal of Applied Crystallography* **2007**, *40*, s223-s228.

318. Petr V. Konarev, Vladimir V. Volkov, Anna V. Sokolova, Michel H. J. Kochb, Dmitri I. Svergun, PRIMUS: a Windows PC-based system for small-angle scattering data analysis, *Journal of Applied Crystallography* **2003**, *36*, 1277-1282.

319. Haydyn D.T. Mertens, Dmitri I. Svergun, Structural characterization of proteins and complexes using small-angle X-ray solution scattering, *Journal of Structural Biology* **2010**, *172*, 128-141.

320. Dmitri I. Svergun, Restoring Low Resolution Structure of Biological Macromolecules from Solution Scattering Using Simulated Annealing, *Biophysical Journal* **1999**, *76*, 2879-2886.

321. Vladimir V. Volkov, Dmitri I. Svergun, Uniqueness of ab initio shape determination in small-angle scattering, *Journal of Applied Crystallography* **2003**, *36*, 860-864.

322. Dmitri I. Svergun, Claudio Barberato, Michel H. J. Koch, CRYSOL- a Program to Evaluate X-ray Solution Scattering of Biological Macromolecules from Atomic Coordinates, *Journal of Applied Crystallography* **1995**, *28*, 768-773.

323. M. B. Kozin, Dmitri I. Svergun, Automated matching of high- and low-resolution structural models, *Journal of Applied Crystallography* **2001**, *34*, 33-41.

324. Marta Passadouro, Ana M. Metelo, Alice S. Melão, Joana R. Pedro, Henrique Faneca, Eugénia Carvalho, M. Margarida C.A. Castro, Study of the antidiabetic capacity of the VO(dmpp)2 complex, *Journal of Inorganic Biochemistry* **2010**, *104*, 987-992.

325. Hiromu Sakurai, Hiroyuki Yasui, Structure-Activity Relationship of Insulinomimetic Vanadyl-Picolinate Complexes in View of Their Clinical Use, *The Journal of Trace Elements in Experimental Medicine* **2003**, *16*, 269-280.

326. Gail R. Willsky, Lai-Har Chi, Michael Godzala III, Paul J. Kostyniak, Jason J. Smee, Alejandro M. Trujillo, Josephine A. Alfano, Wenjin Ding, Zihua Hu, Debbie C. Crans, Anti-diabetic effects of a series of vanadium dipicolinate complexes in rats with streptozotocin-induced diabetes, *Coordination Chemistry Reviews* **2011**, *255*, 2258-2269.

327. Megumi Hamano Nagaoka, Takeshi Yamazaki, Tamio Maitani, Binding patterns of vanadium ions with different valence states to human serum transferrin studied by HPLC/high-resolution ICP-MS, *Biochemical and Biophysical Research Communications* **2002**, *296*, 1207-1214.

328. Shaina L. Byrne, Anne B. Mason, Human serum transferrin: a tale of two lobes. Urea gel and steady state fluorescence analysis of recombinant transferrins as a function of pH, time, and the soluble portion of the transferrin receptor, *Journal of Biological Inorganic Chemistry* **2009**, *14*, 771-781.

329. Erin E. Battin, Ashley Lawhon, Julia L. Brumaghim, David H. Hamilton, Using Proteins in a Bioinorganic Laboratory Experiment: Iron Loading and Removal from Transferrin, *Journal of Chemical Education* **2009**, *86(8)*, 969-972.

330. João Costa Pessoa, Gisela Gonçalves, Somnath Roy, Isabel Correia, Sameena Mehtab, Marino F.A. Santos, Teresa Santos-Silva, New insights on vanadium binding to human serum transferrin, *Inorganica Chimica Acta* **2014**, *420*, 60-68.

331. Nicholas Noinaj, Nicole C. Easley, Muse Oke, Naoko Mizuno, James Gumbart, Evzen Boura, Ashley N. Steere, Olga Zak, Philip Aisen, Emad Tajkhorshid, Robert W. Evans, Andrew R. Gorringe, Anne B. Mason, Alasdair C. Steven, Susan K. Buchanan, Structural basis for iron piracy by pathogenic Neisseria, *Nature* **2012**, *483*, 53-58.

332. Marino F. A. Santos, Isabel Correia, Ana R. Oliveira, Eugenio Garribba, João Costa Pessoa, Teresa Santos-Silva, Vanadium Complexes as Prospective Therapeutics: Structural Characterization of a V(IV) Lysozyme Adduct, *European Journal of Inorganic Chemistry* **2014**, *2014(21)*, 3293-3297.

333. Luís F. Vilas Boas, João Costa Pessoa, Vanadium *in Comprehensive Coordination Chemistry, The Synthesis, Reactions, Properties & Applications of Coordination Compounds – Volume 3, Main Group and Early Transition Elements* edited by George Wilkinson, Robert D. Gillard and Jon A. McCleverty, Pergamon Press, Oxford, UK, **1987**, 1st edition, 453-583.

334. Gunnar I. Berglund, Gunilla H. Carlsson, Andrew T. Smith, Hanna Szöke, Anette Henriksen, Janos Hajdu, The catalytic pathway of horseradish peroxidase at high resolution, *Nature* **2002**, *417*, 463-468.

335. Jochen Wuerges, Jin-Won Lee, Yang-In Yim, Hyung-Soon Yim, Sa-Ouk Kang, Kristina Djinovic Carugo, Crystal structure of nickel-containing superoxide dismutase reveals another type of active site, *Proceedings of the National Academy of Sciences USA* **2004**, *101(23)*, 8569-8574.

336. Erzsébet Kiss, Eugenio Garribba, Giovanni Micera, Tamás Kiss, Hiromu Sakurai, Ternary complex formation between VO(IV)–picolinic acid or VO(IV)–6-methylpicolinic acid and small blood serum bioligands, *Journal of Inorganic Biochemistry* **2000**, *78*, 97-108.

337. Sean S. Amin, Kirk Cryer, Boyan Zhang, Subodh K. Dutta, Sandra S. Eaton, Oren P. Anderson, Susie M. Miller, Benedicte A. Reul, Sonia M. Brichard, Debbie C. Crans, Chemistry and Insulin-Mimetic Properties of Bis(acetylacetonate)oxovanadium(IV) and Derivatives, *Inorganic Chemistry* **2000**, *39*, 406-416.

338. Yanhong Dong, Rama Krishna Narla, Elise Sudbeck, Fatih M. Uckun, Synthesis, X-ray structure, and anti-leukemic activity of oxovanadium(IV) complexes, *Journal of Inorganic Biochemistry* **2000**, *78*, 321-330.

339. Anna M. Kordowiak, Wojciech Dabros, Bozena Kajda, The Influence of a New Vanadium Compound, Bis(2,2'-bipyridine)oxovanadium(IV) Sulphate on Liver Golgi Complexes from Control and Streptozotocin-Diabetic Rats, *Hormone and Metabolic Research* **2002**, *34(10)*, 556-560.

340. Ying Fu, Qin Wang, Xiao-Gai Yang, Xiao-Da Yang, Kui Wang, Vanadyl bisacetylacetonate induced G1/S cell cycle arrest via high-intensity ERK phosphorylation in HepG2 cells, *Journal of Biological Inorganic Chemistry* **2008**, *13*, 1001-1009.

341. Marvin W. Makinen, Marzieh Salehitazangi, The structural basis of action of vanadyl (VO^{2+}) chelates in cells, *Coordination Chemistry Reviews* **2014**, *279*, 1-22.

342. Fabrizio Chiti, Niccolò Taddei, Massimo Stefani, Christopher M. Dobson, Giampietro Ramponi, Reduction of the amyloidogenicity of a protein by specific binding of ligands to the native conformation, *Protein Science* **2001**, *10*, 879-886.

343. Gemma Soldi, Georgia Plakoutsi, Niccolò Taddei, Fabrizio Chiti, Stabilization of a Native Protein Mediated by Ligand Binding Inhibits Amyloid Formation Independently of the Aggregation Pathway, *Journal of Medicinal Chemistry* **2006**, *49*, 6057-6064.

344. Dina Morshedi, Nasrollah Rezaei-Ghaleh, Azadeh Ebrahim-Habibi, Shahin Ahmadian, Mohsen Nemat-Gorgani, Inhibition of amyloid fibrillation of lysozyme by indole derivatives – possible mechanism of action, *The FEBS Journal* **2007**, *274*, 6415-6425.

345. Sajad Shariatizia, Ali Akbar Meratanb, Atiyeh Ghasemia, Mohsen Nemat-Gorganic, Inhibition of amyloid fibrillation and cytotoxicity of lysozyme fibrillation products by polyphenols, *International Journal of Biological Macromolecules* **2015**, *80*, 95-106.

346. Lizbeth Hedstrom, Serine Protease Mechanism and Specificity, *Chemical Reviews* **2002**, *102*, 4501-4523.

347. Michael J. Page, Enrico Di Cera, Serine peptidases: Classification, structure and function, *Cellular and Molecular Life Sciences* **2008**, *65*, 1220-1236.

348. Enrico Di Cera, Serine Proteases, *IUBMB Life* **2009**, *61*, 510-515.

349. Praveen K. Madala, Joel D. A. Tyndall, Tessa Nall, David P. Fairlie, Update 1 of: Proteases Universally Recognize Beta Strands In Their Active Sites, *Chemical Reviews* **2010**, *110*, PR1- PR31.

350. Aaron Moulin, Jason H. Bell, R. F. Pratt, Dagmar Ringe, Inhibition of Chymotrypsin by a Complex of Ortho-Vanadate and Benzohydroxamic Acid: Structure of the Inert Complex and Its Mechanistic Interpretation, *Biochemistry* **2007**, *46*, 5982-5990.

351. Donald Voet, Judith G. Voet, Charlotte W. Pratt, *Fundamentals of Biochemistry – Life at the Molecular Level*, John Wiley & Sons, Inc., 4th edition, **2013**, 339-352.

352. László Polgár, The catalytic triad of serine peptidases, *Cellular and Molecular Life Sciences* **2005**, *62*, 2161-2172.

353. Wolfram Bode, Peter Schwager, The single calcium-binding site of crystalline bovine β-trypsin, *FEBS Letters* **1975**, *56(1)*, 139-143.

354. Salvatore Ulisse, Enke Baldini, Salvatore Sorrenti, Massimino D'Armiento, The Urokinase Plasminogen Activator System: A Target for Anti-Cancer Therapy, *Current Cancer Drug Targets* **2009**, *9*, 32-71.

355. Alessio Metere, Egidio Iorio, Giuseppe Scorza, Serena Camerini, Marialuisa Casella, Marco Crescenzi, Maurizio Minetti, Donatella Pietraforte, Carbon Monoxide Signaling in Human Red Blood Cells: Evidence for Pentose Phosphate Pathway Activation and Protein Deglutathionylation, *Antioxidants & Redox Signaling* **2014**, *20(3)*, 403-416.

356. Jamie Ghuman, Patricia A. Zunszain, Isabelle Petitpas, Ananyo A. Bhattacharya, Masaki Otagiri, Stephen Curry, Structural Basis of the Drug-binding Specificity of Human Serum Albumin, *Journal of Molecular Biology* **2005**, *353*, 38-52.

357. Feng Yang, Chuanbing Bian, Lili Zhu, Gengxiang Zhao , Zixiang Huang , Mingdong Huang, Effect of human serum albumin on drug metabolism: Structural evidence of esterase activity of human serum albumin, *Journal of Structural Biology* **2007**, *157*, 348-355.

358. Ali J. Ryan, Jamie Ghuman, Patricia A. Zunszain, Chun-wa Chung, Stephen Curry, Structural basis of binding of fluorescent, site-specific dansylated amino acids to human serum albumin, *Journal of Structural Biology* **2011**, *174*, 84-91.

359. Kenta Fujita, Yuya Tanaka, Takeya Sho, Shuichi Ozeki, Satoshi Abe, Tatsuo Hikage, Takahiro Kuchimaru, Shinae Kizaka-Kondoh, Takafumi Ueno, Intracellular CO Release from Composite of Ferritin and Ruthenium Carbonyl Complexes, *Journal of the American Chemical Society* **2014**, *136(48)*, 16902-16908.

360. Daniele Sanna, Maria Serra, Giovanni Micera, Eugenio Garribba, Interaction of Antidiabetic Vanadium Compounds with Hemoglobin and Red Blood Cells and Their Distribution between Plasma and Erythrocytes, *Inorganic Chemistry* **2014**, *53*, 1449-1464.

361. Daniele Sanna, Maria Serra, Giovanni Micera, Eugenio Garribba, Uptake of potential anti-diabetic $V^{IV}O$ compounds of picolinate ligands by red blood cells, *Inorganica Chimica Acta* **2014**, *420*, 75-84.

APPENDIX A

Appendix 1 – Structure 1 screen (Molecular Dimensions)

1	0.02 M Calcium chloride dihydrate, 0.1 M Sodium acetate 4.6, 30% 2-Methyl-2,4-pentanediol (MPD)
2	0.2 M Ammonium acetate, 0.1 M Sodium acetate 4.6, 30% PEG 4000
3	0.2 M Ammonium sulfate, 0.1 M Sodium acetate 4.6, 25% PEG 4000
4	2.0 M Sodium formate, 0.1 M Sodium acetate 4.6
5	2.0 M Ammonium sulfate, 0.1 M Sodium acetate 4.6
6	0.1 M Sodium acetate 4.6, 8% PEG 4000
7	0.2 M Ammonium acetate, 0.1 M Sodium citrate 5.6, 30% PEG 4000
8	0.2 M Ammonium acetate, 0.1 M Sodium citrate 5.6, 30% 2-Methyl-2,4-pentanediol (MPD)
9	0.1 M Sodium citrate 5.6, 20% PEG 4000, 20% 2-Propanol
10	1.0 M Ammonium phosphate monobasic, 0.1 M Sodium citrate 5.6
11	0.2 M Calcium chloride dihydrate, 0.1M Sodium acetate 4.6, 20% 2-Propanol
12	1.4 M Sodium acetate trihydrate, 0.1 M Sodium cacodylate 6.5
13	0.2 M Sodium citrate tribasic dihydrate, 0.1 M Sodium cacodylate 6.5, 30% 2-Propanol
14	0.2 M Ammonium sulfate, 0.1M Sodium cacodylate 6.5, 30% PEG 8000
15	0.2 M Magnesium acetate tetrahydrate, 0.1 M Sodium cacodylate 6.5, 20% PEG 8000
16	0.2 M Magnesium acetate tetrahydrate, 0.1M Sodium cacodylate 6.5, 30% 2-Methyl-2,4-pentanediol (MPD)
17	1.0 M Sodium acetate trihydrate, 0.1 M Imidazole 6.5
18	0.2 M Sodium acetate trihydrate, 0.1 M Sodium cacodylate 6.5, 30% PEG 8000
19	0.2 M Zinc acetate dihydrate, 0.1 M Sodium cacodylate 6.5, 18% PEG 8000
20	0.2 M Calcium acetate hydrate, 0.1 M Sodium cacodylate 6.5, 18% PEG 8000
21	0.2 M Sodium citrate tribasic dehydrate, 0.1 M Sodium HEPES 7.5, 30% 2-Methyl-2,4-pentanediol (MPD)
22	0.2 M Magnesium chloride hexahydrate, 0.1 M Sodium HEPES 7.5, 30% 2-Propanol
23	0.2 M Calcium chloride dihydrate, 0.1M Sodium HEPES 7.5, 28% PEG 400
24	0.2 M Magnesium chloride hexahydrate, 0.1 M Sodium HEPES 7.5, 30% PEG 400
25	0.2 M Sodium citrate tribasic dehydrate, 0.1 M Sodium HEPES 7.5, 20% 2-Propanol
26	0.8 M Potassium sodium tartrate tetrahydrate, 0.1 M Sodium HEPES 7.5
27	1.5 M Lithium sulfate, 0.1 M, Sodium HEPES 7.5

28	0.8 M Sodium phosphate monobasic monohydrate/0.8 M Potassium phosphate monobasic, 0.1 M Sodium HEPES 7.5
29	1.4 M Sodium citrate tribasic dehydrate, 0.1 M Sodium HEPES 7.5
30	2.0 M Ammonium sulfate, 0.1 M Sodium HEPES 7.5, 2% PEG 400
31	0.1 M Sodium HEPES 7.5, 20% PEG 4000, 10% 2-Propanol
32	2.0 M Ammonium sulfate, 0.1 M Tris/HCl 8.5
33	0.2 M Magnesium chloride hexahydrate, 0.1 M Tris/HCl 8.5, 30% PEG 4000
34	0.2 M Sodium citrate tribasic dehydrate, 0.1 M Tris/HCl 8.5, 30% PEG 400
35	0.2 M Lithium sulfate, 0.1 M Tris/HCl 8.5, 30% PEG 4000
36	0.2 M Ammonium acetate, 0.1 M Tris/HCl 8.5, 30% 2-Propanol
37	0.2 M Sodium acetate trihydrate, 0.1 M Tris/HCl 8.5, 30% PEG 4000
38	0.1 M Tris/HCl 8.5, 8% PEG 8000
39	2.0 M Ammonium phosphate monobasic, 0.1 M Tris/HCl 8.5
40	0.4 M Potassium sodium tartrate tetrahydrate
41	0.4 M Ammonium phosphate monobasic
42	0.2 M Ammonium sulfate, 30% PEG 8000
43	0.2 M Ammonium sulfate, 30% PEG 4000
44	2.0 M Ammonium sulfate
45	4.0 M Sodium formate
46	0.05 M Potassium phosphate monobasic
47	30 % w/v PEG 1500
48	0.2 M Magnesium formate dihydrate
49	1.0 M Lithium sulfate, 2% PEG 8000
50	0.5 M Lithium sulfate, 15% PEG 8000

Appendix 2 – Structure 2 screen (Molecular Dimensions)

1	0.1 M Sodium chloride, 0.1M BICINE (N,N-Bis(2-hydroxyethyl)glycine) 9.0, 30% PEG 500MME
2	2.0 M Magnesium chloride hexahydrate, 0.1 M BICINE (N,N-Bis(2-hydroxyethyl)glycine)9.0
3	0.1 M BICINE (N,N-Bis(2-hydroxyethyl)glycine) 9.0, 10% PEG 20000, 2% 1,4-Dioxane
4	0.2 M Magnesium chloride hexahydrate, 0.1 M Tris/HCl 8.5, 3.4 M 1,6-Hexanediol
5	0.1 M Tris/HCl 8.5, 25% tert-Butanol
6	1.0 M Lithium sulfate, 0.1 M Tris/HCl 8.5, 0.01 M Nickel(II) chloride hexahydrate
7	1.5 M Ammonium sulfate, 0.1 M Tris/HCl 8.5, 12% Glycerol
8	0.2 M Ammonium phosphate monobasic, 0.1 M Tris/HCl 8.5, 50% 2-Methyl-2,4-pentanediol (MPD)
9	0.1 M Tris/HCl 8.5, 20% Ethanol
10	0.01 M Nickel(II) chloride hexahydrate, 0.1 M Tris/HCl 8.5, 20% PEG 2000 MME
11	0.5 M Ammonium sulfate, 0.1 M Sodium HEPES 7.5, 30% 2-Methyl-2,4-pentanediol (MPD)
12	0.1 M Sodium HEPES 7.5, 10% PEG 6000, 5% 2-Methyl-2,4-pentanediol (MPD)
13	0.1 M Sodium HEPES 7.5, 20% Jeffamine® M-600
14	1.6 M Ammonium sulfate, 0.1 M Sodium HEPES 7.5, 0.1 M Sodium chloride
15	2.0 M Ammonium formate, 0.1 M Sodium HEPES 7.5
16	1.0 M Sodium acetate, 0.05 M Cadmium sulfate, 0.1 M Sodium HEPES 7.5
17	0.1 M Sodium HEPES 7.5, 70% 2-Methyl-2,4-pentanediol (MPD)
18	4.3 M Sodium chloride, 0.1 M Sodium HEPES 7.5
19	0.1 M Sodium HEPES 7.5, 10% PEG 8000, 8 % Ethylene glycol
20	1.6 M Magnesium sulfate heptahydrate, 0.1 M MES [2-(N-morpholino)ethanesulfonic acid] 6.5
21	2.0 M Sodium chloride, 0.1 M Potassium phosphate monobasic, 0.1 M Sodium phosphate monobasic monohydrate, 0.1 M MES 6.5
22	0.1 M MES 6.5, 12% PEG 20000
23	1.6 M Ammonium sulfate, 0.1 M MES 6.5, 10% 1,4-Dioxane
24	0.05 M Cesium chloride, 0.1 M MES 6.5, 30% Jeffamine® M-600
25	0.01 M Cobalt(II) chloride hexahydrate, 0.1 M MES 6.5, 1.8 M Ammonium sulfate
26	0.2 M Ammonium sulfate, 0.1 M MES 6.5, 30% PEG 5000 MME

27	0.01 M Zinc sulfate heptahydrate, 0.1 M MES 6.5, 25% PEG 500 MME
28	0.1 M Sodium HEPES 7.5, 20% PEG 10000
29	2.0 M Ammonium sulfate, 0.1 M Sodium citrate 5.6, 0.2 M Potassium sodium tartrate tetrahydrate
30	1.0 M Lithium sulfate, 0.1 M Sodium citrate 5.6, 0.5 M Ammonium sulfate
31	0.5 M Sodium chloride, 0.1 M Sodium citrate 5.6, 4 % Polyethyleneimine
32	0.1 M Sodium citrate 5.6, 35% tert-Butanol
33	0.01 M Iron(III) chloride hexahydrate, 0.1 M Sodium citrate 5.6, 10% Jeffamine® M-600
34	0.01 M Manganese(II) chloride tetrahydrate, 0.1 M Sodium citrate 5.6, 2.5 M 1,6-Hexanediol
35	2.0 M Sodium chloride, 0.1 M Sodium acetate 4.6
36	0.2 M Sodium chloride, 0.1 M Sodium acetate 4.6, 30% 2-Methyl-2,4-pentanediol (MPD)
37	0.01 M Cobalt(II) chloride hexahydrate, 0.1 M Sodium acetate 4.6, 1.0 M 1,6-Hexanediol
38	0.1 M Cadmium chloride hemi(pentahydrate), 0.1 M Sodium acetate 4.6, 30% PEG 400
39	0.2 M Ammonium sulfate, 0.1 M Sodium acetate 4.6, 30% PEG 2000 MME
40	2.0 M Sodium chloride, 10% PEG 6000
41	0.5 M Sodium chloride, 0.1 M Magnesium chloride hexahydrate, 0.01 M CTAB (Cetyltrimethylammonium bromide)
42	25% Ethylene glycol
43	35% 1,4-Dioxane
44	2.0 M Ammonium sulfate, 5% 2-Propanol
45	1.0 M Imidazole 7.0
46	10% PEG 1000, 10% PEG 8000
47	1.5 M Sodium chloride, 10% Ethanol
48	1.6 M Sodium citrate 6.5
49	15% Polyvinylpyrrolidone
50	2.0 M Urea

Appendix 3 – *In-house* sparse matrix screen (80!)

1	0.2 M Calcium chloride, 0.1 M Acetate buffer 4.5, 30% 2-Methyl-2,4-pentanediol (MPD)
2	1M Potassium/Sodium tartrate, 0.1 M MES 6.5
3	0.4 M Ammonium phosphate
4	0.1 M Tris/HCl 8.5, 3M Ammonium sulfate
5	0.2 M Trisodium citrate, 0.1M HEPES 7.5, 30% 2-Methyl-2,4-pentanediol (MPD)
6	0.2 M Magnesium chloride, 0.1 M Acetate buffer 4.5, 30% PEG 3350
7	1.2 M Sodium citrate, 0.1 M HEPES buffer 7.5
8	0.2 M Trisodium citrate, 2 M Ammonium sulfate
9	0.2 M Ammonium acetate, 0.1 M Citrate buffer 5.5, 30% PEG 400
10	0.1 M Acetate buffer 4.5, 1.5 M Ammonium phosphate
11	0.2 M Ammonium sulfate, 0.1 M HEPES buffer 7.5, 1.5 M Potassium phosphate/1.5 M sodium phosphate
12	0.2 M Trisodium citrate, 0.1 M Tris/HCl 8.5, 20% PEG 400
13	0.2 M Calcium chloride, 0.1 M HEPES buffer 7.5, 25% PEG 3350
14	0.1 M Magnesium chloride, 0.1 M MES buffer 6.5, 30% PEG 8000
15	0.2 M Lithium sulfate, 0.1M Citrate buffer 5.5, 30% PEG 3350
16	1 M Lithium sulfate, 0.1 M Acetate buffer 4.5
17	0.2 M Ammonium phosphate, 0.1 M Tris/HCl 7.5, 30% 2-Methyl-2,4-pentanediol (MPD)
18	0.2 M Ammonium acetate, 0.1 M Tris/HCl 7.5, 1.5 M Potassium phosphate/1.5M sodium phosphate
19	0.1M Ammonium sulfate, 0.1 M Citrate buffer 5.5, 30% PEG 8000
20	0.1 M MES buffer 6.5, 30% 2-Methyl-2,4-pentanediol (MPD)
21	0.2 M Magnesium chloride, 0.1 M HEPES buffer 7.5, 30% PEG 3350
22	0.2 M Sodium acetate, 0.1 M Tris/HCl 8.5, 30% PEG 3350
23	0.1 M Tris/HCl 7.5, 1 M Potassium/Sodium tartrate
24	0.2 M Calcium chloride, 0.1 M Tris/HCl 8.5
25	0.5 M Ammonium acetate, 0.1 M Citrate buffer 5.5, 30% 2-Methyl-2,4-pentanediol (MPD)
26	2 M Sodium acetate. 0.1 M MES buffer 6.5
27	0.2 M Potassium/Sodium tartrate, 0.1 M MES 6.5, 30 % PEG 8000
28	1 M Potassium/Sodium Tartrate, 0.1 M HEPES 7.5

29	0.2 M Ammonium sulfate, 0.1 M Acetate buffer 4.5, 30% PEG 400
30	0.1 M Ammonium sulfate, 0.1 M HEPES buffer 7.5, 20% PEG 3350
31	2 M Ammonium sulfate, 0.1 M MES buffer 6.5
32	0.2 M Sodium chloride, 0.1 M MES 6.5, 30% Ethanol
33	0.2 M Magnesium chloride, 0.1 M HEPES buffer 7.5, 30% Ethanol
34	0.2 M Ammonium acetate, 0.1 M Tris/HCl 8.5, 30% Ethanol
35	0.2 M Calcium chloride, 0.1 M Acetate buffer 4.5, 30% Ethanol
36	0.2 M Sodium acetate, 0.1 M HEPES buffer 7.5, 30% Ethanol
37	0.2 M Magnesium chloride, 0.1 M HEPES 7.5, 30% Isopropanol
38	0.1 M Cacodilate buffer 6.5, 30 % 2-Methyl-2,4-pentanediol (MPD)
39	0.1 M Acetate buffer 4.5, 2 M Sodium formate
40	0.2 M Trisodium citrate, 0.1 M Cacodylate buffer 6.5, 40% isopropanol
41	0.1 M HEPES buffer 7.5, 20% PEG 400, 10% Isopropanol
42	0.1 M HEPES 7.5, 1M Lithium sulfate
43	0.2 M Lithium sulfate, 0.1 M Tris/HCl 8.5, 30% PEG 3350
44	0.2 M Ammonium sulfate, 0.1 M Cacodylate buffer 6.5, 30% PEG 6000
45	0.1 M Acetate buffer 4.5, 1.5 M Sodium acetate
46	0.1 M Trisodium citrate, 1M Ammonium phosphate
47	4 M Sodium formate
48	0.1 M HEPES buffer 7.5, 1.2 M Trisodium citrate
49	0.4 M Potassium/Sodium tartrate
50	0.2 M Magnesium chloride, 0.1 M Tris/HCl 8.5, 30% PEG 3350
51	0.1 M Cacodylate buffer 6.5, 1.4 M Sodium acetate
52	0.2 M Ammonium acetate, 0.1 M Citrate buffer 5.5, 30% PEG 3350
53	0.2 M Ammonium acetate, 0.1 M Acetate buffer 4.5, 30% PEG 3350
54	0.2 M Calcium chloride, 0.1 M HEPES buffer 7.5, 28% PEG 400
55	0.2 M Ammonium sulphate, 0.1 M Cacodylate buffer 6.5, 30% PEG 8000
56	0.2 M Magnesium acetate, 0.1 M Cacodylate buffer 6.5, 20% PEG 8000
57	0.2 M Ammonium acetate, 0.1 M Tris/HCl 8.5, 30% Isopropanol
58	0.2 M Ammonium sulfate, 0.1 M Acetate buffer 4.5, 25% PEG 3350
59	0.2 M Magnesium acetate, 0.1 M Cacodylate buffer 6.5, 20% 2-Methyl-2,4-pentanediol (MPD)
60	0.2 M Calcium chloride, 0.1 Acetate buffer 4.5, 20% Isopropanol
61	0.1 M Imidazole buffer 7.0, 20% Isopropanol
62	0.2 M Trisodium citrate, 0.1 Cacodylate 6.5, 20% Isopropanol

63	0.2 M Sodium acetate, 0.1 M Cacodylate 6.5, 30% PEG 8000
64	0.2 M Ammonium sulfate, 30% PEG 8000
65	0.2 M Ammonium sulfate. 30 % PEG 3350
66	0.1 M HEPES buffer 7.5, 1.6 M Potassium/sodium phosphate
67	0.1 M Tris/HCl 8.5, 8% PEG 8000
68	0.1 M Acetate buffer 4.5, 8% PEG 3350
69	0.1 M HEPES buffer 7.5, 2% PEG 400, 2 M Ammonium phosphate
70	0.1 M Citrate buffer 5.5, 20% Isopropanol, 20% PEG 3350
71	0.05 M Potassium phosphate, 20% PEG 8000
72	30% PEG 8000
73	0.2 M Magnesium formate
74	0.2 M Zinc acetate, 0.1 M Cacodylate buffer 6.5, 18% PEG 8000
75	0.2 M Calcium acetate, 0.1 M Cacodylate 6.5, 18% PEG 8000
76	0.1 M Acetate buffer 4.5, 2 M Ammonium sulfate
77	0.1 M Tris/HCl 8.5, 2 M Ammonium sulfate
78	1 M Lithium sulfate, 2% PEG 8000
79	0.5 M Lithium sulfate, 15% PEG 8000
80	0.2 M Ammonium acetate, 0.1 M Citrate buffer 5.5, 20% Isopropanol, 20% PEG 3350

Appendix 4 – Purification of BSA by gel filtration chromatography using a Superdex S200 column

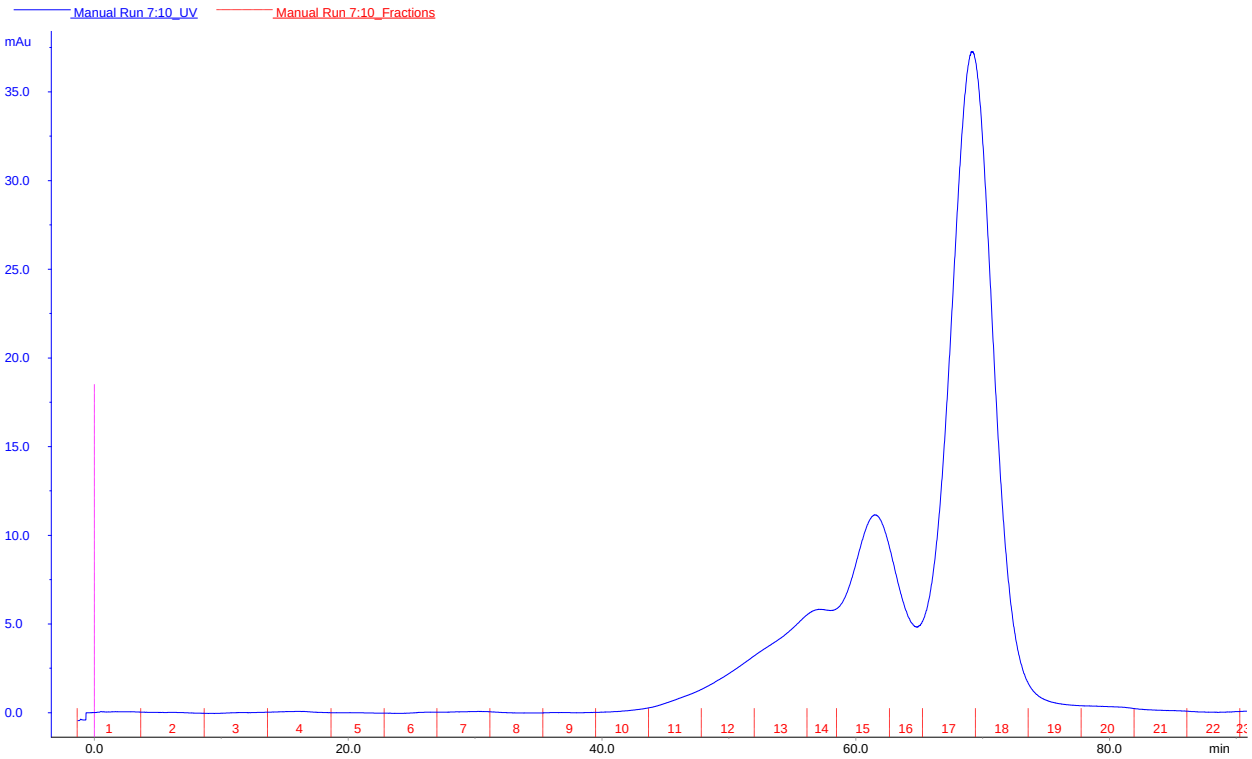

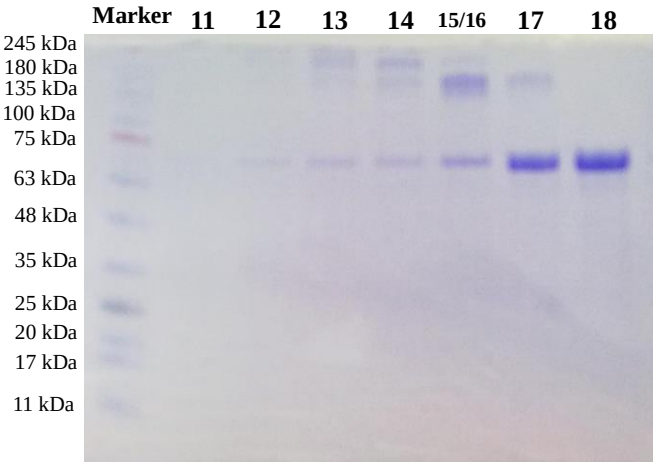

Figure Appendix.1 – Purification of bovine serum albumin by gel filtration chromatography using a Superdex S200 column. Top: Elution profile obtained from the gel filtration column being visible two peaks corresponding to the dimeric and monomeric forms: smaller (fractions 15/16) and larger (fractions 17/18) peaks, respectively. Bottom: SDS-PAGE (10% acrylamide) analysis of the different fractions obtained from the gel filtration (fractions were identified according to the numeration of the chromatogram).